THE DESIGN, SYNTHESIS, AND CHARACTERIZATION OF POLYMETHINE DYES FOR ALL-OPTICAL SIGNAL PROCESSING APPLICATIONS

A Dissertation
Presented to
The Academic Faculty

By

Jonathan D. Matichak

In Partial Fulfillment
Of the Requirements for the Degree
Doctor of Philosophy in Chemistry

Georgia Institute of Technology

August 2010

Copyright © Jonathan D. Matichak 2010

THE DESIGN, SYNTHESIS, AND CHARACTERIZATION OF POLYMETHINE DYES FOR ALL-OPTICAL SIGNAL PROCESSING APPLICATIONS NS

Approved By:

Dr. Seth R. Marder
School of Chemistry and Biochemistry
Georgia Institute of Technology

Dr. Jean-Luc Brédas
School of Chemistry and Biochemistry
Georgia Institute of Technology

Dr. Laren Tolbert
School of Chemistry and Biochemistry
Georgia Institute of Technology

Dr. Joseph Perry
School of Chemistry and Biochemistry
Georgia Institute of Technology

Dr. Anselm Griffin
School of Polymer, Textiles and Engineering
Georgia Institute of Technology

Date Approved: March 31, 2010

ACKNOWLEDGMENTS

I would like to express my appreciation to my advisor, Dr. Seth Marder, for the guidance he has provided over the years and for improving my critical and scientific thinking. He has put together a great research group, the members of which have been my co-workers and friends during my time as a graduate student. I would like to thank my co-workers for the assistance and advice they provided when I needed it. Particularly I would like to thank Dr. Stephen Barlow for editing this thesis and for improving my understanding of science and the English language. I would also like to thank Dr. Barlow, Dr. Mariacristina Rumi and Dr. Joel Hales for answering my numerous questions regarding nonlinear optics. Dr. Hales has also made this work possible by performing all the nonlinear optical measurements within this thesis, which I greatly appreciate his efforts towards this collaboration. I would also like to thank my collaborators Dr. Shino Ohira and Dr. Kada Yesudas for providing quantum-chemical calculations. Finally I would like to thank my family and friends. Particularly, I would like to thank Jenileigh Osborn for being so wonderful.

TABLE OF CONTENTS

ACKNOWLEDGEMENTS iii

LIST OF TABLES vii

LIST OF FIGURES ix

LIST OF SCHEMES xv

LIST OF SYMBOLS xvi

LIST OF ABBREVIATIONS xviii

SUMMARY xix

CHAPTER 1. Introduction 1
1.1. Introduction to Telecommunications and Optical Signal Processing ... 2
1.2. Introduction to Third-Order Nonlinear Optics 5
1.3. Introduction to Selected Nonlinear Optical Modulators 10
1.4. Material Property Requirements for AOSP 15
1.5. Selected Examples of $\chi^{(3)}$-based Optical Devices and Materials From the Literature 19
1.6. Organic $\chi^{(3)}$ Materials 21
1.6.1. Selected Organic Conjugated Polymers from the Literature 21
1.6.2. Selected Organic Conjugated Small Molecules from the Literature .. 30
1.6.2.1. Introduction, Background, and Theory 30
1.6.2.2. Selected Polyenes 36
1.6.2.3. Polymethine Dyes 38
1.7. Organization of the Thesis 45
1.8. References 46

CHAPTER 2. Dioxaborine-Terminated Polymethine Dyes 51
2.1. Introduction 51
2.1.1. Introduction and Background 51
2.1.2. Goals of Chapter 2 59
2.2. Film Forming Properties of a Dioxaborine-Terminated Nonamethine Dye 61
2.3. Effects Upon the Third-Order Nonlinearity Through Extension of Conjugation Beyond the Dioxaborine Termini 65
2.3.1. Synthesis 65
2.3.2. NMR Characterization of 2.3-2.9 66
2.3.3. Electrochemistry of 2.3-2.8 69
2.3.4. Linear Optical Properties of 2.3-2.8 71
2.3.5. Nonlinear Optical Properties of 2.3-2.8 78

2.3.6. Optical Properties of 2.9 81
2.3.7. Conclusions....83
2.4. Experimental Section....84
2.5. References....94

CHAPTER 3. Effects of Bridge Substitution of Dioxaborine-Terminated Polymethine Dyes Upon the Third Order Nonlinear Optical Properties 97
3.1. Introduction....97
3.1.1 Introduction and Background 97
3.1.2 Goals of Chapter 2 109
3.2. Synthesis 109
3.3. NMR Spectroscopy Studies 111
3.4. Electrochemistry 114
3.5. Linear Optical Properties 115
3.6. Nonlinear Optical Properties 121
3.7. Properties of Indole-Terminated Heptamethine Dyes 123
3.8. Conclusions....128
3.9. Experimental 130
3.10. References....136

CHAPTER 4. Third-Order Nonlinear Optical Properties of Anionic Polymethine Dyes with Keto and Dicyano Methylidine Containing Terminal Groups..139
4.1. Introduction....139
4.1.1. Introduction and Background 139
4.1.2. Goals of Chapter 4 144
4.2. Synthesis 146
4.3. NMR Studies 148
4.3.1. NMR Characterization of 4.1-4.7 148
4.3.2 NMR Characterization of 4.8-4.12 151
4.4. Linear and Nonlinear Optical Properties 154
4.4.1. Linear and Nonlinear Optical Properties of 4.1-4.7 154
4.4.2. Linear and Nonlinear Optical Properties of 4.8-4.12 160
4.5. Conclusions....165
4.6. Experimental 167
4.7. References....177

CHAPTER 5. Nonlinear Optical Properties of Chalcogenopyrylium-Terminated Polymethine Dyes 180
5.1. Introduction....180
5.1.1. Brief Literature Survey of the Optical Properties of Polymethine Dyes 181
5.1.2. Chalcogenopyrylium-Terminated Polymethines 185
5.1.3. Goals of Chapter 5 188
5.2. Synthesis and NMR Characterization....189
5.3. Linear Optical Properties 193
5.4. Nonlinear Optical Properties 197

5.5. Conclusions.....200
5.6. Experimental.....202
5.7. References.....212

CHAPTER 6. Conclusions and Future Directions.....215
6.1. Summary of Conclusions.....215
6.2. Future Directions.....219
6.3. References.....224

LIST OF TABLES

Table 1.1 Materials used in all-optical signal processing devices. The fundamental wavelength (λ_f), n_2, , and the T FOM. 21

Table 1.2 Selected conjugated polymers of which the third-order nonlinearity has been measured.....30

Table 1.3 Selected polyene molecules of which the third-order nonlinearity has been measured. 38

Table 1.4 Selected polymethine materials of which the third-order nonlinearity has been measured.....45

Table 2.1 λ_{max} of **2.VII-2.XIV** in various solvents. 58

Table 2.2 Comparison of Linear and Nonlinear Optical Properties of Dye **2.XVI**, **2.1** and **2.2** in DMSO 64

Table 2.3 Electrochemical potentials versus ferrocenium / ferrocene for dyes **2.3-2.8** in THF / 0.1 M $^{n}Bu_4NPF_6$ 71

Table 2.4 Experimental data in DMSO solvent and calculated Intermediate Neglect of Differential Overlap – Configuration Interaction Singles (INDO-CIS) optical data for dyes **2.3-2.6**.....74

Table 2.5 Third-order Nonlinear Optical Properties for **2.3-2.8** in DMSO Determined at 1.3 μm[a] along with Theoretical Estimates of the Static Third-order Polarizabilities.....80

Table 2.6 Comparison of Linear and Nonlinear Optical properties of Dye **2.XVI** and **2.9**.....83

Table 3.1 Hammett parameters and Modified Swain-Lupton constants.....104

Table 3.2 λ_{max} and ε_{max} of **3.III-3.VII**.....105

Table 3.3 λ_{max} and ε_{max} of **3.VI-3XI** in MeOH 108

Table 3.4 Chemical shifts for ^{13}C methine atoms for **3.1-3.4** (CD_3CN) and **3.I'-3.IV'** ($CDCl_3$) 112

Table 3.5 Electrochemical potentials versus ferrocenium / ferrocene for **3.1-3.4** in THF / 0.1 M $^{n}Bu_4NPF_6$ 111

Table 3.6 λ_{max}, ε_{max}, M_{ge}, and the $Re(\gamma)_{calc}$ of polymethine dyes in DMSO solution..... 116

Table 3.7 $Re(\gamma)$, $Im(\gamma)$, $|\gamma|$, Φ, and the $Re(\gamma)_{static}$ of Dioxaborine-Terminated Polymethine Dyes 123

Table 3.8 Electrochemical potentials versus ferrocenium / ferrocene for **3.5'**, **3.6'**, and **3.7'** in THF / 0.1 M $^{n}Bu_4NPF_6$ 126

Table 3.9 λ_{max}, ε_{max}, M_{ge}, and the $Re(\gamma)_{static}$ of polymethine dyes in DMSO solution ... .127

Table 3.10 $Re(\gamma)$, $Im(\gamma)$, $|\gamma|$, Φ, and the $Re(\gamma)_{static}$ of Indole-Terminated Polymethine Dyes 128

Table 4.1 λ_{max}, ε_{max}, M_{ge}, and the $Re(\gamma)_{static}$ of **4.1-4.7** in DMSO solution 158

Table 4.2 $Re(\gamma)$, $Im(\gamma)$, $|\gamma|$, Φ, and the $Re(\gamma)_{static}$ of **1-7** 159

Table 4.3 λ_{max}, ε_{max}, M_{ge}, and the $Re(\gamma)_{static}$ of TCF-terminated polymethine dyes in DMSO solution 164

Table 4.4 $Re(\gamma)$, $Im(\gamma)$, $|\gamma|$, Φ, and the $Re(\gamma)_{static}$ of TCF- terminated polymethine dyes 165

Table 5.1 N_{extra} of terminal groups for **5.I-5.VI** 183

Table 5.2 λ_{max}, ε_{max}, M_{ge}, and the $Re(\gamma)_{calc}$ of chalcogenopyrylium terminated polymethine dyes in $CHCl_3$ solution.....193

Table 5.3 $Re(\gamma)$, $Im(\gamma)$, $|\gamma|$, Φ, and the $Re(\gamma)_{calc}$ of chalcogenopyrylium terminated polymethine dyes 198

LIST OF FIGURES

Figure 1.1 Typical transmission channel in optical communications 4

Figure 1.2 Typical dispersion curve of Im $\chi^{(1)}$ (top left), Re $\chi^{(1)}$ (bottom left), Im $\chi^{(3)}$ (top right) and Re $\chi^{(3)}$ (bottom right).....9

Figure 1.3 A waveguide (Si, n = ~3.5) on glass (SiO_2, n = ~1.5) is coated with an organic film (n = ~1.7)..... 12

Figure 1.4 A schematic of a Mach-Zehnder interferometer. 13

Figure 1.5 Schematic of a ring resonator used to a) multiplex b) demultiplex signals 14

Figure 1.6 Transmission spectra of a resonator with two different indices 13

Figure 1.7 Part A and B show the respective A and B phases of *trans*-polyacetlyne, part C represents the presence of a soliton (a defect between the A and B phases) in *trans*-polyacetlyene, part D and E show the *cis-transoid* and the *trans-cisoid* conformers of polyacetylene respectively, and parts F and G show the phases of polythiophene.. 24

Figure 1.8 Energy diagrams for A) pure polyacetlyene with excitation $h\upsilon_I$, B) a soliton band diagram showing mid-gap transitions $h\upsilon_s$, and C) sub-mid gap transitions ($h\upsilon_1$ and $h\upsilon_2$) for a bipolaron 26

Figure 1.9 Synthetic scheme to perform ROMP on COT and COD co-monomers (top) and R-COT monomors (bottom) with the initiator shown.....28

Figure 1.10 Structure of polydiacetylenes, PDA-PTS and PDA-n_2-BCMU. 26

Figure 1.11 Energy leve diagram of a four state system in which photon energy can be used that is close to the 1PA resonances, but falls between the two 2PA levels, avoiding absorption 30

Figure 1.12 A) The NVB (left) and CT (right) resonance structures. B) The representative structure resulting from the equal mixing of the NVB and CT resonance structures. 32

Figure 1.13 Potential energy surfaces of the NVB (dotted, left) and CT (dotted, right) resonance forms accompanied by the ground state and exited state potential energy surface after mixing the two resonance forms (solid lines)

plotted against the BLA coordinate q for various energy differences (V_0): A) $V_0 < 0$, B) $V_0 = 0$, C) $V_0 > 0$ 34

Figure 1.14 Plots of α, β and γ versus V_0. Trends of α (dash-dot line), β (dashed line), and γ (solid line) as a function of $-V_0$ calculated using the VB–CT model for the model DA molecule $(CH_3)_2N$-(CH = CH)$_4$-CHO 35

Figure 1.15 Symmetric polymethine systems studied for symmetry breaking properties in the literature 43

Figure 2.1 D-π-A chromophores in the literature.....54

Figure 2.2 Chromophores, **2.IV-2.VII**, found in the literature 55

Figure 2.3 Bis(dioxaborine) terminated trimethine dyes from the literature 56

Figure 2.4 Bis(dioxaborine)-terminated nonamethine, **2.XVI**, from the literature.....58

Figure 2.5 Bis(dioxaborine)-terminated dyes discussed in Section 2.3 60

Figure 2.6 Bis(dioxaborine)-terminated dyes discussed in Section 2.3 61

Figure 2.7 Linear absorption spectra of **2.XVI**[21], **2.1**, and **2.2** on a glass substrate....62

Figure 2.8 Variable temperature ^{1}H NMR spectrum of dye **2.5** in $CDCl_3$. A) 243 K. B) 294 K. C) 333 K.....67

Figure 2.9 Possible origins for rotational isomers A and B in bis(dioxaborine) polymethines 68

Figure 2.10 ROESY experiment at 333 K on **2.3**.....69

Figure 2.11 Absorption spectra of **2.3** (—), **2.4** (----), and **2.5** (-·-·-) in DMSO 72

Figure 2.12 Absorption spectra of **2.6** (—), **2.7** (----), and **2.8** (-·-·-) in DMSO 73

Figure 2.13 HOMO (bottom) and LUMO (top) orbital diagrams of **2.3-2.8** 76-77

Figure 2.14 Transition atomic densities and transition dipole moment vectors for **2.3** (top) and **2.5** (below) calculated using INDO-CIS 77

Figure 2.15 Bis(dioxaborine) terminated heptamethine for which *γ* was measured 78

Figure 2.16 Non-degenerate 2PA (ND-2PA) spectra for **2.4** (A), **2.XVI**[21] (B) and **2.9** (C) all in DMSO. The degenerate 2PA (D-2PA) cross-sections determined

from Z-scan measurements are shown as well. The linear absorption spectra for all the dyes are shown in grey.....82

Figure 3.1 Two major contributing resonance structures of $^{+}$BDMP (A, top) and a simple anionic pentamethine (B, top). The ground state structure of $^{+}$BDMP (A, bottom) and the simple anionic pentamethine (B, bottom) are also shown.....98

Figure 3.2 $^{+}$BDMP shown as an odd-alternant system with the α, β, and γ positions shown.....98

Figure 3.3 Orbital energies of even- and odd-alternant hydrocarbons. The arrows represent electrons. A) even-alternant hydrocarbon (*e.g.* polyene), B) a cationic odd-alternate hydrocarbon (*e.g.* cationic polymethine), and C) an anionic odd-alternate hydrocarbon (*e.g.* anionic polymethine).....99

Figure 3.4 Coefficients of the HOMO and LUMO of $^{+}$BDMP.....100

Figure 3.5 Five resonance structures substantially contributing the ground state to $^{+}$BDMP.....101

Figure 3.6 The π-electron densities for the ground and first excited state of $^{+}$BDMP 102

Figure 3.7 Effects upon the orbital energies due to electron withdrawing and electron donating substituents in the γ position of parent dye, $^{+}$BDMP.....103

Figure 3.8 Possible resonance form for the strong π-electron donating substituent of **3.IV**.....106

Figure 3.9 The σ-EW and π-ED effects on the HOMO and LUMO levels due to a substituent on a methine with a large LUMO coefficient. The weak interaction of the π-ED is insufficient to counter the stabilization effects of the σ-EW, so a bathochromic shift is observed.....107

Figure 3.10 Dioxaborine-terminated dyes, **3.1-3.4**, investigated in this study.....109

Figure 3.11 Vinamidinium building blocks to synthesize the polymethine dyes in this study.....110

Figure 3.12 Indole-terminated pentamethine dyes for which the ^{13}C NMR chemical shifts were determined.....111

Figure 3.13 HSQC spectrum (^{1}H NMR on the x-axis with a ^{13}C NMR on the y-axis) of **3.1** in CD_3CN.....112

Figure 3.14 The ^{13}C NMR chemical shifts of the α (A), β (B), and γ (C) methine carbons of **3.1-3.4** and analogous dyes **3.I'-3.IV'** from the literature 114

Figure 3.15 Structure of **3.3'** and **3.4'**.....116

Figure 3.16 Absorption spectra of **3.1** (—), **3.2** (----), **3.3** (-·-·-), and **3.4** (···) in DMSO 117

Figure 3.17 The energy diagram displays the σ-EW and π-ED effects on the HOMO and LUMO levels of the dye due to a Cl substituent on a methine with a large HOMO coefficient. The molecular orbitals of the substituent and the dye have relatively good energy matching leading to strong π-electron interactions.....118

Figure 3.18 Absorption spectra of **3.3** (—) and **3.3'** (----) in DMSO.....119

Figure 3.19 An asymmetric *tris*-terminal polymethine dye with one side of the dye being composed of one endgroup (TG1) and one side being composed of a combination of two endgroups (TG2+TG3=TG2').....120

Figure 3.20 Absorption spectra of **3.4** (—) and **3.4'** (----) in DMSO.....121

Figure 3.21 A possible resonance form of **3.3**, which could contribute to the loss of typical polymethine-like character.....123

Figure 3.22 The structure of the commercial dye HITCI (**3.7'**).....124

Figure 3.23 Absorption spectra of **3.5'** (—), **3.6'** (----) and **3.7'** (-·-·-) in DMSO.....127

Figure 4.1 Two resonance forms of A) the anion of 1,3 indandione and B) the anion of 2,2'-(1H-indene-1,3(2*H*)-diylidene)dimalononitrile.....140

Figure 4.2 Symmetric 1, 3-indandione terminated polymethine dye shown with two extreme resonance structures (top) and the ground state structure.....141

Figure 4.3 Common acceptor groups found in the literature and used in this study.142

Figure 4.4 Donor-acceptor materials using terminal groups relevant to this study ..143

Figure 4.5 Polymethine dyes with terminal groups formed from **S4.4**.....144

Figure 4.6 **S4.1-S4.3** terminated polymethine dyes for which the third-order nonlinear optical properties have been measured by Dr. Joel Hales 145

Figure 4.7 **S4.4** terminated polymethine dyes for which the third-order nonlinear optical properties have been measured 145

Figure 4.8 Starting materials **S4.5-S4.9** used as cyanine bridge precursors 146

Figure 4.9 Aromatic region of the ^{1}H NMR of **4.1** at 243 K (top) and 213 K (bottom) in dichloromethane.....149

Figure 4.10 Possible conformational isomers of **4.1** 150

Figure 4.11 ^{13}C NMR spectra of **4.1** at 298 K (top) and 333 K (bottom) in $CDCl_3$ ...150

Figure 4.12 Multiple sets of peaks can be observed in the aromatic region of the ^{1}H NMR spectrum of **4.2** at 213 K in dichloromethane.....151

Figure 4.13 ^{13}C NMR spectra in $(CD_3)_2SO$ of A) **4.8** and B) **4.9** 152

Figure 4.14 . HSQC NMR spectrum (^{1}H NMR on the X-axis, ^{13}C DEPT135 on the Y-axis) in $(CD_3)_2SO$ of **4.9** 153

Figure 4.15 ^{13}C NMR spectrum of **4.10** in $CDCl_3$ 154

Figure 4.16 Absorption spectra in DMSO solution of **4.1-4.3** 155

Figure 4.17 Absorption spectra in DMSO solution of **4.4** and **4.5**.....156

Figure 4.18 Absorption spectra in DMSO solution of **4.6** and **4.7**.....157

Figure 4.19a Absorption spectra of **4.8** (—), **4.9** (----),, and **4.10** (-·-·-) in DMSO 160

Figure 4.19b Absorption spectra of **4.10** (—), **4.11** (----),, and **4.12** (-·-·-) in DMSO ..161

Figure 4.20 Possible ground state structures of **4.10** (left) and **4.13** (right) with different charge delocalization.....162

Figure 4.21 Benzothiazole terminated dyes from the literature 163

Figure 5.1 Polymethine dyes from the literature.....182

Figure 5.2 Plot of E_{ge} versus N_{π} for representative systems with the dioxaborine terminal units. The solid lines represent fittings to the experimental values from which k and N_{extra} were determined.....183

Figure 5.3 Plots of (a) E_{ge} versus L_{eff}^{-1} and (b) M_{ge} versus L_{eff} for polymethines with various terminal groups.....184

Figure 5.4 Chalcogenopyrylium general structure studied by Detty *et al*.....186

Figure 5.5 Polymethine dyes, which had γ values measured 187

Figure 5.6 Chalcogenopyrylium-terminated dyes, **5.1-5.6**, discussed in this study. The starred positions identify the carbons (and hydrogens attached to them) that consistently did not appear in the room temperature ^{1}H and ^{13}C NMR spectra 189

Figure 5.7 The aromatic region of the ^{1}H NMR spectra of **5.2** in $CDCl_3$ at A) 295 K and B) 333 K.....192

Figure 5.8 The aromatic region of the ^{13}C NMR spectra of **5.6** in $CDCl_3$ at A) 295 K and B) 333 K.....192

Figure 5.9 Absorption spectra of **5.1** (—), **5.2** (----), and **5.3** (-·-·-) in chloroform...194

Figure 5.10 Absorption spectra of **5.2** (—), **5.4** (----), and **5.5** (-·-·-) in chloroform...195

Figure 5.11 Absorption spectra of **5.3** (—) and **5.6** (----) in chloroform 196

Figure 5.12 Non-degenerate 2PA (ND-2PA) spectra in chloroform: (a) **5.1**, (b) **5.2**, (c) **5.3**, and (d) **5.XI**. Different pump wavelengths (shown in legend) were employed to observe the full ND-2PA spectra. Filled circles are degenerate 2PA (D-2PA) cross-sections derived from femtosecond-pulsed Z-scan measurements. 1 GM is defined as 1×10^{-50} cm^4 s $photon^{-1}$. Experimental uncertainties in the values were estimated to be ±15%. Linear absorption spectra are shown as references.....200

Figure 6.1 General structure of a polymethine dye with tunable positions.....216

Figure 6.2 Possible positions to decorate a polymethine dye with dendritic substituents.....222

Figure 6.3 Scheme to form an encapsulated polymethine dye.....223

Figure 6.4 A representation of a random copolymer with a polymethine sidegroup intended to provide third-order nonlinearity and a bulky substituent intended to provide steric bulk.....224

LIST OF SCHEMES

Scheme 2.1 Mechanism for the synthesis of a general 2,2-difluoro-1,3,2-dioxaborine.52

Scheme 2.2 Reaction schemes of 1,3-dicarbonyl (top) and 2,2-difluoro-1,3,2-dioxaborine (bottom) with an aldehyde derivative.. 53

Scheme 2.3 Reaction scheme used to synthesize **2.1** and **2.2** 63

Scheme 2.4 Synthesis of bis(dioxaborine) pentamethines, **2.3**-**2.8** 66

Scheme 2.5 Synthesis of bis(dioxaborine) nonamethine, **2.9**.....66

Scheme 3.1 Preparation of **3.2** and **3.3** 110

Scheme 3.2 Metathesis reaction to prepare **3.1** and **3.4** 110

Scheme 3.3 The synthesis of **3.5'** and **3.6'** 125

Scheme 4.1 Exemplary synthetic scheme for **4.5**.....147

Scheme 4.2 Exemplary synthetic scheme for **4.9** and **4.10** 148

Scheme 5.1 Scheme for the synthesis of **S.8, S5.9** and **S5.10**.....190

Scheme 5.2 Synthetic scheme for dyes **5.2, 5.3, 5.4,** and **5.5**.....191

LIST OF ABBREVIATIONS

1PA – One-Photon Absorption
2PA – Two-Photon Absorption
AOS – All-Optical Switching
AOSP – All-Optical Signal Processing
BDMA – Bis(dimethylamino) Methine Dyes
BLA – Bond Length Alternation
BOA – Bond Order Alternation
BT – Benzothiazole
CARS – Coherent Anti-Stokes Raman Scattering
COT – Cyclooctatetraene
CT – Charge Transfer
DFWM – Degenerate Four Wave Mixing
DMSO – Dimethylsulfoxide
EDG – Electron Donating Group
EFISH – Electronic Field Induced Second Harmonic
EWG – Electron Withdrawing Group
FOM – Figure of Merit
HOMO – Highest Occupied Molecular Orbital
HSQC – Heteronuclear Single Quantum Correlation
LUMO – Lowest Unoccupied Molecular Orbital
MKS – Meters-Kilograms-Seconds
MZI – Mach-Zehnder Interferometer
NOE – Nuclear Overhauser Effect
NLO – Nonlinear Optical
NMR – Nuclear Magnetic Resonance
PDA – Polydiacetylene
PPV – Polyphenylenevinylene
$Re(\gamma)_{static}$ – The Static (zero frequency, infinite wavlength) Third-Order Polarizability
REMZ – Resonator Enhanced Mach-Zehnder
ROESY – Rotating-Frame Overhauser Effect Spectroscopy
ROMP – Ring Opening Metathesis Polymerization
SOH – Silicon Organic Hybrid
TCF – Tricyanofuran, 4,5,5-trimethyl-3-cyano-2(5H)-furanylidenepropanedinitrile
TG – Terminal Group
THG – Third Harmonic Generation
TIR – Total Internal Reflection
UV-vis.-NIR – Ultraviolet-Visible-Near Infrared
NVB – Neutral Valence Bond
WDDM – Wavelength Division Demultiplexing
WDM – Wavelength Division Multiplexing

LIST OF SYMBOLS

Symbol	Meaning
	Chapter 1
E	Electric field
$\mu_{induced}$	Induced dipole
α	First-order polarizability
β	Second-order polarizability
γ	Third-order polarizability
$P_{induced}$	Induced polarization
$\chi^{(n)}$	n-order susceptibility
ω	Angular frequency
N	Number density
L	Local field factor
n_0	Refractive index
n_{total}	Total refractive index
n_2	Nonlinear refractive index
α_L	Linear absorption
β_I	Nonlinear absorption
ε_0	Electric permittivity in free space
c	Speed of light
I	Intensity
$\Delta\varphi$	Phase shift
W	One-photon figure of merit
T	Two-photon figure of merit
λ_f	Fundamental wavelength
V	Potential energy
q	Bond length alternation coordinate
E_{CT}	Energy of charge transfer state
E_{VB}	Energy of the valence bond state
M	Transition dipole moment
g	Ground state
e	Excited state
e'	High lying excited state

Chapter 2-6

λ	Wavelength
δ	Two-photon absorption cross section
ε	Extinction coefficient
M_{ge}	Transition dipole moment (g to e)
$\mathrm{Re}(\gamma)$	Real part of γ
$\mathrm{Im}(\gamma)$	Imaginary part of γ
Φ	phase
$E_{1/2}$	redox potential
$\mathrm{Re}(\gamma)_{static}$	static γ (at zero frequency) (calculated)
E_{ge}	Transition energy

SUMMARY

Material development is necessary before all-optical signal processing (AOSP) can be realized. Traditional AOSP will require materials with a large magnitude of the real part of the third-order polarizability, while having a small imaginary magnitude of third-order polarizability. The aim of this thesis is to investigate the potential for polymethine dyes to be used for AOSP applications. The basic structure of a polymethine dye was synthetically modified in a variety of positions to observe the effects upon the linear and nonlinear optical properties. The modifications included variation in the terminal group, substituents in the polymethine bridge, and exchange of the counterion. The dyes were generally synthesized using the Vilsmeyer-Haack reaction to form simple polymethine precursors, and then complexity was added by performing the Knoevenagel condensation with various acceptors and the polymethine precursor. Ion metathesis was often employed to exchange the initial counterion for a counterion that provided increased solubility in common organic solvents. The third-order nonlinear optical polarizabilities were characterized by Dr. Joel Hales who used the open- and closed-aperture Z-scan technique at 1300 nm and non-degenerate two-photon absorption experiments to identify the position of the two-photon absorption bands.

Chapter 1

Introduction

1. Introduction

The research presented in this thesis is concerned with the design and synthesis of organic polymethine dyes with the goal of optimization of specific nonlinear optical and material properties, which may be useful for the specific application of all-optical signal processing (AOSP). The materials reported in the main chapters (2-5) of this thesis have been developed with the intention to eventually identify materials that could be incorporated in devices designed to perform AOSP. Several of such devices are described in the following introductory chapter; however, the work presented in this thesis was not intended to determine, nor does it explain, how to optimize the devices. While demonstrations of moderately successful devices have been reported in the literature, the specific materials presented in the main chapters of this thesis have not been tested in devices.

This introductory chapter surveys several classes of materials, which the nonlinear optical properties of interest have been investigated and reported in the literature. A wide variety of materials display promising properties that could possibly fulfill requirements for AOSP, which range from inorganic materials such as glass or silicon to both small and large organic materials. The focus of the review of materials is directed toward organic small molecules, because the research reported in the main body chapters of this thesis specifically involves organic dyes.

The telecommunications industry (which signal processing is a primary concern) may be the greatest foreseeable benefactor from the development of these materials for AOSP applications. This thesis begins with a brief description of telecommunications networks, with the intention to provide a framework that will explain where the materials described in the main body of the thesis could be useful. It also provides reasons why certain nonlinear optical properties need to be optimized at wavelengths of 1300-1600 nm, the range of usable telecommunications wavelengths.

1.1. Introduction to Telecommunications and Optical Signal Processing

The telecommunications industry was well established by 1980, by which time optical fibers were being used to transmit information impressed upon optical signals over long distances.[1] Currently, communications in the optical domain (using silica fibers) are generally the best choice for long-distance communications. However, the ever-increasing need for higher rates of information transfer, or equivalently greater bandwidths, may require optical communication to further encroach upon areas electronic communication once dominated, that is, signal processing. Moreover, all-optical technology could have advantages over all-electronic or optical-electronic technology in computing as well.

There are three hardware options to consider for signal processing in telecommunications and computing: all-electronic, hybrid electronic-optical, and all-optical. Each of these options has potential advantages, but they each also have problems associated with them, which must be overcome to improve information processing performance. All-electronic systems have long standing precedence; however, such systems are not ideally-suited for interconnections between devices due to the growing

demands on information bandwidth. Replacement of the electrical interconnections with electro-optic ones would lead to a hybrid device. This is the most likely area for ultrafast (< 1 picosecond) modulators to be inserted into a system: places where a large amount of processing bandwidth is required in a small space.[2] Two potential applications could be interconnections for microprocessor data busses or the backplane of server racks.[2] Microprocessor data busses connect the microprocessor to other components or microprocessors, while the backplanes of server racks interconnect computers dedicated as network servers to other server computers. The integration of optical interconnects in an otherwise electronically dominated system leading to the formation of a hybrid electro-optical system would require suitable interfaces. For example, processing and routing of information would require optical signals to be converted from the optical domain to the electrical domain, processed in the electrical domain, then converted back to the optical domain. An all-optical network would allow information to be transmitted entirely in the optical domain. Signals would remain in the optical domain throughout the entire transmission process, thus increasing the rate of information transfer by eliminating the time-consuming optical to electronic to optical (OEO) conversion steps. However, currently there is a lack of suitable materials to make all-optical networks.

The general components in an optical system to transfer information consist of three parts: a transmitter, a transmission path, and a receiver (Figure 1.1). The transmitter can be broken down further into three parts: an optical source, an input signal, and a modulator. The transmission pathway, or waveguide (the material through which light is guided), in telecommunications is currently comprised of high purity silica fibers.

An outer covering, or cladding, is a material of low refractive index, that surrounds the high index silica fiber. According to Snell's law[3] a range of angles can be found at which the light propagating through the fiber is completely reflected back into the fiber after the light encounters the interface between the fiber and the cladding, which leads to total internal reflection (TIR), thus guiding the light along the fiber. The material of choice in optical communications, high purity silica, has several minima in its attenuation (absorption and scattering) spectra within the range of 1300-1600 nm, which has defined the so-called telecommunications band. Finally the receiver in the transmission channel can be broken down into the optical detector, the demodulator and the output signal.

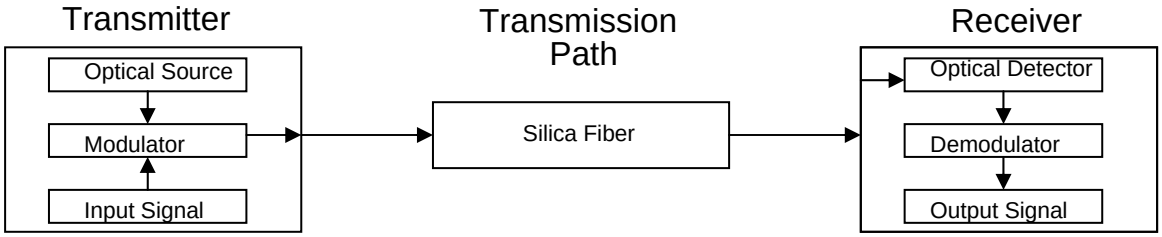

Figure 1.1. Typical transmission channel in optical communications.

The bottleneck in the growing demand for larger bandwidths occurs at the transmitter. First-generation technology in telecommunications relied upon the direct modulation of the laser, where the laser is the optical source and the modulator. This method was able to achieve bandwidths of 1-3 Gbit/s. Signal generation (laser) and modulation can be accomplished with two separate devices to improve the possible bandwidth. The development of optical components, specifically modulators and routers fabricated from $LiNiO_3$ resulted in the development of subsequent generations of long-

distance telecommunications technology.[4] The success of external modulators in telecommunications and the need for greater interconnect speeds for digital computing has led to research in hybrid electronic-optical systems and all-optical systems.

Many of the current devices in hybrid electronic-optical and all-optical systems require nonlinear optical materials. Specifically, all-optical devices require materials with a large third-order optical nonlinearity. The remainder of this chapter will focus upon: an introduction to third-order nonlinear optics (Section 1.2); material property requirements for third-order materials for all-optical signal processing (AOSP) (1.3); a survey of selected nonlinear optical modulators (1.4); selected demonstrations of devices for signal processing (1.5); and finally organic materials to be used as $\chi^{(3)}$ materials (1.6).

1.2. Third-Order Nonlinear Optics

Exposing molecules to electric fields (E) can induce a dipole moment (μ_{induced}). Moderate electric field intensities will induce a dipole moment of a magnitude that is essentially linearly dependent upon the field intensity. Sufficiently large electric fields can induce a nonlinear response in the molecule, giving rise the second- and third-order nonlinearities. More generally the μ_{induced} can be expressed as a power series

$$\mu_{induced} = \alpha E + \beta E^2 + \gamma E^3 + \ldots \qquad \text{E1.1}$$

in which α, β and γ are the first-, second-, and third-order polarizabilities respectively.

The polarization of the bulk material can be expressed in an analogous equation:

$$P_{induced} = \chi^{(1)} E + \chi^{(2)} E^2 + \chi^{(3)} E^3 + \ldots \qquad \text{E1.2}$$

where P is the polarization, and $\chi^{(1)}$, $\chi^{(2)}$ and $\chi^{(3)}$ are the first-order (linear), second-order, and third-order nonlinear susceptibilities in that order.

It is important to note that a second-order nonlinear optical process, known as the Pockels effect, is related to β and $\chi^{(2)}$ and is used in the operation of electro-optic devices. A static electric field is applied across the material (the electro component) to cause a polarization, while light is a signal carrying information (the optic component) passing through the material. The Pockels effect results in a polarization of a material that responds quadratically to the amplitude of an incident electric field.

Several third-order nonlinear optical processes are important for further discussion. These various processes are identified by the fields that result (which possess the modified frequency ω_σ, see below) following interaction of the initial incident fields with the nonlinear medium. The initial frequencies, corresponding to the electric fields from E1.1, are labeled as ω_1, ω_2, and ω_3. The output frequency of the resulting field based upon energy conversion can therefore be written according to the following equation:

$$\omega_\sigma = \pm\omega_1 \pm \omega_2 \pm \omega_3 \qquad \text{E1.3}$$

Two phenomena are third harmonic generation and the intensity dependent refractive index. For example third harmonic generation (THG) mixes the three degenerate initial frequencies (ω_1, ω_2, $\omega_3 = \omega$) to generate a field with a new frequency three times that of the original frequencies (3ω). The oscillating optical frequency polarization operating at the third harmonic only allows high frequency motions (the distortion of the electron cloud) to respond in the material. Therefore, the value of $\chi^{(3)}$ (-3ω; ω_1, ω_2, ω_3) associated with THG is only composed of contributions from the redistribution of the electron cloud, which makes it useful to characterize fast electronic

nonlinearities. In-depth discussions of the processes and techniques used to characterize the processes can be found elsewhere.[5, 6]

The intensity dependent refractive index is the paramount nonlinear optical process for optical signal processing. The modified frequency term, ω_σ, from the nonlinear polarization is driven at the same frequency as the incident electric field (ω_1, -ω_2, $\omega_3 = \omega$). The $\chi^{(3)}(-\omega; \omega, -\omega, \omega)$ term associated with the nonlinear refractive index is analogous to linear optical phenomena associated with $\chi^{(1)}$. This relationship will be explored further in the remainder of this section.

The microscopic contribution of the third-order polarizability (γ), introduced in E1.1, is related to the macroscopic susceptibility ($\chi^{(3)}$) through the following equation:

$$\chi^{(3)} = NL(\omega_{1,2,3})^4 \gamma \qquad \text{E1.4}$$

where N is the number density (number of molecules per unit volume), ω is the angular frequency of the incident fields, and L is the local field factor.[6] The local field experienced by the microscopic species is related to the macroscopic field through the local field factor. The local field factor is a correction factor introduced by Lorentz[7], and it is often approximated as the following:

$$L(\omega_{1,2,3}) = \frac{n(\omega_{1,2,3})^2 + 2}{3} \qquad \text{E1.5}$$

where n is the refractive index of the medium at the frequency ω.

Polarizabilities, susceptibilities and refractive index are complex values, which can be separated into the real and imaginary components. The real part of the susceptibility ($\mathrm{Re}\chi^{(n)}$, where n is an integer) is related to linear or nonlinear refractive indices (depending on the order of the susceptibility). Electric fields (such as the oscillating electric field associated with light) cause weakly bound electrons (such as π-

electrons of organic molecules) to undergo a shift in electron density. The imaginary part of the susceptibilities ($\mathrm{Im}\chi^{(n)}$) indicate there is an exchange of energy between the medium and the field. A positive imaginary susceptibility ($\mathrm{Im}\chi^{(n)}$ is greater than zero) indicates the medium has absorbed some of the of the energy of the field, while negative imaginary susceptibilities ($\mathrm{Im}\chi^{(n)}$ is less than zero) indicate the opposite (the medium has transferred energy to the field). Cases in which there is a gain in the electric field ($\mathrm{Im}\chi^{(n)}$ is less than zero) occur less often than the absorption of the field. Generally the medium must first be energized by external sources for this to occur.[6] When considering the first-order susceptibility, $\chi^{(1)}$: $\mathrm{Re}\chi^{(1)}$ is related to the linear refractive index (n_0) and $\mathrm{Im}\chi^{(1)}$ is related to the linear absorption coefficient, α_L. Note that α_L is not the first-order polarizability α in E1.1; however, they are related. Highly intense pulses of light can cause a nonlinear change in the refractive index, n_2, related to $\mathrm{Re}\chi^{(3)}$. $\mathrm{Im}\chi^{(3)}$ is related to nonlinear absorption, specifically the two photon absorption (2PA) coefficient, β_I. The following two equations can be used to express the total refractive index and the total absorption of a material subjected to high intensity light:

$$n_{total}(\lambda) = n_0(\lambda) + n_2(\lambda)I \qquad \text{E1.6}$$

$$\alpha_{total}(\lambda) = \alpha_L(\lambda) + \beta_I(\lambda)I \qquad \text{E1.7}$$

It is important to note that all factors have wavelength dependence.

Figure 1.2 shows the dispersion of the real and imaginary parts of $\chi^{(1)}$ and $\chi^{(3)}$ as a function of the frequency of incident radiation.[6] A peak in the magnitude of $\mathrm{Im}(\chi^{(1)})$ occurs where there is one photon absorption, in this case at ω_0. The magnitude of $\mathrm{Re}(\chi^{(1)})$ increases as $\omega \rightarrow \omega_0$, resulting in a larger refractive index, which is known as resonance enhancement. The spectral regions where $\mathrm{Re}(\chi^{(1)})$ increases with frequency ($d\mathrm{Re}(\chi^{(1)})/d\omega$

is greater than 0) is said to be normal dispersion. Anomalous dispersion occurs where $\mathrm{Re}(\chi^{(1)})$ decreases with increasing frequency ($d\mathrm{Re}(\chi^{(1)})/d\omega$ is less than 0). The $\mathrm{Re}(\chi^{(1)})$ passes through zero at ω_0, where $\mathrm{Im}(\chi^{(1)})$ is at a maximum. $\chi^{(3)}$ shows similar behavior to $\chi^{(1)}$ however, additional multi-photon resonances can exist.

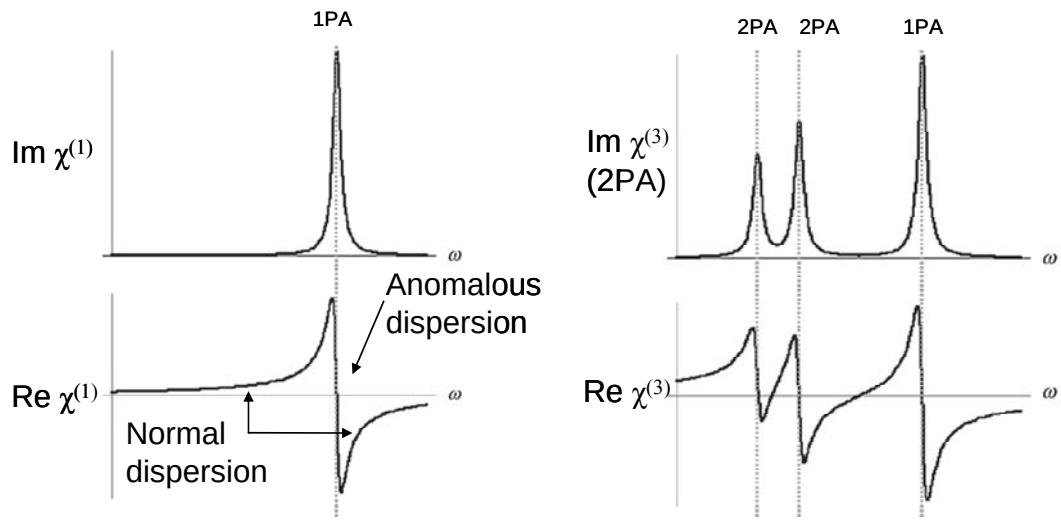

Figure 1.2. Typical dispersion curve of Im $\chi^{(1)}$ (top left), Re $\chi^{(1)}$ (bottom left), Im $\chi^{(3)}$ (top right) and Re $\chi^{(3)}$ (bottom right). Reproduced with permission.[6]

The intensity-dependent changes in refractive index, also known as the optical Kerr effect, can cause self-focusing and self-defocusing. n_2 can be related to the $\mathrm{Re}(\chi^{(3)})$ using E1.8, while β_I is related to $\mathrm{Im}(\chi^{(3)})$ using E1.9:

$$n_2 = \frac{3}{4\varepsilon_0 n_0(\omega)^2 c}\mathrm{Re}[\chi^{(3)}(-\omega;\omega,-\omega,\omega)] \qquad \text{E1.8}$$

$$\beta_I = \frac{3\omega}{2\varepsilon_0 n_0(\omega)^2 c^2}\mathrm{Im}[\chi^{(3)}(-\omega;\omega,-\omega,\omega)] \qquad \text{E1.9}$$

where ε_0 is the electronic permittivity in free space and c is the speed of light.

Self focusing and defocusing occur because a beam from a laser source is generally not uniform. A Gaussian beam has greater intensity at the center than at the

periphery, which leads to larger magnitudes of Δn at the center. If n_2 is positive, then according to E1.6 the n_{induced} in the medium will increase and self focusing will occur due to light at the center of the beam moving slower than light at the periphery. If n_2 is negative, then according to E1.6 the n_{induced} in the medium will be lower, so self defocusing will occur due to light at the center of the beam moving more quickly than light at the periphery. From a material property standpoint for AOSP applications, to a first approximation, it is not important if the material is self-focusing or defocusing.

1.3. A Brief Introduction to Selected Nonlinear Optical Modulators

A large number of devices exist with the purpose of modulating optical signals. The properties of light can be modulated to result in a change in frequency, amplitude and/or phase. The prime method for modulation in telecommunications involves a device that modulates the phase of the light and can, with the introduction of an additional polarization element, lead to a modulation in intensity. Nonlinear optical devices generally rely upon changes in the nonlinear refractive index of materials.

A waveguide is generally fabricated from a high index of refraction material such as silicon (Si) (n = 3.5). A waveguide is often situated on a substrate of low index of refraction, such as glass (SiO_2) (n = 1.5). The outer covering of the waveguide is of low index of refraction, for example air (n = ~1) or organic materials (n = ~1.6-1.8) can be used. Figure 1.3 shows the refractive index profile of a general waveguide. As mentioned in section 1, Snell's law can be used to determine the incident input angles necessary to achieve total internal reflection (TIR). Figure 1.4 shows a ray, with TIR, propagating through the waveguide. A mode describes a well-defined field pattern that remains unchanged as the wave propagates.

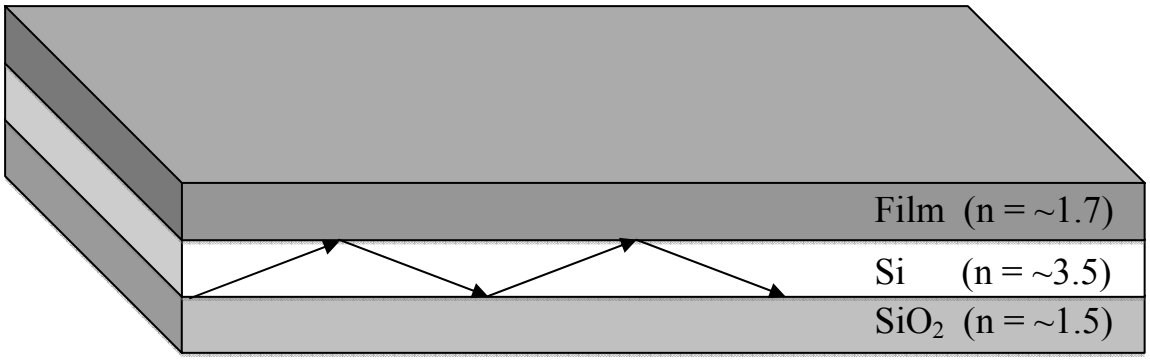

Figure 1.3. A waveguide (Si, n = ~3.5) on glass (SiO_2, n = ~1.5) is coated with an organic film (n = ~1.7).

A typical device used to modulate the phase of light is a Mach-Zehnder interferometer (MZI) (Figure 1.4). Input pulses are split into two waveguides by a Y-junction, typically a 3 dB coupler[8] is used to distribute equal light intensity into both arms of the MZI. The two waves are guided along the separate arms until they are recombined at a second Y-junction. If the optical path lengths differ by an integral number of optical wavelengths (even integer multiple of π), then the two waves will recombine at the second Y-junction in-phase, resulting in constructive interference. If the optical path lengths differ by half the optical wavelength (odd integer multiple of π), then the two waves will recombine at the second Y-junction out of phase, resulting in destructive interference.

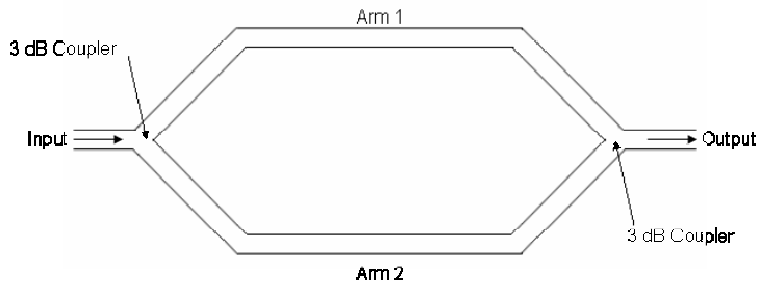

Figure 1.4. A schematic of a Mach-Zehnder interferometer.

Modifications to the MZI can be made to allow the degree of interference to be controlled. For example, increasing the refractive index of the material used in arm 1 will slow the speed of guided light in arm 1 relative to arm 2 and effectively result in a change in relative phase between the two waves. Appropriate changes in this phase can lead to constructive or destructive interference, which can be detected as changes in the output intensity.

A second modulator of great popularity is the ring resonator.[9] In such a device a straight waveguide is placed within close proximity to a ring waveguide. Some of the optical power of a mode exists outside of the waveguide, decreasing exponentially with distance from the guide, which is known as an evanescent wave. Close proximity of the waveguide and resonator allows light to couple between the two components through interaction of the evanescent wave. The strongest coupling occurs when the incident wavelength, λ_0, satisfies the following equation:

$$\frac{n_{eff} L}{\lambda_0} = m \qquad \text{E1.10}$$

where m is an integer, L is the circumference of the ring and n_{eff} is the effective refractive index of the ring. In other words, wavelengths that satisfy this relationship are coupled strongly into the ring.[9]

This coupling of specific wavelengths of light can be useful for routing or signal processing. Figure 1.5 shows an application of wavelength division multiplexing (WDM) on the left and demultiplexing (WDDM) on the right. WDM allows several discrete wavelengths, each individually encoded with information, to be effectively combined prior to traveling within a single waveguide, while WDDM takes signals on different wavelengths and separates the signals onto different waveguides. A device can be set up where two parallel waveguides are separated by a ring resonator (see Figure 1.5). This device can allow multiplexing of signals allowing an input wavelength (λ_1) on waveguide 1 to be combined with a second input wavelength (λ_2) from waveguide 2. Only λ_2 is in resonance with the ring, so it will couple into the ring from waveguide 2 and combine with λ_1 on waveguide 1. WDDM is the reverse scenario, where λ_1 and λ_2 are input on waveguide 1. λ_1 is not in resonance with the ring and continues on waveguide 1, where as λ_2 couples into the ring and subsequently moves to waveguide 2.

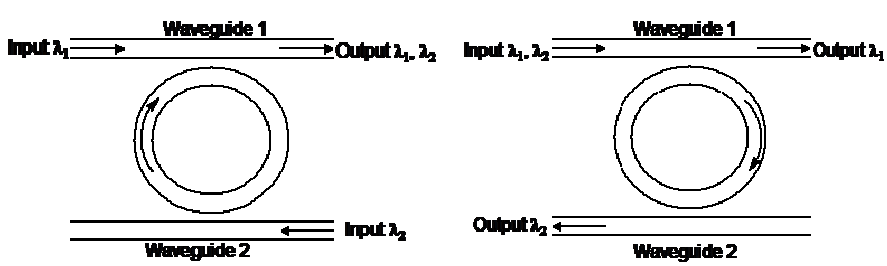

Figure 1.5. Schematic of a ring resonator used to a) multiplex b) demultiplex signals.

According to E1.10, controlling the effective refractive index of the ring can also allow control of the wavelengths in resonance with the ring. Figure 1.6 shows the transmission spectrum obtained by monitoring the output of multiple wavelengths through a waveguide coupled to a ring. The spectrum obtained with the material at an initial refractive index ($n_{eff} = n_0$) is shown as a solid line. A single resonance is shown as a dip in the transmission spectra, which correspond to the wavelengths trapped by the resonator. The same ring can undergo a change in refractive index ($n_{eff} = n_0 - \Delta n$), resulting in a second transmission spectrum shown as a dotted line, with the resonance wavelength shifted from the first spectrum. Changing the refractive index of the ring allows control of either routing (as in a scenario like Figure 1.5) or a method to process signals. Monitoring the transmission at the resonance wavelength of the material with its initial refractive index will indicate if there is a change in transmission caused by a change in refractive index.

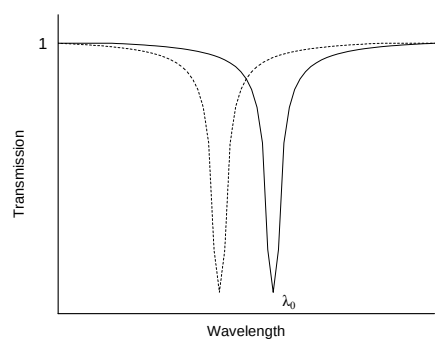

Figure 1.6. Transmission spectra of a resonator with two different indices.

Incorporation of a $\chi^{(2)}$ or $\chi^{(3)}$ material into the MZI or ring resonator would allow the device to become an active nonlinear device, which could process information. For

example, fabricating (or coating) arm 1 of the MZI with a $\chi^{(2)}$ material with electrodes positioned across it could allow strong electric fields to be applied across the $\chi^{(2)}$ material. The electric fields produced by the electrodes in the "on" position would cause a nonlinear change in refractive index of the material compared to that in the "off" position, thus bringing the light in or out of phase, allowing signal processing to occur. On the other hand, fabricating (or coating) arm 1 of the MZI with a $\chi^{(3)}$ material would allow high intensity control pulses of light to be used to induce changes in the refractive index, and also permit signal processing.

Materials with large $\chi^{(2)}$ are utilized in electro-optic devices. The polarization and relaxation times for the π-electrons of conjugated organic chromophores are on the order of femtoseconds, leading to possible bandwidths of hundreds of gigahertz or even terahertz.[10] Such devices remain limited by this electrical component (the build up and dissipation of charge in the capacitor), leading to an operational maximum of ~200 Gb/s.[11] A true all-optical device would use light to control light, both as the signal source and the method of modulation. Because the limitations associated with capacitor charging and discharging no longer apply, $\chi^{(3)}$ materials used in all-optical devices can achieve theoretically larger bandwidths than electro-optic devices.

1.4. Material Property Requirements for AOSP

Photonic devices able to perform the signal processing of data at extremely rapid rates (greater than 100 GHz) have been unable to keep pace with developments in compact, ultrafast (less than 1 picosecond) laser sources. The lag in processing speeds stems from inadequate optical and (or) material-related properties of the nonlinear

medium used in the device. Typical material properties required to perform all optical switching are listed below:[6]

1) Sufficiently large magnitudes of nonlinearity
2) High transparency, both linear and nonlinear, at wavelengths of interest
3) Ultrafast (<1 picosecond) temporal nonlinear response
4) Photochemical stability
5) High optical damage threshold
6) Processability

Large magnitudes of the nonlinearity ($\mathrm{Re}\chi^{(3)}$) allow the optical power density and power consumption to be kept low, and permit devices to be fabricated with small interaction lengths (i.e. to minimize the path length of the light through the nonlinear optical material). Low absorption coefficients at the wavelengths of interest provide greater flexibility in the material interaction length (absorption loss sets an upper limit to device size), while low absorption reduces the buildup of heat that could potentially damage the nonlinear medium. An ultrafast temporal response regarding the nonlinear change in refractive index is necessary to achieve competitive processing speeds with existing technology. Photochemical stability and resistance to optical damage would allow a robust device to be manufactured.

Stegeman *et al.*[12, 13] have developed dimensionless figures of merit (FOM) which allow one to assess the ability of materials to perform all-optical tasks in devices relying on changes in nonlinear phase shift in the presence of linear and nonlinear absorption. These FOMs assume the dominant form of optical loss arises from absorption (i.e. that scattering losses are negligible).

The nonlinear phase shift ($\Delta\Phi$), the most important property for device operation, is given by the following equation:

$$\Delta\phi(\lambda, I) = \frac{2\pi L n_2(\lambda, I) I}{\lambda} \qquad \text{E1.11}$$

where both the $\Delta\phi$ and n_2 have a dependence on the incident wavelength (λ) and intensity (I), and L is the device pathlength. Each type of device requires a different minimal phase shift with a typical range of π to 8π.[14] For example a Mach-Zehnder interferometer requires a phase shift of 2π for operation.

When non-negligible one-photon absorption is considered $\alpha_L >> \beta_I I$ (E1.5 and E1.6) and $\alpha_L^{-1} > L$, one arrives at the expression for the so called one-photon FOM, W:

$$W = \frac{n_2(\lambda) I}{x \alpha_0 \lambda} \qquad \text{E1.12}$$

The x term is a device dependent number arising from the required $\Delta\phi$ for a device (where $\Delta\phi > x\pi$). In order to switch a MZI, where x = 2, W should be >1 for device operation. It is important to note that the W FOM could be met by varying the input intensity however, input intensities are limited by material stability and source output.

Nonlinear absorption is accounted for by the so called two-photon FOM, T, when $\alpha_L << \beta_I$ and $(\beta_I I)^{-1} > L$ is considered:

$$T = \frac{x \beta_I \lambda}{n_2(\lambda)} \qquad \text{E1.13}$$

In order to switch a MZI, T should be <1. The lack of intensity dependence for the T FOM is due to the fact that both β_I and n_2 are dependent on the incident light intensity. The T FOM can be rewritten in terms of $\chi^{(3)}$ as in the following equation:[12]

$$2x\pi \frac{\mathrm{Im}(\chi^{(3)})}{\mathrm{Re}(\chi^{(3)})} < 1 \qquad \text{E1.14}$$

For example a typical device operating in telecommunications wavelengths (λ = 1550 nm) could be on a silica wafer with the waveguide fabricated from silicon or silicon nitride (Si_3N_4). An approximate path length of 1 mm and a cross-sectional area of ~1 μm^2 is typical for NLO devices. If a compact mode-locked-laser is used as a light source with a 100 mW average power and 100 GHz repetition rate (1 pJ pulse energy (E) and 10 ps pulsewidth (τ)), then the intensity can be calculated for a beam with a Gaussian shape:

$$I = \frac{E}{\pi^{(\frac{3}{2})}\omega_0^2\tau} \approx 100\frac{MW}{cm^2} \qquad \text{E1.15}$$

the ω_0 (assumed to be ~0.4 μm) is a factor related to the radius of the beam width, while the other variables were described previously.

According to E1.11 ($\Delta\varphi = \pi$, $\lambda = 1.55 \times 10^{-6}$ m, $L = 1 \times 10^{-3}$ m, and $I = 1 \times 10^{12}$ W/m^2), under the described conditions the required nonlinear refractive index (n_2) for device operation is approximately 8×10^{-16} m^2/W. The nonlinear refractive index (in SI units) can be converted to $\chi^{(3)}$ (in esu) through the following equation:

$$n_2[SI] = \left(\frac{\pi}{3\varepsilon_0 c n^2}\cdot 10^{-8}\right)\chi^{(3)}[esu] \qquad \text{E1.16}$$

where ε_0 is the electric permittivity in free space (8.85×10^{-12} J^{-1} C^2 m^{-1}) , c is the speed of light (3.0×10^8 ms^{-1}) and n is the linear refractive index (generally ~1.7 for organic materials). Using the n_2 value obtained previously (8×10^{-16} m^2/W) the minimal $\mathrm{Re}(\chi^{(3)})$ necessary to effect the π-phase shift can be calculated to be ~6×10^{-10} esu.

1.5. Selected Examples of χ^3-Based Optical Devices and Materials From the Literature

The low cost of using silica fibers over long distances and the extremely low optical absorption losses (a fraction of a decibel per kilometer) were important factors leading to the incorporation of silica fibers in telecommunications. The low loss of the material readily makes it a candidate for investigation of its potential use in all-optical devices. The nonlinear refractive index, n_2, of SiO_2 in the telecommunications spectral region is 3×10^{-16} cm^2W^{-1}.[15] Even though $Re(\chi^{(3)})$ is relatively small, extremely low losses allows silica to meet the FOM material requirements (Table 1.1, entry 1).[14, 15] However, fabricating a device which relies on the nonlinear refractive index of silica to acquire an appropriate phase shift would require interaction lengths that are impractical for use. Heebner *et al.* proposed all-optical switches fabricated using a MZI coupled to a ring resonator on one arm, leading to resonator-enhanced Mach-Zehnder (REMZ) devices.[16] Such devices could theoretically operate as a nonlinear switch at reduced power levels (from 240 W for an MZI to 12 mW for the REMZ) however, the size of the device would still be too large (10 m ring length) to be practical.

Ferroelectronic inorganic materials have had a large impact on the devices utilizing photorefractive materials. Materials composed of a pair of elements from groups 13 and 15 (previously III and V) or groups 12 and 16 (previously II and VI) are inorganic ferroelectronic materials, which have undergone a great deal of research as $\chi^{(3)}$ materials.

One example of a III-V material is GaAs, which has a bandedge at ~800 nm. The material shows large third-order nonlinearities near the bandgap due to the polarization of electrons.[17] However, it has been shown that two-photon absorption (TPA) can be

significant in regions of 1PA transparency for III-V and II-VI materials.[18] Free carriers (unpaired holes and electrons) generated from the TPA in several III-V and II-VI materials also show significant nonlinear refractive indices, but have associated slow relaxation times.[19] The optical Kerr effect dominates at low intensities, while free carrier refraction dominates at high intensities. Said *et al.* used the Z-scan method to determine the contributions of free carrier refraction, optical Kerr effects and TPA to the overall non-linearity of GaAs and several other materials at 532 and 1064 nm.[19] Dinu *et al.* used Z-scan to measure GaAs at the telecommunications wavelength 1540 nm, which did not show a favorable *T* FOM (Table 1.1, entry 2).[20]

An all-optical nonlinear switch operating at 1.55 μm using a micro-ring resonator coupled to a straight waveguide, fabricated from GaAs-AlGaAs, was developed by Van *et al*.[21] Generation of free carriers was used to tune the resonance wavelength of the cavity. The switching time for the device was ~100 ps, while the recovery time after the termination of the pump beam was ~50 ps, which was due to recombination of the charges on the micro-ring sidewalls. This long lifetime for the recombination of carriers makes it difficult to use such materials in ultrafast optical devices.

The material of choice in the electronics industry, silicon, has been a material making great progress in photonics over recent years. The nonlinear refractive index, intensity-dependent absorption and the two-photon FOM for crystalline silicon <111> was reported by Dinu *et al.* (Table 1.1, entry 3).[20] Electro-optic devices have been fabricated using a silicon-on-insulator (SOI) design in which silicon is the waveguide. Liu *et al.* demonstrated high speed optical-phase modulation in a MZI with a modulation bandwidth exceeding 1 GHz.[22] The refractive index of silicon was not controlled using

the optical Kerr effect, but controlled using the free carrier refraction in which charges were injected into the arms of the MZI using a metal-oxide-semiconductor capacitor. The device size, on the order of millimeters, would need to be reduced for on-chip integration.

Soon after, Almeida *et al.* demonstrated the all-optical control of a 20 μm long structure using a micro-ring resonator.[23] The change in the refractive index, utilizing changes in the concentration of free-carriers, was induced by two-photon absorption (TPA). The rate of TPA is proportional to the square of the peak pump power (I^2) circulating in the ring. The relaxation time of the free carriers found in this device: τ_{fc} = 450 ps, is not the fundamental limit and could possibly be improved to as low as 100 ps.

The development of silicon-organic hybrid (SOH) devices may be necessary to achieve higher processing speeds. Organic materials show adequate material response times and large nonlinearities required for device operation however, their development in devices has been largely hindered by unacceptable absorption losses. A functional SOH device was demonstrated by Koos *et al*.[24] In this device a small organic molecule, DDMEBT (Table 1.1, entry 4), was deposited upon a slotted waveguide SOI wafer using molecular beam deposition. All-optical demultiplexing at transmission speeds above 100 Gb s^{-1} at 1.55 μm was then demonstrated.

Table 1.1 summarizes several of the material properties discussed in the preceding device demonstrations.

Table 1.1. Materials used in all-optical signal processing devices. The fundamental wavelength (λ_f), n_2, , and the T FOM.					
Entry	Material	λ_f (nm)	n_2 (cm^2W^{-1})	β ($cmGW^{-1}$)	T
1	SiO_2	1064	3×10^{-16}	-	<<1
2	GaAs	1540	1.59×10^{-13}	0.88	3.1
3	Silicon <111>	1540	0.43×10^{-13}	10.2	10
4	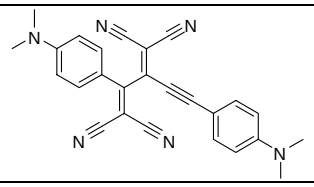	1500	$(1.7 \pm 0.8) \times 10^{-13}$	-	-

1.6. Organic $\chi^{(3)}$ Materials

As mentioned previously, the relatively large nonlinear refractive indices and ultra-fast response times suggest organic materials are promising third-order nonlinear optical materials. This section separates conjugated polymers and conjugated small molecules into two parts. This section only gives a selected review of materials, a thorough review of the third-order properties of a large variety of materials has been given by Nalwa.[25]

1.6.1. Selected Organic Conjugated Polymers From the Literature

Large conjugated systems such as conjugated polymers show strong, low energy 1PA, which depending on the transition dipole moment between the ground state and the first excited state (M_{ge}) and the transition dipole moment between the first excited state and higher lying excited states ($M_{ee'}$) may give rise to high $\chi^{(3)}$ (see section 1.6.2.1 for further details). The polymers can be thought of as organic molecular wires (a molecular-scale object that can conduct charge), which have a continuous set of π-orbitals along the conjugated backbone of the material. The strongest coupling along a

chain is a polymer using all-polyene units. The addition of aromatic rings and triple bonds causes the effective conjugation to be decreased, which may decrease the nonlinearity. However, there are advantages of using conjugated polymers with aromatic groups or triple bonds, such as the overall stability of the polymer can be improved. The following section reviews some of the more popular conjugated polymers being investigated.

Polyacetylene (Table 1.2, entry 1) is the simplest conjugated polymer, with all polyene units. *Trans*-polyacetylene has two valence bond isomers, the A and B phases (Figure 1.7 A and B). It is important to note that the A and B phases are not resonance forms, because the polymer retains the alternation of single and double bond character, instead of all carbon - carbon bonds being equal.[5] If *trans*-polyacetylene has an odd number of carbons, then it will have one unpaired electron, which is delocalized over several carbon atoms. This region of delocalization of the radical is known as a soliton. The double bonds change from phase A *trans*-polyacetylene to phase B *trans*-polyacetylene through the soliton region (Figure 1.7, C).[26] The degenerate phases of *trans*-polyacetylene allow the soliton to be a center for high non-linear optical activity.

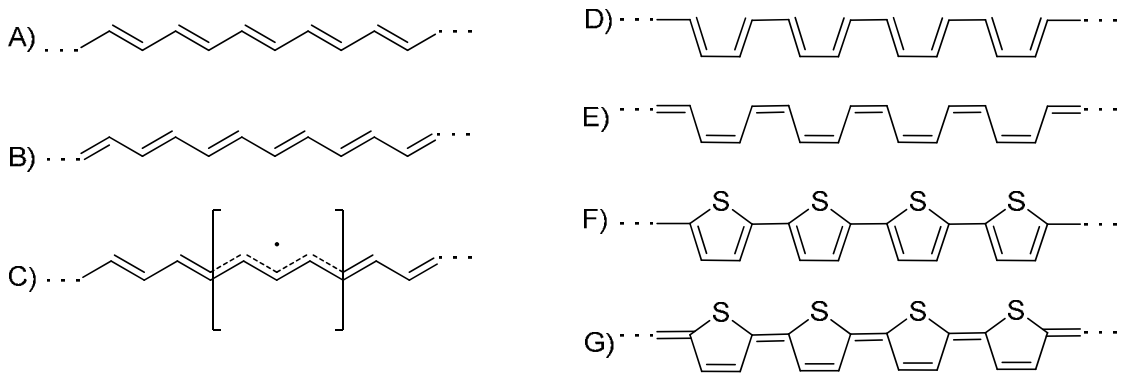

Figure 1.7. Part A and B show the respective A and B phases of *trans*-polyacetlyne, part C represents the presence of a soliton (a defect between the A and B phases) in *trans*-polyacetlyene, part D and E show the *cis-transoid* and the *trans-cisoid* conformers of polyacetylene respectively, and parts F and G show the phases of polythiophene.

Heeger *et al*.[27] claimed that an intense pump can cause the formation of electron-hole pairs, which can subsequently lead to states in the band gap, similar to the state created by a soliton. The states appear due to geometry relaxation in the polymer structure in a localized area (assumed to be ultrafast, 10^{-13} s), which traps the charge.[27] The states in the middle of the band gap, caused by the presence of the soliton redistribute the oscillator strength from the inter-band transition ($h\upsilon_I$) (Figure 1.8 A) to transitions involving the soliton state ($h\upsilon_s$) (Figure 1.8 B).

The origins of the difference in $\chi^{(3)}$ for *trans*- and *cis*- polyacetlyene is controversial[5]; however, Heeger *et al*.[27] have attempted to explain it. *cis*-Polyacetylene does not have a doubly degenerate ground state like trans-polyacetylene. Part D and E show the *cis-transoid* and the *trans-cisoid* forms of polyacetylene respectively. The total-energy of the two forms is different; the *trans-cisoid* form is higher in energy by ~10 kJ/mol per C_2H_2 unit.[28] The loss of degeneracy leads to a decrease in the third-order nonlinear optical activity of *cis*-polyacetylene. The lack of energetic degeneracy for the phases of

cis-polyacetylene (Figure 1.7 D and E) leads to the instability of solitons. Bipolarons are the lowest energy defect that can exist for such conjugated materials. A bipolaron is a region in a conjugated polymer that is doubly charged (2^+ or 2^-) and has two states in the bandgap. Figure 1.8 C shows the energy diagram for a dicationic bipolaron. As was the case for solitons, there is a redistribution of oscillator strength from the $h\upsilon_I$ excitation to the $h\upsilon_1$ and $h\upsilon_2$ excitations, involving the states in the gap. Halvorson *et al.*[29] used THG to measure *trans*- and *cis*-polyacetylene from 0.5 to 1.3 eV. The $\chi^{(3)}$ values measured for *trans*-polyacetylene, ~1.8×10^{-9} esu at 1500 nm, were generally an order of magnitude larger than the *cis* form. A derivative of polyacetylene able to form optical quality films after being cast from solution (Table 1.2, entry 2) showed similar results in terms of the magnitudes of $\chi^{(3)}$ compared to polyacetylene.[30]

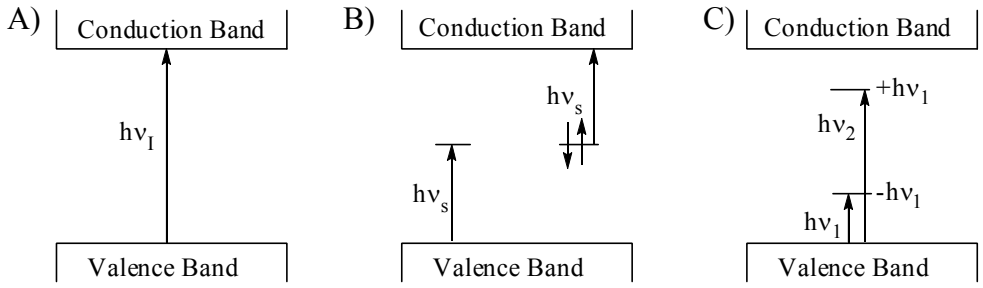

Figure 1.8. Energy diagrams for A) pure polyacetlyene with excitation $h\upsilon_I$, B) a soliton band diagram showing mid-gap transitions $h\upsilon_s$, and C) sub-mid gap transitions ($h\upsilon_1$ and $h\upsilon_2$) for a bipolaron.[27]

Marder *et al.*[31] synthesized soluble polymers, which were the product of a ring opening metathesis polymerization (ROMP) of copolymers cyclooctatetraene (COT) and 1,5 cyclooctatetraene (COD) using a tungsten carbene complex (Figure 1.9). The mole fraction was varied with a tendency for longer conjugation segments in samples with

more COT. The nonlinear optical susceptibilities, measured using THG at 1.907 nm, showed $\chi^{(3)}$ values as high as 1.6×10^{-12} esu for samples with 32% COT (compared to 3.3×10^{-13} esu for 8% COT), due to the segments of longer conjugation. Chi *et al.*[32] prepared polymers from substituted cyclooctatetraenes (R-COT) monomers using the ROMP methodology with a variety of initiators (Figure 1.9). The side-groups made the processing of thick (2-200 μm), large-area (greater than 1 cm × 1 cm) films of good optical quality. An ultrafast response time (less than 100 fs) and large $|\chi^{(3)}|$ values (as large as 2.1×10^{-10} esu) were reported for telecommunications wavelengths (1300-1550 nm) using the Z-scan technique.

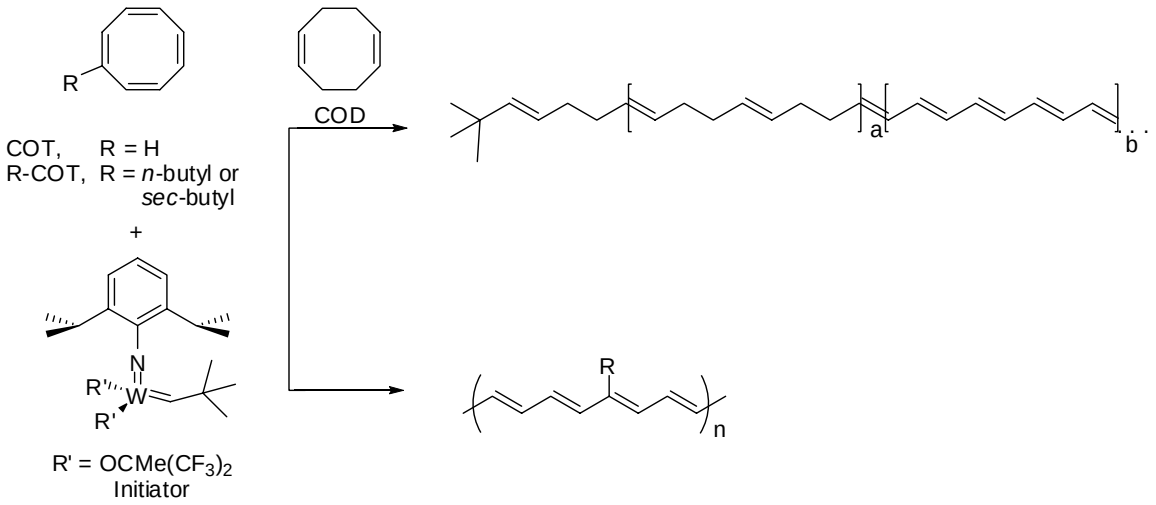

Figure 1.9. Synthetic scheme to perform ROMP on COT and COD co-monomers (top) and R-COT monomors (bottom) with the initiator shown.

Poly(2,5-thiophenes are closely related to the *cis-transoid* and *trans-cisoid* conformers of polyacetylene (removing the sulfur atoms from F and G of Figure 1.7 leaves the hydrocarbon skeletons of D and E); however, the thiophene units have

aromatic stabilization, so the total energy difference between the F and G phases of polythiophene will be larger than the *cis-transoid* and *trans-cisoid* phases of polyacetylene. Dorsinville *et al*.[33] measured poly(2,5-thiophene) by degenerate four-wave mixing (DFWM) to be 0.3×10^{-10} esu at 1064 nm (Table 1.2, entry 4). Poly(3-alkylthiophene) generally have good solubility in common organic solvents and can form amorphous films which are all properties desirable for AOSP applications.[34] Okawa *et al*.[34] studied the third-order nonlinear optical properties of thin films of several Poly(3-alkylthiophene) of different alkyl length using the THG technique at 1540 nm and 1910 nm. The magnitude of $\chi^{(3)}$ was found to depend slightly on the alkyl chain length with shorter chains giving larger values, most likely due to dilution effects. There was a strong dependence on the wavelength, due to a three-photon resonance at 1540 nm (the linear λ_{max} being ~514 nm), which gave significantly larger values of $\chi^{(3)}$ (~2 times larger). Torruellas *et al*.[35] subsequently mapped the dispersion of $\chi^{(3)}$ using THG for two poly(3-alkylthiophene) in a range of 953-1904 nm. The dispersion measurements confirmed the existence of a peak at ~1540 nm.

Polydiacetylenes (PDAs) are another class of polymers investigated as $\chi^{(3)}$ materials due to their π-conjugated backbones. PDAs have alternating single-double-single-triple bonds, with side groups attached at the vinylene positions. The properties of PDAs was reviewed by Bloor and Chance.[36] Two of the more widely studied PDAs are poly[2,4-hexadiyne-1,4-diyl bis(para-toluenesulfonate) (PDA-PTS) (Table 1.2, entry 3), and poly[2,4-hexadiyne-1,4-diyl bis(alkoxycorbonylmethylurethane) (PDA-*n*-BCMU), which are shown in Figure 1.10. The side groups on the polymer are generally designed to 1) provide steric strain, which keeps the polymer elongated and 2) possibly form hydrogen

bonds with adjacent sidegroups leading to a more planar structure, such as the urethane groups of PDA-n_2-BCMU.[25] The polymerization of the diacetylene monomers can occur in the solid state though thermal and photochemical initiation.

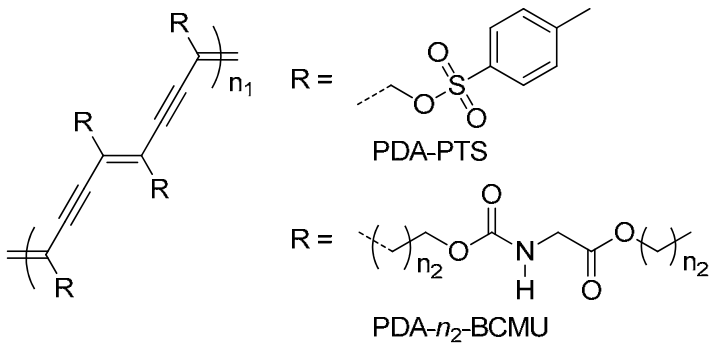

Figure 1.10. Structure of polydiacetylenes, PDA-PTS and PDA-n_2-BCMU.

PDAs are often crystalline material (preservation of crystallinity of monomors upon polymerization[36]), which can be advantageous because it gives a high degree of orientation. Large induced polarizations in the direction of the long axis of the chain can be induced. Sauteret *et al.*[37] were the first to measure the Re($\chi^{(3)}$) in such crystals (PDA-PTS), and the values were found to be 2×10^{-12} esu at 2.62 μm, and 10×10^{-12} esu at 1.89 μm. Lequime *et al.*[38] reported substantial nonlinear absorbance, β_I, over a wavelength range of 667-1111 nm for PDA-PTS crystals. After this pioneering work, Polyakov *et al.*[39] subjected PDA-PTS to measurements of the n_2 and β_I over a broad range of wavelengths, which covered the telecommunications region. At 1.3 μm, the n_2 term was determined to be 7.5×10^{-17} m^2W^{-1}, while the β_I term was found to be 6×10^{-11} mW^{-1}. The magnitude of the third-order response is sensitive to the orientation of the PDA, due to the high order in the crystals. Kanetake *et al.*[40] used THG at 1.90 μm to measure

oriented films (parallel and perpendicular) and unoriented films of PDA-C_4UC_n (Figure 1.10, R = $(CH_2)_4$-O-CO-NH-$(CH_2)_{n-1}$-CH_3). The anisotropy of the films revealed parallel oriented films to have $\chi^{(3)}$ values several orders of magnitude larger than the perpendicularly oriented films (2.9×10^{-10} versus 0.03×10^{-10} esu).

Another popular conjugated polymer is poly(*para*-phenylene vinylene) (PPV). PPV has alternating *para*-substituted phenyl rings and double bonds. The effective conjugation is diminished compared to polyacetylene, because the aromatic stabilization of the phenyl rings. Bradley *et al.*[41] studied the increase of the third-order nonlinearity of a polymer precursor that was converted into PPV, which is consistent with a nonlinearity arising from a π-conjugated system. Kurihara *et al.*[42] performed similar experiments leading to similar results on the poly(3,6-dimethoxy-*para*-phenylene vinylene) (MO-POV). McBranch *et al.*[43] compared the THG properties of films of PPV and PDA-4-BCMU at 1.06 μm. The magnitude of $\chi^{(3)}$ at this wavelength was found to be similar for both polymers ($2 \pm 1.5 \times 10^{-10}$ esu). Thus PPV materials can be competitive with other conjugated polymers. However, PPV has a tendency to be highly crystalline[44], which is a cause of undesirable scattering. Bahtiar *et al.*[45] investigated the effects on optical loss as alkoxy substituents on the PPVs was varied, like poly[2-methoxy-5-(2-ethyl-hexy-loxy)-1,4-phenylene vinylene (MEH-PPV). It was found that loss in a waveguide could be reduced from 20 dB/cm for PPV to less than 1 dB/cm by controlling the sidechain alkoxy groups extending from the backbone of the PPV.

Table 1.2. Selected conjugated polymers of which the third-order nonlinearity has been measured.				
Entry	Chemical	λ_I (nm)	$\lvert\chi^{(3)}\rvert$ (10^{-10} esu)	Method
1	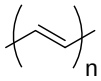	1500	17	THG
2	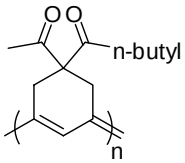	1500	1.2	THG
3	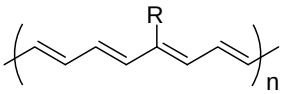	1300	2.1	Z-Scan
4	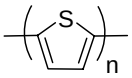	1064	0.3	DFWM
5	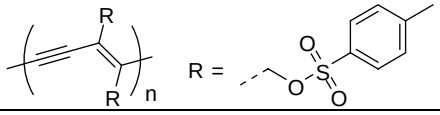	1500	0.80	Z-scan
6	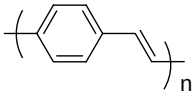	1064	2 ± 15	THG

1.6.2. Selected Organic Conjugated Small Molecules From the Literature

Hans Kuhn suggested the three most important organic dyes can be grouped into three categories: polyenes, symmetrical polymethines, and porphyrins.[46] Porphyrin molecules are not the focus of the remainder of this thesis and the nonlinear optical properties of this class of materials has been reviewed by Torre *et al.*,[47] so these materials will not be discussed further. A brief introduction and selected review of the third-order nonlinear optical properties of polyenes and symmetrical polymethines is given below.

1.6.2.1. Introduction, Background and Theory

The tailorability of small organic molecules gives them an advantage over other materials, given that more careful studies of structure-property relationships have been performed on such systems. The material requirements of low absorption losses and ultra-fast response times can be easily satisfied if the operational wavelength of the

device is non-resonant with one and two photon absorption bands of the material (where $Re(\chi^{(3)}) \neq 0$ and $Im(\chi^{(3)}) \sim 0$). However, this often does not lead to favorable device performance because changes in the nonlinear refractive index are generally smaller at non-resonant wavelengths (see Figure 1.2). Working below the one photon absorption band but between any deleterious two-photon bands can provide resonance enhancement to obtain large third-order nonlinearities, while minimizing 1PA and 2PA, which can potentially allow the *W* and *T* FOMs to be met. The rational design of organic molecules may allow a situation to be achieved where the aforementioned situation exists (see Figure 1.11). However, the propensity for organic molecules with large $Re(\chi^{(3)})$ measured in the telecommunications region to be accompanied by significant $Im(\chi^{(3)})$ causes such molecular design approaches to be challenging.

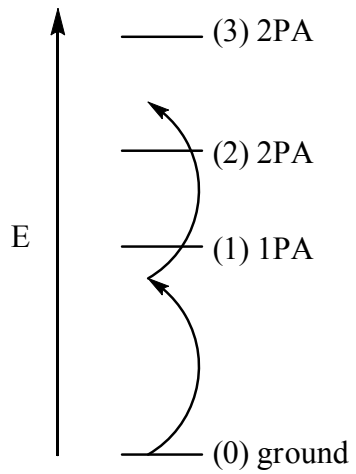

Figure 1.11. Energy-level diagram of a four state system in which photon energy can be used that is close to the 1PA resonances, but falls between the two 2PA levels, avoiding absorption.

Polyenes are conjugated molecules with delocalized π systems, which can be modified to give rise to several desired optical effects. The geometry of polyenes change

as various donors and acceptors are added as terminal groups. A neutral valence bond (NVB) structure can be drawn if there is little coupling between the terminal groups, leading to little charge transfer. On the other hand strong coupling between the terminal groups would result in a valence bond structure with a significant amount of charge transfer (CT). A representation of the NVB (left) and CT (right) structures are shown in Figure 1.12 A. If the NVB and CT structures contributed equally to a molecule, with half a charge on each end group accompanied by carbon – carbon bond orders of 1.5, then the ground state representative structure from this equal mixing of the two extreme resonance forms would be anticipated to look like that which is depicted in Figure 1.12 B.

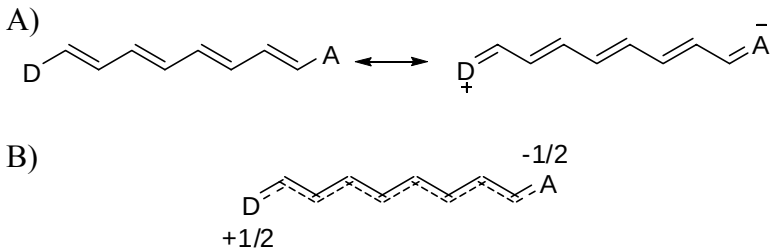

Figure 1.12. A) The NVB (left) and CT (right) resonance structures. B) The representative structure resulting from the equal mixing of the NVB and CT resonance structures.

The geometry of the polyene in the ground state is dependent on the relative contributions of the two resonance forms. The degree of contribution depends upon the relative energy of the resonance forms. The strength of the donor and acceptors, as well as the loss and gain of aromaticity[48] and the polarity of the solvent all play a role in these relative contributions. For instance, a low polarity solvent will favor the neutral form of the molecule, while increasing the solvent polarity can favor the charge-transfer form.[49,50]

Potential wells for the limiting resonance forms can be drawn, displaying the potential energy (V) surface in correlation with the geometrical bond length alternation coordinates (q) of the resonance forms (Figure 1.13).[51] The geometry and energy of the ground state structure formed after the mixing of the individual NVB and CT potential wells is strongly dependent upon the relative energies of the NVB and CT structures. The relative energies at the minimum of each well are associated with a BLA coordinate (where q_{NVB}, q_{CT}, and q_{opt} are the NVB, CT and ground state coordinates, respectively) and the difference in energy (V_0) between the adiabatic potential wells can be expressed using the following equation:

$$V_0 = E_{CT} - E_{NVB} \qquad \text{E1.17}$$

where E_{CT} is the lowest potential energy of the CT potential well at q_{CT} and E_{NVB} is the lowest potential energy of the NVB potential well at q_{NVB}.

When V_0 is greater than 0, the mixed ground state resonance structure mostly resembles the NVB structure with significant bond length alternation (BLA)[52] (Figure 1.13 A, q_{NVB} is similar to q_{opt}), on the other hand when V_0 is less than 0 the ground state resonance structure mostly resembles the CT structure, with significant BLA of opposite sense to that in the case of $V_0>0$ (Figure 1.13 C, q_{CT} is similar to q_{opt}). When V_0 is equal to zero, then the ground state resonance structure is an equal mix of the two forms leading to a BLA of 0. The case where V_0 and BLA are equal to zero is known as the cyanine limit (Figure 1.13 B).

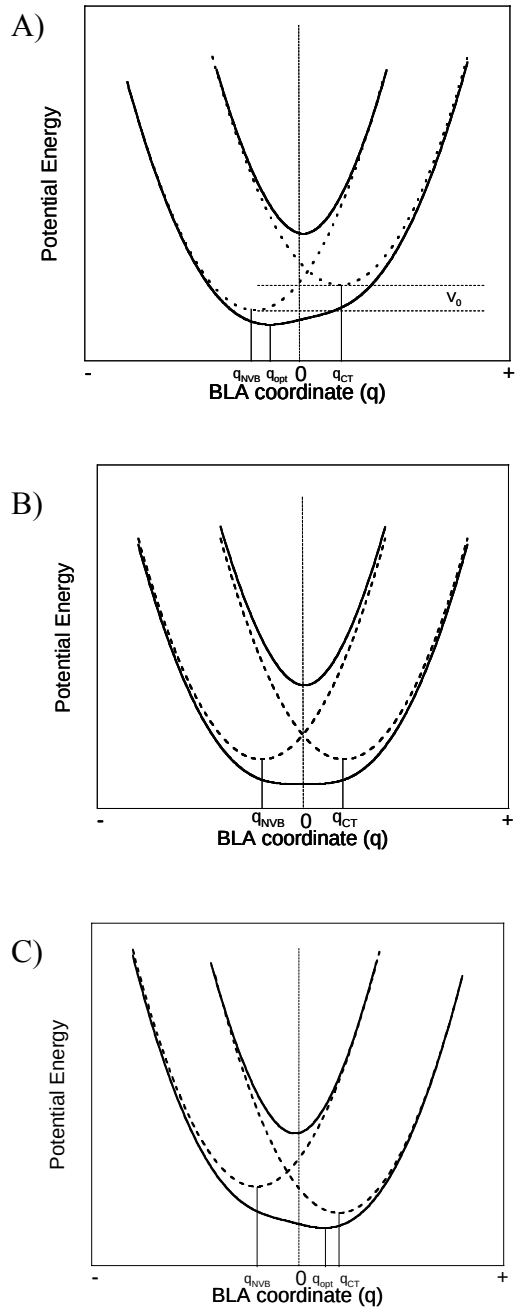

Figure 1.13. Potential energy surfaces of the NVB (dotted, left) and CT (dotted, right) resonance forms accompanied by the ground state and exited state potential energy surface after mixing the two resonance forms (solid lines) plotted against the BLA coordinate q for various energy differences (V_0): A) $V_0 < 0$, B) $V_0 = 0$, C) $V_0 > 0$. The vertical dashed line is the zero BLA position.

Plots of α, β and γ versus V_0 are shown in Figure 1.14. The q_{opt} changes as V_0 is varied from -2 to +2, which affects the magnitude of α, β and γ. Variations in donor and acceptor strength and the electric fields generated by solvents are reflected in V_0. In the case where BLA equals 0 ($V_0 = 0$), α is at a maximum, β is zero and γ is at a negative maximum. Similar plots can be generated with similar shape as those in Figure 1.14 for the real parts of the polarizabilities (α, β, γ) of conjugated donor acceptor polyenes versus their BLA (or BOA).[50, 53]

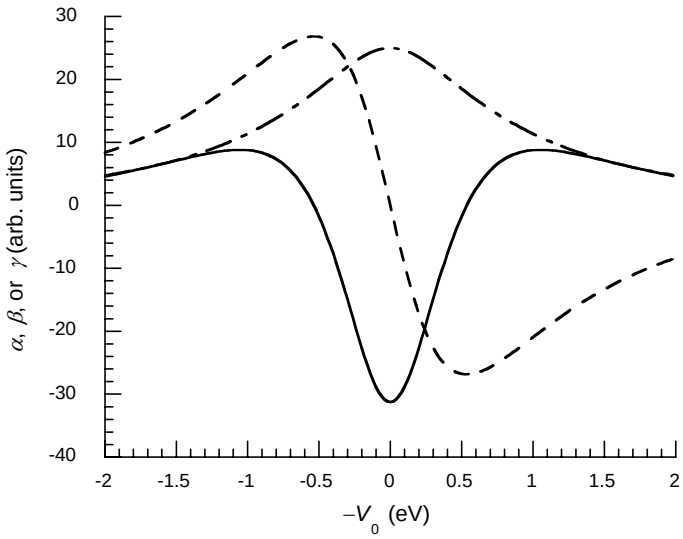

Figure 1.14. Plots of α, β and γ versus V_0. Trends of α (dash-dot line), β (dashed line), and γ (solid line) as a function of $-V_0$ calculated using the VB–CT model for the model DA molecule $(CH_3)_2N$-$(CH = CH)_4$-CHO. Reproduced with permission.[6]

The Re(γ) for donor/acceptor polyenes and polymethine dyes can be expressed as the combination of a three-term equation based upon simplified perturbation theory: the dipolar term (D), the negative term (N) and the two photon term (TP):[54]

$$\mathrm{Re}(\gamma) \propto \sum_{e'} \frac{M_{ge}^2 M_{ee'}^2}{E_{ge}^2 E_{ee'}} - \frac{M_{ge}^4}{E_{ge}^3} + \frac{M_{ge}^2 \Delta\mu_{ge}^2}{E_{ge}^3} \qquad \text{E1.18}$$

TP N D

where g represents the ground state, e represents the excited state, e' the higher lying excited states, M is the transition dipole moment, $\Delta\mu$ is the difference in the dipole between states ($\mu_{ee} - \mu_{gg}$) and the E is the difference in energy between states.

The TP, N and D term and consequently γ are dependent on the BLA.[54] The N term (negative) opposes the D and TP terms (positive). The contributions to γ from the TP term and the contributions from the N term each reach a maximum at the cyanine limit. The N term typically dominates the TP term at the cyanine limit, even if $M_{ee'}$ is similar in magnitude to M_{ge}, because the N term has a smaller E_{ge} than $E_{ge'}$. The D term arises from a change in dipole moment upon excitation from the ground state to the excited state. At the cyanine limit (BLA ~ 0), the D term is reduced to zero because there is no change in dipole moment between the ground state and excited state ($\Delta\mu_{ge}$= 0). At this limit the N term dominates and an overall large negative value of γ is observed.

1.6.2.2. Selected Polyenes

β-carotene (Table 1.3, entry 1) is a benchmark material concerning third-order nonlinear optical measurements using THG. Marder *et al.* synthesized and characterized the magnitude of γ for a series of asymmetric carotenoid derivatives with one terminal group substituted with acceptors of various strengths (for example Table 1.3, entry 2).[55] The wavelength dependent THG values of γ were measured at the peak three-photon resonance and were compared to the value for the symmetrically substituted β-carotene. An increase in λ_{max} and γ_{max} followed with increasing acceptor strength. The increase in

γ arises from greater contributions of the D term described in equation 16. Electro-absorption (Stark) spectroscopy was used to probe the excited state dipole moment, which revealed a large change in dipole moment ($|\mu_{ee} - \mu_{gg}|$). Stabilization of the CT form (stronger acceptors) leads to an increased mixing of the VB and CT potential surfaces, thus γ would move closer to the first positive maximum in the BLA curve.

Haas *et al.*[56] synthesized carotenoid derivatives known as astaxanthene molecules. These carotenoids were also subjected to γ measurements using THG. A $\chi^{(3)}$ value of 1.2 $\times$ 10^{-10} esu was observed for the longest derivative (Table 1.3, entry 3). This discrete polyene molecule has a similar $\chi^{(3)}$ compared to the polymeric materials discussed previously.

Pucceti *et al.* measured γ values using third harmonic generation or electric field induced second harmonic (EFISH) generation for several series of disubstitued polyenes of increasing chain length with the following terminal groups: symmetric aldehyde terminations (Table 1.3, entry 4), symmetric dimethylaminophenyl terminations (Table 1.3, entry 5), and asymmetric dimethylaminophenyl – aldehyde terminations (Table 1.3, entry 6).[57] Observed trends in γ versus conjugation length led to the equation $\gamma = kN^a$, where k is a constant and N is the number of double bonds (phenyl groups were counted as 1.5 double bonds). The exponent values, a, for the symmetric aldehyde terminated series and the dimethylaminophenyl terminated series measured using EFISH at 1.34 μm were 2.3 and 4.65 respectively. Large γ values were obtained for the long conjugation length dimethylaminophenyl terminated series due to electron donation into the π-system however, these values may have been enhanced by TPA resonances. The series of donor acceptor compounds interrogated using THG at 1.91 μm resulted in an exponent value of

3.4 (a maximum value of 7600 ± 600 × 10^{-36} esu). Drawing conclusions by making comparisons between the asymmetric and the symmetric systems is complicated due to wavelength dependent dispersion.

Table 1.3. Selected polyene molecules of which the third-order nonlinearity has been measured.

Entry	Chemical	λ_I (nm)	γ	$\lvert\chi^{(3)}\rvert$	method
1	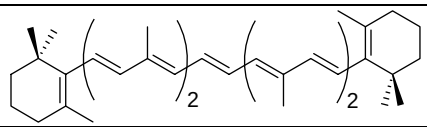	1392	1	-	THG
2	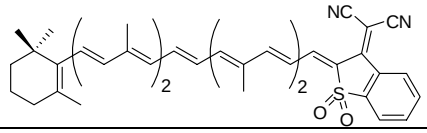	2220	35	-	THG
3	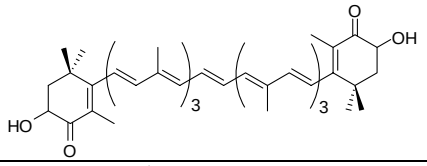	1500	-	1.2×10^{-10}	THG
4	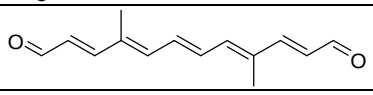	1340	0.05	-	EFISH
5	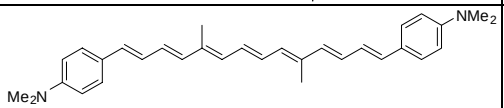	1340	1.2	-	EFISH
6	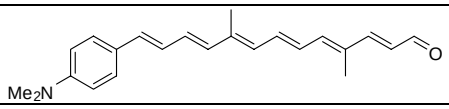	1910	0.4	-	THG

1.6.2.3. Polymethine Dyes

Symmetric, ionic polymethine dyes with an odd number of methine units, such as cyanine dyes (typically represented as cationic polymethine dyes terminated with nitrogen atoms), have several properties which make them interesting materials to use in nonlinear optical devices. The symmetry of the dye results in the hybrid resonance structure which has a bond-order alternation of 1.5 (BLA = 0). Several crystal structures

of cyanine dyes have confirmed that polymethine dyes have zero BLA.[58] Zero BLA results in the theoretical negative maximum of Re(γ). Polymethine dyes of relatively long conjugation length generally have large M_{ge} and small E_{ge} which are linear optical properties that should be optimized to obtain large γ according to E1.18. Finally, narrow absorption bands allow interrogating pump and probe signals to operate with small detuning from the band edge allowing for potential resonance enhancement without incurring large linear absorption losses. A more in depth discussion of the properties of polymethine dyes is discussed in chapter 3.

Hermann studied the dependence of γ on chain length in cyanines using THG as early as 1974.[59] A strong power law dependence on the number of double bonds was observed, resulting in values up to ~2×10^{-30} esu for the longest compound (Table 1.4, entry 1). Subsequently Matsumoto *et al.*[60] incorporated the same dye into films. Films of sodium polystyrene sulfonate with different doping levels by weight percent of dye (as high as 50%) were cast using the spin coating technique from an acetic acid/water solution. The $\chi^{(3)}$ was measured for the films using the THG technique at various wavelengths, including 1.9 μm, at which the maximum $\chi^{(3)}$ value was obtained (2×10^{-11}). The magnitude of $\chi^{(3)}$ increased linearly with the percent of doping with chromophore until ~50%, at which point a deviation occurred. The deviation was most likely caused by aggregation.

Wernke *et al.*[61] studied the linear and nonlinear optical properties of simple bis(dimethylamino) methine dyes (BDMA dye, Table 1.4, entry 2) and a more complex benzothiazole dye (BT dye, Table 1.4, entry 3) series. The BDMA series showed similar absorption band shapes for increasing chain lengths with a typical ~100 nm bathochromic

shift in λ_{max} for each additional vinylene group.[27] The BT series showed a similar trend for dyes of relatively short conjugation length, but the trend broke down at longer conjugation lengths. Dyes of longer conjugation length showed significantly broader absorption bands than typical short-chain cyanines. The broadened absorption spectra could be representative of the onset of symmetry breaking.

Symmetry breaking is a result of the localization of the charge, leading to imperfections in the delocalization of π-electrons and subsequent non-zero BLA. Now, the polyene-like molecule would have one of the two extreme resonance forms dominating the ground state distribution of bonds, leading to the formation of long and short bonds in the polymethine chain much like Peierls distortion in polyacetylene.[62]

Early models proposed by Dähne and Redaglia predicted there would be no band gap for polymethines of infinite chain length, resulting in metallic behavior.[63] However, more recent theoretical work predicted that polymethines of long chain length (30 carbon atoms) would have an asymmetric ground state, thus being non-convergent (they will not show metallic behavior upon lengthening).[64] A polymethine of infinite chain length can be put in perspective when comparing it to polyacetylene, which was described in a previous section to be a bond-alternant system with non-convergent band edges. Upon doping of the polymer, the charged centers formed (solitons) have been theoretically found to be localized centers ~spanning 30 carbons, which have equivalent bond lengths throughout the geometrical defect.[65]

Tolbert *et al.*[66] studied symmetry breaking behavior in long chain (n = 4 and 6) polymethine dyes of type **1.I** (Figure 1.15). Experimental evidence for charge localization in the longer dyes (n = 4 and 6) was given by comparison of UV-vis.-NIR

spectra of the shorter symmetrical (n = 0, 1, 2) dyes. The longer dyes were shown to have broad absorption bands compared to the shorter analogues. The longest dye (n = 6) was shown to have pronounced solvatochromic behavior, indicating the dye may have had more D-π-A type charge-transfer upon excitation. These results have led others to draw comparisons between these chromophores[66, 67] with Robin-Day class II mixed valence systems (a two minimum potential surface, with degenerate ground state energies), while a typical cyanine was considered to be analogous to a class III system (one minimum on the potential surface).[68]

The Robin-Day classification system uses two key parameters: electronic coupling between the extreme localized structures (V) and the reorganization energy of Marcus theory (λ). The reorganization energy in polymethine dyes is attributed to the sense of bond-length alternation of the bridge, and the end groups. Barlow *et al.*[67, 69] choose to use metallocene endgroups of type **1.II** (Figure 1.15), to investigate the dependence of the type of endgroup and the reorganization energy involved, which could lead to symmetry breaking. The crystal structure of the ruthenacene-terminated dye was obtained showing the first evidence of symmetry breaking in the solid state, which was attributed to the strong interaction of the α-carbon of the polymethine bridge and the metal center (η^6-fulvene-ruthenium).[69]

Lepkowicz *et al.*[70] studied the linear optical and excited-state absorption properties of the short (Figure 1.15, **1.III**) and long (Figure 1.15, **1.IV**) versions of benzothiazole terminated dyes. The linear optical properties of **1.III** were consistent with typical cyanines in that the absorption spectrum consisted of a sharp long wavelength absorbing peak, which showed little dependence on the polarity of the solvent (ranging

from low polarity (*ortho*-dichlorobenzene) to high polarity (methanol)). Similar behavior was observed for a series of thiopyrylium terminated dyes studied by Kachkovski *et al.* (Figure 1.15, **1.V**).[71] The low energy band (~1000 nm) of **1.IV** showed little dependence on the solvent polarity either; however, as the polarity of the solvent increased a broad absorption band appeared at ~800 nm. The existence of the two absorption bands was hypothesized to be both the symmetric dye and the symmetry broken dye in solution. Pump-probe experiments were used to determine if the hypothesis was correct. In two separate experiments the low energy band (~1000 nm) and the higher energy broad band (~800 nm) were pumped, while the probe was used to determine the saturation of the two peaks. **1.IV** was found to have both symmetric and asymmetric forms in polar solvents (CH_3CN).

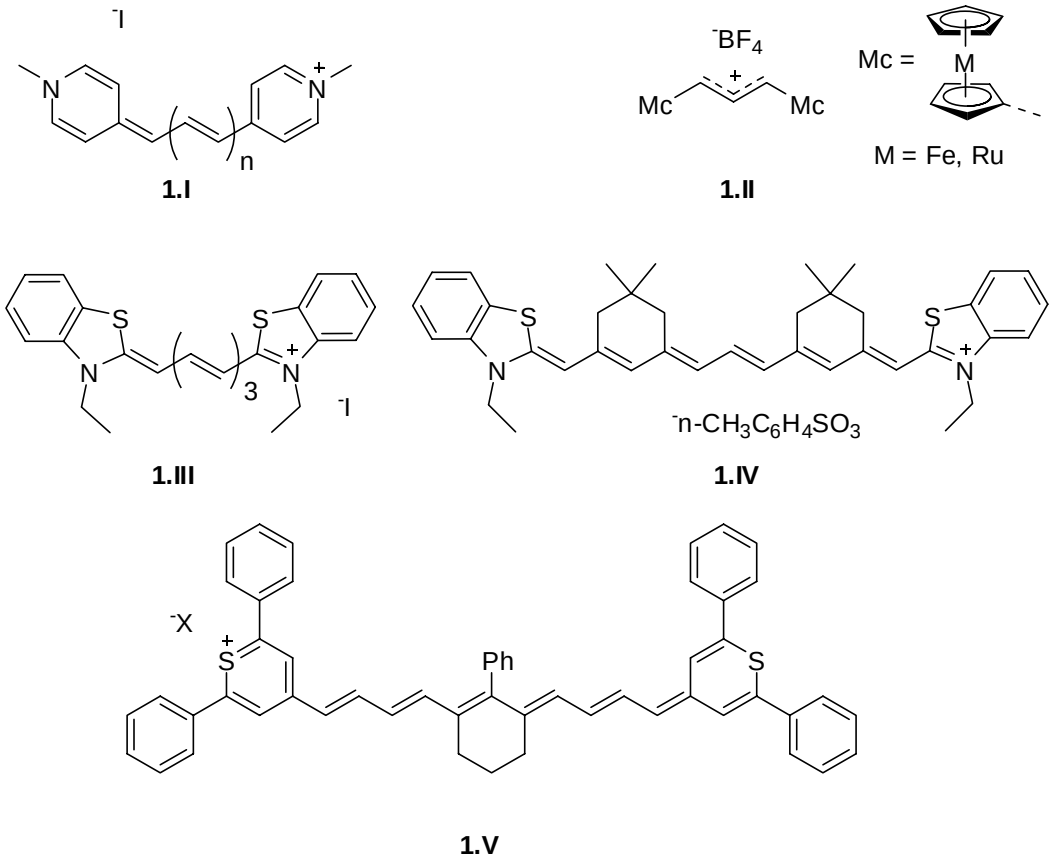

Figure 1.15. Symmetric polymethine systems studied for symmetry breaking properties in the literature.[66, 67, 69-71]

As the conjugation length of a polymethine dye increases, Re(γ) is generally found to increase with a steep power law dependence.[59, 72, 73] Pierce[74] showed theoretically that the absolute value of the nonresonant π-electron component of the third-order polarizability ($|\gamma_\pi|$) will increase more rapidly with conjugation length than polyenes. Plotting the number of π-electrons, N, against $|\gamma_\pi|$ led to a power law dependence of N^8, compared to polyenes with a power law dependence of N^4. Polyenes have indeed been shown experimentally to have power law dependencies of $N^{\sim 4}$.[57] Wernke *et al.*[61] investigated γ values for dyes in the BDMA and BT series, which were extrapolated from coherent anti-Stokes Raman scattering (CARS), and showed a steep

increase in magnitude as the conjugation length increased. The BT series has larger γ values than the BDMA dyes when relatively short chain lengths are compared with the same number of π-electrons in the bridge. This increase in γ is most likely due to larger transition dipoles for the BT series (important according to E1.18) as a result of the increased conjugation of the BT series extending from the central core of the dye.

Thorley *et al.*[75] synthesized a porphyrin terminated dye with the structure shown as entry 4 in Table 1.4. This porphyrin terminated dye exhibited cyanine-like behavior, even though it did not contain a bridge fragment composed of conjugated methine units.[76] The dye showed strong absorption at 1243 nm. Extremely large Re(γ) values were measured for the dye using the Z-scan technique at 1550 nm. Another significant feature was the ratio of the Re(γ) to Im(γ) (-20×10^{-32} and 4.5×10^{-32} esu, respectively). The favorable ratio of Re(γ)/Im(γ) suggested these systems could be promising materials for AOSP.

Hales *et al.*[77] reported the synthesis and characterization of a bis(dioxaborine)-terminated nonamethine dye (Table 1.4, entry 5). It exhibited very large, predominantly real, γ values in the telecommunications bands (real and imaginary parts are -5.7×10^{-32} and 7.9×10^{-33} esu, respectively, at 1.3 μm), and was fabricated into amorphous films that exhibited correspondingly large $\chi^{(3)}$ (real and imaginary parts are -3.6×10^{-10} and 3.8×10^{-11} esu, respectively, at 1.3 μm).[77] Even though the magnitude of the Re(γ) is smaller than that of the previously mentioned porphyrin dye, the ratio between Re(γ) and Im(γ) (and similar for $\chi^{(3)}$) is more favorable, suggesting this as a promising material for AOSP.

Table 1.4. Selected polymethine materials of which the third-order nonlinearity has been measured.					
Entry	Chemical	λ_I (nm)	γ (10^{-32} esu)	$\lvert\chi^{(3)}\rvert$ (esu)	method
1	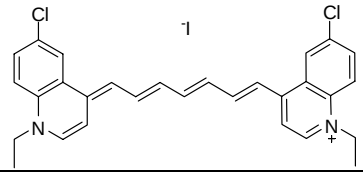	1890	-19	2×10^{-11} (50% loading)	THG
2	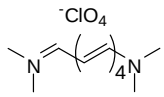	-	-0.08 (Re(γ_{static}))	-	CARS
3	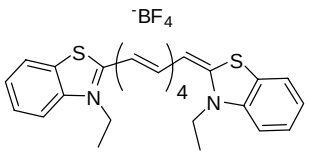	-	-0.07 (Re(γ_{static}))	-	CARS
4	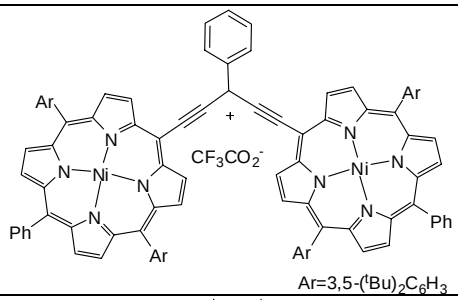	1550	-20.5	-	Z-scan
5	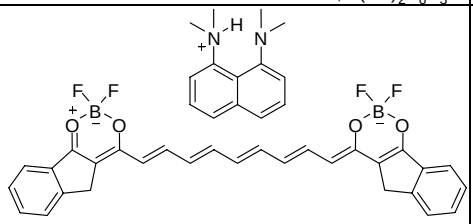	1300	-5.7	3.6×10^{-10}	DFWM and Z-Scan

1.7. Organization of the Thesis

A general introduction to $\chi^{(3)}$ materials and their use in AOSP has been presented. The specific projects detailed in chapters 2-5 predominantly involve the rational design, synthesis and third-order characterization of novel polymethine dyes for AOSP applications. More focused literature discussions pertaining to aspects of the specific project areas of this thesis will be presented as necessary. In addition to specific background information, each chapter will include experimental details, results, and a

discussion of the results. Chapter 2 will discuss the synthesis of dioxaborine-terminated polymethine dyes with various degrees of conjugation and the effects of conjugation length on γ. Chapter 3 will discuss the investigation of the effects of electron donating and electron accepting groups in the bridge of dioxaborine terminated polymethine dyes. Investigations involving the γ properties of anionic polymethine dyes with various terminal groups are discussed in chapter 4. The structure-property relationships of pyrylium terminated polymethine dyes are discussed in chapter 5. Chapter 6 discusses the use of several heavy atom containing polymethine dyes and their potential use in optical limiting applications. Finally, general statements regarding these results and potential future directions will be discussed in chapter 7.

1.8. References

1. Gowar, J., *Optical Communication Systems*. Second Edition ed.; Prentice Hall International (UK) Ltd: 1993.
2. Salib, M.; Liao, L.; Jones, R.; Morse, M.; Liu, A.; Samara-Rubio, D.; Alduino, D.; Paniccia, M., Silicon Photonics. *Intel Technol. J.* **2004,** 8, (2), 143-160.
3. Snell's law relates the refractive index of two optical medium and the angle of refraction as the light changes from one medium to the other. The law is summarized in the following equation:

$$n_1 \times \sin(\theta_1) = n_2 \times \sin(\theta_2)$$

Where the values correspond to variables defined in the following figure:

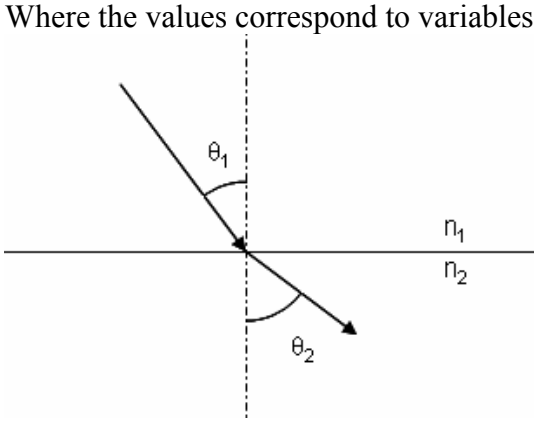

4. Suchoski Jr., P. G.; Leonberger, F. J., Commercialization of Lithium Niobate Modulators. In *Integrated Optical Ciruits and Components: Design and applications*, Murphy, E. J., Ed. Marcel Dekker, Inc: New York, 1999; pp 9-19.

5. Brédas, J. L.; Adant, C.; Tackx, O.; Persoons, A.; Pierce, B. M., Third-Order Nonlinear Optical Response in Organic Materials: Theoretical and Experimental Aspects. *Chem. Rev.* **1994,** 94, 243-278.
6. Hales, J. M.; Perry, J. W., 3rd-Order Nonlinear Optical Materials and Device Applications. In *Introduction to Organic Electronic and Optoelectronic Materials and Devices*, Sun, S.-S.; Dalton, L., Eds. CRC Press: Orlando, 2008; pp 521-579.
7. Lorentz, H. A., *The Theory of Electrons and its Applications to the Phenomena of Light and Radient Heat*. 2nd ed. ed.; Dover Publications: New York, 1952.
8. Decibels are a logarithmic unit used to measure the ratio between an input versus an output. In the case of optical losses, input light intensities are related to output light intensities through the following equation:

$$L = 10 \times \log(\frac{I_{output}}{I_{input}})$$

Three decibels is an important number because this signifies a loss (or splitting of the intensity) by 50%.
9. Lipson, M., Guiding, Modulating, and Emitting Light on Silicon - Challenges and Opportunities. *J. Lightwave Technol.* **2005,** 23, 4222-4238.
10. Dalton, L., Organic electro-optic materials. *Pure Appl. Chem.* **2004,** 76, 1421-1433.
11. Lee, M.; Katz, H. E.; Erben, C.; Gill, D. M.; Gopalan, P.; Heber, J. D.; McGee, D. J., Broadband Modulation of Light by Using an Electro-Optic Polymer. *Science* **2002,** 298, 1401-1403.
12. Mizrahi, V.; DeLong, K. W.; Stegeman, G. I., Two-photon absorption as a limitation to all-optical switching. *Opt. Lett.* **1989,** 14, 1140-1142.
13. Stegeman, G. I.; Stolen, R. H., Waveguides and figures for nonlinear optics. *J. Opt. Soc. of Am. B: Opt. Phys.* **1989,** 6, 652-662.
14. Stegeman, G. I., Material figures of merit and implications to all-optical waveguide switching. *Proc. SPIE Int. Soc. Opt. Eng.* **1993,** 1852, 75-89.
15. Kim, K. S.; Stolen, R. H.; Reed, W. A.; Quoi, K. W., Measurement of the nonlinear index of silica-core and dispersion-shifted fibers. *Opt. Lett.* **1994,** 19, 257-259.
16. Heebner, J. E.; Boyd, R. W., Enhanced all-optical switching by use of a nonlinear fiber ring resonator. *Opt. Lett.* **1999,** 24, 847-849.
17. Gibbs, H. M.; McCall, S. L.; Venkatesan, T. N. C.; Gossard, A. C.; Passner, A.; Wiegmann, W., Optical Bistability in Semiconductors. *Appl. Phys. Lett.* **1979,** 35, 451-453.
18. Van Stryland, E. W.; Wu, Y. Y.; Hagan, D. J.; Soileau, M. J.; Mansour, K., Optical Limiting with Semiconductors. *J. Opt. Soc. Am. B: Opt. Phys.* **1988,** 5, 1980-1988.
19. Said, A. A.; Sheik-Bahae, M.; Hagan, D. J.; Wei, T. H.; Wang, J.; Young, J.; Van Stryland, E. W., Determination of bound-electronic and free-carrier nonlinearities in ZnSe, GaAs, CdTe and ZnTe. *J. Opt. Soc. Am. B: Opt. Phys.* **1992,** 9, 405-414.
20. Dinu, M.; Quochi, F.; Garcia, H., Third-order nonlinearities in silicon at telecom wavelengths. *Appl. Phys. Lett.* **2003,** 82, 2954-2956.
21. Van, V.; Ibrahim, T. A.; Ritter, K.; Absil, P. P.; Johnson, F. G.; Grover, R.; Goldhar, J.; Ho, P.-T., All-Optical Nonlinear Swiching in GaAs-AlGaAs Microring Resonators. *IEEE Photonics Technol. Lett.* **2002,** 14, 74-76.

22. Liu, A.; Jones, R.; Liao, L.; Samara-Rubio, D.; Rubin, D.; Cohen, O.; Nicolaescu, R.; Paniccia, M., A high-speed silicon optical modulator based on a metal-oxide-semiconductor capacitor. *Nature* **2004,** 427, 615-618.
23. Almeida, V. R.; Barrios, C. A.; Panepucci, R. R.; Lipson, M., All-optical control of light on a silicon chip. *Nature* **2004,** 431, 1081-1084.
24. Koos, C.; Vorreau, P.; Vallaitis, T.; Dumon, P.; Bogaerts, W.; Baets, R.; Esembeson, B.; Biaggio, I.; Michinobu, T.; Diederich, F.; Freude, W.; Leuthold, J., All-optical high-speed signal processing with silicon-organic hybrid slot waveguides. *Nat. Photonics* **2009,** 3, 216-219.
25. Nalwa, H. S., Organic Materials for Third-Order Nonlinear Optics. In *Nonlinear Optics of Organic Molecules and Polymers*, Nalwa, H. S.; Miyata, S., Eds. CRC Press: Boca Raton, 1997; pp 611-797.
26. Brédas, J.-L.; Street, G. B., Polarons, Bipolarons, and Solitons in Conducting Polymers. *Acc. Chem. Res.* **1985,** 18, 309-315.
27. Heeger, A. J.; Moses, D.; Sinclair, M., Semiconducting Polymers: Fast Response Nonlinear Optical Materials. *Synth. Met.* **1986,** 15, 95-104.
28. Karpfen, A.; Petkov, J., Ab Initio Studies on Polymers. II. All-trans Polyene. *Theo. Chim. Acta* **1979,** 53, 65-74.
29. Halvorson, C.; Hagler, T. W.; Moses, D.; Cao, Y.; Heeger, A. J., Conjugated polymers with degenerate ground state. *Chem. Phys. Lett.* **1992,** 200, 364-368.
30. Halvorson, C.; Wu, R.; Moses, D.; Wudl, F.; Heeger, A. J., Third Harmonic spectra. *Chem. Phys. Lett.* **1993,** 212, 85-89.
31. Marder, S. R.; Perry, J. W.; Klavetter, F. L.; Grubbs, R. H., Third-Order Susceptibilities of Soluble Polymers Derived from the Ring-Opening Metathesis Copolymerization of Cyclooctatetraene and 1,5-cyclooctadiene. *Chem. Mater.* **1989,** 1, 171-173.
32. Chi, S.-H.; Hales, J. M.; Fuentes-Hernandez, C.; Tseng, S.-Y.; Cho, J.-Y.; Odom, S. A.; Zhang, Q.; Barlow, S.; Schrock, R. R.; Marder, S. R.; Kippelen, B.; Perry, J. W., Thick Optical-Quality Films of Substituted Polyaceylenes with Large, Ultrafast Third-Order Nonlinearities and Application to Image Correlation. *Adv. Mater.* **2008,** 20, 3199-3203.
33. Dorsinville, R.; Yang, L.; Alfano, R. R.; Zamboni, R.; Danieli, R.; Ruani, G.; Taliani, C., Nonlinear-Optical Response in Polythiophene Films Using Four-Wave Mixing Techniques. *Opt. Lett.* **1989,** 14, 1321-1323.
34. Okawa, H.; Wada, T.; Yamada, A.; Sasabe, H., Third-Order Optical Nonlinearity of Soluble Polythiophenes. *Mat. Res. Soc. Symp. Proc.* **1991,** 214, 23-28.
35. Torruellas, W. E.; Neher, D.; Zanoni, R.; Stegeman, G. I.; Kajzar, F.; Leclerc, M., Dispersion Measurements of the Third-Order Nonlinear Susceptibility of Polythiophene Thin Films. *Chem. Phys. Lett.* **1990,** 175, 11-16.
36. Bloor, D.; Chance, R. R., *Polydiacetylenes: Synthesis, Structure and Electronic Properties*. Martinus Nijhoff Publishers: Dordrecht, 1985.
37. Suteret, C.; Hermann, J.-P.; Frey, R.; Padère, F.; Ducuing, J.; Baughman, R. H.; Chance, R. R., Optical Nonlinearities in One-Dimensional–Conjugated Polymer Crystals. *Phys. Rev. Lett.* **1976,** 36, 956-959.
38. Lequime, M.; Hermann, J.-P., Reversible Creation of Defects by Light in One Dimensional Conjugated Polymers. *Chem. Phys.* **1977,** 26, 431-437.

39. Polyakov, S.; Yoshino, F.; Liu, M.; Stegeman, G., Nonlinear refraction and multiphoton absorption in polydiacetlenes from 1200-2200 nm. *Phys. Rev. B: Condens. Matter* **2004,** 69, 115421-1-115421-11.
40. Kanetake, T.; Ishikawa, K.; Hasegawa, T.; Koda, T.; Takeda, K.; Hasegawa, M.; kubodera, K.; Kobayashi, H., Nonlinear Optical Properties of Highly Oriented Polydiacetylene Evaporated Films. *Appl. Phys. Lett.* **1989,** 54, 2287-2289.
41. Bradley, D. D. C.; Mori, Y., Third Harmonic Generation in Precursor Route Poly(*p*-Phenylene Vinylene). *Jpn. J. of Appl. Phys.* **1989,** 28, 174-177.
42. Kurihara, T.; Mori, Y.; Kaino, T.; Murata, H.; Yakada, N.; Tsutsui, T.; Saito, S., Spectra of $\chi^{(3)}$ (-3ω; ω, ω, ω) in Poly(2,5-dimethoxy *p*-phenylene vinylene) (MO-PPV) for various conversion levels. *Chem. Phys. Lett.* **1991,** 183, 534-538.
43. McBranch, D.; Sinclair, M.; Heeger, A. J.; Patil, A. O.; Shi, S.; Askari, S.; Wudl, F., Linear and Nonlinear Optical Studies of Poly(p-Phenylene Vinylene) Derivatives and Polydiacetylene-4BCMU. *Synth. Met.* **1989,** 29, E85-E90.
44. Moon, Y. B.; Rughooputh, S. D. D. V.; Heeger, A. J.; Patil, A. O.; Wudl, F., X-Ray Scattering Study of The Conversion of Poly(p-Phenylene Vinylene Precursor to the Conjugated Polymer. *Synth. Met.* **1989,** 29, E79-E84.
45. Bahtiar, A.; Koynov, K.; Mardiyati, Y.; Hörhold, H.-H.; Bubeck, C., Slab Waveguide of Poly(p-Phenylenevinylene)s for All-Optical Switching: Impact of Side-Chain Substitution. *J. Mater. Chem.* **2009,** 19, 7490-7497.
46. Kuhn, H., A Quantum-Mechanical Theory of Light Absorption of Organic Dyes and Similar Compounds. *J. Chem. Phys.* **1949,** 17, 1198-1212.
47. de La Torre, G.; Vázquez, P.; Agulló-López, F.; Torres, T., Role of Structural Factors in the Nonlinear Optical Properties of Phthalocyanines and Related Compounds. *Chem. Rev.* **2004,** 104, 3723-3750.
48. Gorman, C. B.; Marder, S. R., An Investigation of the Interrelationships Between Linear and Nonlinear Polarizabilities and Bond-Length Alternation in Conjugated Organic Molecules. *PNAS* **1993,** 90, 11297-11301.
49. Bourhill, G.; Brédas, J.-L.; Cheng, L.-T.; Marder, S. R.; Meyers, F.; Perry, J. W.; Tiemann, B. G., Experimental Demonstration of the Dependence of the First Hyperpolarizability of Donor-Acceptor-Substituted Polyenes on the Ground-State Polarization and Bond Length Alternation. *J. Am. Chem. Soc.* **1994,** 116, 2619-2620.
50. Marder, S. R.; Gorman, C. B.; Meyers, F.; Perry, J. W.; Bourhill, G.; Brédas, J.-L.; Pierce, B. M., A Unified Description of Linear and Nonlinear Polarization in Organic Polymethine Dyes. *Science* **1994,** 265, 632-635.
51. Lu, D.; Chen, G.; Perry, J. W.; Goddard, W. A. I., Valence-Bond Charge-Transfer Model fro Nonlinear Optical Properties of Charge-Transfer Organic Molecules. *J. Am. Chem. Soc.* **1994,** 116, 10679-10685.
52. Bond length alternation is defined as the difference between the long and short bonds of a conjugated molecule as follows:
$BLA = R_{long} - R_{short}$
The BLA can be useful to determine the extent of π-electron delocalization, where a small value is highly delocalized (aromatic) and a large value indicates localization (non-aromatic).

53. Marder, S. R.; Perry, J. W.; Bourhill, G.; Gorman, C. B.; Tiemann, B. G.; Mansour, K., Relation Between Bond-Length Alternation and Second Electronic Hyperpolarizability of Conjugated Organic Molecules. *Science* **1993,** 261, (5118), 186-189.
54. Meyers, F.; Marder, S. R.; Pierce, B. M.; Bredas, J. L., Electric-Field Modulated Nonlinear-Optical Properties of Donor-Acceptor Polyenes - Sum-over-States Investigation of the Relationship between Molecular Polarizabilities (Alpha, Beta, and Gamma) and Bond-Length Alternation. *J. Am. Chem. Soc.* **1994,** 116, (23), 10703-10714.
55. Marder, S. R.; Torruellas, W. E.; Blanchard-Desce, M.; Ricci, V.; Stegeman, G. I.; Gilmour, S.; Brédas, J.-L.; Li, J.; Bublitz, G. U.; Boxer, S. G. B., Large Molecular Third-Order Optical Nonlinearities in Polarized Carotenoids. *Science* **1997,** 276, 1233-1236.
56. Haas, K.-H.; Ticktin, A.; Esser, A.; Fisch, H.; Paust, J.; Schrof, W., Chi(3) Dispersion Measurements of the Conjugation Length Dependence of Carotenoid Derivatives. *J. Phys. Chem.* **1993,** 97, 8675-8677.
57. Puccetti, G.; Blanchard-Desce, M.; Ledoux, I.; Lehn, J.-M.; Zyss, J., Chain-Length Dependence of the Third-Order Polarizability of Disubstituted Polyenes. *J. Phys. Chem.* **1993,** 97, 9385-9391.
58. Smith, D. L., Structure of Dyes and Dye Aggregates - Evidence from Crystal Structure Analysis. *Photographic Science and Engineering* **1974,** 18, 309-322.
59. Hermann, J.-P., Non-Linear Susceptibilities of Cyanine Dyes. Application to Frequency Tripling. *Opt. Commun.* **1974,** 12, 102-104.
60. Matsumoto, S.; Kubodera, K.-i.; Kurihara, T.; Kaino, T., Third-Order Nonlinar Optical Properties of Cyanine Dyes and Polymer Films Containing these Dyes. *Opt. Commun.* **1990,** 76, 147-150.
61. Werncke, W.; Pfeiffer, M.; Johr, T.; Lau, A.; Grahn, W.; Johannes, H.-H.; Dähne, L., Increase and saturation of the third order hyperpolarizabilities in homologous series of symmetric cyanines. *Chem. Phys.* **1997,** 216, 337-347.
62. Peierls, R. E., *Quantum Theory of Solids*. OUP: Oxford, 1955.
63. Dähne, S.; Radeglia, R., Revision Der Lewis-Calvin-Regel Zur Charakterisierung Vinyloger. Polyen- Und Polymethinahnlicher Verbindungen. *Tetrahedron* **1971,** 27, 3673-3693.
64. Kuhn, C., Step Potential Model for Nonlinear Optical Properties of Polyenes, Push-Pull Polyenes and Cyanines and the Motion of Solutions in Long-Chain Cyanines. *Synth. Met.* **1991,** 41-43, 3681-3688.
65. Craw, J. S.; Reimers, J. R.; Bacskay, G. B.; Wong, A. T.; Hush, N. S., Solitons in finite- and infinite-length negative-defect trans-polyacetlyene and the corresponding Brooker (polymethinecyanine) cations. I. Geometry. *Chem. Phys.* **1992,** 167, 77-99.
66. Tolbert, L. M.; Zhao, X., Beyond the Cyanine Limit: Peierls Distortion and Symmetry Collapse in a Polymethine Dye. *J. Am. Chem. Soc.* **1997,** 119, 3253-3258.
67. Barlow, S.; Henling, L. M.; Day, M. W.; Schaefer, W. P.; Green, J. C.; Hascall, T.; Marder, S. R., Metallocene-Terminated Allylium Salts: The Effect of End Group on Localization in Polymethines. *J. Am. Chem. Soc.* **2002,** 124, 6285-6296.
68. Robin, M. B.; Day, P., Mixed Valence Chemistry - A Survey and Classification. In *Advances in Inorganic Chemistry and Radiochemistry*, Emeléus, H. J.; Sharpe, A. G., Eds. Academic Press: New York and London, 1967; Vol. 10, pp 247-422.

69. Barlow, S.; Henling, L. M.; Day, M. W.; Marder, S. R., Effect of the End-Groups Upon Delocalisation in Polymethines: the First Crystallographically Characterised Bond-Alternated Cyanine. *Chem. Commun.* **1999**, 1567-1568.
70. Lepkowicz, R. S.; Przhonska, O. V.; Hales, J. M.; Fu, J.; Hagan, D. J.; Van Stryland, E. W.; Bondar, M. V.; Slominsky, Y. L.; Kachkovski, A. D., Nature of the Electronic Transitions in Thiacarbocyanines with a Long Polymethine Chain. *Chem. Phys.* **2004,** 305, 259-270.
71. Kachkovski, O. D.; Tolmachov, O. I.; Slominskii, Y. L.; Kudinova, M. O.; Derevyanko, N. O.; Zhukova, O. O., Electronic Properties of Polymethine Systems 7: Soliton Symmetry Breaking and Specral Features of Dyes with Long Polymethine Chain. *Dyes Pigm.* **2005,** 64, 207-216.
72. Johr, T.; Werncke, W.; Pfeiffer, M.; Lau, A.; Dähne, L., Third-order Nonlinear Polarizabilities of a Homologous Series of Symmetric Cyanines. *Chem. Phys. Lett.* **1995,** 246, 521-526.
73. Albert, I. D. L.; Das, P. K.; Ramasesha, S., Optical Nonlinearities in Symmetric Cyanine Dyes and Related Systems. *J. Opt. Soc. Am. B.* **1993,** 10, 1365-1371.
74. Pierce, B. M., A Theoretical Analysis of the Third-Order Nonlinear Optical Properties of Linear Cyanines and Polyenes. *Proc. SPIE Int. Soc. Opt. Eng.* **1991,** 1560, 148-161.
75. Thorley, K. J.; Hales, J. M.; Anderson, H. L.; Perry, J. W., Porphyrin Dimer Carbocations with Strong Near Infrared Absorption and Third-Order Optical Nonlinearity. *Angew. Chem. Int. Ed.* **2008,** 47, 7095-7098.
76. Ohira, S.; Hales, J. M.; Thorley, K. J.; Anderson, H. L.; Perry, J. W.; Brédas, J.-L., A new class of cyanine-like dyes with large Bond-Length Alternation. *J. Am. Chem. Soc.* **2009,** 131, 6099-6101.
77. Hales, J. M.; Zheng, S.; Barlow, S.; Marder, S. R.; Perry, J. W., Bisdioxaborine Polymethines with Large Third-Order Nonlinearities for All-Optical Signal Processing. *J. Am. Chem. Soc.* **2006,** 128, 11362-11363.

Chapter 2

Dioxaborine-Terminated Polymethine Dyes

2.1. Introduction

Several derivatives of dioxaborine-terminated dyes were synthesized. The first series (Section 2.2) investigated the film forming properties of nonamethine dyes with various terminal groups. Section 2.3 examined the structure-property relationship between the extent of conjugation in the post-termini position of six pentamethine dyes and the linear and nonlinear optical properties. Increased extended conjugation was expected to reduce the transition energy and increase the transition dipole moment, both being changes expected to increase Re(γ).

2.1.1. Introduction and Background

Many enolizable 1,3-dicarbonyl compounds (*i.e.*, β-diketones) can be condensed with boronic acid complexes to give 1,3,2-dioxaborines. Condensation of 1,3-dicarbonyl compounds with boron trifluoride or its complexes gives stable diketoboronates known as 2,2-difluoro-1,3,2-dioxaborines. Meerwein *et al.*[1] used 2,2-difluoro-1,3,2-dioxaborine intermediates to synthesize 1,3-dicarbonyls from esters in which normal Claisen-type reactions could not be performed owing to base sensitivity of the starting materials. The condensation was performed between the enol and acetic anhydride in the presence of boron trifluoride. Young *et al.*[2] and Hauser *et al.*[3] proposed a mechanism to convert enol-esters into β-diketones through the use of BF_3 and acetic anhydride. A key intermediate was the 2,2-difluoro-1,3,2-dioxaborine. A similar mechanism (based upon that proposed for the conversion of enol-esters) is shown in Scheme 2.1 for the reaction between a ketone, acetic anhydride and two equivalents of BF_3.

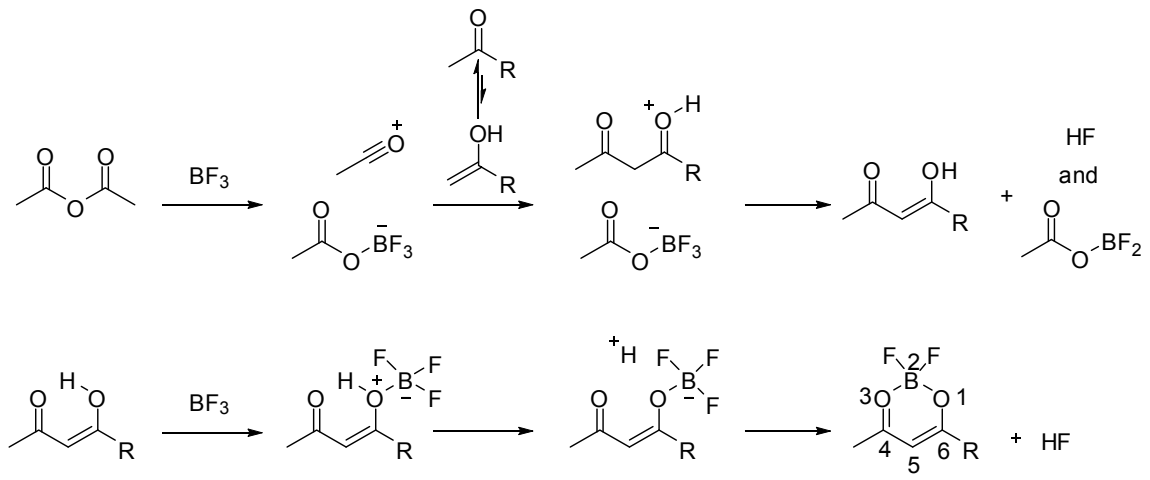

Scheme 2.1. Mechanism for the synthesis of a general 2,2-difluoro-1,3,2-dioxaborine.

The reactivity of 1,3-dicarbonyls and 2,2-difluoro-1,3,2-dioxaborines (with one degree or two degree alkyl groups in the 4 and 6 positions) are quite different as indicated by Halik *et al.*[4] Scheme 2.2 shows the reactivity of a 1,3-dicarbonyls and a 2,2-difluoro-1,3,2-dioxaborine after the loss of an acidic proton. The most acidic proton of the 1,3-dicarbonyl is between both carbonyl groups (or the –O-H in the enol form), while the methyl group of the 2,2-difluoro-1,3,2-dioxaborine has the most acidic proton. The reaction of the conjugate base of each compound with aldehyde derivatives results in different substitution products as shown. The proposed structure of the intermediate, the conjugate base of 2,2-difluoro-1,3,2-dioxaborine, results from an activated methyl group, which can react with functional groups that can extend the overall conjugation pathway of the π-electrons.[5-7]

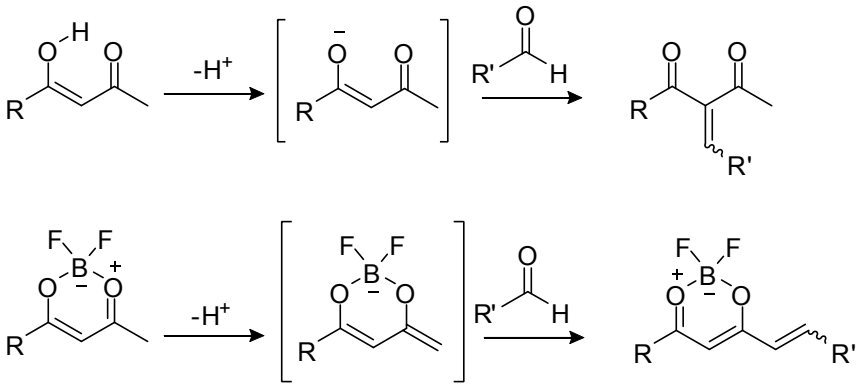

Scheme 2.2. Reaction schemes of 1,3-dicarbonyl (top) and 2,2-difluoro-1,3,2-dioxaborine (bottom) with an aldehyde derivative.

2,2-difluoro-1,3,2-dioxaborine (This name will be shortened to dioxaborines for the remainder of this chapter) have attracted attention in previous studies as strong π-electron accepting groups in D-π-A chromophores.[8] Figure 2.1 shows three D-π-A chromophores synthesized by VanAllan *et al.*[5] The λ_{max} associated with the charge transfer band, increases from **2.I** (428 nm in CH_3CN) to **2.II** (570 nm in CH_3CN) as the conjugation length was increased. A similar D-π-A chromophore with the widely used 4,5,5-trimethyyl-3-cyano2(5H)-furanylidenepropanedinitrile (the so-called TCF) acceptor (**2.IIIb**) has a bathochromically shifted absorption maximum (588 nm in $CHCl_3$)[9] to dioxaborine containing D-π-A chromophore **2.IIIa** (530 nm in $CHCl_3$),[8] which indicates dioxaborines are typically not as strong of π-electron acceptors as TCF.

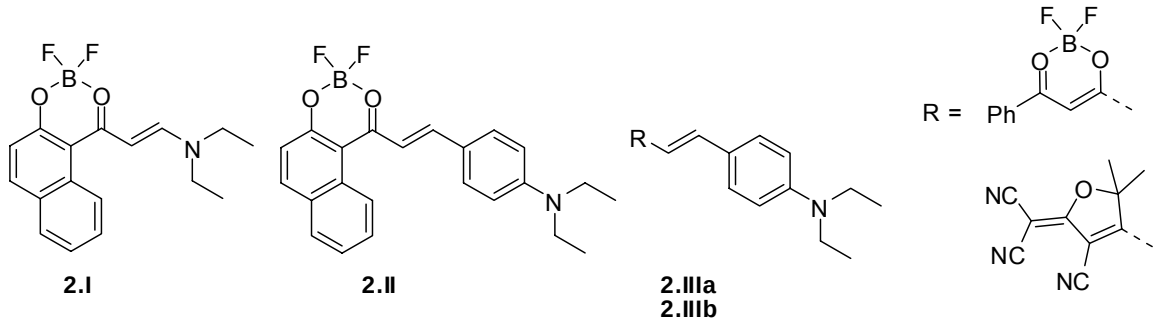

Figure 2.1. D-π-A chromophores in the literature.[5, 8, 9]

Several compounds in which two dioxaborines bridged by various conjugated π-systems have been investigated regarding mixed valence anions[10], electron-transport properties[11], and two-photon absorption properties[12]. These studies demonstrate dioxaborines are strong electron acceptors in both the electron transfer sense (*i.e.*, dioxaborine materials are easily reduced) and as π-acceptors (i.e., they effectively couple to π -systems through the four and (or) six positions (See bottom right structure of Scheme 1.1 for numbering) and withdraw electron density). **2.IV** (Figure 2.2) was shown to have two reversible reductions at moderate potentials (Cyclic voltammetry in CH_3CN with 0.1 M [$^nBu_4N$][PF_6] reveals two reversible reductions at -970 and -1180 mV versus ferrocenium—ferrocene), in which the first reduction corresponded to a system with complete delocalization of the charge between the two sites (Robin and Day Class III system).[10] The electron-transport properties of **2.V** and **2.VI** (Figure 2.2) were measured by Domercq *et al.*[11] Time-of-flight measurements indicated that **2.VI** has electron mobility up to two orders of magnitude higher than tris(8-hydroxyquinolate)aluminum (AlQ_3), a commonly used electron-transport material. Halik *et al.*[12] showed that A-π-A chromophores can also have moderate two-photon absorption cross sections, for example in CH_2Cl_2 chromophore **2.II** has a two-photon absorption peak at *ca.* 612 nm

characterized by a cross section (δ_{max}) of 490 GM. Cogné-Laage *et al.*[13] explored substituted dioxaborines of the general structure, **2.VII,** to be used *in vivo* as fluorescent labels. The two-photon absorption peaks were characterized by cross sections ranging from <5 to 200 GM in the near-IR region.

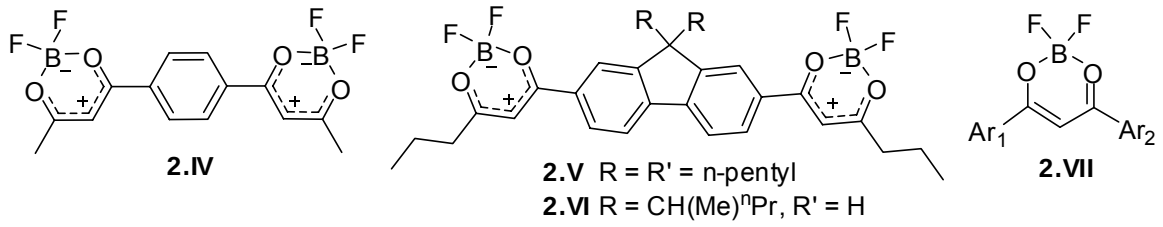

Figure 2.2. Chromophores, **2.IV-2.VII**, found in the literature.[10-13]

As strong π-accepting groups with a large amount of internal conjugation, dioxaborines are candidates for terminal groups of anionic polymethine chromophores. The active methyl positions allow the acceptor to readily undergo the Knoevenagel condensation with a simple polymethine dye. Indeed, several polymethine dyes with dioxaborine terminal groups can be found in the literature. Trimethines **2.VIII-2.XV** are shown in Figure 2.3.

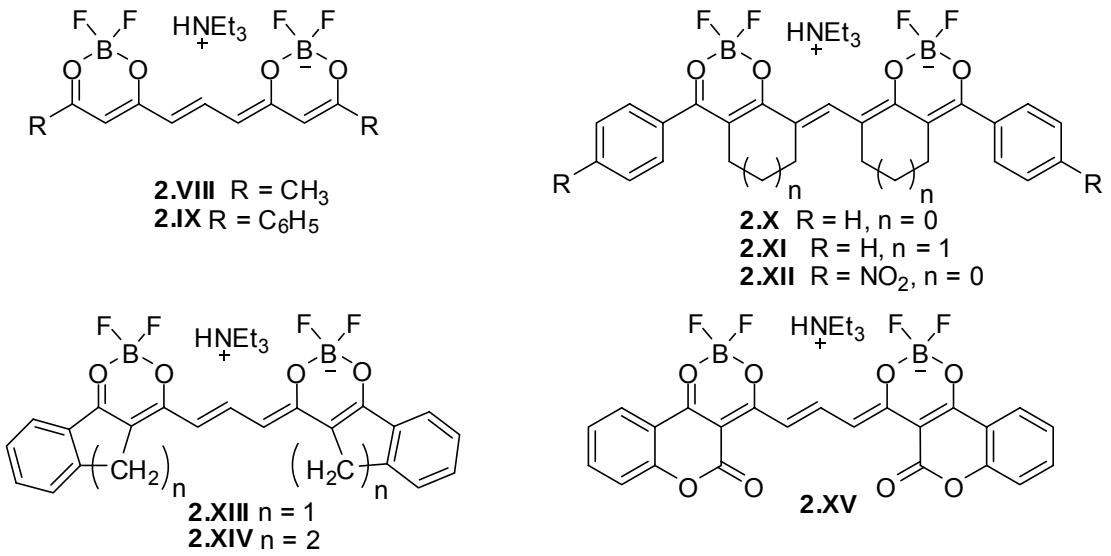

Figure 2.3. Bis(dioxaborine) terminated trimethine dyes from the literature.[4, 14-17]

The simplest dye shown is **2.VIII**, synthesized by Zyabrev *et al.* [14], which has terminal methyl groups extending from the bis(dioxaborine) trimethine core. Markin *et al.*[16] and Traven *et al.*[15] synthesized **2.IX**. **2.IX** has phenyl groups extended from the bis(dioxaborine) trimethine core, providing additional possible conjugation pathways. The λ_{max} has a bathochromic shift compared to **2.VIII** (although the spectra were determined in different solvents the difference is still significant), thus providing some evidence of a more extensive π-system for **2.IX**. **2.X** and **2.XI** are similar to **2.IX**, except there are two additional rings connecting the dioxaborine ring and the α-carbons of the bridge. The small electronic effects of the rings would be anticipated to cause a bathochromic shift in λ_{max} according to the Dewar-Knott rules (see Chapter 3 for details). The rings would also have the effect of increasing the planarity of the dye, which a bathochromic shift in λ_{max} would be anticipated. Zyabrev *et al.*[17] reported the λ_{max} of **2.X** and **2.XI**, which show a bathochromic shift compared to **2.IX**. Halik *et al.*[4]

synthesized a variety of dyes with long wavelength absorption, one of which being **2.XII**. Halik *et al*. noted that nitro substituted dyes (such as **2.XII**) usually had significant red shifts compared to parent compounds with H substituents, most likely due to increased conjugation. A direct comparison of λ_{max} between **2.X** and **2.XII** is difficult due to the difference in solvents in which the spectra were acquired. **2.XIII**, synthesized by Zyabrev *et al*.[17], contains rings similar to **2.X** and **2.XI**; however, the rings are no longer connected to the polymethine bridge. The λ_{max} of **2.XIII** and **2.XIV** were found to have a bathochromic shift compared to **2.IX**. The reason for this is due to a locked configuration leading to an increase in the planarity of the π-system and the subtle electron donating ability of alkyl groups (see Chapter 3 for more details). Dioxaborines derived from coumarin derivatives, reported by Traven *et al*.[15], were used to synthesize **2.XV**. The ring substituent is no longer a simple alkyl ring as in **2.XIV**, but has a lactone functional group, which should be electron withdrawing. However, this provided a similar bathochromic shift in λ_{max} relative to **2.IX** as that provided by **2.XI**, **2.XIII**, and **2.XIV**. Additional chromophores similar to **2.XV** were reported by Gerasov *et al*.[18, 19] and more exotic dioxaborine derivatives were reported by Zyabrev et al.[20]

Table 2.1. λ_{max} of **2.VII-2.XIV** in various solvents.

Dye	λ_{max} (nm), CH_2Cl_2	λ_{max} (nm), other
2.VIII	-	519, CH_3CN
2.IX	600[a]	562[b], $CHCl_3$
2.X	671	-
2.XI	625	-
2.XII	-	734, DMF
2.XIII	613	-
2.XIV	625	-
2.XV	-	581, $CHCl_3$

[a] From Markin *et al.*[16]

[b] From Traven *et al.*[15]

Recently Hales *et al.*[21] have found that a bis(dioxaborine)-terminated nonamethine dye (Figure 2.4, **2.XVI**) appears to be less affected by symmetry breaking (Please see Chapter 1) than other cyanine-like dyes with similar absorption maxima.[22] It also exhibits very large, predominantly real γ in the telecommunications bands of the near-IR (real and imaginary parts are -5.7×10^{-32} and 7.9×10^{-33} esu, respectively, at 1.3 μm). It was shown that thin films can be fabricated, which exhibit correspondingly large $\chi^{(3)}$ (real and imaginary parts are -3.6×10^{-10} and 3.8×10^{-11} esu, respectively, at 1.3 μm).[21]

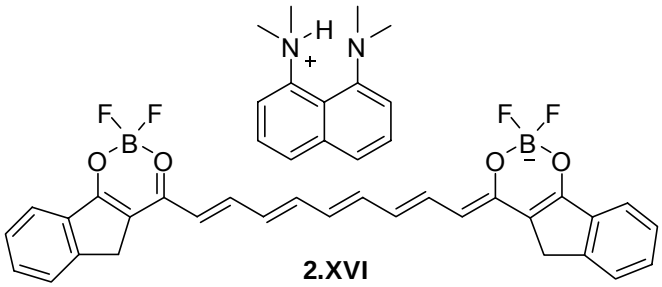

Figure 2.4. Bis(dioxaborine)-terminated nonamethine, **2.XVI**, from the literature.[21]

2.1.2. Goals of Chapter 2

The research aims of this chapter are to determine viable strategies to improve the processability and the nonlinearity of this class of chromophore. **2.XVI** has low solubility in most common organic solvents and has a tendency to be semi-crystalline in the solid state, which lead to limitations in the processing of optical quality films. These are issues that need to be addressed before the dye could be used for AOSP applications. Additionally, a larger magnitude of Re(γ) than that of **2.XVI** at telecommunications wavelengths would be desirable before it could be used for AOSP applications. As noted previously (see chapter one), there is a strong dependence of γ with an increasing number of π-electrons (vinylene groups) in the core of polymethine dyes. Simply extending the core of **2.XVI** to form the undecimethine may be impractical for several reasons. The first reason being that undecimethine is synthetically challenging relative to the nonamethine due to the additional number of steps required to make starting materials. Attempts made by this author to synthesize the dimethylamine-terminated nonamethine resulted in a mixture of products. The second reason against simply extending the core is the stability (this would include chemical stability and an increasing tendency for symmetry breaking to occur) of the dye, because the stability of polymethine dyes generally decreases as the number of methine units is increased. A series of dioxaborine-terminated dyes synthesized by Zyabrev *et al.*[20] showed much broader absorption spectra for the analogous nonamethine, than the shorter homologues (tri-, penta-, and heptamethines), which may be near the onset of symmetry breaking. Finally, if the desired product is obtained, the optical losses may be large in the region of interest. It is important to note **2.XVI** was shown to have optical transparency at telecommunications

wavelengths (1.3-1.6 μm); however, the position of λ_{max} is likely to bathochromoically shift as additional vinylene groups. This effect may truncate the available wavelengths in the telecommunications region usable for AOSP.

Thus, section 2.2 will be concerned with improving the processability of **2.XVI**, by performing ion metathesis of the protonated-proton sponge cation for tetra-alkyl ammoniums, **2.1** and **2.2** (Figure 2.5). Section 2.3 is concerned with testing strategy for further increasing γ in bis(dioxaborine)-terminated polymethines without significantly lowering the excited-state energies in a manner that leads to increased linear or nonlinear loss in the telecommunications range. This is a study on the relationships between chemical structure and optical properties for a set of modified bis(dioxaborine)-terminated pentamethines, **2.3-2.8**, (Figure 2.6) in which the aryl end group of the dioxaborine is varied to incorporate π-donors, π-acceptors, and additional conjugation. The nonamethine analogue of **2.5**, labeled **2.9**, was also synthesized for comparison with **2.XVI**.

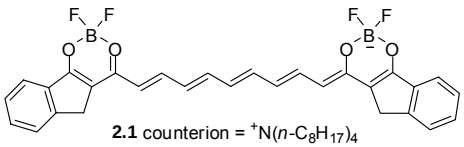

2.1 counterion = $^{+}N(n\text{-}C_8H_{17})_4$
2.2 counterion = $^{+}N(n\text{-}C_4H_9)_4$

Figure 2.5. Bis(dioxaborine)-terminated dyes discussed in Section 2.3.

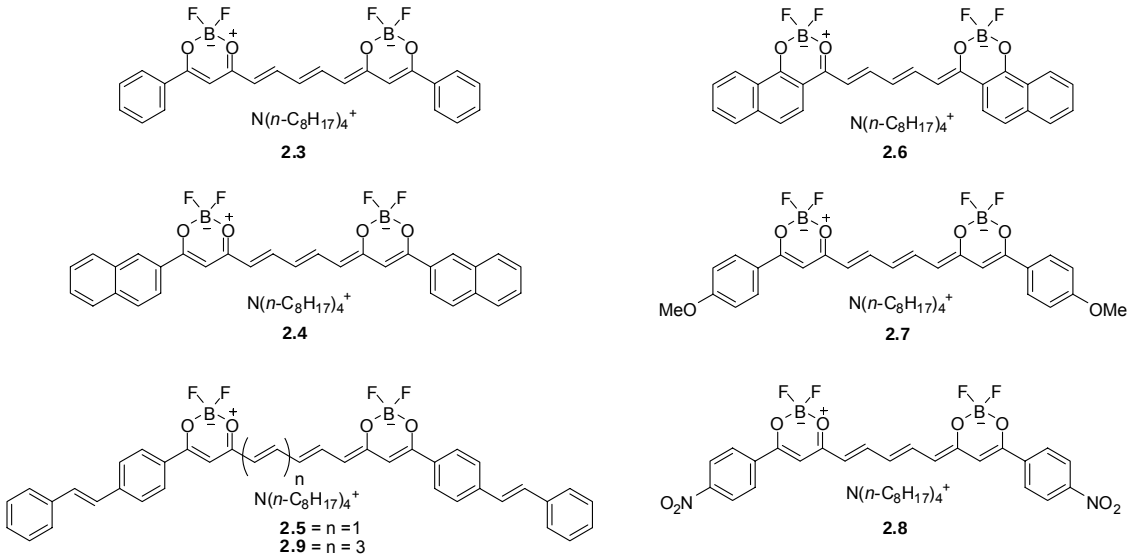

Figure 2.6. Bis(dioxaborine)-terminated dyes discussed in Section 2.3.

2.2. Film-Forming Properties of a Dioxaborine-Terminated Nonamethine Dye

Hales *et al.*[21] showed **2.XVI** could be solution processed from DMSO to form neat solid films. The formation of neat films is important to achieve high number density of chromophore to maintain high bulk nonlinearities. The absorption spectrum of a neat film (Figure 2.7), processed by the spin-coating, exhibited broadening of the band relative to the solution spectrum and a splitting into two absorption maxima, each of similar magnitude.[21] As mentioned in the introduction, the Z-scan technique was performed on the thin film of **2.XVI** at 1300 nm, which exhibited large $\chi^{(3)}$ with Re($\chi^{(3)}$) (-3.6×10^{-10} esu) being almost an order of magnitude larger than Im($\chi^{(3)}$) (-3.8×10^{-11} esu).[21] The splitting of the absorption band into two maxima in the solid state shows both maxima to have nearly equal distribution of the oscillator strength (related to the area under the peaks). Consequently the bathochromically shifted peak would be expected to have larger resonance enhancement, while the hypsochromically shifted peak is expected

to have smaller resonance enhancement when measurements are taken at 1300 nm. These effects could balance in such a way to provide $\chi^{(3)}$ values that would be expected from making extrapolations from the solution measurements.

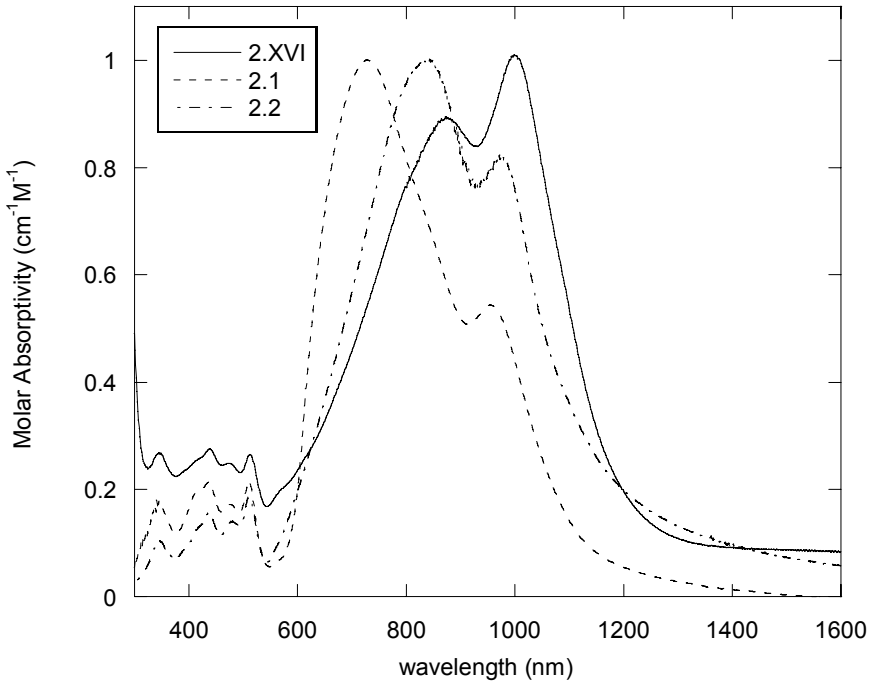

Figure 2.7. Linear absorption spectra of **2.XVI**[21], **2.1**, and **2.2** on a glass substrate.[23]

Hales *et al*.[21] noted that the film of **2.XVI** was semi-crystalline, which would lead to scattering and is therefore undesirable if one is to fabricate a device for AOS and AOSP. The optical loss in the absorption spectrum of **2.XVI** in the region of 1300-1600 may be due to scattering loss rather than absorption. **2.1** and **2.2** were synthesized and reported in this chapter to a) create ion pairs more soluble in common organic solvents than **2.XVI** and b) to create more amorphous films than those formed by **2.XVI**. Ion metathesis was chosen as the route to modify the solubility and crystallinity, because it

was potentially a more synthetically accessible to path than modification of the dye itself. Scheme 2.3 shows the reaction to form **2.1** and **2.2** from **2.XVI**; Sodium hydride was used as a base to deprotonate the proton sponge (1,8-bis(dimethylamino)naphthalene) of **2.XVI**. Sodium bromide quickly precipitated, while the tetra-*n*-alkylammonium paired with the dye and remained in solution.

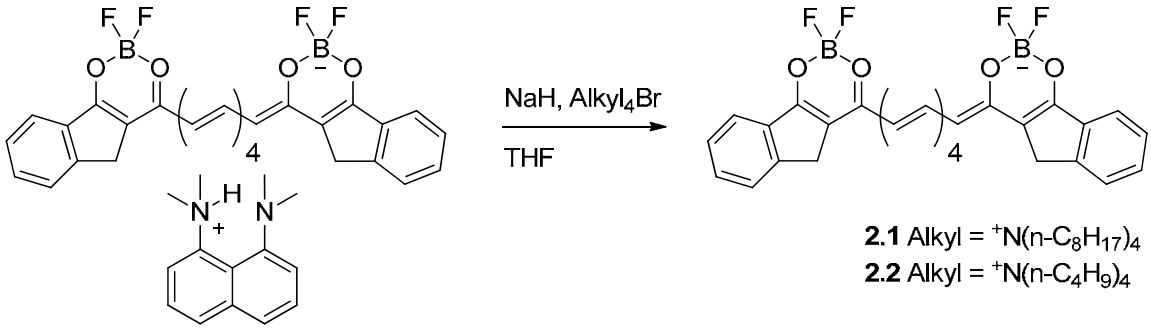

2.XVI

Scheme 2.3. Reaction scheme used to synthesize **2.1** and **2.2**.

The new ion pairs **2.1** and **2.2** had increased solubility compared to **2.XVI** in many common organic solvents (*i.e.* tetrahydrofuran and chloroform) as well as less common solvents (*i.e.* cyclopentanone). The linear and nonlinear optical properties of **2.XVI**, **2.1** and **2.2** are collected in Table 2.2, which exhibit relatively small variations.[23]

Table 2.2. Comparison of Linear and Nonlinear Optical Properties of Dye **2.XVI**, **2.1** and **2.2** in DMSO.

Dye	λ_{max} (nm)	ε_{max} (10^5 $M^{-1}cm^{-1}$)	M_{ge} (D)	Re(γ) (10^{-33} esu)	Im(γ) (10^{-33} esu)	Φ (°)
2.XVI	944	1.79	18	-57	7.9	172
2.1	944	1.99	19	-38	4.1	173
2.2	944	1.98	19	-27	3.1	174

The high boiling point and high viscosity (two desirable solvent properties for spin-coating) of cyclopentanone make it a reasonable choice to spin-coat thin films on substrates. Films of **2.1** and **2.2** were spin-coated onto glass substrate. Visual inspection of the films showed the films of **2.1** and **2.2** to be of much better optical quality (homogeneity and little evidence of crystalline domains) than those of **2.XVI**.

Figure 2.6 shows the absorption spectrum of the thin films of **2.XVI**, **2.1,** and **2.2**. While the spectra of **2.1** and **2.2** are fairly similar, there are large differences between them and **2.XVI**. The strongest peak of **2.1** (730 nm) and **2.2** (845 nm) have a hypsochromic shift from the λ_{max} of **2.XVI** (999 nm). The telecommunications region (1300-1600 nm) appears to have somewhat less absorption/scattering in the spectra for **2.1** and **2.2** than in **2.XVI.** However, **2.1** and particularly **2.2** still have non-zero long wavelength absorption tails extending into the telecommunications wavelengths. Contributions further decreasing the utility of **2.1** and **2.2** for telecommunication applications that $\chi^{(3)}$ in the telecommunications region are expected to receive less resonance enhancement due to the hypsochromic shift of the band. Indeed, the $\chi^{(3)}$ value of **2.1** and **2.2** are nearly an order-of-magnitude lower than **2.XVI** at 1300 nm.

The most likely cause of the different absorption spectra in the solid state is aggregation. While many options could be explored to prevent aggregation, such as

'bulking up' the dye with dendrimers or mixing the dye in polymer matrices, the dye concentration will be diluted and a high number density of chromophore would not be achieved. A dye with larger magnitudes of $\chi^{(3)}$ would most likely be required. Therefore the structure-property relationships discussed in the remainder of this chapter were pursued to determine if the magnitude of Re(γ) (and Re($\chi^{(3)}$) could be increased.

2.3. Effects Upon the Third-Order Nonlinearity Through Extension of Conjugation Beyond the Dioxaborine Termini

A significant amount of section 2.3 was previously published, and has been reproduced here with permission, Copyright Wiley-VCH Verlag GmbH & Co. KGaA.[24]

2.3.1. Synthesis

The pentamethine dyes **2.3**-**2.8** were synthesized by condensation of the known dioxaborine acceptors, **S2.3**-**S2.8** respectively, and the bis(phenylamino)termethine salt, **S2.1**, in the presence of a base (see Scheme 2.4). With the exception of **S2.5**, which was synthesized from *E*-4-acetylstilbene, boron trifluoride, and acetic anhydride, all the dioxaborine acceptors have been previously reported in the literature.[25] Attempts to incorporate a stronger π-donor into the bis(dioxaborine) pentamethines by treating **S2.9** with 4-[4-(dimethylamino)phenyl]-2,2-difluoro-6-methyl-1,3,2(2*H*)-dioxaborine[25] were unsuccessful. The triethylammonium analogues of **2.3** and **2.6** have previously been synthesized;[16] however, in this study, the dyes with tetra-*n*-octylammonium counterions were isolated to facilitate purification (the salts can be purified by chromatography on silica gel), to improve dye solubility, and potentially to improve their processibility during the fabrication of films. The crude $DBUH^+$ (protonated diaza(1,3)bicyclo[5.4.0]undecane) or triethylammonium salts were converted to sodium

salts by treatment with sodium hydride; these were then converted to the final products by exchanging sodium with tetra-*n*-octylammonium bromide. **2.9**, the nonamethine analogue of **2.5**, was synthesized from **S2.5** in a similar manner to **XVI**,[21] i.e., using proton sponge (1,8-bis(dimethylamino)naphthalene) as the base and **S2.2** as the source of the polymethine bridge (Scheme 2.5), followed by counterion metathesis analogous to that performed for **2.3-2.8.**

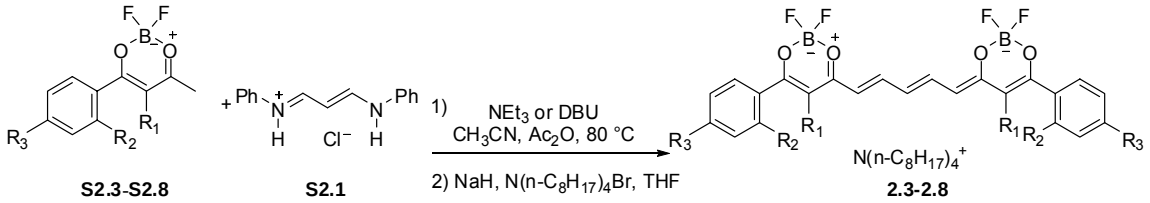

Scheme 2.4. Synthesis of bis(dioxaborine) pentamethines, **2.3-2.8**.

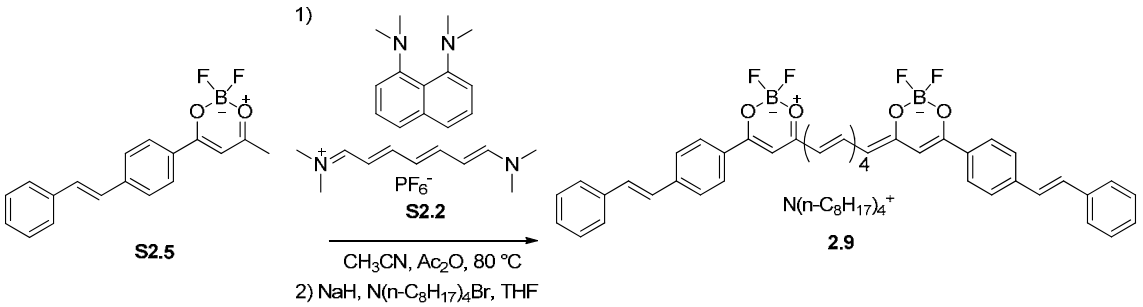

Scheme 2.5. Synthesis of bis(dioxaborine) nonamethine, **2.9**.

2.3.2. NMR Characterization of 2.3-2.9

NMR characterization of **2.3-2.9** with the exception of **2.6** was complicated by the observation of some severely broadened resonances at room temperature, in particular some of the ^{1}H and ^{13}C resonances assigned to atoms in the polymethine bridge.

Variable-temperature experiments were used to investigate the origin of this broadening. For **2.3**-**2.9** both heating and cooling the sample leads to sharpening of the spectra, with additional ^{1}H resonances being seen at 240 K in $CDCl_3$, as shown in Figure 2.8 for the case of **2.5**. These data suggest the presence of a major and a minor conformer (present in a ratio of *ca*. 15:1 for **2.5** at 240 K), the rate of inter-conversion of which at low temperatures is slow on the NMR timescale.

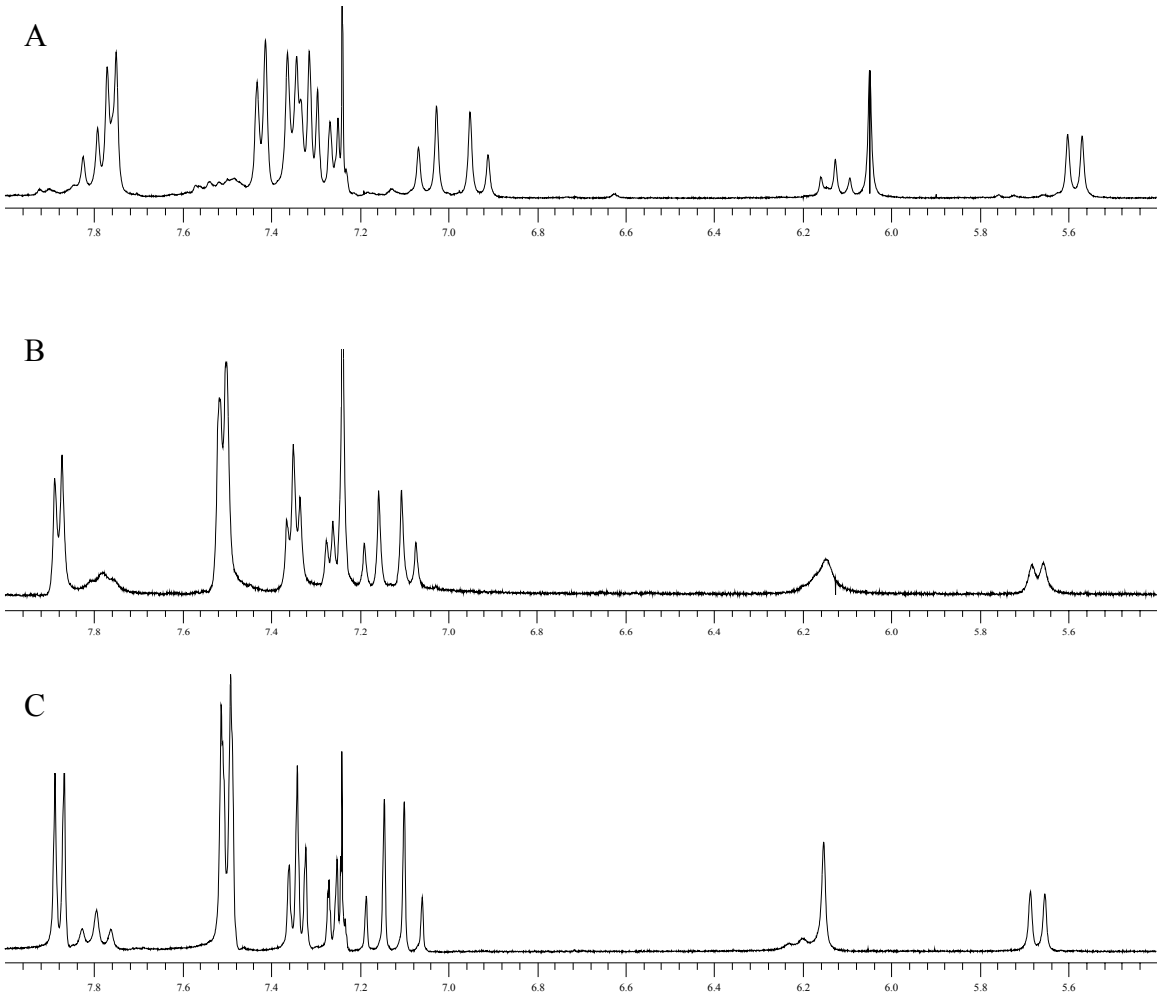

Figure 2.8. Variable temperature ^{1}H NMR spectrum of **2.5** in $CDCl_3$. A) 243 K. B) 294 K. C) 333 K. Reproduced with permission.[24]

These conformers likely result from restricted rotation about the dioxaborine—CH bonds, as shown schematically in Figure 2.9. Nuclear Overhauser effect (NOE) experiments could be used to identify the major and minor isomers. A rotating-frame Overhauser effect spectroscopy (ROESY) experiment at 333 K on **2.3** (Figure 2.10) shows a correlation between the proton on carbon 1 and the proton on the α-carbon 2, while there is no correlation seen between the protons on carbons 1 and 3, thus indicating that species A (Figure 2.9) is the major conformer in solution. Unfortunately, analogous low-temperature experiments did not yield definitive structural information on the minor conformer due to its low concentration and accordingly poorly resolved signals, and to overlap between the spectra of minor and major conformers.

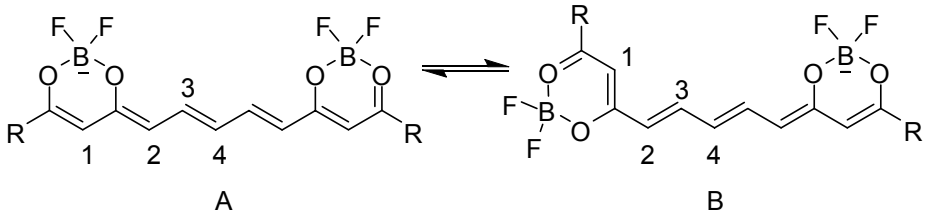

Figure 2.9. Possible origins for rotational isomers A and B in bis(dioxaborine) polymethines.

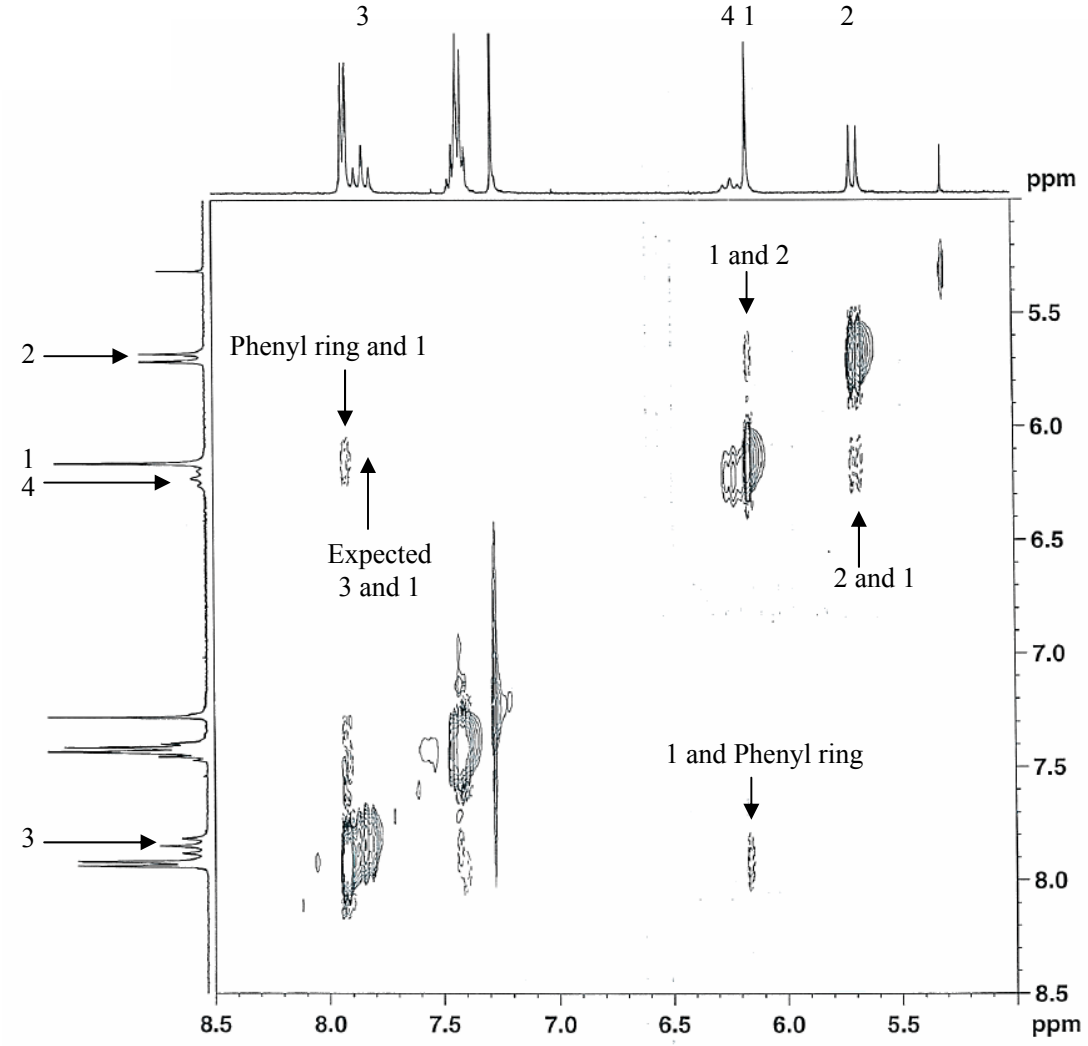

Figure 2.10. ROESY experiment at 333 K on **2.3.**

2.3.3. Electrochemistry of 2.3-2.8

The redox properties of **2.3-2.8** were investigated using cyclic voltammetry in THF. The redox potentials are compared in Table 2.3. Although the bis(dioxaborine) polymethines have an overall negative charge, the negative charge is formally localized on each boron atom and a positive charge is delocalized over the conjugated π system; the most reversible process observed for **2.3-2.7** is a molecular reduction ($E_{1/2}^{1-/2-}$) and, therefore,

corresponds to neutralization of this positive charge. In addition, **2.3**, **2.4**, **2.6**, and **2.7** exhibit a second reduction with characteristics of an EC-type process (i.e., one in which the electron transfer itself is reversible but where the reduced species undergoes a chemical reaction on a time scale comparable with that of the electron transfer) and an irreversible oxidation. The second reduction for **2.5**, on the other hand, appears to be more reversible. In contrast, the nitrophenyl-terminated example, **2.8**, shows three successive reversible reductions, some of which may be associated with local reductions of the nitrophenyl group; indeed nitrobenzene is reduced reversibly at –1.73 V in THF.[26] **2.3-2.5** showed similar potentials to one another for the oxidations and the first reduction, whereas the methoxy π-donors of **2.7** leads to more facile oxidation and less facile reduction, indicating that the terminal aryl groups indeed influence the electronic structure of the bis(dioxaborine) pentamethine core to some extent. Similarly, the nitro derivative, **2.8**, undergoes the most facile first reduction and the least facile oxidation. Interestingly, fusion of the naphthalene and dioxaborine on the terminal unit of **2.6** leads to redox potentials that approach those of **2.8** (*i.e.*, more facile reduction and less facile oxidation than for the other dyes).

Table 2.3. Electrochemical potentials versus ferrocenium / ferrocene for dyes **2.3-2.8** in THF / 0.1 M $^{n}Bu_4NPF_6$.

Dye	$E_{1/2}^{2-/3-}$, V	$E_{1/2}^{1-/2-}$, V	$E_{ox}^{1-/0}$, V
2.3	-2.62[a]	–1.49[b]	–0.12[d]
2.4	-2.33[a]	–1.46[b]	–0.01[d]
2.5	-2.25[b]	–1.47[b]	–0.04[d]
2.6	-2.55[a]	–1.32[b]	+0.14[d]
2.7	-2.50[a]	–1.58[b]	–0.28[d]
2.8	-1.45[b],[c]	–1.21[b]	+0.18[d]

[a] EC-type process
[b] Reversible
[c] A third reversible reduction is seen at $E_{1/2}^{3-/4-}$ = –1.64 V
[d] Irreversible

2.3.4. Linear Optical Properties of 2.3-2.8

2.3-2.8 all show strong absorption maxima in the visible-near-IR spectrum (Figures 2.11 and 2.12); parameters characterizing these absorptions are given in Table 2.4. Increasing the conjugation of the terminal aryl group of the dioxaborines in the series **2.3-2.5** leads to an increasing bathochromic shift in the absorption maximum, λ_{max}, associated with the optical transition from the ground state to the lowest-lying excited state, and an increase in the corresponding transition dipole moment, M_{ge}. However, these effects are relatively minor compared to those obtained upon increasing the number of methine groups at the core (between acceptor groups) of the chromophore. For instance, the low-energy transitions of typical cyanine-type dyes show *ca.* 100 nm bathochromic shifts upon addition of a vinylene group (incorporating an additional 2 π-electrons) to the polymethine bridge, whereas the absorption maxima of **2.3** and **2.5** differ by only *ca.* 50

nm, despite the presence of two additional 8 π-electron styryl groups. A similar effect was noted by Wernke *et al.*[27] when comparing dimethylamino- and benzothiazole-terminated polymethines: for a given chain length between the two nitrogen atoms, a member of the latter class has 12 additional π-electrons relative to its analogue in the former class, but the red-shift observed is similar to what would be obtained on adding one vinylene group to the bridge. This suggests that the terminal groups provide less contribution to the frontier molecular orbitals than the polymethine bridge of the dye, a feature that will be discussed in more detail below.

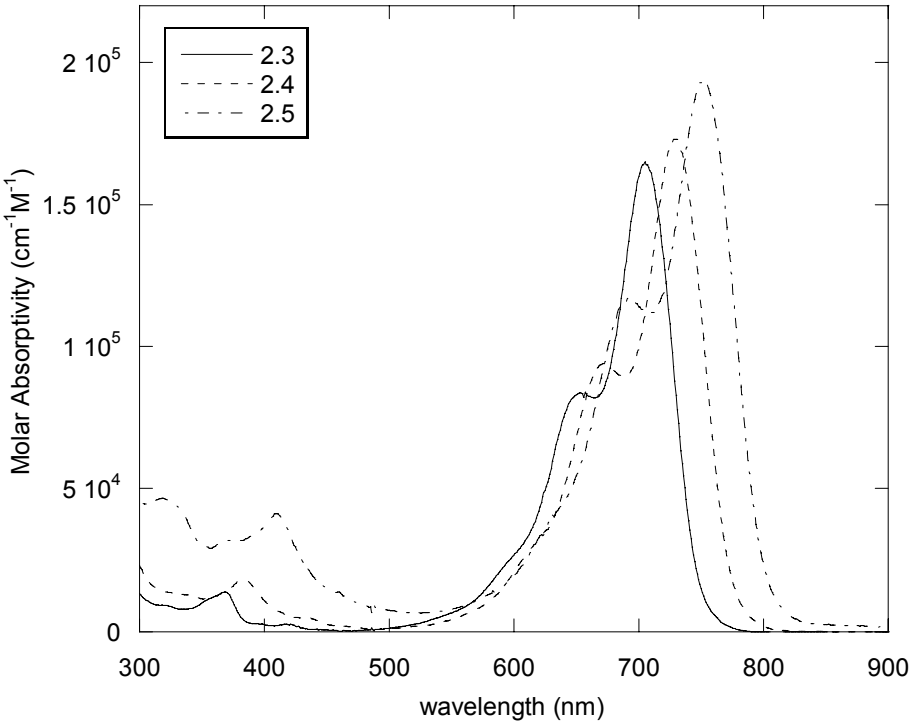

Figure 2.11. Absorption spectra of **2.3** (—), **2.4** (----), and **2.5** (-·-·-) in DMSO.

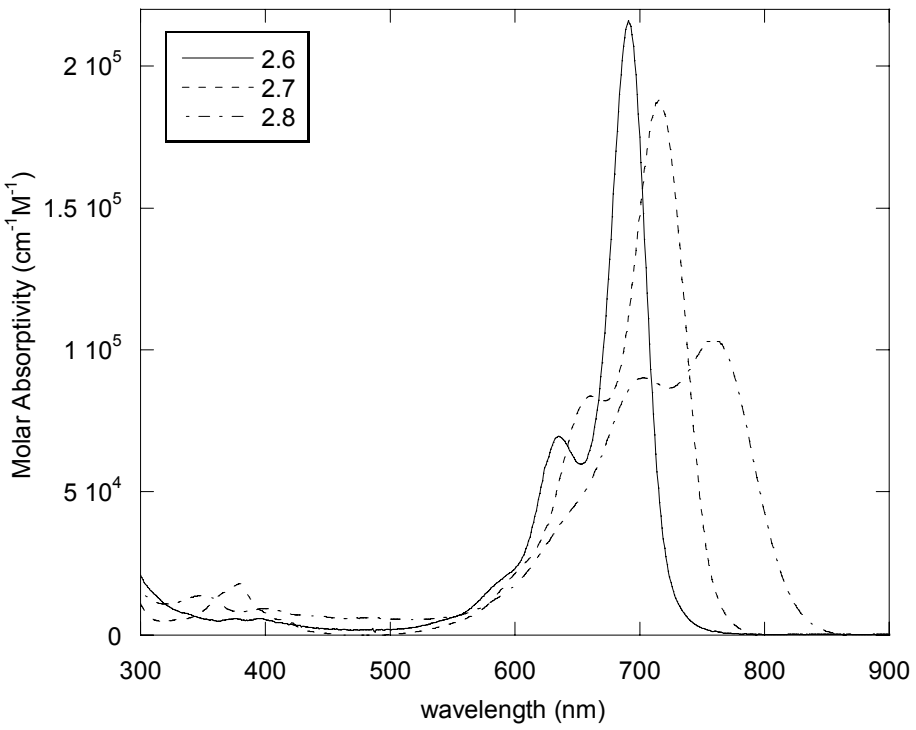

Figure 2.12. Absorption spectra of **2.6** (—), **2.7** (----), and **2.8** (-·-·-) in DMSO.

Although dye **2.6** has 4 additional π-electrons relative to **2.3**, λ_{max} is hypsochromically shifted. Moreover, the aromaticity of the fused six-membered ring may to some extent hinder delocalization of the positive charge to the terminal oxygen of the dioxaborine donor, effectively reducing the length of the main conjugation path, thus reducing the overall polarizability of the dye. Adding either a weak π-donor (**2.7**) or a strong π-acceptor (**2.8**) to the termini leads to bathochromic shifts in λ_{max} compared to **2.3**; this again shows that these substituents can, to some extent, couple to the π-system of the dye, with the nitro compound having the lowest energy absorption of the molecules examined here. This behavior is consistent with that reported for zwitterionic bis(dioxaborine) heptamethine derivatives with phenyl, *p*-methoxyphenyl, and *p*-nitrophenyl end groups.[4] Although the value of the maximum absorptivity for the nitro

compound is lower than that of the other dyes, the absorption spectrum is considerably broader as shown in Figure 2.11. The most likely explanation for the broadened spectrum is different vibronic coupling. Consequently, the transition dipole moments for **2.8** as well as **2.7** are both larger than that of **2.3**.

Table 2.4. Experimental data in DMSO solvent and calculated Intermediate Neglect of Differential Overlap – Configuration Interaction Singles (INDO-CIS) optical data for dyes **2.3-2.6**.

Dye	Exp. λ_{max} (nm)	Calc. λ_{max} (nm)	ε_{max} (10^5 M^{-1} cm^{-1})	Exp. M_{ge} (D)[a]	Calc. M_{ge} (D)
2.3	705	512	1.65	13.9	16.9
2.4	729	517	1.73	14.7	18.1
2.5	752	525	1.94	16.6	19.1
2.6	691	504	2.16	13	16.7
2.7	715	515	1.78	14.3	17.2
2.8	761	544	1.01	14.3	17.8

[a] Obtained from integration of the absorption spectra as $M_{ge} = 0.9584(\int \varepsilon \, d\nu / \nu_{max})^{0.5}$ where ε is in $M^{-1}cm^{-1}$ and ν is in cm^{-1}

In order to gain a better understanding of the nature of the lowest energy optical bands, the transition energies and transition dipole moments for **2.3-2.8** were calculated by Dr. Shino Ohira using the Intermediate Neglect of Differential Overlap[28, 29] – Configuration Interaction Singles (INDO-CIS) computational method (Table 2.4), which has been extensively used for that purpose in earlier work.[30] The calculated transition energies are overestimated (which is typical for this method and can, in part, be attributed to neglect of solvent effects); the calculated transition dipole moments are also all slightly overestimated. However, the calculations generally well reproduce the experimentally observed trends in both quantities. The calculations indicate that, in all cases, the $S_0 \rightarrow S_1$

transitions are predominantly HOMO-to-LUMO excitations; however, other configurations can also be important, with, for instance, the HOMO-to-LUMO+2 excitation contributing significantly in the case of **2.4**, **2.5**, and, in particular, **2.8**.

The frontier orbitals, determined by Dr. Shino Ohira, as obtained from hybrid Density Functional Theory (DFT) B3LYP[31-35] level of theory using the 6-31G** basis set (TURBOMOLE[36] package), are shown for **2.3-2.8** in Figure 2.13. The HOMOs of all the dyes are rather similar; importantly, the associated electron density is primarily localized in the dioxaborine heterocycles and the polymethine bridge, with only minor contributions from the terminal aryl groups. The lack of electron density on the terminal groups in the HOMO may explain why the impact on the optical properties of the dyes originating from the terminal groups is small compared to modifications in the polymethine bridge. The terminal substituents play a more significant role in the LUMOs (Figure 2.12). The LUMOs can be regarded as in-phase combination of the local LUMO of the bis(dioxaborine) pentamethine and the local LUMOs of the terminal aryl groups. This can be seen for the example of **2.5** in Figure 2.13, in which the LUMO is extensively delocalized over the stilbenyl substituents. Contributions from the terminal substituents to the LUMO are, not surprisingly, particularly important in the *p*-nitrophenyl-terminated compound, **2.8**. The LUMO+2 orbitals which, as mentioned above, are important as well in determining the spectra of some of the compounds, also consist of combinations of the local LUMO of the bis(dioxaborine) pentamethine with end-group-based orbitals, the relative contributions from each depending on the particular substituent.

2.3

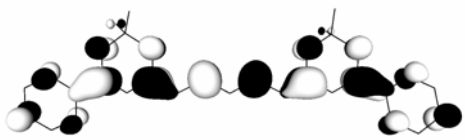

LUMO

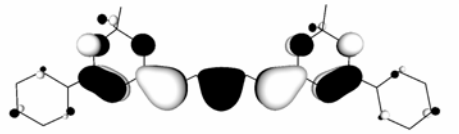

HOMO

2.4

LUMO

HOMO

2.5

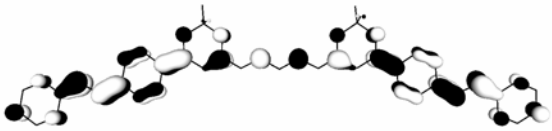

LUMO

HOMO

2.6

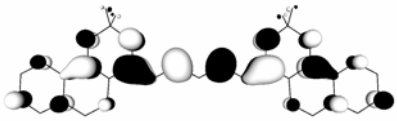

LUMO

HOMO

2.7

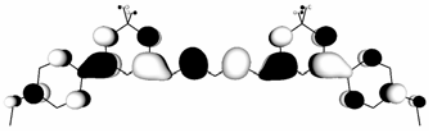

LUMO

HOMO

2.8

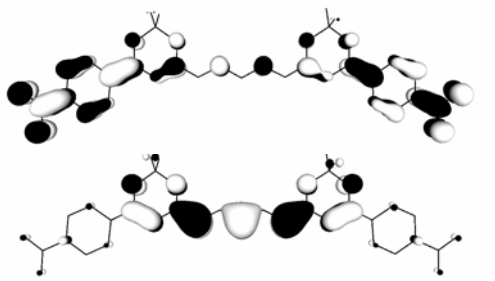

Figure 2.13. HOMO (bottom) and LUMO (top) orbital diagrams of **2.3-2.8**.[24, 37]

The differences in the experimental and calculated transition dipole moments between **2.5** (for which M_{ge} is largest) and the simplest dye examined, **2.3**, can be understood from transition density plots (*i.e.*, plots showing the contribution of each atom to the transition dipole moments) computed from INDO-CIS and shown pictorially in Figure 2.14 for **2.3** and **2.5**. The differences in M_{ge} can be partly attributed to contributions to the transition density from the vinylene groups of the terminal stilbenyl groups of **2.5**.

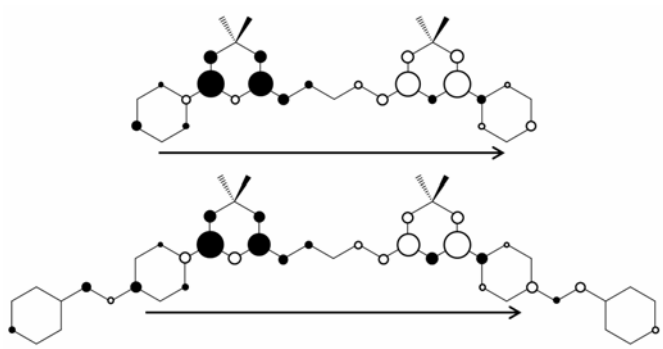

Figure 2.14. Transition atomic densities and transition dipole moment vectors for **2.3** (top) and **2.5** (below) calculated using INDO-CIS.[24, 37] Reproduced with permission.[24]

2.3.5. Nonlinear Optical Properties of 2.3-2.8

The third-order nonlinear optical properties of **2.3-2.8** were investigated in DMSO solutions using open- and closed-aperture Z-scan techniques by Dr. Joel Hales[38,39] (Table 4) to determine Im(γ) and Re(γ), respectively, with ~100 fs pulses at a wavelength of 1.3 μm. The values of Re(γ) vary among the compounds by almost a factor of two. The largest values are similar to those previously reported for a zwitterionic bis(dioxaborine) heptamethine at the same wavelength (**2.XVII**, Figure 2.15),[21] and are around an order-of-magnitude smaller than that for the nonamethine **2.XVI**.[21] In the series **2.3-2.5**, Re(γ) increases with the extension of conjugation in the terminal aryl groups. Both the absorption maxima and the values of Re(γ) depend much less strongly on conjugation length in the end group than would be expected on extension of the polymethine core; this can again be attributed to the relatively small participation of the terminal groups in the HOMO levels.

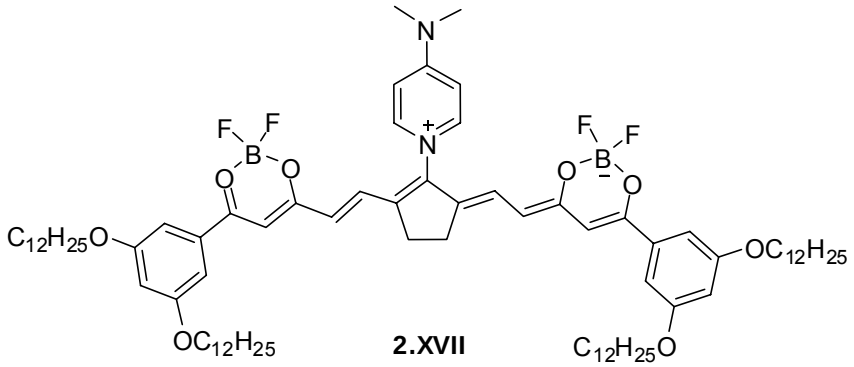

Figure 2.15. Bis(dioxaborine) terminated heptamethine for which γ was measured.[21]

In polymethines, the sum-over-states expression[40] for Re(γ) is typically dominated by a two-state term in which the key quantities are the transition energy and transition

dipole moment both associated with the lowest energy one-photon absorption. Values of the undamped (peak broadness was unaccounted for due to the long distance between the λ_{max} and the excitation wavelength), static (zero-frequency) Re(γ) were estimated by the two-state expression:

$$\mathrm{Re}(\gamma)_{\mathrm{static}} = -\left((2.998)^4 \times 10^{23}\right) \times \left(\frac{1}{5}\right) \times 4 \times \frac{M_{ge}^4}{E_{ge}^3} \qquad \text{(E2.1)}$$

the factor of 1/5 is due to orientational averaging of the quasi-one dimensional (only one axis of significant polarizability) chromophores and the prefactor is a conversion factor between the input MKS units (values for E_{ge} in Joules and M_{ge} in C·m) and the resulting cgs (esu) units for Re(γ)$_{static}$. These values are included in Table 2.5 and show that the observed trends in experimental Re(γ) at 1300 nm can largely be rationalized in terms of the transition energies and transition dipole moments associated with the low-energy transitions. While the trends are well-reproduced, overall the calculated values are underestimated with respect to the experimentally determined ones. This discrepancy is likely a result of neglecting resonance enhancement effects by employing the static approximation to Re(γ) (detuning factors were ignored in E2.1).

Despite the fact that the values for Re(γ) are roughly ten times smaller than the previously reported value for **2.XVI** at the same wavelength, the values of Im(γ) are only slightly smaller than those previously reported for **2.XVI** at the same wavelength.[41] Therefore, in the present compounds, Im(γ) is similar in magnitude to Re(γ), as can also be seen from the phase of γ, Φ (Table 2.5). Given that Im(γ) is directly related to the 2PA cross-section,[42] non-degenerate 2PA (ND-2PA) spectra were acquired by Dr. Joel Hales for compounds **2.4** and **2.XVI** in order to investigate the origin of this difference in Φ. The ND-2PA spectra (shown in Figure 2.14) reveal two dominant peaks located at ~1.1×

E_{ge} and ~1.7× E_{ge}, typical of 2PA spectra of shorter chain cyanines reported in the literature.[43] The region between these two peaks shows reduced two-photon response and, therefore, exhibits smaller Im(γ) and a value of ϕ closer to 180°. Excitation of **2.4** at 1.3 μm is quite close to the lowest lying two-photon band and, therefore, results in similar magnitudes for both the real and imaginary parts of γ, i.e. ϕ~130°. Since excitation of **2.XVI** falls between the two 2PA bands, the phase falls closer to ~170°.[41] While **2.XVI** does possess an additional 2PA band within this window, its smaller 2PA cross-section coupled with the order-of-magnitude increase in Re(γ) for the nonamethine **2.XVI** compared to the pentamethine **2.4** results in the significant difference in the phases.

Table 2.5. Third-order Nonlinear Optical Properties for **2.3-2.8** in DMSO Determined at 1.3 μm[a] along with Theoretical Estimates of the Static Third-order Polarizabilities.

Dye	Re(γ) (10^{-33} esu)	Im(γ) (10^{-33} esu)	|γ| (10^{-33} esu)[b]	Φ (°)[b]	Re(γ)$_{static}$ (10^{-33} esu)[c]
2.3	-3.5	3.0	4.6	140	-1.3
2.4	-4.0	4.4	5.9	130	-1.9
2.5	-5.4	4.8	7.2	140	-3.3
2.6	-2.9	2.3	3.7	140	-1.0
2.7	-4.6	4.4	6.3	140	-1.6
2.8	-3.0	2.9	4.2	140	-1.9

[a] Experimental values for third order properties have associated errors determined to be ±10%. The errors for the phase are ±7%.

[b] The magnitude and phase of γ are defined as $|\gamma|^2 = \mathrm{Re}(\gamma)^2 + \mathrm{Im}(\gamma)^2$ and $\phi = \arctan[\mathrm{Im}(\gamma)/\mathrm{Re}(\gamma)]$, respectively.

[c] Calculated from E2.1 using experimentally determined values of M_{ge} and E_{ge} from Table 2.4.

2.3.6. Optical Properties of 2.9

Since **2.5** showed the largest Re(γ) among the pentamethines discussed above, the nonamethine **2.9** was synthesized and characterized to determine if extension of conjugation in the terminal aryl group would result in a derivative of **2.XVI** with enhanced nonlinearity. The results are presented in Table 2.6. As expected for an elongation of the polymethine chain by two vinylene units, the absorption maximum for **2.9** is bathochromically shifted *ca.* 230 nm compared to that of **2.5**. Furthermore, the value of Re(γ) for **2.9** is over an order-of-magnitude larger than that of **2.5**, and slightly larger than that for **2.XVI**. Unfortunately, the value of Im(γ) at 1.3 μm for **2.9** is approximately three times larger than for **2.XVI**, resulting in a value of ϕ of 160.5°, further reduced from 180° (although still significantly closer to 180° than the phases observed for **2.3-2.8**). According to the ND-2PA spectrum of **2.9** shown in Figure 2.16, excitation at 1.3 μm should still fall within the aforementioned window of relative 2PA transparency; however, the 2PA cross-sections throughout this region are substantially larger than for **2.XVI**. One possible explanation for this phenomenon is that extending the conjugation beyond the terminal dioxaborine units in this manner could lead to the onset of Peierls-type symmetry breaking resulting in additional two-photon activity (increased Im(γ)); however, there is little evidence for this in the linear absorption spectrum. Despite the slight increase in Re(γ) for **2.9** compared to **2.XVI**, the larger nonlinear optical loss results in a considerably less favorable AOSP figure-of-merit[44, 45] in this region, at least in solution.

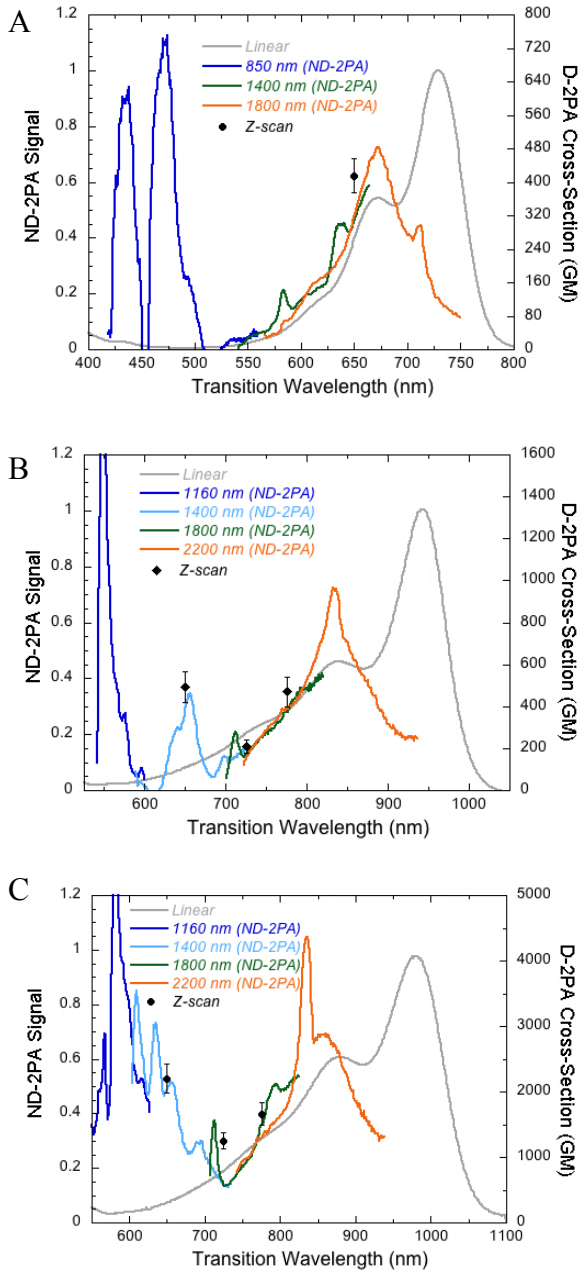

Figure 2.16. Non-degenerate 2PA (ND-2PA) spectra for **2.4** (A), **2.XVI**[21] (B) and **2.9** (C) all in DMSO. The degenerate 2PA (D-2PA) cross-sections determined from Z-scan measurements are shown as well. The linear absorption spectra for all the dyes are shown in grey.[23] Reproduced with permission.[24]

Table 2.6. Comparison of Linear and Nonlinear Optical properties of Dye **2.XVI** and **2.9**.[a]

Dye	λ_{max} (nm)	ε_{max} (10^5 $M^{-1}cm^{-1}$)	M_{ge} (D)	Re(γ) (10^{-33} esu)	Im(γ) (10^{-33} esu)	Φ (°)
2.XVI	944	1.79	18.2	-57	7.9	172
2.9	981	1.78	19.8	-66	23	161

[a] Experimental values for third order properties have associated errors determined to be ±10%. The errors for the phase are ±3%.

2.3.7. Conclusions

The introduction of extended conjugation into the terminal aryl groups of bis(dioxaborine) pentamethines leads to bathochromically-shifted absorption maxima and increased transition dipole moments. In accordance with expectations for polymethines where the sum-over-states expression for Re(γ) is typically dominated by a two-state term, these modifications result in an increased negative value of Re(γ), although these increases are smaller than those observed upon addition of vinylene groups to the core of the polymethine dye. We have further applied this strategy to obtain a new bis(dioxaborine) nonamethine, **2.9**, which exhibits somewhat enhanced Re(γ) compared to the previously investigated nonamethine, **2.XVI**. **2.9** also shows increased Im(γ), due to two-photon absorption, relative to **2.XVI** at 1.3 μm, resulting in less suitability for AOSP applications at this wavelength. Broadband nonlinear absorption spectroscopy reveals the window of relative two-photon transparency that aids in the favorable AOSP figure-of-merit for **2.XVI** is decreased for **2.9**, possibly indicating the onset of symmetry-breaking in this extended nonamethine. Therefore, while extending conjugation beyond the terminal unit results in increased Re(γ) for these polymethine-based cyanines,

different substituents and/or terminal groups may have to be investigated further to simultaneously reduce Im(γ) in this spectral range.

2.4. Experimental Section

General. Starting materials were obtained from commercial sources and used without further purification. Compounds **S2.3-S2.8,**[25] **S2.1**, and **S2.2** (The 1,7-bis(dimethylamino)heptamethine cyanine was synthesized according to the procedure of Nikolajewski *et al*.[46] as a hexafluorophosphate salt instead of the perchlorate salt to avoid possible shock hazards) with the exception of **S2.5**, were synthesized according to the literature. Where necessary tetrahydrofuran was dried by passage through two columns of activated alumina.[47] Electrochemical measurements were carried out under nitrogen on dry deoxygenated tetrahydrofuran solutions ca. 10^{-4} M in analyte and 0.1 M in tetra-*n*-butylammonium hexafluorophosphate using a BAS Potentiostat, a glassy carbon working electrode, a platinum auxiliary electrode, and, as a pseudo-reference electrode, a silver wire anodized in 1 M aqueous potassium chloride. Potentials were referenced to ferrocenium / ferrocene by using decamethylferrocene (measured at –0.45 V vs. ferrocenium / ferrocene) as an internal reference. Cyclic voltammograms were recorded at a scan rate of 50 mVs^{-1}. UV-vis.-NIR spectra were recorded in 1 cm cells using a Varian Cary 5E spectrometer. NMR spectra were recorded on a Varian 300 and a Bruker 400 MHz spectrometer. Elemental analyses were performed by Atlantic Microlabs. The EI mass spectra were recorded on a VG instruments 70SE and the ESI mass spectra were recorded on a Micromass Quattro LC.

2.1

2.XVI (0.493 g, 0.661 mmol) and tetra-*n*-octylammonium bromide (0.343 g, 0.628 mmol) were combined in dry tetrahydrofuran (10 mL) under a nitrogen atmosphere. A slurry of sodium hydride (0.130 g, 5.42 mmol) in tetrahydrofuran (10 mL) was cannulated dropwise into the solution with stirring. The solution was sonicated for 1 h, then quickly filtered. The precipitate was rinsed with dry tetrahydrofuran, then the filtrate was concentrated under reduced pressure. Hexane (50 mL) was added to precipitate a solid. The solution was filtered, followed by dissolving the precipitate in dichloromethane (10 mL) and precipitating in hexanes (50 mL). The precipitate was filtered off and passed through a silica gel plug (made basic by treatment with triethylamine) using dichloromethane as the eluent. The solvent was removed from the collected fractions to give shiny brown solid (319 mg, 0.320 mmol, 48.4%). ^{1}H NMR (400 MHz, $CDCl_3$): δ (ppm) 7.63 (d, J = 7.2 Hz, 2H), 7.59 (t, J = 12.8 Hz, 2H), 7.42 (d, J = 7.6 Hz, 2H), 7.36 (t, J = 7.2 Hz, 2H), 7.31 (t, J = 7.2 Hz, 2H), 6.85 (t, J = 12.4 Hz, 2H), 6.24 (m, 3H), 5.71 (d, J = 12.4 Hz, 2H), 3.48 (s, 4H), 3.10 (m, 8H), 1.54 (m, 8H), 1.32-1.14 (m, 40H), 7.57 (t, J = 12.8, 2H), 0.84 (t, J = 6.8 Hz, 12H). ^{13}CNMR (100 MHz, $CDCl_3$): δ (ppm) 171.3, 165.9, 148.8, 145.4, 145.1, 137.6, 129.9, 127.0 125.1, 124.6, 123.8, 121.2, 111.2, 107.9, 58.7, 31.7, 31.3, 29.2, 29.1, 26.4, 22.7, 22.0, 14.2. MS (MALDI) (+) m/z = 466.5 [M^+ cation] (-) m/z = 531.2 [M^+ anion]. Anal. Calcd. for $C_{61}H_{89}B_2F_4NO_4$: C, 73.41, H, 8.99, 1.40. Found: C, 73.55, H, 9.07, N, 1.60.

2.2

2.XVI (296 mg, 0.397 mmol) was combined with tetra-*n*-butylammonium bromide (201 mg, 0.624 mmol) and dissolved in dry tetrahydrofuran (20 mL) under a nitrogen

atmosphere. A slurry of sodium hydride (58 mg, 2.42 mmol) in tetrahydrofuran (10 mL) was added dropwise, and stirred for 5 min. The solution was quickly filtered and the solvent of the filtrate was removed. The residue was dissolved in dichloromethane (10 mL) and precipitated by adding hexanes (50 mL). The product was collected by filtration. The desired product was separated through silica gel (made basic by treatment with triethylamine) chromatography using dichloromethane/ethylacetate (9:1). The solvent was removed under vacuum and the residue was precipitated from acetone using hexanes, followed by filtration to collect the brown product (60 mg, 0.078 mmol, 20%). ^{1}H NMR (400 MHz, CD_3CN): δ (ppm) 7.62 (d, J = 7.0 Hz, 2H) 7.56 (t, J = 12.9 Hz, 2H) 7.53 (d, J = 7.1 Hz, 2H) 7.46 (td, J = 7.4, 1.3 Hz, 2H) 7.40 (td, J = 7.3, 1.3 Hz, 2H) 7.06 (t, J = 12.6 Hz, 2H) 6.35 (m, 3H) 5.84 (d, J = 12.7 Hz, 2H) 3.56 (s, 4H) 3.05 (m, 8H) 1.58 (m, 8H) 1.33 (sextet, J = 7.5 Hz, 8H) 0.95 (t, J = 7.4 Hz, 12H). ^{13}C NMR (100 MHz, $(CD_3)_2SO$): δ (ppm)170.4, 165.7, 149.9, 145.7, 145.1, 136.9, 130.3, 127.3, 125.7, 125.2, 124.3, 120.6, 111.3, 107.9, 57.5, 30.7, 23.0, 19.2, 13.5 . MS (ESI) (+) m/z = 242.1 [M^+ cation] (-) m/z = 619.3 [M^- anion]. Anal. Calcd. for $C_{45}H_{47}B_2F_4NO_4$: C, 69.87, H, 7.43, N, 1.81. Found: C, 69.64, H, 7.21, N, 2.02.

_E_-2,2-difluoro-6-methyl-4-(4-styrylphenyl)-1,3,2(2_H_)-dioxaborine, S2.5.

Acetic anhydride (5 mL) and boron trifluoride acetic acid complex (3.1 mL, 72 mmol) was added dropwise to a stirred slurry of *E*-4-acetylstilbene (trans-4-acetylstilbene was synthesized using similar Heck coupling conditions as those reported by Barlow *et al.*[48], while the ^{1}H NMR was consistent with that reported by Arvela *et al.*[49]) (2.0 g, 9.0 mmol) in acetic anhydride (20 mL) at 0 °C under a nitrogen atmosphere over 3 h. The solution was stirred 16 hours at room temperature. After the solution was cooled to -20 °C, it was

poured into a saturated aqueous sodium carbonate (150 mL) and the product was extracted using dichloromethane (3 × 30 mL). The organic layers were combined, dried with magnesium sulfate, filtered, and then concentrated under reduced pressure. Chromatographic separation on silica gel using dichloromethane as eluent led to isolation of a fluorescent, yellow solid. (1.06 g, 3.41 mmol, 38%). ^{1}H NMR ($(CD_3)_2SO$, 400 MHz): δ (ppm) 8.18 (d, J = 8.6 Hz, 2H), 7.86 (d, J = 8.6 Hz, 2H), 7.69 (d, J = 7.2 Hz, 2H), 7.58 (d, J = 16.5 Hz, 1H), 7.43–7.38 (m, 4H), 7.27 (s, 1H), 2.45 (s, 3H). ^{13}C NMR ($(CD_3)_2SO$, 100 MHz, 333 K): δ (ppm) 193.4, 180.4, 144.6, 136.4, 133.1, 129.7, 129.1, 128.9, 128.7, 127.2, 127.1, 127, 98.0, 24.2. MS (GC/MS) *m/z* 264 [M^+-48]. Anal. Calcd. for $C_{18}H_{15}BF_2O_2$: C, 69.27, H, 4.84. Found: C, 69.51, H, 4.88.

2.3

A stirred solution of **S2.3** (0.218 g, 1.04 mmol) and **S2.1** (0.122 g, 0.473 mmol) in acetonitrile (4 mL) and acetic anhydride (0.25 mL) was heated to reflux. Diaza(1,3)bicycle[5.4.0]undecane (DBU) (0.25 mL) in acetonitrile (1 mL) was added dropwise and the mixture was stirred for 5 min. The solution was allowed to cool to room temperature, then a hexanes/ether (1:1, 100 mL) was added and the solution cooled to -20 ˚C. After 2 h, the resultant precipitate was filtered, the solid was reprecipitated from dichloromethane with hexanes, and collected again by filtration. The green residue was combined with tetra-*n*-octylammonium bromide (0.285 g, 0.522 mmol) and put under a nitrogen atmosphere. Dry tetrahydrofuran (10 mL) was used to dissolve the compounds. A slurry of sodium hydride (70 mg, 2.8 mmol) in tetrahydrofuran (10 mL) was added dropwise, and the resultant mixture was stirred for 5 min. The solution was quickly filtered and the solvent of the filtrate was removed under reduced pressure to give a

residue that was purified by silica gel column chromatography using ethylacetate/hexanes (1:2) as eluent (259 mg, 0.281 mmol, 59%). ^{1}H NMR (400 MHz, $CDCl_3$, 333 K): δ (ppm) 7.89 (dd, J = 1.6 Hz, 7.9, 4H), 7.81 (t, J = 12.8 Hz, 2H), 7.43-7.35 (m, 6H), 6.19 (t, J = 12.9 Hz, 1H), 6.12 (s, 2H), 5.65 (d, J = 13.2 Hz, 2H), 3.20 (m, 8H), 1.68 (m, 8H), 1.35 (m, 40H), 0.86 (t, J = 7.2 Hz, 12H). ^{13}C NMR (100 MHz, $CDCl_3$, 333 K): δ 173.9, 168.7, 151.6, 134.9, 131.1, 128.4, 126.9, 119.1, 108.9, 96.5, 59.3, 31.6, 28.99, 28.95, 26.4, 22.5, 22.1, 13.9. MS (ESI)(+) *m/z* 467 [M^+ cation] (–) *m/z* = 455 [M^- anion]. Anal. Calcd. for $C_{55}H_{85}B_2F_4NO_4$: C, 71.66, H, 9.29, N, 1.52. Found: C, 71.78, H, 9.40, N, 159.

2.4

A solution of **S2.4** (0.304 g, 1.17 mmol) and **S2.1** (0.140 g, 0.542 mmol) in acetonitrile (8 mL) and acetic anhydride (0.4 mL) was heated to reflux with stirring. DBU (0.25 mL) was added dropwise and then stirred for 15 min. The solution was allowed to cool to room temperature then hexanes/ether (1:1, 100 mL) was added. The precipitate was collected by filtration, and then re-precipitated. The oily residue was dried under vacuum, then combined with tetra-*n*-octylammonium bromide (0.315 g, 0.577 mmol) and put under a nitrogen atmosphere. Dry tetrahydrofurnan (20 mL) was used to dissolve the compounds. A slurry of sodium hydride (40 mg, 1.7 mmol) in tetrahydrofuran (10 mL) was added dropwise, and stirred for 5 min. The solution was quickly filtered and the solvent of the filtrate was removed. The desired product (0.108 g, 0.106 mmol, 18%) was obtained after silica gel chromatography of the residue using dichloromethane as the eluent, followed by a final precipitation from dichloromethane using hexanes. ^{1}H NMR (400 MHz, $CDCl_3$, 333 K): δ (ppm) 8.46 (s, 2H), 7.88-7.78 (m, 10H), 7.50-7.46 (m, 4H), 6.29 (s, 2H), 6.24 (t, J = 12.4 Hz, 1H) 5.71 (d, J = 13.2 Hz, 2H) 3.12 (m, 8H) 1.60 (m,

8H) 1.31-1.22 (m, 40H) 0.83 (t, J = 6.8 Hz, 12H). ^{13}C NMR (100 MHz, $CDCl_3$, 333 K): δ (ppm) 173.8, 168.4, 151.3, 134.9, 133.2, 132.1, 129.2, 128.1, 127.7, 127.6, 127.5, 126.6, 123.4, 119.6, 109.3, 97.0, 59.3, 31.6, 29.0, 28.9, 26.4, 22.4, 22.0, 13.9. MS (ESI) (+) *m/z* 467 [M^+ cation] (–) *m/z* 555 [M^- anion]. Anal. Calcd. for $C_{63}H_{89}B_2F_4NO_4$: C, 74.04, H, 8.78, N, 1.37. Found: C, 74.15, H, 8.84 N, 1.51.

2.5

The **S2.5** (0.312 g, 1.00 mmol) and **S2.1** (0.126 g, 0.488 mmol) were dissolved in acetonitrile (4 mL) and acetic anhydride (0.25 mL). The solution was then heated to reflux with stirring. Triethylamine (0.21 mL) in acetonitrile (2 mL) was added dropwise and then stirred for 45 min. The solution was allowed to cool to room temperature, then hexanes/ether (1:1, 75 mL) was added and the solution put in the freezer. After 1 h. a precipitate was filtered, the solid was redissolved in acetonitrile and precipitated with ether (75 mL). The precipitate was collected by filtration and then combined with tetra-*n*-octylammonium bromide (0.285 g, 0.522 mmol) and put under a nitrogen atmosphere. Dry tetrahydrofuran (10 mL) was used to dissolve the compounds. A slurry of sodium hydride (70 mg, 2.8 mmol) in tetrahydrofuran (10 mL) was added dropwise, and stirred for 5 min. The solution was quickly filtered and the solvent of the filtrate was removed. The desired product was separated from the residue through silica gel chromatography with ethylacetate/hexanes (1:1) eluent (89 mg, 0.079 mmol, 16%). ^{1}H NMR (400 MHz, $CDCl_3$, 333 K): δ (ppm) 7.88 (d, J = 8.4 Hz, 4H), 7.80 (t, J = 13.0 Hz, 2H), 7.50 (d, J = 8.8 Hz, 8H), 7.34 (t, J = 7.6 Hz, 4H), 7.25 (t, J = 7.3 Hz, 2H overlap with chloroform), 7.17 (d, J = 16.3 Hz, 2H), 7.08 (d, J = 16.3 Hz, 2H), 6.20 (m, 3H), 5.67 (d, J = 13.0 Hz, 2H), 3.17 (m, 8H), 1.67 (m, 8H), 1.45-1.20 (m, 40H), 0.85 (t, J = 7.1 Hz, 12H). ^{13}C NMR

(100 MHz, $CDCl_3$, 333 K): δ(ppm) 173.5, 168.0, 151.1, 140.4, 137.2, 133.7, 133.7, 130.6 128.7, 128.0 (2 peaks overlapped), 127.3, 126.8, 126.5, 119.5, 109.3, 96.5, 59.3, 31.6, 29.0 (2 peaks overlapped), 26.4, 22.5, 22.0, 13.9. MS (ESI) (+) *m/z* 466.7 [M^+ cation] (–) *m/z* 659 [M^- anion]. Anal. Calcd. for $C_{63}H_{89}B_2F_4NO_4$: C, 75.72, H, 8.68, N, 1.24. Found: C, 76.00, H, 8.83 N, 1.22.

2.6

A solution of **S2.6** (0.399 g, 1.71 mmol) and **S2.1** (0.203 g, 0.785 mmol) in acetonitrile (8 mL) and acetic anhydride (0.5 mL) was heated to reflux with stirring. Triethylamine (0.4 mL) was added dropwise and then stirred for 20 min. The solution was allowed to cool to room temperature at which the solution was added to diethyl ether (200 mL) and cooled to -20 °C. A precipitate was collected by filtration, and reprecipitated from acetonitrile using ether at -20 °C. The precipitate collected by filtration was sonicated in acetic acid for 1 min. The remaining solid was collected by filtration on filter paper and rinsed with water. The crude material (0.114 g) was combined with tetra-*n*-octylammonium bromide (0.133 g, 0.243 mmol) and dissolved in dry tetrahydrofuran (10 mL) under a nitrogen atmosphere. A slurry of sodium hydride (18 mg, 0.75 mmol) in tetrahydrofuran (10 mL) was added dropwise, and stirred for 5 min. The solution was quickly filtered and the solvent was removed from the filtrate under reduced pressure. The desired product (156 mg, 0.161 mmol, 21%) was separated from the residue through silica gel (made basic by treatment with triethylamine) chromatography using dichloromethane as the eluent. ^{1}H NMR (400 MHz, $CDCl_3$): δ(ppm) 8.50 (d, J = 8.2 Hz, 2H), 8.14 (t, J = 12.7 Hz, 2H), 7.69 (d, J = 8.0 Hz, 2H), 7.58-7.53 (m, 4H), 7.45 (t, J = 7.3 Hz, 2H), 7.23 (d, J = 10.3, 2H), 6.54-6.51 (m, 3H), 3.10 (m, 8H), 1.58 (m, 8H), 1.27-

1.17 (m, 40H), 0.80 (t, J = 7.0 Hz, 12H). ^{13}C NMR (100 MHz, CD_2Cl_2): δ (ppm) 173.8, 159.7, 155.0, 137.7, 130.1, 127.9, 126.6, 126.3, 124.8, 123.3, 122.5, 119.5, 112.0, 107.1, 59.2, 32.0, 29.3 (2 peaks overlapped), 26.5, 22.9, 22.1, 14.2. MS (ESI) (+) *m/z* 467 [M^+ cation] (–) *m/z* 503 [M^- anion]. Anal. Calcd. for $C_{59}H_{85}B_2F_4NO_4$: C, 73.06, H, 8.83, N, 1.44. Found: C, 73.28, H, 8.82 N, 1.49.

2.7

A solution of **S2.7** (0.496 g, 2.07 mmol) and **S2.1** (0.243 g, 0.940 mmol) in acetonitrile (8 mL) and acetic anhydride (0.5 mL) was heated to 75 °C with stirring. Triethylamine (0.5 mL) was added dropwise and then heated to 80 °C stirred for 25 min. The solution was allowed to cool to room temperature and was then added to ether (100 mL) and the solution was kept at -20°C for 1 h. The dark oily precipitate was collected by decanting the solvent and the precipitation procedure was repeated. The residue was combined with tetra-*n*-octylammonium bromide (0.156 g, 0.286 mmol) and put under a nitrogen atmosphere. Dry tetrahydrofuran (20 mL) was used to dissolve the compounds. A slurry of sodium hydride (0.048 g, 2.0 mmol) in tetrahydrofuran (10 mL) was added dropwise and the resulting mixture was stirred for 5 min. The solution was quickly filtered and the filtrate was evaporated under reduced pressure. The desired product (0.110 g, 0.178 mmol, 19%) was separated from the residue using silica gel (made basic by treatment with triethylamine) chromatography with dichloromethane as the eluent. ^{1}H NMR (400 MHz, $CDCl_3$, 333 K): δ (ppm) 7.85 (d, J = 8.9 Hz, 4H), 7.74 (t, J = 13.0 Hz, 2H), 6.89 (d, J = 8.9 Hz, 4H), 6.14 (d, J = 12.0 Hz, 1H), 6.03 (s, 2H), 5.61 (d, J = 13.1 Hz, 2H), 3.83 (s, 6H), 3.20 (m, 8H), 1.69 (m, 8H), 1.45-1.20 (m, 40H), 0.85 (t, J = 7.1 Hz, 12H). ^{13}C NMR (100 MHz, $CDCl_3$, 333 K): δ (ppm) 173.5, 168.6, 162.6, 128.8, 127.4, 116.0,

114.0, 108.2, 95.5, 59.5, 55.4, 31.6, 29.0 (two peaks overlapped), 26.4, 22.5, 22.1, 13.9. MS (ESI) (+) *m/z* 467 [M^+ cation] (–) *m/z* = 515 [M^- anion]. Anal. Calcd. for $C_{57}H_{89}B_2F_4NO_6$: C, 69.72, H, 9.14, N, 1.43. Found: C, 70.00, H, 9.19 N, 1.42.

2.8

A solution of **S2.8** (0.526 g, 2.06 mmol) and **S2.1** (0.257 g, 0.994 mmol) in acetonitrile (8 mL) and acetic anhydride (0.5 mL) was heated to reflux with stirring. Triethylamine (0.42 mL) in acetonitrile (2 mL) was added dropwise and then stirred for 1 min. Upon cooling to room temperature a mixture of hexanes/diethylether (1:1, 150 mL) was added, then the kept at -20 °C for 1 h. The precipitate was collected by filtration and dried under vacuum. The precipitate was combined with tetra-*n*-octylammonium bromide (0.60 g, 1.1 mmol) and put under a nitrogen atmosphere. Dry tetrahydrofuran (10 mL) was used to dissolve the compounds. A slurry of sodium hydride (0.144 mg, 6.0 mmol) in tetrahydrofuran (10 mL) was added dropwise, and the resulting mixture stirred for 5 min. The solution was quickly filtered and the filtrate was evaporated under reduced pressure. The desired product (0.57 g, 0.56 mmol, 56%) was separated from the residue through silica gel (made basic by treatment with triethylamine) chromatography with Ethyl acetate/hexanes (1:2) as the eluent. ^{1}H NMR (400 MHz, $CDCl_3$, 333 K): δ (ppm) 8.22 (d, J = 9.0 Hz, 4H), 8.02 (d, J = 9.0 Hz, 4H), 7.86 (t, J = 13.1 Hz, 2H), 6.27 (t, J = 12.6 Hz, 1H), 6.21 (s, 2H), 5.75 (d, J = 13.1 Hz, 2H), 3.21 (m, 8H), 1.70 (m, 8H), 1.45-1.20 (m, 40H), 0.85 (t, J = 7.1 Hz, 12H). ^{13}C NMR (100 MHz, $CDCl_3$, 333 K): δ (ppm) 173.9, 165.6, 152.7, 149.3, 140.6, 127.5, 123.6, 121.2, 110.6, 59.5, 31.6, 29.0, 28.9, 26.4, 22.5, 22.1, 13.9. MS (ESI) (+) *m/z* 467 [M^+ cation] (–) *m/z* 545 [M^- anion]. Anal. Calcd. for $C_{55}H_{83}B_2F_4N_3O_8$: C, 65.28, H, 8.27, N, 4.15. Found: C, 65.51, H, 8.39 N, 4.15.

2.9

A solution of **S2.5** (0.442 g, 1.42 mmol), **S2.2** (0.220 g, 0.678 mmol) and 1,8-bis(dimethylamino)naphthalene (proton sponge) (0.487 g, 2.28 mmol) in acetonitrile (8 mL) and acetic anhydride (0.25 mL) was heated to reflux with stirring for 35 min. The reaction mixture was filtered upon cooling. The crude solid (0.341 g, 0.350 mmol crude) was combined with tetra-*n*-octylammonium bromide (0.309 g, 0.566 mmol) and put under a nitrogen atmosphere and dissolved in dry tetrahydrofuran (30 mL). A slurry of sodium hydride (38 mg, 1.6 mmol) in dry tetrahydrofuran (15 mL) was added dropwise and the resulting mixture was stirred for 10 min. The solution was quickly filtered and the solvent of the filtrate was removed under reduced pressure. The residue was purified by chromatography on silica gel (made basic by treatment with triethylamine), using hexanes/dichloromethane (3:1), followed by a second column prepared in the same manner using hexanes/dichloromethane (1:1), followed by dichloromethane as the eluents. The solvent was removed under reduced pressure and a black powder was collected by filtration after precipitating it from dichloromethane with hexanes. (0.184 g, 0.156 mmol, 23%). ^{1}H NMR (400 MHz, $CDCl_3$, 333 K): δ (ppm) 7.84 (d, J = 8.4 Hz, 4H), 7.57 (t, J = 13.0 Hz, 2H), 7.45 (d, J = 8.2 Hz, 8H), 7.31 (t, J = 7.7 Hz, 4H), 7.22 (m, 2H), 7.12 (d, J = 16.3 Hz, 2H), 7.01 (d, J = 16.3 Hz, 2H), 6.88 (t, J = 12.9 Hz, 2H), 6.21 (t, J = 12.8 Hz, 2H), 6.13 (s, 2H), 5.65 (d, J = 12.9 Hz, 2H), 3.10 (m, 8H), 1.58 (m, 8H), 1.31-1.26 (m, 40H), 0.87 (t, J = 7.1 Hz, 12H). A satisfactory ^{13}C NMR spectrum was not obtained for this compound due to expected complications related to the restricted rotations as shown in Figure 2.7 at room temperature, which would lead to broad peaks in the spectrum and rapid decomposition of the dye at 333 K. MS (ESI) (+) *m/z* 466 [M^+

cation] (–) *m/z* 711 [M⁻ anion]. Anal. Calcd. for $C_{75}H_{101}B_2F_4NO_4$: C, 76.45, H, 8.64, N, 1.19. Found: C, 76.17, H, 8.74 N, 1.25.

2.5. References

1. Meerwein, H.; Vossen, D., Synthesis of ketones and beta-ketones with boron fluoride. *J. Prakt. Chem.* **1934,** 141, 149-166.
2. Young, F. G.; Frostick Jr, F. C.; Sanderson, J. J.; Hauser, C. R., Conversion of Ketone Enol Esters to beta-diketones by Intramolecular Thermal Rearrangement and by Intermolecular Acylations Using Boron Trifluoride. *J. Am. Chem. Soc.* **1950,** 72, 3635-3642.
3. Hauser, C. R.; Frostick Jr, F. C.; Man, E. H., Mechanism of Acetylation of Ketone Enol Acetates with Acetic Anhydride by Boron Trifluoride to Form *β*-ketones. *J. Am. Chem. Soc.* **1952,** 74, 3231-3233.
4. Halik, M.; Hartmann, H., Synthesis and Characterization of New Long-Wavelength-Absorbing Oxonol Dyes from the 2,2-Difluoro-1,3,2-dioxaborine Type. *Chem. Eur. J.* **1999,** 5, 2511-2517.
5. VanAllan, J. A.; Reynolds, G. A., The Reactions 2,2-difluoro-4-methylnaphtho[1,2-*e*]-1,3,2-dioxaborin and Its [2,1-*e*] Isomer with Carbonyl Compounds and with Aniline. *J. Heterocycl. Chem.* **1969,** 6, 29-35.
6. Reynolds, G. A.; VanAllan, J. A., The reactions of 2,2-Difluoro-4-methylnaphtho[1,2-*e*]-1,3,2-dioxaborin and Its [2,1-*e*] Isomer with *N,N*-Dimethylformamide. *J. Heterocycl. Chem.* **1969,** 6, 375-377.
7. Reynolds, G. A.; VanAllan, J. A.; Seidel, A. K., Synthesis of Chromones. *J. Heterocycl. Chem.* **1979,** 16, 369-370.
8. Kammler, R.; Bourhill, G.; Jin, Y.; Bräuchle, C.; Görlitz, G.; Hartmann, H., Second-Order optical non-linearity of new dioxaborine dyes. *J. Chem. Soc., Faraday Trans.* **1996,** 92, 945-947.
9. Han, L.; Jiang, Y.; Li, W.; Li, Y.; Hao, P., Spectroscopic Investigations of A Novel Tricyanofuran Dye for Nonlinear Optics. *Spectrochim. Acta, Part A* **2008,** 71, 86-89.
10. Risko, C.; Barlow, S.; Coropceanu, V.; Halik, M.; Brédas, J.-L.; Marder, S. R., An Anionic Organic Mixed-Valence System with Remarkably Well-Resolved Vibrational Structure in its Intervalence Band. *Chem. Commun.* **2003**, 194-195.
11. Domercq, B.; Grasso, C.; Maldonado, J.-L.; Halik, M.; Barlow, S.; Marder, S. R.; Kippelen, B., Electron-Transport Properties and Use in Organic Light-Emitting Diodes of a Bis(dioxaborine)fluorene Derivative. *J. Phys. Chem. B* **2004,** 108, 8647-8651.
12. Halik, M.; Wenseleers, W.; Grasso, C.; Stellacci, F.; Zojer, E.; Barlow, S.; Brédas, J.-L.; Perry, J. W.; Marder, S. R., Bis(dioxaborine) compounds with large two-photon cross sections, and their use in the photodepostion of Silver. *Chem. Commun.* **2003**, 1490-1491.
13. Cogné-Laage, E.; Allemand, J.-F.; Ruel, O.; Baudin, J.-B.; Croquette, V.; Blanchard-Desce, M.; Jullien, L., Diaroyl(methanato)boron Difluoride Compounds as Medium-Sensitive Two-Photon Fluorescent Probes. *Chem. Eur. J.* **2004,** 10, 1445-1455.

14. Zyabrev, K. V.; Il'chenko, A. Y.; Slominskii, Y. L.; Tolmachev, A. I., *Ukr. Khim. Zh.* **2006,** 72, 56-63.
15. Traven, V. F.; Chibisova, T. A.; Manaev, A. V., Polymethine dyes derived from Boron Complexes of acetylhydroxycoumarins. *Dyes Pigm.* **2003,** 58, 41-46.
16. Markin, V. S.; Abramenko, P. I.; Boiko, I. I., Polymethine dyes - derivatives of organic complexes of boron. *Zhurnal Vsesoyuznogo Khimicheskogo Obshchestva im. D. I. Mendeleeva* **1984,** 29, (4), 457-459.
17. Zyabrev, K. V.; Il'chenko, A. Y.; Slominskii, Y. L.; Romanov, N. N.; Tolmachev, A. I., Polymethine Dyes Derived from 2,2-difluoro-3,1,2-(2H)-oxaoxoniaboratines with Polymethylene Bridge Groups in the Chromophore. *Dyes Pigm.* **2006,** 71, 199-206.
18. Gerasov, A. O.; Shandura, M. P.; Kovtun, Y. P., Polymethine Dyes Derived from the Boron Trifluoride Complex of 3-acetyl-5,7-di(pyrrolidin-1-yl)-4-hydroxycoumarin. *Dyes Pigm.* **2008,** 79, 252-258.
19. Gerasov, A. O.; Shandura, M. P.; Kovtun, Y. P., Series of polymethine dyes derived from 2,2-difluoro-1,3,2-(2*H*)-dioxaborine of 3-acetyl-7-diethylamino-4-hydroxycoumarin. *Dyes Pigm.* **2008,** 77, 598-607.
20. Zyabrev, K.; Doroshenko, A.; Mikitenko, E.; Slominskii, Y.; Tolmachev, A., Design, Synthesis and Spectral Luminescent Properties of a Novel Polycarbocyanine Series Based on the 2,2-difluoro-1,3,2-dioxaborine Nucleus. *Eur. J. Org. Chem.* **2008**, 1550-1558.
21. Hales, J. M.; Zheng, S.; Barlow, S.; Marder, S. R.; Perry, J. W., Bisdioxaborine Polymethines with Large Third-Order Nonlinearities for All-Optical Signal Processing. *J. Am. Chem. Soc.* **2006,** 128, 11362-11363.
22. Ryabitsky, A. B.; Kachkovski, A. D.; Przhonska, O. V., Symmetry breaking in cationic and anionic polymethine dyes. *J. Mol. Struct. THEOCHEM* **2007,** 802, 75-83.
23. *Performed by Dr. Joel Hales*.
24. Matichak, J. D.; Hales, J. M.; Ohira, S.; Barlow, S.; Jang, S.-H.; Jen, A. K.-Y.; Brédas, J.-L.; Perry, J. W.; Marder, S. R., Using End Groups to Tune the Linear and Nonlinear Optical Properties of Bis(dioxaborine)-Terminated Polymethined Dyes. *ChemPhysChem* **2010,** 11, 130-138.
25. Görlitz, G.; Hartmann, H., On the Formation and Solvolysis of 4-Aryl-2,2-difluoro-6-methyl-1,3,2-(2H)-dioxaborines. *Heteroat. Chem.* **1997,** 8, (2), 147-155.
26. Barlow, S.; Bunting, H. E.; Ringham, C.; Green, J. C.; Bublitz, G. U.; Boxer, S. G.; Perry, J. W.; Marder, S. R., Studies of the Electronic Structure of Metallocene-Based Second-Order Nonlinear Optical Dyes. *J. Am. Chem. Soc.* **1999,** 121, 3715-3723.
27. Werncke, W.; Pfeiffer, M.; Johr, T.; Lau, A.; Grahn, W.; Johannes, H.-H.; Dähne, L., Increase and saturation of the third order hyperpolarizabilities in homologous series of symmetric cyanines. *Chem. Phys.* **1997,** 216, 337-347.
28. Ridley, J.; Zerner, M., *Theor. Chim. Acta* **1973,** 32, 111-134.
29. Pople, J. A.; Beveridge, D. L.; Dobosh, P. A., Approximate Self-Consistent Molecular-Orbital Theory. V. Intermediate Neglect of Differential Overlap. *J. Chem. Phys.* **1967,** 47, 2026-2033.
30. Ohira, S.; Rudra, I.; Schmidt, K.; Barlow, S.; Chung, S.-J.; Zhang, Q.; Matichak, J.; Marder, S. R.; Brédas, J. L., Electronic and Vibronic Contributions to Two-Photon Absorption in Donor-Acceptor-Donor Squaraine Chromophores. *Chem. Eur. J.* **2008,** 14, 11082-11091.

31. Becke, A. D., Density-functional exchange-energy approximation with correct asymptotic behavior. *Phys. Rev. A* **1988,** 38, 3098-3100.
32. Becke, A. D., Density-functional thermochemistry. III. The role of exact exchange. *J. Chem. Phys.* **1993,** 98, 5648-5652.
33. Dirac, P. A. M., *Proc. Royal Soc. (London) A* **1929,** 123, 714-733.
34. Lee, C.; Yang, W.; Parr, R. G., *Phys. Rev. B* **1988,** 37, 785-789.
35. Slater, J. C., A Simplification of the Hartree-Fock Method. *Phys. Rev.* **1951,** 81, 385-390.
36. Ahlrichs, R.; Bär, M.; Häser, M.; Horn, H.; Kölmel, C., Electronic Structure Calculations on Workstation Computers: The Program System Turbomole. *Chem. Phys. Lett.* **1989,** 162, 165-169.
37. Performed by Dr. Shino Ohira.
38. Thorley, K. J.; Hales, J. M.; Anderson, H. L.; Perry, J. W., Porphyrin Dimer Carbocations with Strong Near Infrared Absorption and Third-Order Optical Nonlinearity. *Angew. Chem. Int. Ed.* **2008,** 47, 7095-7098.
39. Sheik-bahae, M.; Said, A. A.; Van Stryland, E. W., High-sensitivity, single-beam n_2 measurements. *Opt. Lett.* **1989,** 14, 955-957.
40. Dirk, C. W.; Cheng, L.-T.; Kuzyk, M. G., A Simplified Three-Level Model Describing the Molecular Third-Order Nonlinear Optical Susceptibility. *Int. J. of Quantum Chem.* **1992,** 43, 27-36.
41. Hales, J. M.; Zheng, S.; Barlow, S.; Marder, S. R.; Perry, J. W., Bisdioxaborine Polymethines with Large Third-Ordr Nonlinearities for All-Optical Signal Processing. *J. Am. Chem. Soc.* **2006,** 128, 11362-11363.
42. Zojer, E.; Beljonne, D.; Kogej, T.; Vogel, H.; Marder, S. R.; Perry, J. W.; Brédas, J.-L., Tuning the Two-Photon Absorption Response of Quadrupolar Organic Molecules. *J. Chem. Phys.* **2002,** 116, 3646-3658.
43. Fu, J.; Padilha, L. A.; Hagan, D. J.; Van Stryland, E. W., Molecular Structure—Two-Photon Absorption Property Relations in Polymethine Dyes. *J. Opt. Soc. Am. B: Opt. Phys.* **2007,** 24, 56-66.
44. Stegeman, G. I.; Stolen, R. H., Waveguides and figures for nonlinear optics. *J. Opt. Soc. of Am. B: Opt. Phys.* **1989,** 6, 652-662.
45. Mizrahi, V.; DeLong, K. W.; Stegeman, G. I., Two-photon absorption as a limitation to all-optical switching. *Opt. Lett.* **1989,** 14, 1140-1142.
46. Nikolajewski, H. E.; Dähne, S.; Hirsch, B., Vilsmeir-Formylierung von Polenaldehyden. *Chem. Ber.* **1967,** 100, 2616-2619.
47. Pangborn, A. B.; Giardello, M. A.; Grubbs, R. H.; Rosen, R. K.; Timmers, F. J., Safe and Convenient Procedure for Solvent Purification. *Organometallics* **1996,** 15, 1518-1520.
48. Barlow, S.; Risko, C.; Chung, S.-J.; Tucker, N. M.; Coropceanu, V.; Jones, S. C.; Levi, Z.; Brédas, J.-L.; Marder, S. R., Intervalence Transitions in the Mixed-Valence Monocations of Bis(triarylamines) Linked with Vinylene and Phenylene-Vinylene Bridges. *J. Am. Chem. Soc.* **2005,** 127, 16900-16911.
49. Arvela, R. K.; Leadbeater, N. E., Microwave-Promoted Heck Coupling Using Ultralow Metal Catalyst Concentrations. *J. Org. Chem.* **2005,** 70, 1786-1790.

Chapter 3

Effects of Bridge Substitution of Dioxaborine-Terminated Polymethine Dyes upon the Third-Order Nonlinear Optical Properties

3.1. Introduction

The Dewar-Knott rules, developed to predict the effects upon the absorption spectra of chromophores caused by substituent effects, were examined in the context of their effects on the third-order nonlinear optical properties of a series of dioxaborine pentamethine dyes and indole-terminated heptamethine dyes. Substituents in the polymethine bridge classified as electron donating or withdrawing groups would be expected to have different effects on the third-order nonlinear optical properties of analogous dyes.

3.1.1. Introduction and Background

Valence bond theory predicts polymethine dyes to have two major, limiting resonance structures of equal energy.[1] The dominance of these two resonance structures lead to a molecular structure that has zero C—C bond length alternation in both the ground and excited states for atoms in the polymethine bridge. Figure 3.1 shows the two primary contributing resonance structures for a simple bis(dimethylamino)pentamethine cationic dye (A, which will henceforth be referred to as $^{+}$BDMP), and a simple anionic dye (B). The bottom of parts of both A and B of Figure 3.1 illustrate a delocalized representation for the ground-state electronic structures of the dyes.

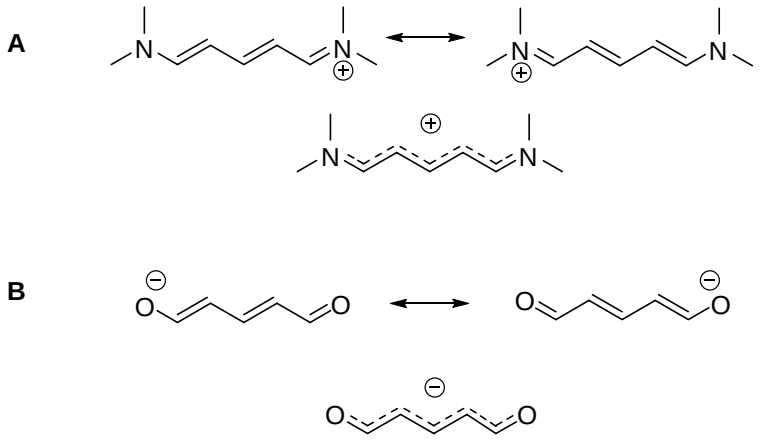

Figure 3.1. Two major contributing resonance structures of $^{+}$BDMP (A, top) and a simple anionic pentamethine (B, top). The ground state structure of $^{+}$BDMP (A, bottom) and the simple anionic pentamethine (B, bottom) are also shown.

In this chapter the methine carbons in the bridge will be labeled α, β, γ, *etc*. depending on the position from the terminal groups, as shown for $^{+}$BDMP in Figure 3.2. $^{+}$BDMP and all other polymethine dyes are analogous to odd-alternant hydrocarbons. If the atoms of the conjugated system can be marked, in this case with stars (*) and no stars, in an alternating pattern without any two atoms with or without stars adjacent to one another, then the system is alternant. The uneven distribution of starred atoms and unstarred atoms makes the system odd (*e.g.* $^{+}$BDMP has 4 starred and 3 unstarred π-conjugated atoms). Even- and odd-alternate hydrocarbons, and how they relate to polmethine dyes, as well as the color-structure relationship between polymethine and related dyes was reviewed by Griffiths.[1]

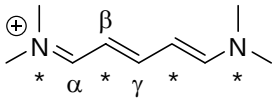

Figure 3.2. $^{+}$BDMP shown as an odd-alternant system with the α, β, and γ positions shown.

Dewar[2] proposed that even-alternant hydrocarbons form an equal number of bonding and antibonding orbitals of equal and opposite energy (+E and –E) for each pair of atoms in the π-system (Figure 3.3, A). However, odd-alternant hydrocarbons have an atom, which cannot be paired with another atom in the conjugated system. This leads to a non-bonding molecular orbital. For cationic polymethines the non-bonding molecular orbital is unfilled, while for anionic polymethine dyes the non-bonding molecular orbital is filled. The energy gap between the HOMO's and LUMO's of a cationic odd-alternant hydrocarbon (*e.g.* cationic polymethine) and an anionic odd-alternant hydrocarbon (*e.g.* anionic polymethine) are the same (Figure 3.3, B and C).

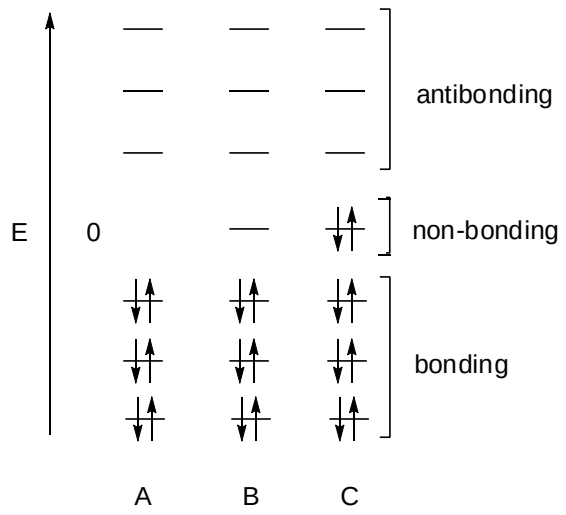

Figure 3.3. Orbital energies of even- and odd-alternant hydrocarbons. The arrows represent electrons. A) even-alternant hydrocarbon (*e.g.* polyene), B) a cationic odd-alternate hydrocarbon (*e.g.* cationic polymethine), and C) an anionic odd-alternate hydrocarbon (*e.g.* anionic polymethine).[2]

Typically the low energy transition of a polymethine dye from the ground state to the excited state is well described by the excitation of a single electron from the highest occupied molecular orbital (HOMO) to the lowest unoccupied molecular orbital

(LUMO). The presence of the non-bonding molecular orbital (the HOMO in anionic dyes and the LUMO in cationic dyes) creates relatively small energy gaps for transitions, generally resulting in bathochromic shifts compared to even-alternant hydrocarbons (polyenes). The orbital coefficients on the atoms in the HOMO alternate between vanishingly small and relatively large (similar to the starred and unstarred positions) along the participating atoms of the π-conjugated system of the polymethine dye. An opposite trend in the magnitude of coefficients is observed in the lowest occupied molecular orbital (LUMO); those atoms with large coefficients in the HOMO will have a small coefficient in the LUMO and vice versa. An example of this is shown for $^{+}$BDMP in Figure 3.4.

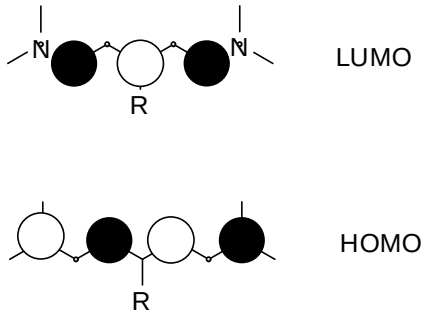

Figure 3.4. Coefficients of the HOMO and LUMO of $^{+}$BDMP.

Five resonance structures substantially contributing the ground state of $^{+}$BDMP are drawn in Figure 3.5, which collectively demonstrate from a valence bond point of view that some atoms are electron rich and some are electron poor (the positive charge can only be drawn on the α and γ carbons of the polymethine bridge. Konig[3] was the first to propose that polymethine dyes had an alternating charge density among the methine atoms. This charge alternation was first shown experimentally by Dähne *et al.*[4] through

the use of NMR. The atoms with higher electron density generally correspond to those that have larger HOMO coefficient, while the electron poor atoms generally track the atoms with larger LUMO coefficient.

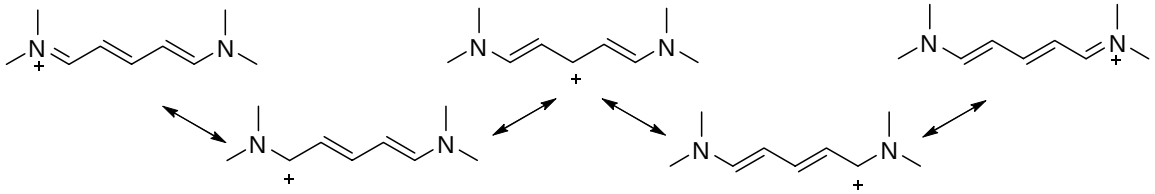

Figure 3.5. Five resonance structures substantially contributing the ground state to $^{+}$BDMP.

Accompanying the first one-photon excitation from the HOMO to the LUMO is significant charge transfer. The charge-transfer occurs from the alternating electron rich atoms to the electron poor atoms (In the case of D-π-A polyenes the charge transfer occurs between the change in electron densities between bonds). In the ground state of $^{+}$BDMP the electron rich atoms are the starred atoms (those with significant HOMO coefficient). Klessinger[5] used the Pariser-Parr-Pople molecular orbital theory to calculate the π-electron densities of various cyanines including $^{+}$BDMP, which the values for the ground state and excited state are shown in Figure 3.6. Upon excitation the electron rich atoms transfer some of the charge to the electron poor atoms.

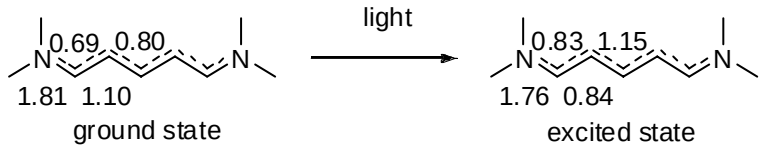

Figure 3.6. The π-electron densities for the ground and first excited state of $^{+}$BDMP[5].

Dewar[6] and Knott[7] have formulated some general rules to predict the color of dyes. A bathochromic shift is produced if electron withdrawing groups (EWG) (or atoms of higher electronegativity replace carbon) are substituents at unstarrred position or if electron donating groups (EDG) (or atoms with lower electronegativity replace carbon) are substituents on starred positions. A hypsochromic shift occurs if electron donating groups are substituents on unstarred positions or electron withdrawing groups are substituents on starred positions.

A simple treatment of molecular orbital theory can be used to predict the effects of EDGs and EWGs substituted into the polymethine bridge. Figure 3.7 shows a diagram of $^{+}$BDMP with a Y substituent on the γ position of the polymethine bridge. Substituents on the γ position should have greater interaction with the LUMO, due to its nonzero-orbital coefficient on that atom, relative to zero-orbital coefficient on the HOMO. If Y is an EWG, the HOMO will only be stabilized slightly relative to $^{+}$BDMP (Y = H), while the LUMO will be significantly stabilized. In this case the energy gap should be reduced causing a bathochromic shift in absorption maxima. In the case where Y is an EDG the LUMO will be destabilized relative to $^{+}$BDMP, significantly more than the destabilization of the HOMO, resulting in a larger energy gap.

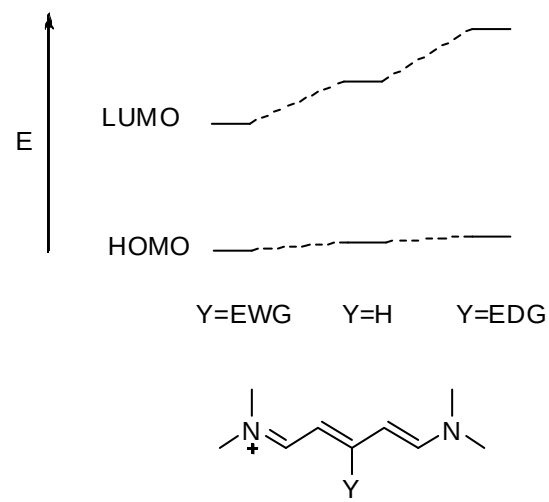

Figure 3.7. Effects upon the orbital energies due to electron withdrawing and electron donating substituents in the γ position of parent dye, $^{+}$BDMP.

Classification of substituents into EDG and EWG is complicated due to σ-bond (inductive effects) and π-bond (lone pair donation or lone pair acceptance) effects that can be in opposition. Hammett did extensive work concerning the electronic effects caused by substituents on reaction mechanisms.[8] He looked at the relative acidities of substituted benzoic acids (**3.I**) to determine the σ_p parameters defined in the following equation:

$$\sigma_p = \log K_Y - \log K_H \qquad \text{E3.1}$$

where K_H is the ionization constant of benzoic acid in water at 25 °C and K_Y is the equilibrium constant for *para*-substituted benzoic acid. A positive value indicates the derivative is more acidic than benzoic acid (the substituent is electron withdrawing and can stabilize the formation of a negative charge), while a negative value indicates lower acidity of the derivative (the substituent is electron donating and destabilizes the negative charge). The σ_p values of selected Hammett parameters are given in Table 3.1. Roberts and Moreland[9] examined the difference in equilibrium constants of substituted

bicyclooctane carboxylic acids of **3.II** to determine the field and inductive effects (F) of substituents. **3.II** only has single bonds, so only inductive or field effects should be observed, because resonance effects (R) require π-bonds. The field (F) and resonance (R) terms determined by Swain and Lupton[10] and subsequently modified by Charton[11] can be expressed through the following equation:

$$\sigma_p = F + R \qquad \text{E3.2}$$

A positive F value corresponds to a σ-electron withdrawing group, while a positive R value is π-electron withdrawing. A negative R value would correspond to a π -electron donating group. The number of analyzed substituents was extended by Hansch *et al*[12], from which selected F and R values are reported in Table 3.1.

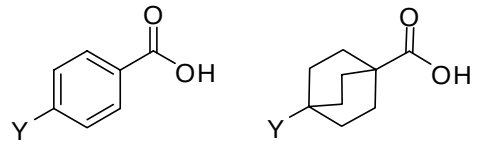

3.I **3.II**

Table 3.1. Hammett parameters and Modified Swain-Lupton constants[12]

Substituent (Y)	σ_p	F	R
H	0.00	0.03	0.00
NO_2	0.78	0.65	0.13
CN	0.66	0.51	0.15
Cl	0.23	0.42	-0.19
OPh	-0.03	0.37	-0.40
SPh	0.07	0.30	-0.23
OMe	-0.27	0.29	-0.56
NMe_2	-0.83	0.15	-0.98

Examples of bridge-substituted polymethine dyes can be found in the literature. Slominski *et al*.[13] and Encinas *et al*.[14] have reported on a series of benzothiazole heptamethine cyanines, **3.III-3.VII**, which have a variety of substituents attached to the ε carbon of the polymethine bridge. The ε carbon has increased coefficient on the LUMO, so electron donating groups should cause a hypsochromic shift, while the withdrawing groups should cause a bathochromic shift in λ_{max} relative to Y = H (**3.III**). The substituent, λ_{max}, and extinction coefficient (ε_{max}) are given in Table 3.2.

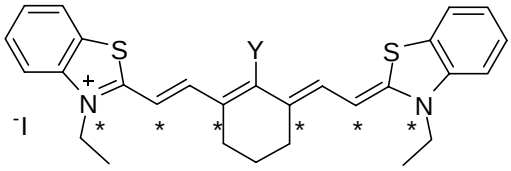

Table 3.2. λ_{max} and ε_{max} of **3.III-3.VII**.

Dye	Y	λ_{max} (nm)	ε (10^5 $M^{-1}cm^{-1}$)
3.III	H	766	-
3.IV	NMe_2	698	1.11[a]
3.V	Cl	799	2.10[b]
3.VI	SPh	805	2.64[a]
3.VII	CN	884	1.80[a]

[a]From Slominski *et al* in MeOH.[13]
[b]From Encinas *et al* in EtOH.[14]

According to the modified Swain and Lupton constants, the dimethylamino substituent is a strong π-electron donating group (R = -0.98), and only a mild σ-electron withdrawing group (F = 0.15). A hypsochromic shift in λ_{max} was observed for **3.IV**, which is, therefore, consistent with predictions using the Dewar-Knott rule. The shift in λ_{max} was accompanied by a large decrease in molar absorptivity. Similar amine-

substituted dyes have absorption spectra with extensive broadening of the lowest energy absorption band, which deviates significantly from typical polymethine absorption spectra.[15] This broadened shape of the first absorption band may be caused by a new dominant resonance form, which delocalizes the charge between the dimethylamine to the indole-terminal groups, as shown in Figure 3.8.

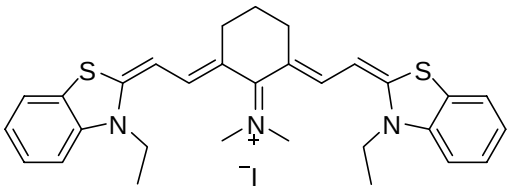

3.IV

Figure 3.8. Possible resonance form for the strong π-electron donating substituent of **3.IV**.

It would be expected that chloro (**3.V**) and phenylsufanyl (**3.VI**) substituents have both π-electron donating abilities and σ-electron withdrawing abilities. Indeed, this is seen in the modified Swain-Lupton constants in Table 3.1. These counteracting effects on the energy level of the HOMO and LUMO make it difficult to strictly define these substituents as electron withdrawing or electron donating. In this case, where the substituent is on a methine carbon with a significant coefficient in the LUMO, the LUMO of the dye will be stabilized more than the HOMO. The carbon directly bonded to the substituent has no coefficient, but the methine carbons one bond away (δ carbons) have substantial coefficient, so the HOMO is still affected by the substituent due to inductive effects through two bonds. The HOMO (with zero-coefficient) is unaffected by the π-ED effects; however, the LUMO is substantially destabilized. Evidently, in this case the π-

ED effects do not outweigh the σ-EW effects, so a bathochromic shift is observed in λ_{max} (Figure 3.9).

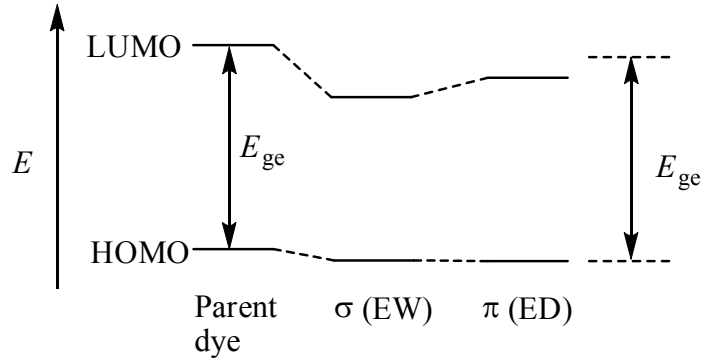

Figure 3.9. The σ-EW and π-ED effects on the HOMO and LUMO levels due to a substituent on a methine with a large LUMO coefficient. The weak interaction of the π-ED is insufficient to counter the stabilization effects of the σ-EW, so a bathochromic shift is observed.

According to the Swain-Lupton constants, the cyano substituent is both σ and π-electron withdrawing (F = 0.51, R = 0.15), so the cyano-substituent gives a bathochromic shift in λ_{max} for **3.VII**, which follows expectations from the Dewar-Knott Rule. Toxic conditions (use of sodium cyanide) are required to form the dye and it is noted by the authors that it is difficult to prepare the dye with the cyano compared to dyes with dimethylamino and phenylsufanyl groups.

Lepkowski *et al.*[16] investigated the substituent effects for a series of indole-terminated dyes, **3.VIII-3.XIII**. The substituent, $\lambda_{max,}$ and extinction coefficients (ε_{max}) are given in Table 3.3 for this series.

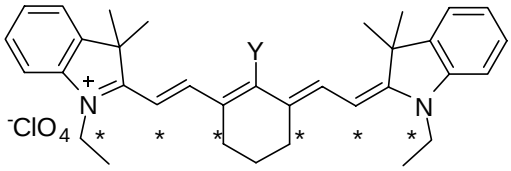

Table 3.3. λ_{max} and ε_{max} of **3.VI-3XI** in MeOH

Dye	Y	λ_{max} (nm)	ε (10^5 $M^{-1}cm^{-1}$)
3.VIII	H	747	2.62
3.IX	NHMe	615	0.84
3.X	Cl	778	2.19
3.XI	OMe	753	1.82
3.XII	OPh	764	2.06
3.XIII	SPh	790	1.68

In this series the amine substituted dye, **3.IX**, behaves similarly to **3.IV**, a hypsochromic shift was observed with a dramatic decrease in extinction coefficient. The chlorine substituted dye, **3.X**, also behaves similar to **3.V**. A bathochromic shift in λ_{max} is observed compared to **3.VIII**, due to the dominant σ-electron withdrawing abilities of the substituent.

3.XI, **3.XII**, and **3.XIII** have -OMe, -OPh, and -SPh substituents, respectively. Each of these substituents is strongly inductively withdrawing (F = 0.29, 0.37, and 0.30 respectively). However, the -SPh group has relatively lower π-electron donating abilities. According to Figure 3.7, the σ-electron withdrawing abilities of these three substituents should stabilize the LUMO by similar energies. However the -SPh group, would have a destabilizing effect on the LUMO less than that of -OMe and OPh, due to the reduced π-electron donation effects. This leads to the greater bathochromic shift observed for **3.XIII** (790 nm) than **3.XI** (753 nm) and **3.XII** (764 nm).

3.1.2. Goals of Chapter 2

This chapter aims to understand the effects upon the third-order nonlinear polarizabilities in polymethine dyes caused by substituent effects in the bridge of the polymethine dyes. In this study a series of bis(dioxaborine)-terminated pentamethine dyes was synthesized in which the γ methine of the polymethine bridge has a variety of substituents (Figure 3.10). The electronic effects caused by the various substituents were investigated through NMR spectroscopy, cyclic voltammetry, and UV-vis absorption spectroscopy. The effects caused by the substituents upon the third-order nonlinear polarizability were investigated using the Z-scan technique.

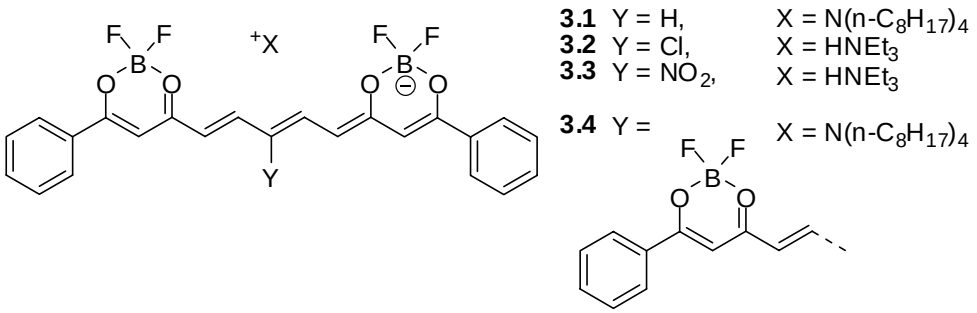

Figure 3.10. Dioxaborine-terminated dyes, **3.1-3.4**, investigated in this study.

3.2. Synthesis

The vinamidinium salts used in this study (**S3.1**, **S3.2**,[17] **S3.3**[17, 18], and **S3.4**[19]) are shown in Figure 3.11 and were synthesized by known methods.

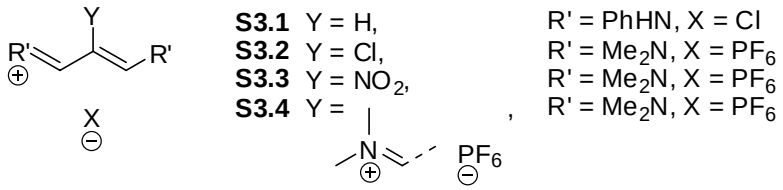

Figure 3.11. Vinamidinium building blocks to synthesize the polymethine dyes in this study.

The polymethine dyes were synthesized under the Knoevenagel reaction conditions using the vinamidinium salts, **S3.1**-**S3.4**, with the known dioxaborine acceptor **S3.5** in the presence of base (Scheme 3.1). The crude $HNEt_3^+$ salts of **3.1**, and **3.4** were converted to the sodium salt by treatment of sodium hydride, followed by ion metathesis with tetra-*n*-octylammonium bromide to obtain the final products (Scheme 3.2).

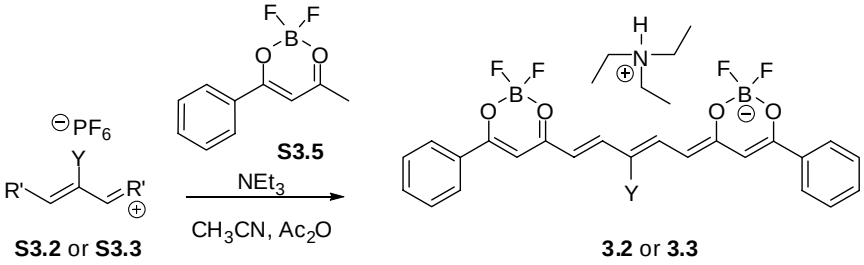

Scheme 3.1. Preparation of **3.2** and **3.3**.

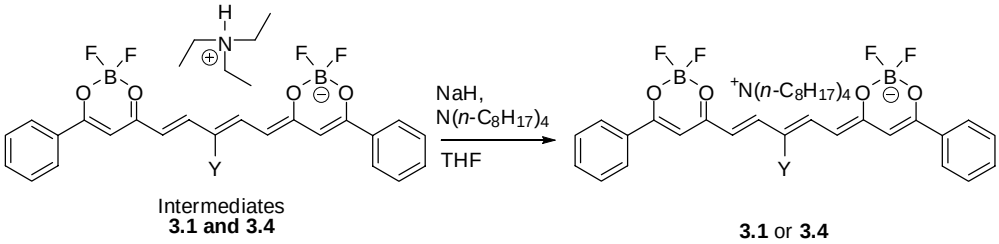

Scheme 3.2. Ion Metathesis reaction to prepare **3.1** and **3.4**.

3.3. NMR Spectroscopy Studies

The electron density on each atom of the core of the polymethine dye is reflected in ^{1}H NMR and ^{13}C NMR spectroscopy. Grahn *et al.*[20, 21] have studied the electronic effects of various γ substituents on the chemical shift of the methine carbons of a series of indole-terminated pentapolymethine dyes shown in Figure 3.12.

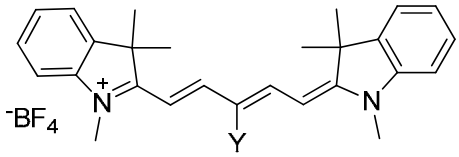

3.I'-3.IV'

Figure 3.12. Indole-terminated pentamethine dyes for which the ^{13}C NMR chemical shifts were determined.[20, 21]

A similar investigation was performed in this study on **3.1**-**3.4** in which the chemical shift of the γ carbon of each dye was determined in deuterated acetonitrile. The identification of the γ carbon for **3.1** was determined using heteronuclear single quantum correlation (HSQC) NMR spectroscopy, which shows direct correlations between directly bonded proton-carbon atoms. The assignments for the atoms are given in Figure 3.13.

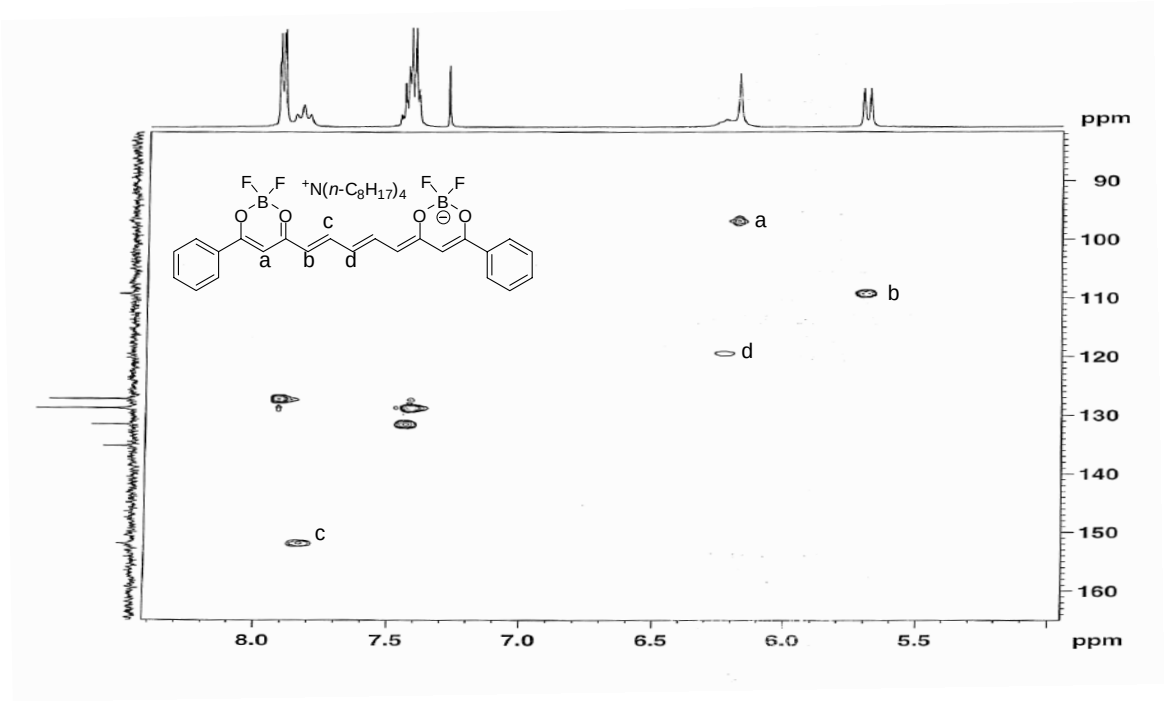

Figure 3.13. HSQC spectrum (^{1}H NMR on the x-axis with a ^{13}C NMR on the y-axis) of **3.1** in CD_3CN.

Table 3.4 shows the chemical shift of the methine carbons for **3.1-3.4** and **3.I'-3.IV'** from the literature.[20, 21]

Table 3.4. Chemical shifts for ^{13}C methine atoms for **3.1-3.4** (CD_3CN) and **3.I'-3.IV'** ($CDCl_3$)

Dye	α	β	γ	Dye	α	β	γ
3.1	110.6	152.6	121.5	**3.I'**[21]	103.3	154	125.2
3.2	108.1	146.6	120.5	**3.II'**[21]	100	147.4	122.3
3.3	110.2	140.4	130.8	**3.III'**[21]	102.3	141.5	131.5
3.4	112.7	147	118	**3.IV'**[20]	106.5	149.5	121.8

The α and γ methine carbons are generally shifted further downfield relative to the β carbons, which is consistent with the alternating charges on the atoms the polymethine bridges. Plotting the chemical shifts of the methine carbons of **3.1-3.4** with the chemical shifts of analogous compounds **3.I'-3.IV'** from the literature[20, 21] show similar trends observed for the chemical shifts for both sets of polymethine dyes despite being recorded in different solvents (Figure 3.14). There is generally little solvent dependence upon the chemical shift of the ^{13}C resonances of polymethine dyes, for example Wähnert *et al*.[22] obtained ^{13}C NMR spectra of $^{+}$BDMP in a variety of solvents with a large range of polarities, with little change observed in the chemical shift of the methine carbons.

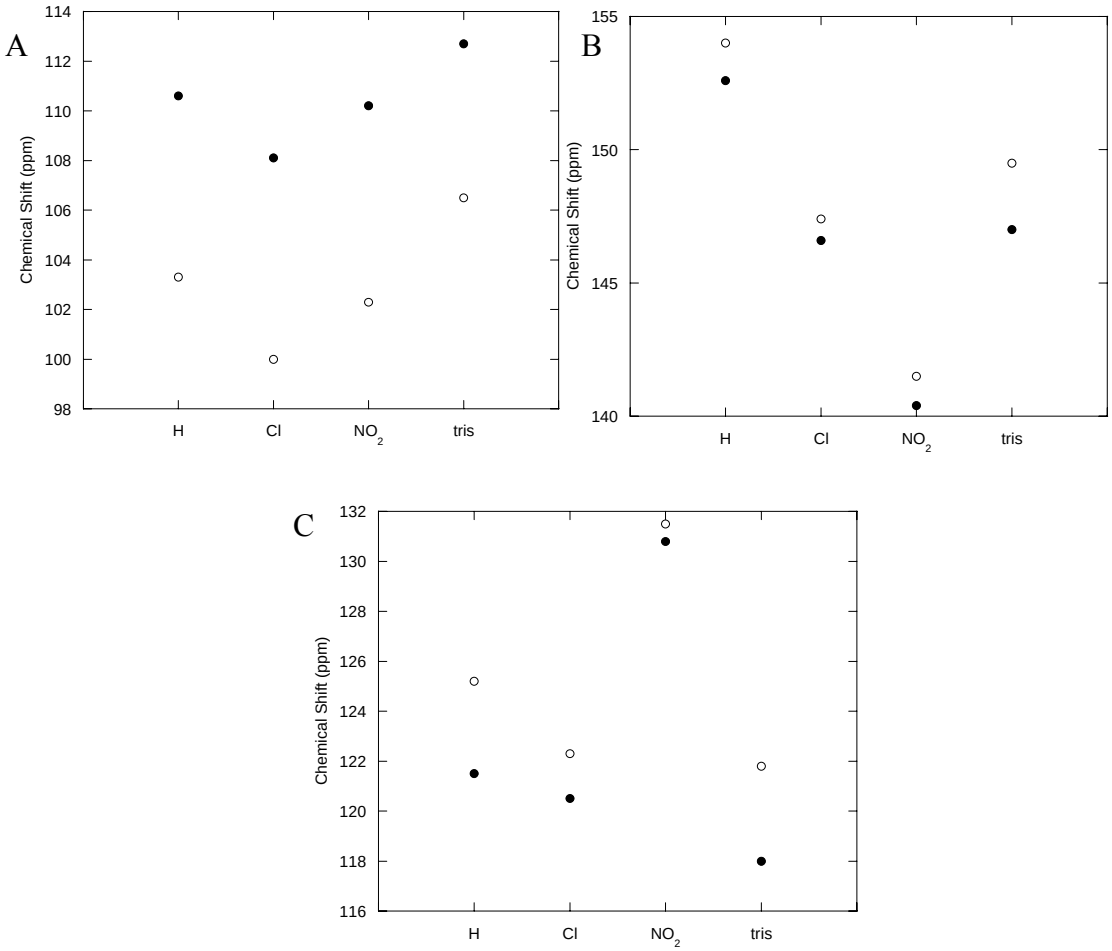

Figure 3.14. The ^{13}C NMR chemical shifts of the α (A), β (B), and γ (C) methine carbons of **3.1-3.4** and analogous dyes **3.I'-3.IV'** from the literature.[20, 21]

3.4. Electrochemistry

The redox properties of **3.1-3.4** were investigated using cyclic voltammetry in order to complement optical data in assigning the separate effects of the electron donating and withdrawing abilities of the substituents. The voltammagrams were obtained in tetrahydrofuran solution with ferrocene/ferrocenium used as a reference, and the potentials are reported in Table 3.5. Although the dioxaborine-terminated polymethine dyes have an overall negative charge, which is formally localized on each boron atom, a

positive charge is delocalized over the conjugated π system. The oxidation potentials of **3.1-3.4** range from an E_{ox} of -0.12 to +0.40. **3.3** and **3.4** would be expected to be the most difficult to oxidize due to the presence of strong electron withdrawing group, which is consistent with observations. The first reduction potentials for **3.1-3.4** have a range of -1.41 V to -1.49 V, with a difference of 0.08 V. A larger difference in oxidation potentials (0.52 V) versus reduction potentials (0.08 V) was observed for **3.1-3.4** due to the non-zero orbital coefficient in the HOMO and zero orbital coefficient in the LUMO.

Table 3.5. Electrochemical potentials versus ferrocenium / ferrocene for **3.1-3.4** in THF / 0.1 M $^{n}Bu_4NPF_6$.

Dye	$E_{1/2}^{2-/3-}$, V	$E_{1/2}^{1-/2-}$, V	$E_{ox}^{0/1-}$, V
3.1	–2.62[a]	–1.49[b]	–0.12[d]
3.2	–2.13[a]	–1.43[b]	–0.03[a]
3.3[c]	–1.41[a]	–1.41[a]	+0.40[a]
3.4	-	–1.41[a]	+0.12[a]

[a] EC-type process
[b] Reversible
[c] A third reversible reduction is seen at $E_{1/2}^{3-/4-}$ = –2.00 V
[d] Irreversible

3.5. Linear Optical Properties

The Dewar-Knott rules lead to a prediction that compounds with electron donating substituents would have a bathochromic shift in λ_{max} compared to **3.1**, while substituents with electron withdrawing groups are predicted to hypsochromically shift in λ_{max}. The linear absorption properties (λ_{max}, ε_{max}, M_{ge}) of **3.1-3.4** and **3.3'** and **3.4'** are collected in Table 3.6. The structure of dyes 3.3' and 3.4' are shown in Figure 3.15.

Table 3.6. λ_{max}, ε_{max}, M_{ge}, and the $Re(\gamma)_{calc}$ of polymethine dyes in DMSO solution

Dye	λ_{max} (nm)	ε_{max} (10^5 M^{-1} cm^{-1})	M_{ge} (D)[a]	$Re(\gamma)_{static}$ (10^{-33} esu)[b]
3.1	705	1.65	13.9	-1.3
3.2	700	1.92	14.4	-1.5
3.3	636	0.93	12.9	-0.73
3.4	701	1.23	15.7	-2.1
3.3'	598	0.76	12.3	-0.5
3.4'	643	1.54	13.6	-0.93

[a] Obtained from integration of the absorption spectra as $M_{ge} = 0.9584(\int \varepsilon d\upsilon / \upsilon_{max})^{0.5}$ where ε is in $M^{-1}cm^{-1}$ and υ is in cm^{-1}.

[b] Calculated from E3.3 using experimentally determined values of M_{ge} and E_{ge} from this table.

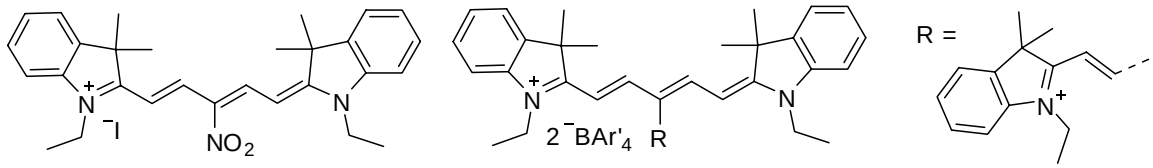

3.3' **3.4'**

Figure 3.15. Structure of **3.3'** and **3.4'**.

The linear absorption spectra of **3.1**-**3.4** (Figure 3.10) are shown in Figure 3.16. **3.1** and **3.3** show typical polymethine absorption, while **3.3** and **3.4** have atypical absorption spectra and will be discussed in further detail below. The low energy absorption bands of **3.1** and **3.2** are strong and narrow with small vibronic shoulders, which is a line shape characteristic of a molecule with a ground state and excited state with little change in geometry.

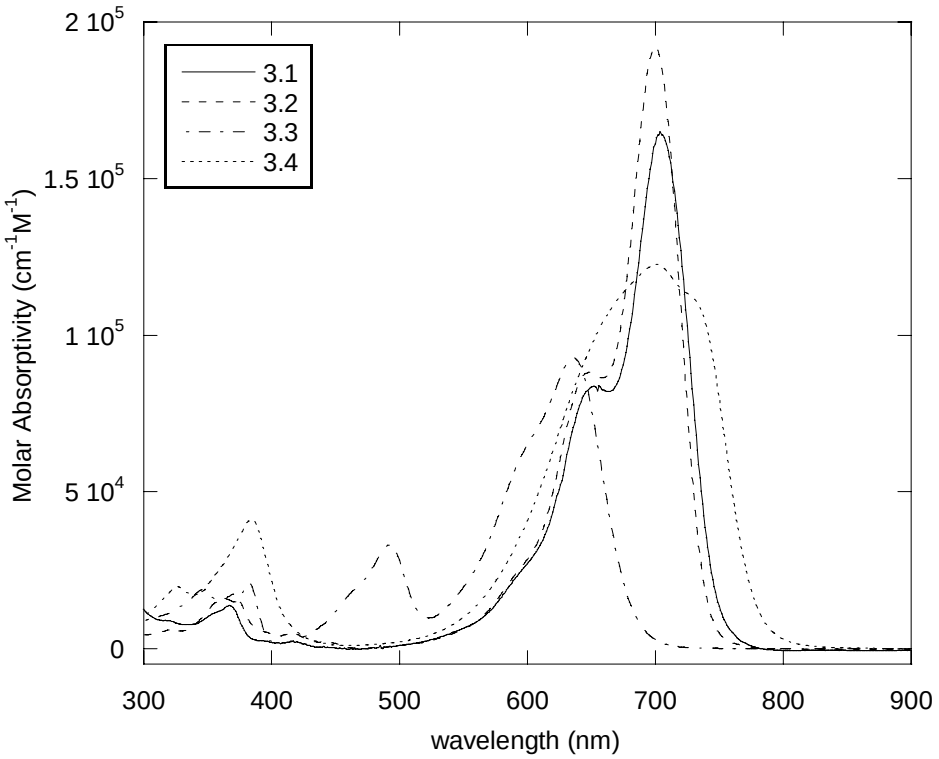

Figure 3.16. Absorption spectra of **3.1** (—), **3.2** (----), **3.3** (-·-·-), and **3.4** (···) in DMSO.

The Swain-Lupton constants for the chloro substituent indicate it is weakly π-electron donating (R = -0.19) and inductively σ withdrawing (F = 0.42). The higher HOMO coefficient of the parent dye leads to significant σ and π effects; however, the evidently dominant σ effects cause the Cl substituent to behave as an electron withdrawing group in the Dewar-Knott sense (Figure 3.17). In the pentamethine series (*e.g.* **3.2**) the substituents have greater interaction with the HOMO, for which the π-effects have good energy matching leading to a strong interaction. In the heptamethine series described in the introduction, **3.X** and **3.XI** each exhibit a bathochromic shift compared to **3.VIII**. In that series the substituent has greater interaction with the LUMO, for which the π-effects have poor energy matching, leading to a weak interaction.

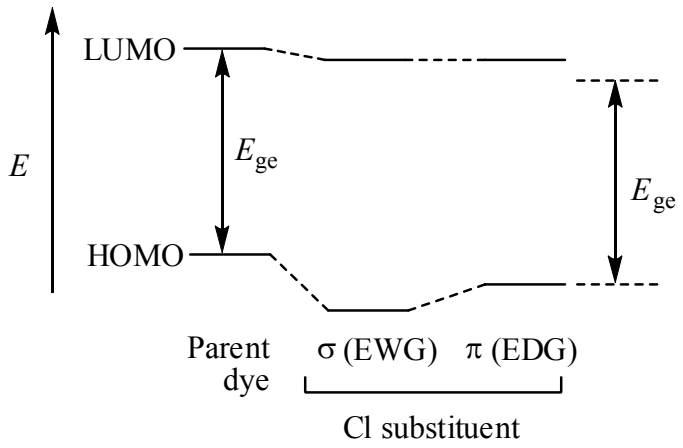

Figure 3.17. The energy diagram displays the σ-EW and π-ED effects on the HOMO and LUMO levels of the dye due to a Cl substituent on a methine with a large HOMO coefficient. The molecular orbitals of the substituent and the dye have relatively good energy matching leading to strong π-electron interactions.

Figure 3.18 shows the absorption spectra of **3.3** and **3.3'** in DMSO. **3.3'** is an analogous dye to **3.3** with indole-termini, which has a hypsochromic shift in λ_{max}. **3.3** shows a dramatic hypsochromic shift in λ_{max} relative to **3.1**, which **3.3** is also accompanied by a reduction in extinction coefficient. There is a second band of higher energy observed in the absorption spectrum for **3.3** and **3.3'**, which is occupying a region where typical polymethine dyes have an absorption window. The additional high energy bands may be due to charge transfer between the terminal groups of the parent dye to the nitro substituent.

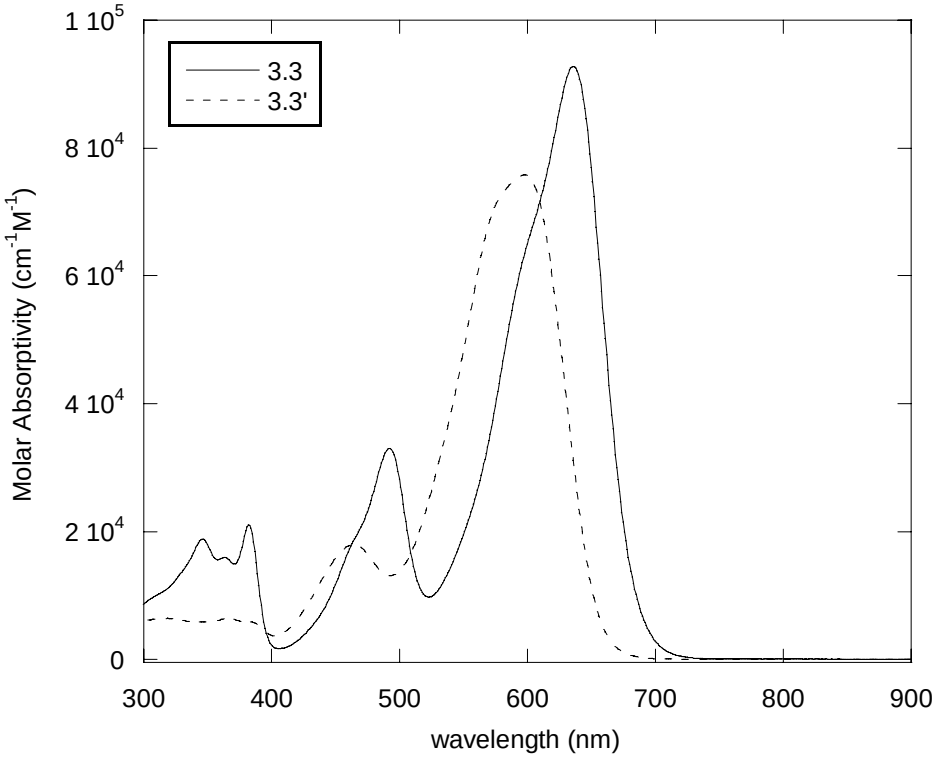

Figure 3.18. Absorption spectra of **3.3** (—) and **3.3'** (----) in DMSO.

Tris-terminal polymethine dyes are similar to *bis*-terminal analogues; however, *tris*-terminal dyes differ in the degree of bond length alternation between the atoms of the methine chain due to asymmetry. For example, in Figure 3.19 the bonds between the methine carbons leading from the terminal group (TG) to the central carbon (γ carbon) are drawn as double- single-double, while the bonds leading from TG2 and TG3 are single double single. The three bond alternation patterns lead to more *trans* character between the α and β carbons of the *tris*-terminal dyes. Evidence for this is observed in the large coupling constants in the ^{1}H NMR spectrum between the protons on the α and β carbons (J = 15.6 Hz, a coupling constant more similar for a typical *trans*-bond[23]). According to Bricks *et al.* [24], the *tris*-terminal dyes can be considered as an asymmetric dye with one terminal group (TG1) being a combination of two terminal groups (TG2')

(Figure 3.19). This leads to an increased number of rotational isomers and additional vibronic coupling resulting in broadened absorption spectrum.

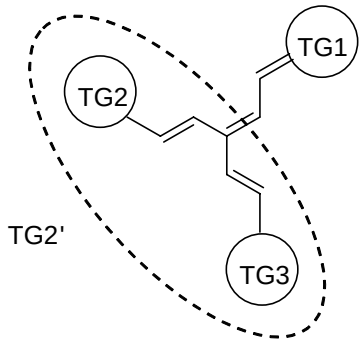

Figure 3.19. An asymmetric *tris*-terminal polymethine dye with one side of the dye being composed of one endgroup (TG1) and one side being composed of a combination of two endgroups (TG2+TG3=TG2').[24]

The third terminal group of the *tris*-terminal dyes acts as a substituent to a parent bis-terminated dye, which should be an electron withdrawing group in the case of **3.4**. **3.4** has a broadened spectra compared to **3.1** as shown in Figure 3.20. The broadness of the absorption band in the spectra for **3.4** seems to distribute the oscillator strength of the band to the higher energy side and lower energy side of the absorption band of the parent dye, **3.1.** Indole-terminated dye **3.4'** also has an uncharacteristically broad absorption band for a polymethine dye.

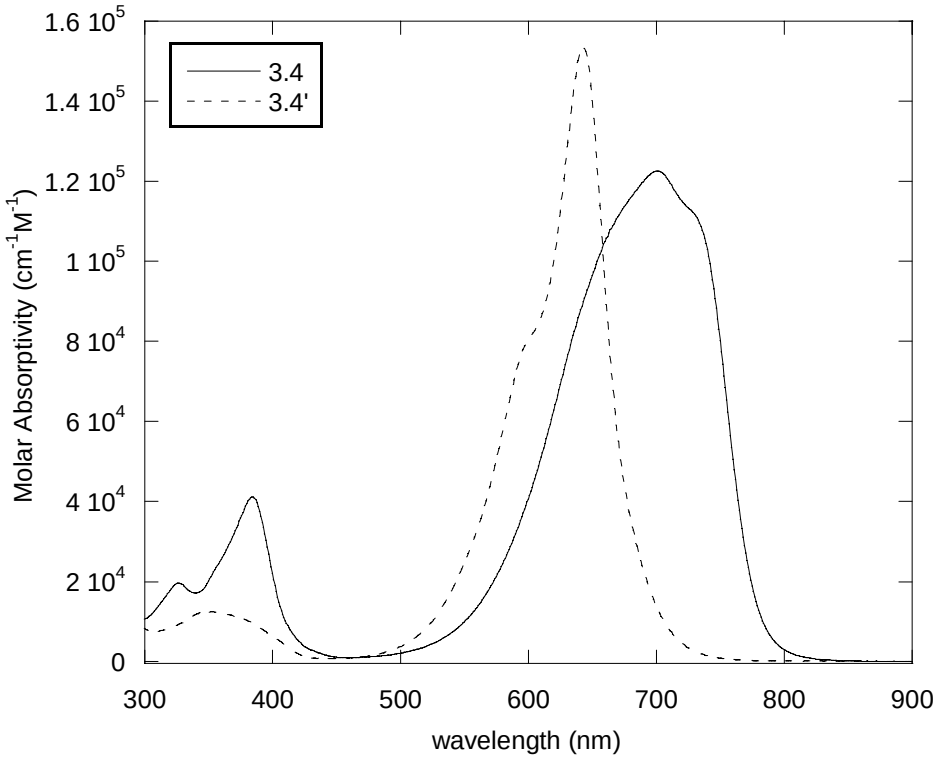

Figure 3.20. Absorption spectra of **3.4** (—) and **3.4'** (----) in DMSO.

3.6. Nonlinear Optical Properties[25]

The sum-over states expression[26] introduced in Chapter 2 (shown below as E3.3) was used to estimate Re(γ) at the static limit (wavelength = ∞, frequency = 0). This estimate will be henceforth referred to as $\mathrm{Re}(\gamma)_{static}$. As mentioned in chapter 1, polymethine dyes are typically dominated by a two-state term in which the key quantities are the transition energy and transition dipole moment, both associated with the lowest energy one-photon absorption.

$$\mathrm{Re}(\gamma)_{static} = -\left((2.998)^4 \times 10^{23}\right) \times \left(\frac{1}{5}\right) \times 4 \times \frac{M_{ge}^4}{E_{ge}^3} \qquad \text{E3.3}$$

The values from the calculations for dyes **3.1-3.4** and **3.3'** and **3.4'** are shown in Table 3.6. The calculations lead to predictions that the dioxaborine-terminated dyes are of larger magnitude of $Re(\gamma)_{static}$ than the indole-terminated dyes, due to a bathochromic shift in λ_{max} and larger transition dipole moments.

Dr. Joel Hales investigated the third-order nonlinear optical properties of **3.1-3.4** in DMSO solutions using open- and closed-aperture Z-scan techniques[27, 28] (Table 3.7) to determine Im(γ) and Re(γ), respectively, with ~100 fs pulses at a wavelength of 1.3 μm. Calculations of Re(γ) made using the 2-state model calculations would indicate that **3.1**, **3.2** and **3.4** would have similar static Re(γ). The z-scan measurements at 1300 nm indicate there is significant Im(γ) (due to 2PA), implying these measurements are not completely non-resonant (resonant with 2PA). The experimental values of Re(γ) remain fairly similar for **3.1**, **3.2**, and **3.4**. However, a comparison between **3.1** and **3.2** reveals that even though the λ_{max} is similar, the Im(γ) is quite different, which may be caused by a change in position of the 2PA bands.

3.3 was calculated to have the lowest Re(γ) value according to the two-state model calculations, which was experimentally confirmed to have the lowest Re(γ) at 1300 nm. Within a two level approximation the reduction in Re(γ) is related to the hypsochromic shift in λ_{max} and reduced transition dipole moment. The positive sign for Re(γ) for **3.3** is uncharacteristic of polymethine dyes. As can be seen in the absorption spectrum in Figure 3.18, there is a change in the shape from the typical polymethine low energy absorption. The polymethine character (BLA=0) may be lost due to the presence of the strong electron withdrawing group. Further evidence for the loss of polymethine character was observed in the ^{1}H NMR, which showed unusually high coupling constants

for a polymethine. For example **3.2** has a *J* coupling constant of 12.5 Hz, while **3.3** has a *J* coupling constant of 14.5 Hz. A possible resonance structure, which has a formal minus charge on the nitro-group, that may contribute to the disruption of the polymethine chain is shown in Figure 3.21.

Table 3.7. Re(γ), Im(γ), |γ|, Φ, and the $Re(\gamma)_{static}$ of Dioxaborine-Terminated Polymethine Dyes.[a]

Dye	$Re(\gamma)_{static}$ (10^{-33} esu)[b]	Re(γ) (10^{-33} esu)	Im(γ) (10^{-33} esu)	|γ| (10^{-33} esu)	Φ (°)
3.1	-1.3	-3.5	2.9	4.6	141
3.2	-1.5	-2.6	3.7	4.5	125
3.3	-0.73	0.50	0.27	0.57	29
3.4	-2.1	-3.3	3.2	4.6	136

[a] Measured in DMSO at 1300 nm using the Z-scan technique. The magnitude and phase of γ are defined as $|\gamma|^2 = Re(\gamma)^2 + Im(\gamma)^2$ and $\theta = \arctan[Im(\gamma)/Re(\gamma)]$, respectively.
[b] Calculated from E3.3 using experimentally determined values of M_{ge} and E_{ge} from Table 3.6.

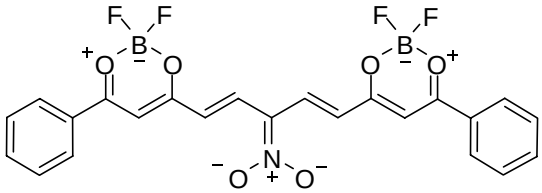

Figure 3.21. A possible resonance form of **3.3**, which could contribute to the loss of typical polymethine-like character.

3.7. Properties of Indole-Terminated Heptamethine Dyes

3.5' and **3.6'** were prepared to test the effects of donor and acceptor substituents upon the third-order nonlinear optical properties of heptamethine dyes (Scheme 3.3). A commercial unsubstituted dye (purchased from Exciton) known as HITC (Figure 3.22)

was used as a reference. The HITC dye will henceforth be referred to as **3.7'** in this chapter. The sodium tetrakis(3,5-bis(trifluoromethyl)phenyl)borate ($NaBAr'_4$) used for the ion exchange reaction was prepared according to a literature procedure.[29] This counterion provided enhanced solubility for the dyes in common organic solvents. Similar to series **3.I-3.V**, the ε carbon is an unstarred position, which based upon the Dewar-Knott rule, one would predict electron donating groups to give a hypsochromic shift, while electron withdrawing groups would give a bathochromic shift in λ_{max}.

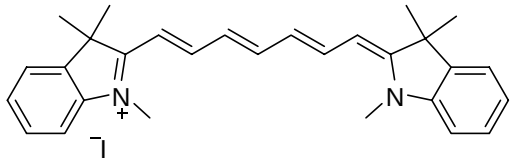

Figure 3.22. The structure of the commercial dye HITCI (**3.7'**).

3.5' and **3.6'** were synthesized through the addition/elimination reactions shown in Scheme 3.3 at the ε carbon of **S3.7** (**S3.7** was prepared in a similar manner to the procedure by Strewkowski *et al.*[16]), in which the chloro group can act as a nucleofuge. The 4-(N,N-dimethylamino)pyridinium (DMAP) substituent should act primarily as a σ-electron withdrawing group, which should stabilize the LUMO and cause a bathochromic shift in λ_{max}. The 4-methylphenylsufanyl substituent would be expected to act as a π-electron donating group, and a σ-electron withdrawing group. It is worth noting that phenylsulfanyl substituents have been described as π-electron acceptors.[30] The interaction of the π-electron donating abilities of the 4-methylphenylsulfanyl substituent should destabilize the LUMO, while the σ-electron withdrawing abilities would stabilize the LUMO.

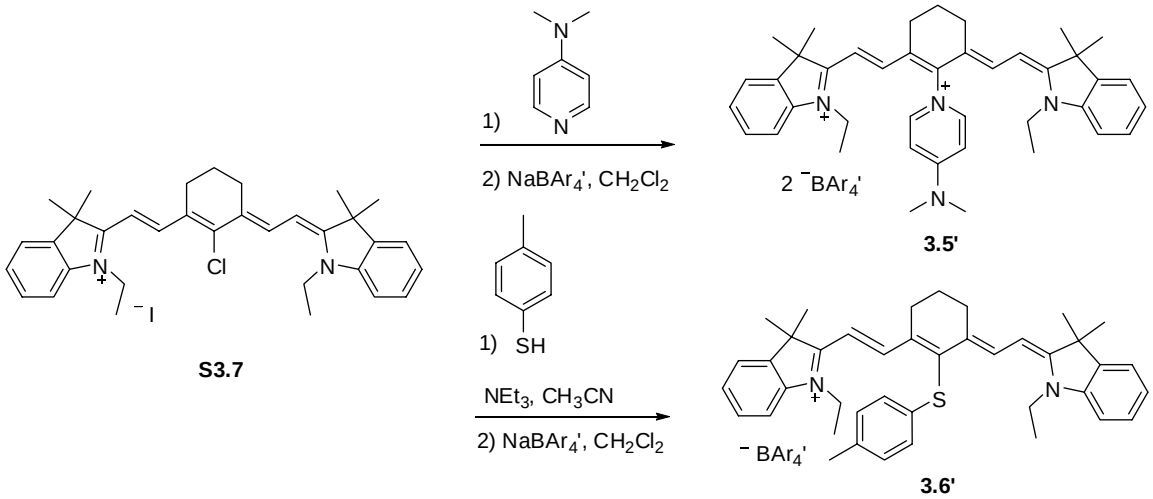

Scheme 3.3. The synthesis of **3.5'** and **3.6'**.

Cyclic voltammetry was performed on **3.5'**-**3.7'** to determine the oxidation and reduction potentials of these dyes to complement the optical data in assigning the separate effects of the electron donating and withdrawing abilities of the substituents. The conditions were similar to those used in electrochemistry Section 3.4. The redox potentials are collected in Table 3.8. **3.7'** was more difficult to reduce ($E_{red}^{1+/0}$ = -1.13 V) and easier to oxidize ($E_{ox}^{1+/2+}$ = -0.11 V) than **3.5'** and **3.6'** which is consistent with the substituents being electron withdrawing. A reversible oxidation was observed for **3.5'** at $E_{1/2}^{2+/3+}$ = +0.16, while a similar, reversible oxidation peak was observed for **3.6'** at $E_{1/2}^{1+/2+}$ = +0.11. The electron withdrawing ability of the DMAP substituent in **3.5'** has apparently shifted the HOMO lower in energy relative to **3.6'**. Reversible reduction peaks are observed for **3.5'** ($E_{1/2}^{2+/3+}$ = -0.95) and **3.6'** ($E_{1/2}^{2+/3+}$ = -1.05). The difference in reduction potentials between **3.5'** and **3.6'** is 0.10 V, more than twice the difference in their oxidation potentials (0.04 V). This indicates there is greater interaction of the substituents with the LUMO as expected from the Dewar-Knott rules. It is interesting to note that the oxidation and reduction potentials were reversible for **3.5'** and **3.6'**, while

they were not reversible for **3.7'**. The bridge substituents most likely reduce the reactivity of the radicals through steric hindrance.

Table 3.8. Electrochemical potentials versus ferrocenium / ferrocene for **3.5'**, **3.6'**, and **3.7'** in THF / 0.1 M $^{n}Bu_4NPF_6$.

Dye	$E_{1/2}^{2+/3+}$, V	$E_{1/2}^{1+/2+}$, V	$E_{1/2}^{2+/1+}$, V	$E_{1/2}^{1+/0+}$, V
3.5'	+0.16[a]	-	-0.95[a]	-
3.6'	-	+0.11[a]	-	-1.05[a]
3.7'	+0.06[b]	-0.11[b]		-1.13[c]

[a] Reversible
[b] EC-type process, E_{ox} potentials reported
[c] EC-type process, E_{red} potential reported

The linear absorption spectra for **3.5'**, **3.6',** and **3.7'** in dimethylsulfoxide solution are presented in Figure 3.23, while the optical properties extracted from the spectra are reported in Table 3.9. The value for λ_{max} and extinction coefficient for **3.7'** in dimethylsulfoxide has been reported in the literature (λ_{max} = 750 nm, $\varepsilon_{max} = 2.03 \times 10^5$ M^{-1} cm^{-1})[31] and is similar to the value obtained for the samples used in this Chapter. The λ_{max}, ε_{max}, and M_{ge} are very similar for **3.5'** and **3.6'**. The substituent effects should be dominated by σ-withdrawing characteristics, leading to the observed bathochromic shift in λ_{max}. Calculations of static Re(γ), performed as described in Section 3.5, are unsurprisingly similar for the two dyes due to the similarities in the linear absorption properties. However, the value for **3.7'** was calculated to be larger than **3.5'** and **3.6'** despite having a hypsochromic shift of ~50 nm. The extinction coefficient at λ_{max} were found to be similar, but the shape of the absorption band of **3.7'** appears to be slightly more broad than **3.5'** and **3.6'**, which leads to a larger transition dipole moment.

Table 3.9. λ_{max}, ε_{max}, M_{ge}, and the $Re(\gamma)_{static}$ of polymethine dyes in DMSO solution

Dye	λ_{max} (nm)	ε_{max} (10^5 M^{-1} cm^{-1})	M_{ge} (D)[a]	$Re(\gamma)_{static}$ (10^{-33} esu)[b]
3.5'	800	2.22	15.0	-2.6
3.6'	804	2.10	14.8	-2.5
3.7'	751	2.10	16.0	-2.8

[a] Obtained from integration of the absorption spectra as $M_{ge} = 0.9584(\int \varepsilon d\upsilon / \upsilon_{max})^{0.5}$ where ε is in $M^{-1}cm^{-1}$ and υ is in cm^{-1}.
[b] Calculated from E3.3 using experimentally determined values of M_{ge} and E_{ge} from this table.

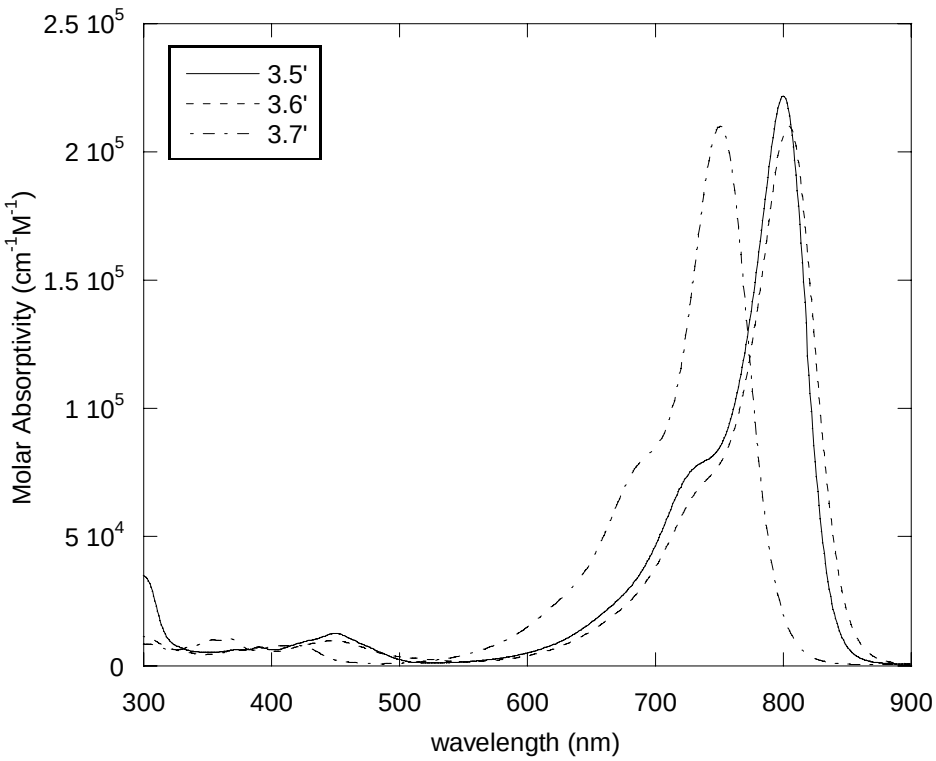

Figure 3.23. Absorption spectra of **3.5'** (—), **3.6'** (----) and **3.7'** (-·-·-) in DMSO.

The nonlinear optical properties, measured by Dr. Joel Hales, of **3.5'-3.7'** are collected in Table 3.10. The overall trends in Re(γ) calculated using the two-state model

well reproduce the experimental results. As the calculation from the two state-model predicted, **3.5'** and **3.6'** have very similar nonlinear optical properties. **3.7'** has much larger Re(γ) and Im(γ) compared to **3.5'** and **3.6'**. The larger Im(γ) of **3.7'** indicates it closer to a 2PA resonance, which would also lead to larger Re(γ) values due to resonance enhancement. The calculation of $Re(\gamma)_{static}$ does not include resonance enhancement (Im(γ) = 0), while significant magnitudes of Im(γ) was found for all three dyes at 1300 nm, meaning that the apparent agreement in trends between experimental Re(γ) and $Re(\gamma)_{static}$ is coincidental.

Table 3.10. Re(γ), Im(γ), |γ|, Φ, and the $Re(\gamma)_{static}$ of Indole-Terminated Polymethine Dyes.[a]

Dye	$Re(\gamma)_{static}$ (10^{-33} esu)[b]	Re(γ) (10^{-33} esu)	Im(γ) (10^{-33} esu)	|γ| (10^{-33} esu)	Φ (°)
3.5'	-2.6	-8.9	2.7	9.3	163
3.6'	-2.5	-8.1	2.3	8.4	164
3.7'	-2.8	-10.1	5.9	11.7	150

[a] Measured in DMSO at 1300 nm using the Z-scan technique. The magnitude and phase of γ are defined as $|\gamma|^2 = Re(\gamma)^2 + Im(\gamma)^2$ and $\theta = \arctan[Im(\gamma)/Re(\gamma)]$, respectively.

[b] Calculated from E3.3 using experimentally determined values of M_{ge} and E_{ge} from Table 3.9.

3.8. Conclusions

Surveying the literature regarding substituted heptamethine dyes on the ε carbon reveals that consideration of the σ and π-electron effects is necessary to determine if a substituent will act as an electron donating or electron withdrawing group. Modified

Swain-Lupton coefficients were employed to explain the substituent effects observed for a series of dyes from the literature. **3.5'** was synthesized with a substituent typically considered to be an EWG (pyridinium), while **3.6'** was synthesized with a substituent that would typically be considered an electron donating group (4-methylphenylsufanyl); however both behaved as electron withdrawing groups. According to the 2-state model and experiment, **3.5'** and **3.6'** have very similar third-order nonlinear optical properties. A comparison with **3.7'** reveals that at 1300 nm, **3.5'** and **3.6'** are farther from a 2PA resonance, which leads to moderately reduced Re(γ) but more significantly reduced Im(γ).

A series of dioxaborine terminated dyes, **3.1-3.4**, with different substituents in the γ position of the polymethine bridge were also synthesized. The electronic properties of the dyes were compared using ^{13}C NMR spectroscopy, cyclic voltammetry, and absorption spectroscopy. The substituent effects generally followed expectations from the Dewar-Knott rules. Anomalies found in the absorption spectra of the dioxaborine-terminated dyes (**3.3** and **3.4**), were also present in analogous indole-terminated dyes, **3.3'** and **3.4'**.

The nonlinear optical properties of **3.1-3.4** were characterized by the Z-scan technique at 1300 nm. The magnitudes of Re(γ) were larger for the indole-terminated heptamethine series than the dioxaborine-terminated series, which is to be expected due to the longer conjugation length. Re(γ) followed similar trends as to be expected from a two state model based upon the linear optical properties of the dyes. **3.1**, **3.2** and **3.4** have similar magnitudes and phases of Re(γ) similar to the dioxaborine-terminated pentamethine dyes discussed in Chapter 2. The linear optical properties for **3.1**, **3.2** and

3.4 had minor changes, which was reflected in concomitant minor variation in the magnitudes of Re(γ) and Im(γ). **3.3** was experimentally found to have lower, positive Re(γ), which is consistent with predictions from the 2-state model. The reduction in the magnitude of Re(γ) is perhaps due to a loss of polymethine character as shown by UV-vis.-NIR spectroscopy, ^{1}H NMR coupling constants and positive Re(γ). Overall, these systems are not useful for AOSP applications; however, they do indicate that polymethine bridge substitution can be used to tune the position of the one and two photon absorption bands in larger systems.

3.9. Experimental

Starting materials were obtained from commercial sources and used without further purification. When necessary tetrahydrofuran and dichloromethane was dried by passage through two columns of activated alumina.[32] Electrochemical measurements were carried out under nitrogen on dry deoxygenated tetrahydrofuran solutions *ca.* 10^{-4} M in analyte and 0.1 M in tetra-*n*-butylammonium hexafluorophosphate using a BAS Potentiostat, a glassy carbon working electrode, a platinum auxiliary electrode, and, as a pseudo-reference electrode, a silver wire anodized in 1 M aqueous potassium chloride. Potentials were referenced to ferrocenium/ferrocene by using decamethylferrocene (measured at –0.45 V vs. ferrocenium/ferrocene) as an internal reference. UV-vis.-NIR spectra were recorded in 1 mm cells using a Varian Cary 5E spectrometer. Varian 300, Bruker 400 and Bruker 500 megahertz NMR spectrometers were used to record NMR spectra. Elemental analyses were performed by Atlantic Microlabs. The ESI mass spectra were recorded on a Micromass Quattro LC.

S3.4

Synthesized according to the literature, except potassium hexafluorophosphate was used to precipitate the product[19] rather than sodium perchlorate and was obtained as a light brown solid (1.96 g, 4.13 mmol, 31% yield). The ^{1}H NMR was consistent with that in the literature.[33]

3.1

Synthesized according to chapter 2.

3.2

S3.2 (0.292 g, 0.952 mmol) and **S3.5** (0.419 g, 2.00 mmol) and were dissolved in acetonitrile (8 mL) and acetic anhydride (0.5 mL). Triethylamine (0.5 mL) was added drop wise and the reaction mixture was heated with stirring for ten min. The reaction mixture was allowed to cool to room temperature at which time a mixture of hexanes (50 mL) and ether (50 mL) was added. The solvent was decanted to leave a blue residue. The residue was dissolved in a minimal amount of acetonitrile (~3 mL) and precipitated by adding the solution to a mixture of hexanes (75 mL) and ether (125 mL). A green solid was collected by filtration, which was rinsed with acetic acid, then water. The green solid was once again precipitated from acetonitrile by adding the solution into a mixture of hexanes (50 mL) and ether (150 mL). The product was collected as a green solid by filtration (336 mg, 0.568 mmol, 60% yield). ^{1}H NMR (500 MHz, $CDCl_3$): δ (ppm) 7.93 (m, 6H), 7.54 (t, J = 7.5 Hz, 2H), 7.48 (t, J = 7.5 Hz, 4H), 6.57 (s, 2H), 5.98 (d, J = 12.5 Hz, 2H), 3.12 (q, J = 7 Hz, 6H), 1.22 (t, J = 7.5 Hz, 9H). ^{13}C NMR (125 MHz, $CDCl_3$, 333 K): δ (ppm) 175.1, 168.5, 145.4, 133.5, 131.6, 128.4, 126.5, 118.7,

106.6, 95.5, 45.9, 8.4. (ESI) (+) m/z = 102.0 [M^+] (-) m/z = 489.0 [M^-]. Anal. Calcd. for $C_{29}H_{32}B_2ClF_4NO_4$: C, 58.87; H, 5.45; N, 2.37. Found: C, 59.01; H, 5.51; N, 2.46.

3.3

S3.3 (0.281 g, 0.886 mmol) and **S3.5** (0.398 g, 1.90 mmol) were dissolved in acetonitrile (6 mL) and acetic anhydride (0.5 mL). Triethylamine (0.5 mL) was added drop wise and the reaction mixture was heated with stirring for ten min. The reaction mixture was allowed to cool to room temperature at which time ether (50 mL) was added and the mixture was cooled to -20 °C. The liquid was decanted, leaving a residue which was dissolved in a minimal amount of acetonitrile (~3 mL) and precipitated by adding the solution to a mixture of hexanes and ether. The solid was then recrystallized in acetic acid. The product was collected as a green solid by filtration (0.305 g, 0.507 mmol, 57% yield). ^{1}H NMR (500 MHz, $(CD_3)_2SO$): δ (ppm) 8.82 (s, 1H), 8.36 (d, J = 14.5 Hz, 2H), 8.08 (dm, J = 7.0 Hz, 4H), 7.66 (tm, J = 7.5 Hz, 2H), 7.57 (t, J = 7.0 Hz, 4H), 7.12 (s, 2H), 6.77 (d, J = 15.0 Hz, 2H), 3.08 (q, J = 7.5 Hz, 6H), 1.16 (t, J = 7.5 Hz, 9H). ^{13}C NMR (125 MHz, $(CD_3)_2SO$): δ (ppm) 179.9, 173.7, 138.3, 133.5, 132.6, 129.1, 128.8, 127.6, 109.2, 97.4. (ESI) (+) m/z = 101.9 [M+] (-) m/z = 499.9 [M-]. Anal. Calcd. for $C_{29}H_{32}B_2F_4N_2O_6$: C, 57.84, H, 5.36, N, 4.65. Found: C, 57.70, H, 5.45, N, 4.81.

3.4

S3.4 (220 mg, 0.465 mmol) and **S3.5** (338 mg, 1.61 mmol) were dissolved in a solution of acetonitrile (4 mL) and acetic anhydride (0.3 mL). Triethylamine (0.4 mL) was added dropwise with stirring at 80 °C. After 7 min. the reaction was removed from heat and allowed to cool to room temperature. The product was separated from the reaction mixture by directly applying the solution to a size exclusion column (SX1 biobeads) with

dichloromethane as the eluent. The crude product was mixed with tetra-n-octylammonium bromide (254 mg, 465 mmol) and was dissolved in dry tetrahydrofuran. A slurry of sodium hydride (82 mg, 3.4 mmol) in dry tetrahydrofuran (10 mL) was added. The solution was filtered after 5 min of stirring. The solvent was removed from the filtrate and the residue was purified by silica gel chromatography using dichloromethane/ethylacetate (9:1) as an eluent. The product was obtained as a blue solid (160 mg, 0.140 mmol, 30% yield). ^{1}H NMR (500 MHz, CD_2Cl_2): δ (ppm) 8.27 (d, J = 14.5 Hz, 3H), 8.01 (d, J = 7.0 Hz, 6H), 7.56 (t, J = 6.5 Hz, 3H), 7.51 (t, J = 7.5 Hz, 6H), 6.54 (s, 3H), 6.46 (d, J = 14.5 Hz, 3H), 3.06 (m, 8H), 1.59 (m, 8H), 1.33-1.22 (m, 40 H), 0.87 (t, J = 7.1 Hz, 12H). ^{13}C NMR (125 MHz, CD_2Cl_2): δ (ppm) 178.5, 174.6, 145.9, 133.8, 133.3, 129.2, 127.9, 117.0, 111.4, 97.7, 59.4, 32.0, 29.34, 29.31, 26.6, 22.9, 22.2, 14.2. (ESI) (+) m/z = 466.6 [M+] (-) m/z = 675.0 [M-]. Anal. Calcd. for $C_{66}H_{92}B_3F_6NO_2$: C, 69.42, H, 8.12, N, 1.23. Found: C, 69.52, H, 7.93, N, 1.29.

3.3'

S3.6 (345 mg, 1.09 mmol) and **S3.3** (169 mg, 0.533 mmol) and sodium acetate (203 mg, 2.48 mmol) were combined in acetic anhydride (3 mL) and heated with stirring at 85 °C for 15 min. Upon cooling a brown crystalline solid was collected by filtration and rinsed with distilled water (195 mg, 0.334 mmol, 63% yield). ^{1}H NMR (400 MHz, $CDCl_3$): δ (ppm) 8.74 (d, J = 15.6 Hz, 2H), 7.50-7.44 (m, 4H), 7.39 (t, J = 7.2 Hz, 2H), 7.32 (d, J = 8.0 Hz, 2H), 7.01 (d, J = 15.6 Hz, 2H), 4.58 (q, J = 7.6 Hz, 4H), 1.84 (s, 12H), 1.53 (t, J = 7.6 Hz, 6H). ^{13}C NMR (125 MHz, $(CD_3)_2SO$: δ (ppm) 178.2, 142.3, 141.9, 140.9, 131.7, 128.9, 127.1, 122.8, 113.0, 101.6, 50.4, 40.3, 26.9, 12.4. (ESI) (+) m/z = 456 [M+] (-)

m/z = 127 [M-]. Anal. Calcd. for $C_{29}H_{34}N_3IO_2$: C, 59.69, H, 5.87, N, 7.20. Found: C, 59.50, H, 5.89, N, 7.17.

3.4'

S3.6 (503 mg, 1.60 mmol), **S3.4** (238 mg, 0.503 mmol), and sodium acetate (253 mg, 3.08 mmol) were combined in acetic anydride (4 mL). The solution was heated to 80 °C, and after 20 min. of stirring the solution was allowed to cool to room temperature. The solution was filtered to remove excess sodium acetate was decanted into ether (50 mL). The supernatant was decanted and the residue was dissolved in dichloromethane (~5 mL). NaBAr'$_4$ (473 mg, 0.534 mmol) was added to the solution and allowed to stir for five min. The residue was purified by silica gel chromatography using dichloromethane as the eluent, followed by purified using size-exclusion chromatography (SX-1 biobeads, and dichloromethane eluent) to give a blue solid (180 mg, 0.077 mmol, 15% yield). ^{1}H NMR (400 MHz, $CDCl_3$): δ (ppm) 8.14 (d, J = 15.0 Hz, 3H), 7.59 (s, 16H), 7.53 (t, J = 8.0 Hz, 3H), 7.49 (t, J = 7.6 Hz, 3H), 7.42 (d, J = 7.0 Hz, 3H), 7.39 (s, 8H), 7.28 (d, J = 7.5 Hz, 3H), 6.48 (d, J = 15.0 Hz, 3H), 4.15 (d, J = 7.5 Hz, 6H), 1.63 (s, 18H), 1.45 (t, J = 7.6 Hz, 9H). ^{13}C NMR (100 MHz, $CDCl_3$): δ (ppm) 178.9, 162.6 (1:1:1:1 q, J = 50 Hz), 150.4, 142.7, 142.2, 135.7, 130.1, 129.9 (1:2:2:1 q, J = 36 Hz), 128.7, 124.5 (1:1:1:1 q, J = 270 Hz), 123.7, 121.34, 118.8, 114.0, 106.2, 52.1, 42.0, 26.5, 12.3. (ESI) (+) m/z = 304.8 [M^{2+}] (-) m/z = 862.9 [M-]. Anal. Calcd. for $C_{107}H_{75}B_2F_{48}N_3$: C, 55.01, H, 3.24, N, 1.80. Found: C, 55.29, H, 3.39, N, 1.88.

3.5'

S3.7 (116 mg, 0.182 mmol) was combined with dimethylaminopyridine (115 mg, 0.943 mmol) in acetonitrile (8 mL) under a nitrogen atmosphere. The solution was heated at 60

°C for fifty min. The sample was concentrated under vacuum, then the solid was precipitated by the addition of ether. The crude solid was dissolved in dichloromethane (3 mL), to which $NaBAr_4'$ (318 mg, 0.359 mmol) was added. After 5 min. of stirring the product was separated using silica gel chromatography with dichloromethane as the eluent. The product was obtained as a green solid (349 mg, 0.150 mmol, 82% yield). ^{1}H NMR (400 MHz, CD_3CN): δ 7.93 (d, J = 7.2 Hz, 2H), 7.69 (broad s, 16H), 7.66 (broad s, 8H), 7.42 (m, 4H), 7.28 (m, 4H), 7.11 (d, J = 6.8 Hz, 2H), 6.83 (d, J = 14.0 Hz, 2H), 6.27 (d, J = 14.0 Hz, 2H), 4.13 (q, J = 7.2 Hz, 4H), 3.36 (s, 6H), 2.76 (d, J = 6.4 Hz, 4H), 2.01 (quint., J = 6.0 Hz, 2H), 1.341 (t, J = 7.2 Hz, 6H), 1.337 (s, 12H). ^{13}C NMR (100 MHz, $CDCl_3$): δ (ppm) 173.7, 162.6 (1:1:1:1 q, J = 49 Hz), 157.5, 151.8, 143.6, 142.8, 142.6, 141.6, 135.7, 130.0 (1:2:2:1 q, J = 26 Hz), 129.8, 127.6, 126.8, 125.5 (1:2:2:1 q, J = 271 Hz), 123.3, 118.7, 112.5, 109.0, 102.8, 50.35, 41.31, 40.73, 28.02, 25.4, 21.2, 12.7. (ESI) (+) m/z = 299 [M^{2+}] (-) m/z = 863 [M-]. Anal. Calcd. for $C_{105}H_{74}B_2F_{48}N_4$: C, 54.24, H, 3.21, N, 2.41. Found: C, 54.35, H, 3.08, N, 2.42.

3.6'

S3.7 (97 mg, 0.152 mmol) and 4-methylbenzenethiol (205 mg, 1.65 mmol) were combined in acetonitrile (10 mL). The solution was heated to 50 °C and triethylamine (0.20 mL, 1.4 mmol) was added. After five minutes a white solid was precipitated by the addition of ether (50 mL) and hexanes (30 mL). The solid was filtered and the solvent was removed from the filtrate under vacuum. The residue was combined with $NaBAr_4'$ (154 mg, 0.174 mmol) in dichloromethane (10 mL) and stirred for 5 min. The product was purified by silica gel chromatography using dichloromethane as the eluent, then the product was precipitated from dichloromethane (5 mL) by adding hexanes (50 mL) and

collected as a brown solid (107 mg, 0.073 mmol, 48% yield). ^{1}H NMR (400 MHz, $CDCl_3$): δ (ppm) 8.74 (d, J = 14.4 Hz, 2H), 7.70 (s, 8H), 7.50 (s, 4H), 7.34 (t, J = 7.6 Hz, 2H), 7.29 (d, J = 7.2 Hz, 2H), 7.20 (t, J = 7.6 Hz, 2H), 7.07 (d, J = 8.4 Hz, 2H), 7.02 (d, J = 8.0 Hz, 2H), 7.01 (d, J = 8.0 Hz, 2H), 6.02 (d, J = 14.0 Hz, 2H), 3.96 (q, J = 7.2 Hz, 4H), 2.60 (t, J = 6.0 Hz, 4H), 2.19 (s, 3H), 1.88 (quint., J = 5.6 Hz, 2H), 1.47 (s, 12H), 1.35 (t, J = 7.2 Hz, 6H). ^{13}C NMR (100 MHz, $CDCl_3$): δ (ppm) 172.2, 161.9 (1:1:1:1 q, J = 49 Hz), 153.7, 147.0. 141.4, 141.1, 135.9, 134.8, 133.5, 130.2, 128.9 (1:2:2:1 q), 128.8, 126.2, 125.5, 124.5 (1:2:2:1 q, J = 271 Hz), 122.3, 117.5, 110.1, 100.3, 49.3, 39.2, 27.8, 26.2, 20.8, 20.6, 12.0. (1 peak not observed presumably due to overlap with other peaks) (ESI) (+) m/z = 599 [M+] (-) m/z = 863 [M-]. Anal. Calcd. for $C_{73}H_{59}BF_{24}SN_2$: C, 59.95, H, 4.06, N, 1.91. Found: C, 60.17, H, 3.98, N, 1.88.

3.10. References

1. Griffiths, J., *Colour and Constitution of Organic Molecules*. Academic Press Inc.: London, 1976.
2. Dewar, M. J. S., Some Recent Developments in Theoretical Organic Chemistry. In *Progress in Organic Chemistry 2*, Cook, J. W., Ed. Academic Press inc.: New York, 1953; pp 1-28.
3. König, W., Conception of the "Polymethine Dyes" and a General Dye Formula Derived Therefrom as the Basis of a New. *Journal fuer Praktische Chemie (Leipzig)* **1926,** 112, 1-36.
4. Daehne, S.; Ranft, J., Proton Resonance Spectra of Simple Polymethine Dyes. *Zeitschrift fuer Physikalische Chemie (Leipzig)* **1963,** 224, 65-73.
5. Klessinger, M., Pariser-Parr-Pople-Rechnungen an Molekülen mit Aminogruppen II. Cyanine, Merocyanine und Qudrupol-merocyanine. *Theoret. Chim. Acta.* **1966,** 5, 251-265.
6. Dewar, M. J. S., Colour and Constitution. Part I. Basic Dyes. *J. Chem. Soc.* **1950**, 2329-2334.
7. Knott, E. B., The Colour of Organic Compounds. Part I. A General Colour Rule. *J. Chem. Soc.* **1951**, 1024-1028.
8. Hammett, L. P., The Effect of Structure upon the Reactions of Organic Compounds. Benzene Derivatives. *J. Am. Chem. Soc.* **1937,** 59, 96-103.
9. Roberts, J. D.; Moreland, W. T. J., Electrical Effects of Substituent Groups in Saturated Systems. Reactivities of 4-Substituted Bicyclo [2.2.2]octane-1-carboxylic Acids. *J. Am. Chem. Soc.* **1953,** 75, 2167-2173.

10. Swain, C. G.; Lupton, E. C. J., Field and Resonance Components of Substituent Effects. *J. Am. Chem. Soc.* **1968,** 90, 4328-4337.
11. Charton, M., Electrical Effect Substituent Constants for Correlation Analysis. In *Progress in Physical Organic Chemistry*, Taft, R. W., Ed. Interscience: New York, 1981; Vol. 13, pp 119-251.
12. Hansch, C.; Leo, A.; Taft, R. W., A Survey of Hammett Substituet Constants and Resonance and Field Parameters. *Chem. Rev.* **1991,** 91, 165-195.
13. Slominskii, Y. L.; Popov, S. V.; Dyadyusha, G. G.; Kachkovskii, A. D.; Tolmachev, A. I., Polymethine Dyes With Hydrocarbon Bridges. Anionic Dyes With An o-Phenylene Group in the Chromophore. *Zh. Org. Khim. (English translation)* **1986,** 21, 1950-1959.
14. Encinas, C.; Miltsov, S.; Otazo, E.; Rivera, L.; Puyol, M.; Alonso, J., Synthesis and Spectoscopic Characterisation of Heptamethincyanine NIR dyes for their use in Optical Sensors. *Dyes Pigm.* **2006,** 71, 28-36.
15. Peng, X.; Song, F.; Lu, E.; Wang, Y.; Zhou, W.; Fan, J.; Gao, Y., Heptamethine Cyanine Dyes with a Large Stokes Shift and Strong Fluorescence: A Paradigm for Excited-State Intramolecular Charge Transfer. *J. Am. Chem. Soc.* **2005,** 127, 4170-4171.
16. Strekowski, L.; Lipowska, M.; Patonay, G., Substitution Reactions of a Nucleofugal Group in Heptamehtine Cyanine Dyes. Synthesis of an Isothiocyanato Derivative for Labeling of Proteins with a Near-Infrared Chromophore. *J. Org. Chem.* **1992,** 57, 4578-4580.
17. Davies, I. W.; Marcoux, J.-F.; Wu, J.; Palucki, M.; Corley, E. G.; Robbins, M. A.; Tsou, N.; Ball, R. G.; Dormer, P.; Larsen, R. D.; Reider, P. J., An Efficient Preparation of Vinamidiniuim Hexafluorophosphate Salts. *J. Org. Chem.* **2000,** 65, 4571-4574.
18. Malhotra, S. S.; Whiting, M. C., Researches on Polyenes. Part VII.* The Preparation and Electronic Absorption Spectra of Homologous Series of Simple Cyanines, Merocyanines, and Oxonols. *J. Chem. Soc.* **1960**, 3812-3822.
19. Jameleddine, K.; Adnen, H. A. M.; Béchir, B. H., An efficient preparation and some reactions of 2-dimethylaminomethylene-1,3-bis(dimethylimonio)propane diperchlorate. *Tetrahedron Lett.* **2006,** 47, 2973-2975.
20. Grahn, W., 13C-Spektren Von di- und trinuclearen polymethincyanin-farbstoffen. *Tetrahedron* **1976,** 32, 1931-1939.
21. Grahn, W.; Reichardt, C., 13C-NMR-Spektren Von gamma-Substituierten pentamethincyanin-farbstoffen mit indolenin-edngruppen. *Tetrahedron* **1976,** 32, 125-134.
22. Wähnert, M.; Dähne, S.; Radeglia, R., The Effect of Solvents on the Electronic Structure of Symmetrical Polymethines ^{1}H- and ^{13}C-NMR Spectroscopic Investigations. *Advances in Molecular Relaxation and Interaction Processes* **1977,** 11, 263-282.
23. Silverstein, R. M.; Webster, F. X.; Kiemle, D. J., *Spectrometric Identification of Organic Compounds*. Seventh ed.; John Wiley & Sons, Inc: 2005.
24. Bricks, Y. L.; Ishchenko, A. A.; Kachkovski, A. D.; Tolmachev, A. I., Nature of Electronic Transitions in Trinuclear Polymethine Dyes. *Dyes Pigm.* **1987,** 8, 353-369.
25. *Performed by Dr. Joel Hales*.
26. Dirk, C. W.; Cheng, L.-T.; Kuzyk, M. G., A Simplified Three-Level Model Describing the Molecular Third-Order Nonlinear Optical Susceptibility. *Int. J. of Quantum Chem.* **1992,** 43, 27-36.

27. Thorley, K. J.; Hales, J. M.; Anderson, H. L.; Perry, J. W., Porphyrin Dimer Carbocations with Strong Near Infrared Absorption and Third-Order Optical Nonlinearity. *Angew. Chem. Int. Ed.* **2008,** 47, 7095-7098.
28. Sheik-bahae, M.; Said, A. A.; Van Stryland, E. W., High-sensitivity, single-beam n_2 measurements. *Opt. Lett.* **1989,** 14, 955-957.
29. Brookhart, M.; Grant, B.; Volpe, A. F. J., [(3,5-(CF3)2C6H3)4B]-[H(OEt2)2]$^+$: A Convenient Reagent for Generation and Stabilization of Catioinic, Highly Electrophilic Organometallic Complexes. *Organometallics* **1992,** 11, 3920-3922.
30. Cheng, Y.-J.; Luo, J.; Huang, S.; Zhou, X.; Shi, Z.; Kim, T.-D.; Bale, D. H.; Takahashi, S.; Yick, A.; Polishak, B. M.; Jang, S.-H.; Dalton, L. R.; Reid, P. J.; Steier, W. H.; Jen, A. K.-Y., Donor-Acceptor Thiolated Polyenic Chromophores Exhibiting Large Optical Nonlinearity and Excellent Photostability. *Chem. Mater.* **2008,** 20, 5047-5054.
31. Davidson, Y. Y.; Gunn, B. M.; Soper, S. A., Spectroscopic and Binding Properties of Near-Infrared Tricarbocyanine Dyes to Double-Stranded DNA. *Appl. Spectrosc.* **1996,** 50, 211-221.
32. Pangborn, A. B.; Giardello, M. A.; Grubbs, R. H.; Rosen, R. K.; Timmers, F. J., Safe and Convenient Procedure for Solvent Purification. *Organometallics* **1996,** 15, 1518-1520.
33. Davies, I. W.; Tellers, D. M.; Shultz, C. S.; Fleitz, F. J.; Cai, D.; Sun, Y., A [2+2] Cycloaddition Route to Dimethylaminomethylene Vinamidinium Salts. *Org. Lett.* **2002,** 4, 2969-2972.

Chapter 4

Third-Order Nonlinear Optical Properties of Anionic Polymethine Dyes with Keto and Dicyano Methylidine Containing Terminal Groups

4.1. Introduction

In this chapter three series of anionic polymethine dyes were synthesized with various keto- and dicyano methylidine-terminal groups. It was hypothesized that dyes with terminal groups considered to be stronger accepting groups would have larger third-order polarizabilities due to generally having longer conjugation lengths. A related series of anionic polymethine dyes with the so-called TCF acceptor as the terminal group was synthesized and the linear and nonlinear optical properties were characterized in a similar manner.

4.1.1. Introduction and Background

The majority of polymethine dyes studied in the literature are cationic with the positive charge delocalized between two electron donating groups across a hydrocarbon skeleton with an odd number of methine units. The dioxaborine-terminated dyes discussed in previous chapters have a net negative charge causing them to be anionic. However, the two negative charges are formally localized on the boron atoms of the dioxaborine group. It is a positive charge that is delocalized between the oxygens of the dioxaborine unit. Oxonol dyes are analogous anionic dyes to the cationic counterparts, usually synthesized using two electron withdrawing terminal groups in which oxygen atoms bear the negative charge. A variety of oxonol dyes (and oxonol-like dyes) have been examined as silver halide sensitizers[1] and in optical recording applications.[2]

However, γ measurements comparing oxonol-like polymethines w/ different end groups are not common.

A simple example of an oxonol dye is the deprotonated form of 1,3 indandione (Figure 4.1 top). The ketone functional groups bear the negative charge and delocalize the charge between them. The double condensation product of 1,3 indandione with malononitrile is known[3] and at least two equivalent resonance forms contributing greatly to the overall ground state can be drawn (Figure 4.1 bottom). The acceptor strength of the terminal groups and the conjugation path length of the π-system are dramatically increased. Evidence for this is readily visible by comparing the colors of the two dyes, which anionic 1,3 indandionate is yellow and the anionic dimalononitrile condensation product is blue.

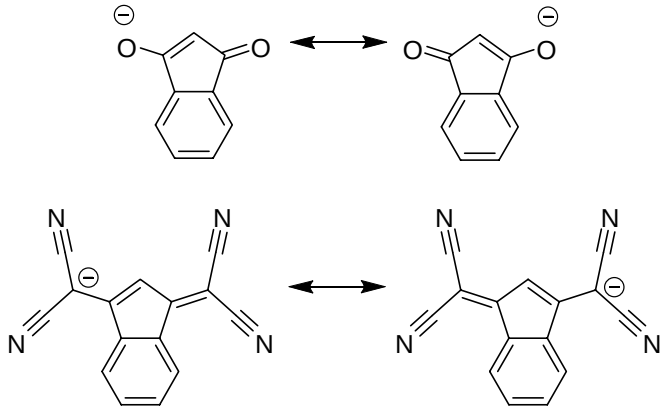

Figure 4.1. Two resonance forms of A) the anion of 1,3 indandione and B) the anion of 2,2'-(1H-indene-1,3(2*H*)-diylidene)dimalononitrile.

Oxonol dyes are commonly synthesized through a double Knoevenagel condensation of acceptor moieties with a simple polymethine bridge. 1,3-Indandione has been shown to form more complex oxonol dyes, with the connectivity shown in Figure

4.2.[4] The charge can now be delocalized across the bridge to form equivalent extreme resonance structures, two of which are shown in Figure 4.2. The full charge delocalization of the ground state is represented in the bottom structure of Figure 4.2.

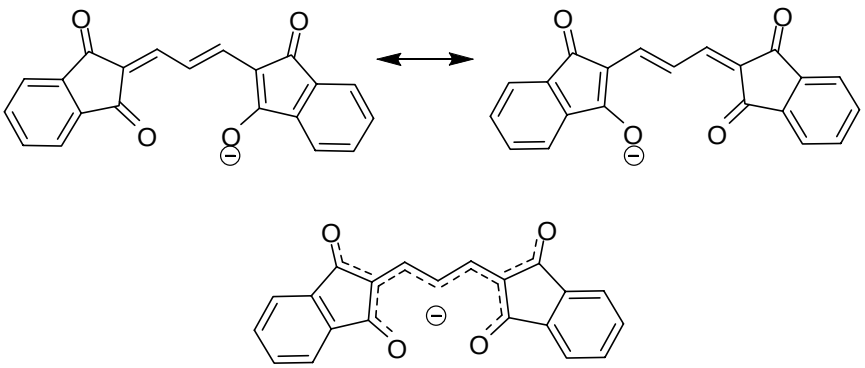

Figure 4.2. Symmetric 1, 3-indandione terminated polymethine dye shown with two extreme resonance structures (top) and the ground state structure.

A large amount of research in nonlinear optics has targeted organic materials with π-electron conjugated systems with donating (D) and accepting (A) groups to probe structure-property relationships, especially for second-order nonlinear optics. Several acceptors (benzo[*b*]thiophen-3(2H)-one 1,1-dioxide (**S4.1**), 2-(3-oxo-2,3-dihydro-1H-inden-1-ylidene)malononitrile (**S4.2**), [3-(dicyanomethylidene)-2,3-dihydrobenzothiophen-2-ylidene-1,1-dioxide] (**S4.3**) and 4,5,5-trimethyl-3-cyano-2(5H)-furanylidenepropanedinitrile (**S4.4**)) are shown in Figure 4.3. Acceptor **S4.4**, is commonly called tricyanofuran, or TCF. The acceptor strength of the closely related structures **S4.1**-**S4.3** is expected to increase from **S4.1** to **S4.2** to **S4.3**. Accepter **S4.1** has received less attention in the literature as an acceptor group relative to **S4.2** and **S4.3** due to the lower acceptor strength. The strong electron accepting abilities of **S4.3** and

comparable accepting abilities of **S4.4** has lead to several studies of making analogous materials comparing these terminal groups.

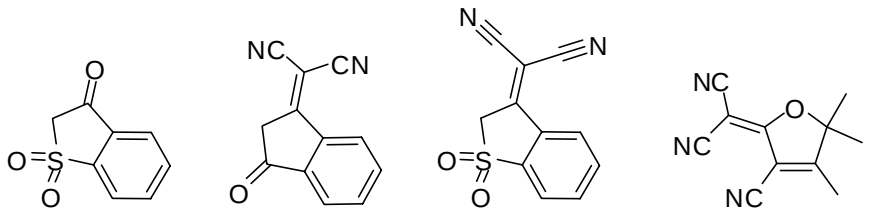

S4.1 **S4.2** **S4.3** **S4.4**

Figure 4.3. Common acceptor groups found in the literature and used in this study.

Ahlheim *et al.*[5] have investigated dipolar donor-acceptor (D-A) chromophore **4.I** (Figure 4.4), using **S4.3** as the acceptor as an electro-optic material. Similarly, Shi *et al.*[6] investigated chromophore **4.II**[6] (Figure 4.4), using **S4.4** as the acceptor in similar electro-optic applications. **4.I** has five π-bonds between the dicyanomethylidene and the aryl-diethylamine portion of the acceptor, while **4.II** has six bonds, which gives **4.II** a longer conjugation length. However, comparison of the λ_{max} of **4.I** (744 nm in CH_2Cl_2) and **4.II** (688 nm in $CHCl_3$[7]) reveals a significant hypsochromic shift in chromophore **4.II**. The hypsochromic shift in λ_{max} for **4.II** (In similar solvents) despite the increased conjugation length indicates that acceptor **S4.3** may be slightly more strongly electron withdrawing than **S4.4**. Dipolar molecules with **S4.3** and **S4.4** accepting groups were also investigated by Beverina *et al.*[8] to determine the two-photon absorption (2PA) properties. Dyes **4.III** and **4.IV** contained auxiliary acceptors (A', thiazole) and donors (D', pyrrole) in the π-conjugated bridge between the primary D and A groups. Large magnitudes (>1000 GM) of degenerate 2PA were observed at transition energies near their respective 1PA

transitions, which, chromophore **4.III** (812 nm) showed a bathochromic shift in λ_{max} compared to **4.IV** (691) in THF solution. The 2PA properties of quadrapolar A-D-A dyes **4.V** and **4.VI** were investigated by Zheng *et al*.[9] The dyes were found to have 2PA cross sections (δ) from 2400-5900 GM in a wavelength rage of 1.0-1.3 nm. Dye **4.V** and **4.VI** have the same number of double bonds between the donor groups and the dicyanovinylene portion of the acceptor, but once again the **S4.3** terminated chromophore of **4.V** (719 nm in THF) has a significant bathochromic shift in λ_{max} compared to **4.VI** (616 nm in THF).

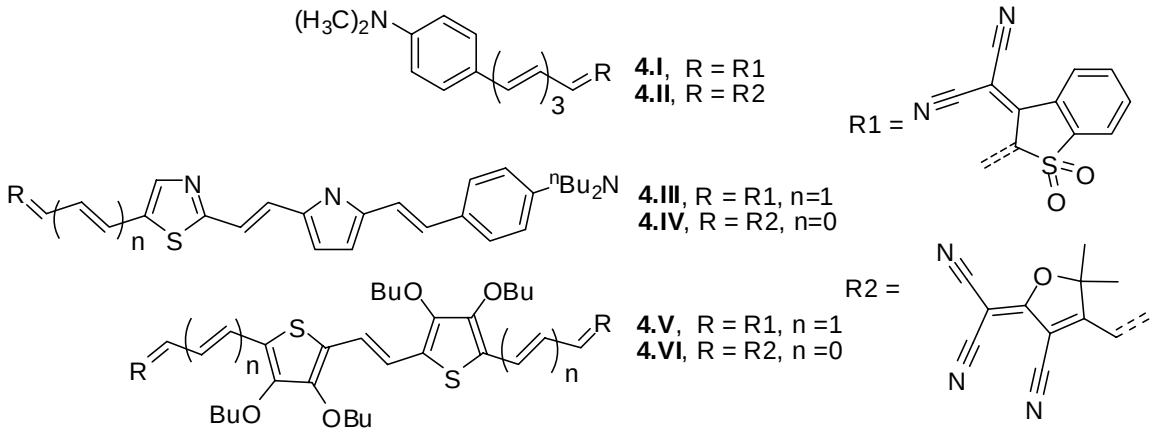

Figure 4.4. Donor-acceptor materials using terminal groups relevant to this study.

The synthesis of **S4.4**-terminated polymethine dyes (Figure 4.5) has recently been reported in the literature[10] and have been found to be promising materials to be used in photovoltaic applications.[11] Dye **4.VII** was found to absorb in the near IR (900 nm in dichloromethane) with a large extinction coefficient (>300,000 L/mol/cm) and a cyanine-like absorption shape. Dye **4.VIII** had a significant hypsochromic shift relative to **4.VII** and diminished extinction coefficient, which is similar to results found for amine-substituted cationic cyanine counterparts.[12] The contributions to the absorbance spectrum

of dye **4.IX** from the anion (The same anion as **4.VII**) are relatively unchanged in the cyanine-cyanine pair indicating there was little interaction between the two polymethine ions in the ground state.

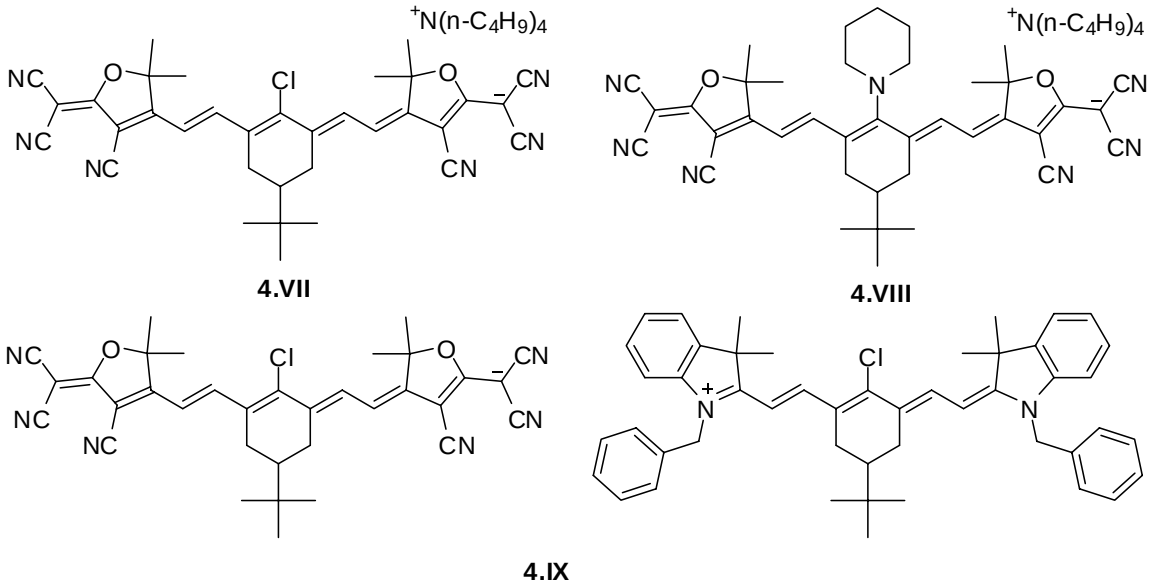

Figure 4.5. Polymethine dyes with terminal groups formed from **S4.4**.

4.1.2. Goals of Chapter 4

This chapter examines the linear absorption properties and third-order NLO properties of anionic dyes synthesized using terminal groups **S4.1**-**S4.4.** The three series of anionic cyanines synthesized using **S4.1**-**S4.3** are shown in Figure 4.6. The dyes were synthesized at several unsubstituted hydrocarbon bridge lengths.

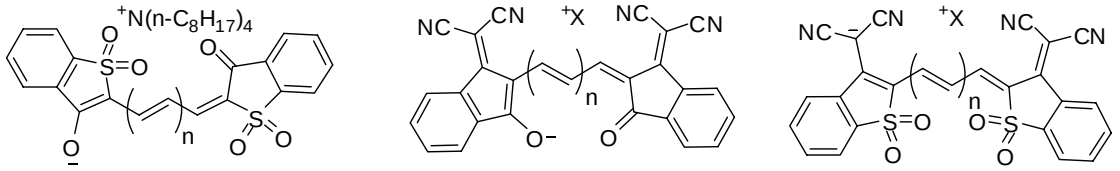

4.1, n=1
4.2, n=2
4.3, n=3

4.4, n=1, X = $HNEt_3$
4.5, n=2, X = $N(n\text{-}C_8H_{17})_4$

4.6, n=1, X = $N(n\text{-}C_8H_{17})_4$
4.7, n=2, X = Proton sponge

Figure 4.6. **S4.1-S4.3** terminated polymethine dyes for which the third-order nonlinear optical properties have been measured by Dr. Joel Hales.

The series of dyes terminated with **S4.4** are shown in Figure 4.7. Dyes **4.8-4.10** were synthesized with unsubstituted bridges, similar to the dyes in Figure 4.6. Dye **4.11** is similar to dye **4.VII** synthesized from the literature with minor changes that do not add to the overall conjugation (note the *tert*-butyl group on the ring of the bridge in **4.VII** and the different alkyl chain lengths in the counterioins). Finally **4.12** has bridge substitution which can increase the total available conjugation.

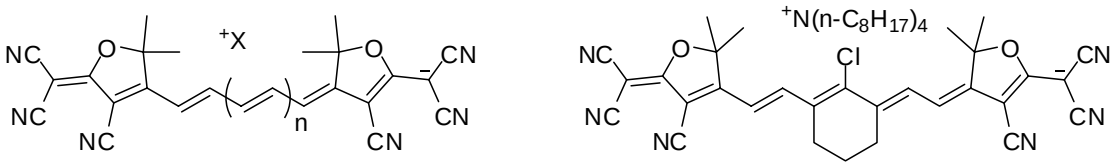

4.8 X=proton sponge, n=1
4.9 X=proton sponge, n=2
4.10 X=$N(n\text{-}C_8H_{17})_4$, n=2

4.11

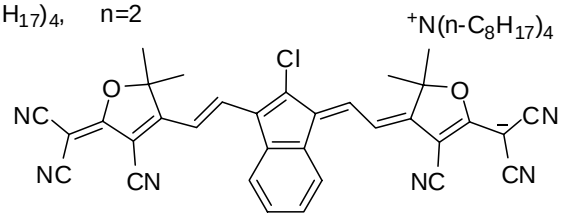

4.12

Figure 4.7. **S4.4** terminated polymethine dyes for which the third-order nonlinear optical properties have been measured by Dr. Joel Hales.

4.2. Synthesis

The acceptor starting materials (**S4.1**,[13] **S4.2**,[14] **S4.3**,[15] and **S4.4**[16] shown in Figure 4.3**)** and the simple polymethine bridges (**S4.5, S4.6, S4.7** (The 1,7-bis(dimethylamino)heptamethine cyanine was synthesized according to the procedure of Nikolajewski *et al*.[17] as a hexafluorophosphate salt instead of the perchlorate salt to avoid possible shock hazards), **S4.8, and S4.9**[18] shown in Figure 4.8**)** have been reported in the literature.

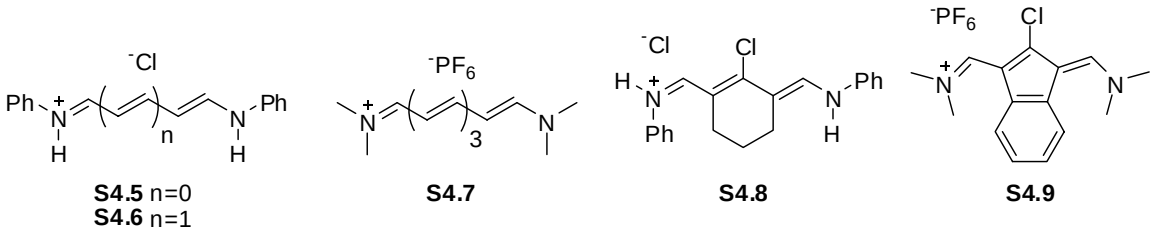

Figure 4.8. Starting materials **S4.5-S4.9** used as cyanine bridge precursors.

4.1-4.7 were synthesized following similar procedures to the exemplary reaction scheme of **4.5** (Scheme 4.1). Each dye is fully characterized by ^{1}H and ^{13}C NMR, mass spectrometry and elemental analysis, with the exception of **4.7**, for which a satisfactory ^{13}C NMR spectrum was not obtained. Also, two sets of unidentifiable peaks were observed in the ^{1}H NMR for **4.7** at ~8.7 and 8.5 ppm, which appear to be in 3% abundance by integration. Synthesizing dyes with additional vinylene groups in the bridge (such as reacting **S4.2** or **S4.3** with **S4.7**) were unsuccessful using the procedures similar to that shown in Scheme 4.1. Additionally, conditions described in Scheme 4.1 were unsuccessful in the condensation of **S4.5-S4.7** with 2,2'-(1H-indene-1,3(2H)-diylidene)dimalononitrile (Figure 4.1 bottom). Dyes **4.1** and **4.2** were first synthesized

by Rumyantseva *et al.*[19] as the acid (no counterion), then later by Patel *et al.*[20] as the triethylammonium salt. The dye with an additional vinylene unit (**4.3)** was previously unknown in the literature. Patel *et al*[1] previously synthesized **4.4**, while **4.5** was synthesized with a trioctadecylammonium counterion. In this work **4.5** was prepared with the tetra-*n*-octylammonium counterion. The chromophores of dyes **4.6** and **4.7** are previously unknown in the literature.

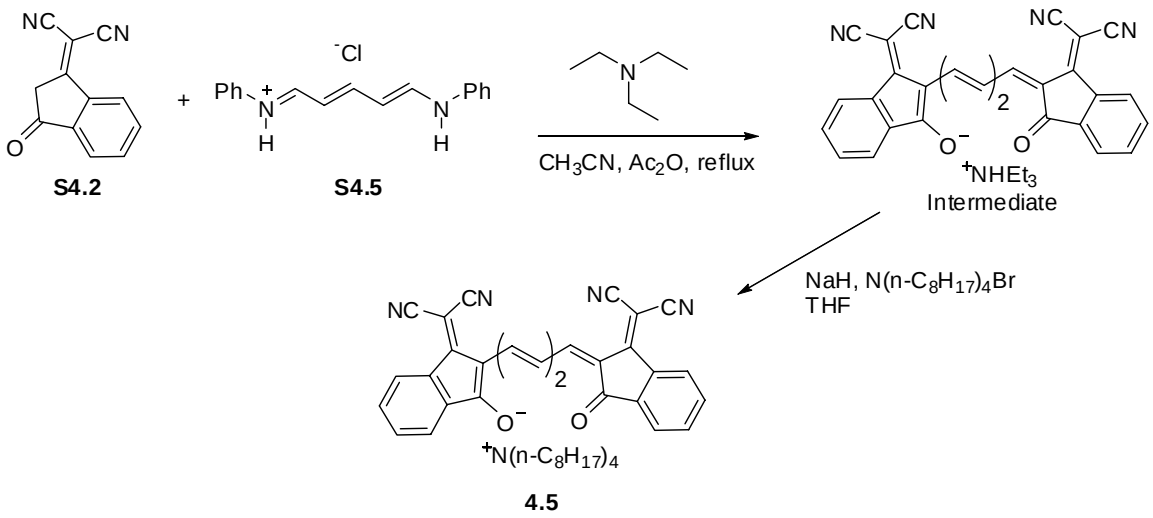

Scheme 4.1. Exemplary synthetic scheme for **4.5**.

4.8 and **4.9** were synthesized by the double Knoevenagel condensation of **S4.4** with **S4.5** and **S4.6** respectively. The condensation was performed in refluxing acetonitrile in the presence of acetic anhydride and base. Employing the use of proton sponge as the base allowed the desired product to precipitate from the solution and to be collected by a simple filtration. Dye intermediates for **4.10**-**4.12** were synthesized in a similar manner, then an ion metathesis reaction was performed using sodium hydride as a base in the presence of tetra-*n*-octylammonium bromide. The excess sodium hydride and

sodium bromide were then removed by filtration leaving the tetra-*n*-octylammonium-polymethine dye product. An exemplary synthetic scheme is shown in Scheme 4.2 for **4.9** and **4.10**.

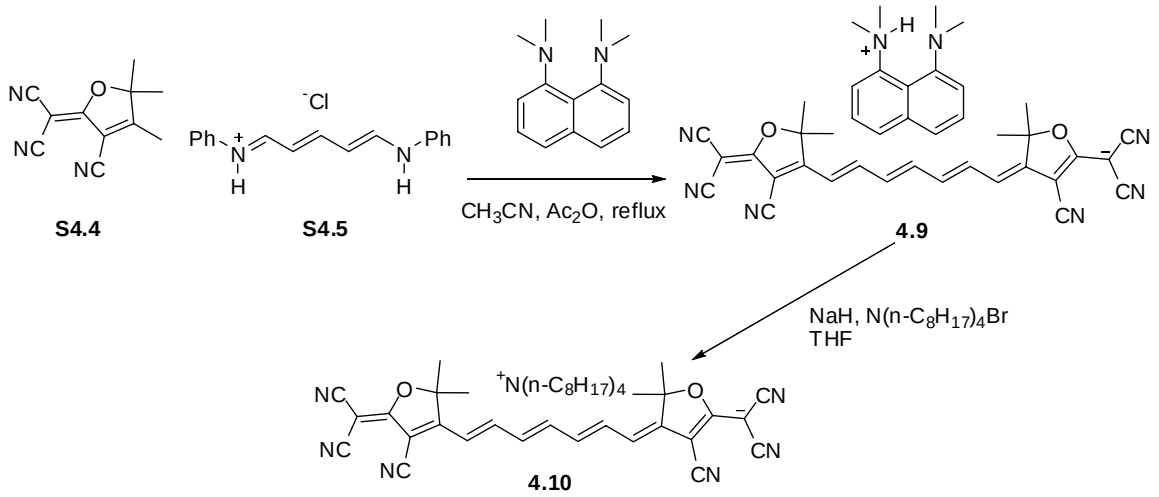

Scheme 4.2. Exemplary synthetic scheme for **4.9** and **4.10**.

4.3. NMR Studies

4.3.1. NMR Characterization of 4.1-4.7

Dyes **4.1-4.6** were characterized by ^{1}H and ^{13}C NMR spectroscopy. The peaks in the ^{1}H NMR spectrum of **4.1-4.3** were severely broadened at room temperature. Variable temperature NMR was employed to further probe dyes **4.1-4.3**. The aromatic region in the ^{1}H NMR of **4.1** shows broadened peaks at temperatures of 243 K (Figure 4.9). At 213 K the peaks in the spectrum sharpen and an additional peak can be observed (Figure 4.9). The temperature-dependent peak resolution gives evidence that two conformational isomers are present in solution (Figure 4.10). The rate of interconversion of these isomers is comparable to the NMR timescale at room temperature, but slow on the NMR timescale at 213 K. The doublet at ~7.6 ppm most likely belongs to the protons on the α

carbon of the major isomer and the doublet at ~7.3 ppm most likely belongs to the protons on the α carbon of the minor isomer.

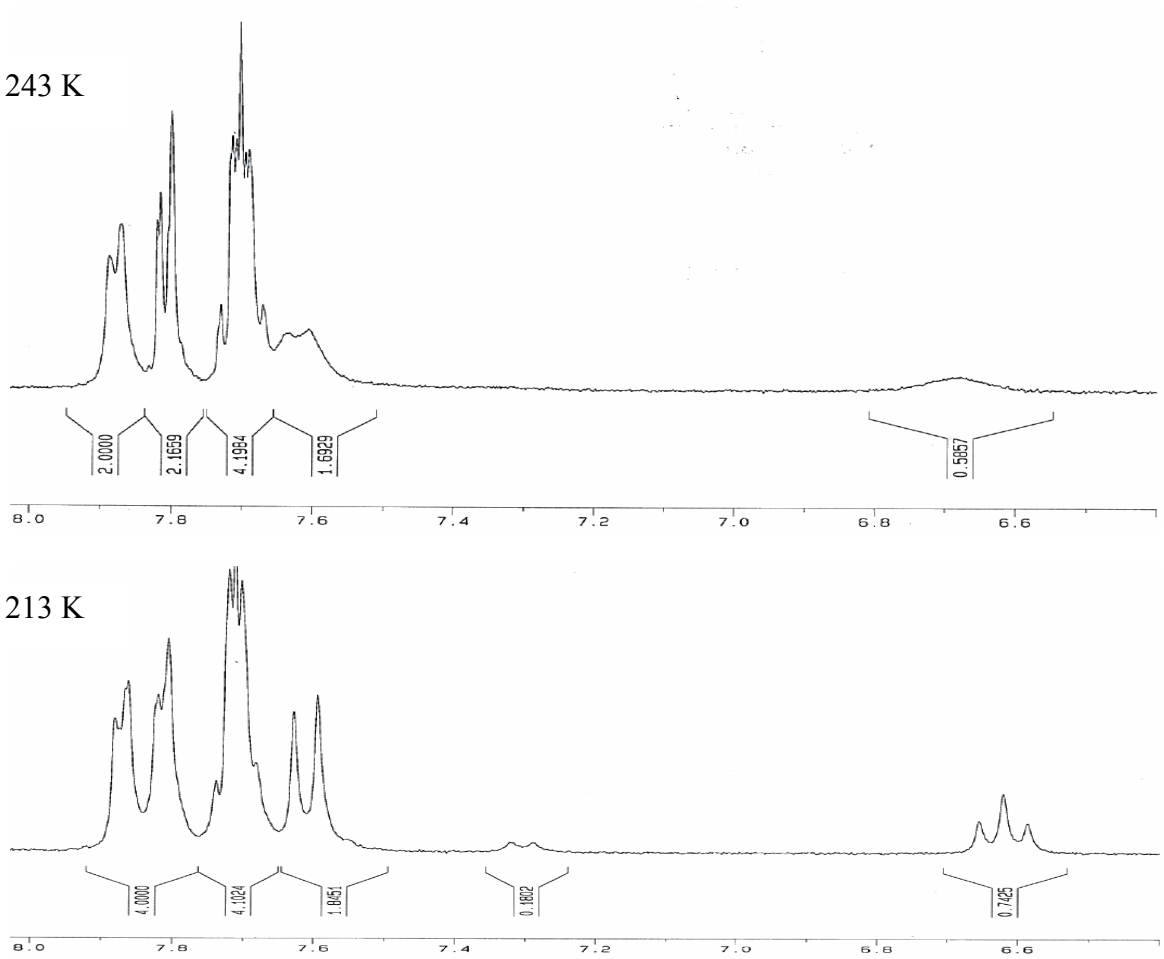

Figure 4.9. Aromatic region of the ^{1}H NMR of **4.1** at 243 K (top) and 213 K (bottom) in dichloromethane.

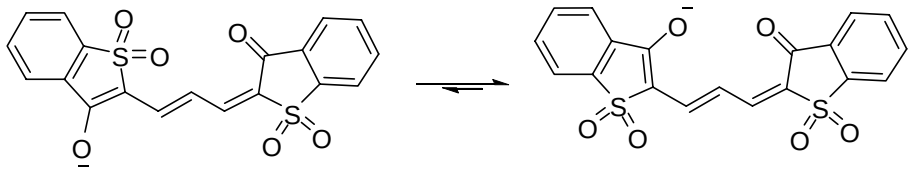

Figure 4.10. Possible conformational isomers of **4.1**.

The ^{13}C NMR spectrum of 4.1 at room temperature shows a set of peaks for the major and the minor isomer (Figure 4.11 A). However, heating the sample to 333 K shows only one set of peaks.

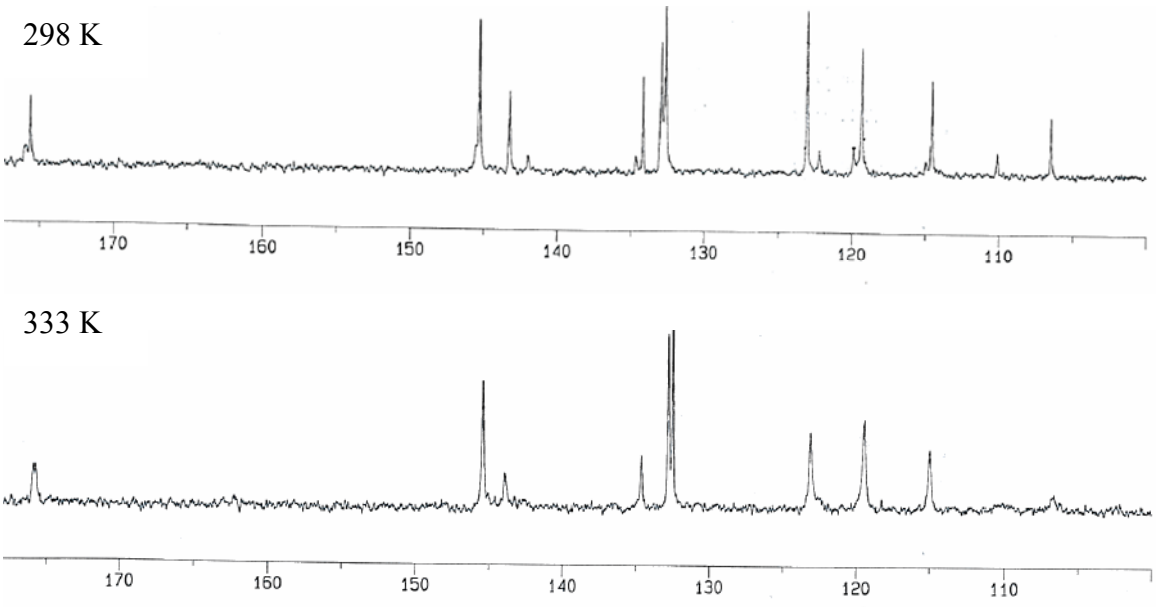

Figure 4.11. ^{13}C NMR spectra of **4.1** at 298 K (top) and 333 K (bottom) in $CDCl_3$.

Similarly, the aromatic region of the ^{1}H NMR spectrum of **4.2** and **4.3** had broad peaks at room temperature. Resolved peaks were observed at sufficiently low temperatures for **4.2** (Figure 4.12), but once again multiple sets of peaks can be observed due to multiple isomers. Only one set of peaks was observed for **4.3** at high temperatures

(333 K). The aromatic region of the ^{13}C NMR spectrum at room temperature showed only one set of peaks for **4.2** and **4.3**.

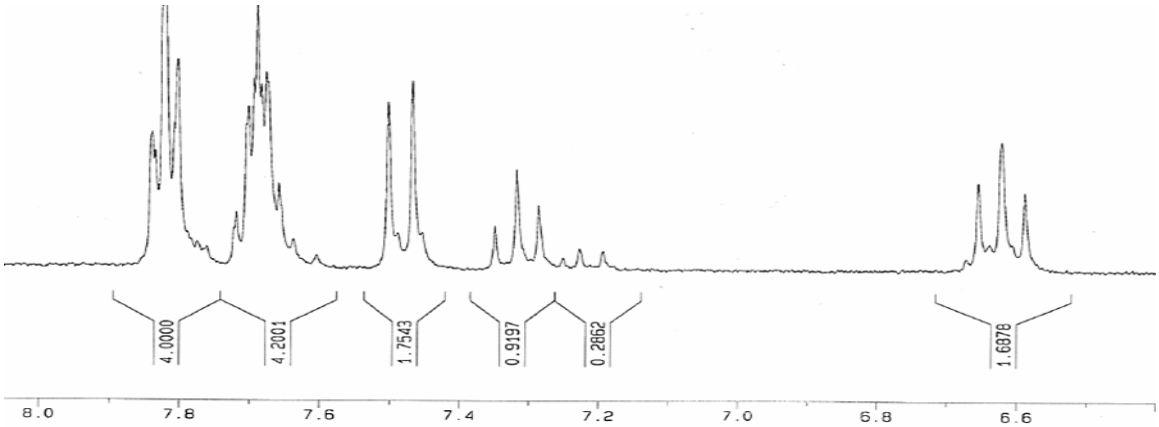

Figure 4.12. Multiple sets of peaks can be observed in the aromatic region of the ^{1}H NMR spectrum of **4.2** at 213 K in dichloromethane.

4.3.2. NMR Characterization of 4.8-4.12

Dyes **4.8-4.12** have been characterized through ^{1}H, ^{13}C NMR spectroscopy, ESI mass spectrometry and elemental analysis, each being consistent with the desired product. The ^{13}C spectra for **4.8** and **4.9** are shown in Figure 4.13. Dye **4.9** should have one additional carbon resonance than **4.8**; however, the same number of carbons was observed indicating there was probably overlap of two peaks. The heteronuclear single bond coherence (HSQC) NMR technique was used to correlate the ^{1}H resonances with the ^{13}C resonances for **4.9** (Figure 4.14). The feature seen at 127 ppm in the spectrum of **4.9** was found to be due to the overlap of two peaks, while the additional peak (not seen for **4.8**) was found to appear at 152 ppm.

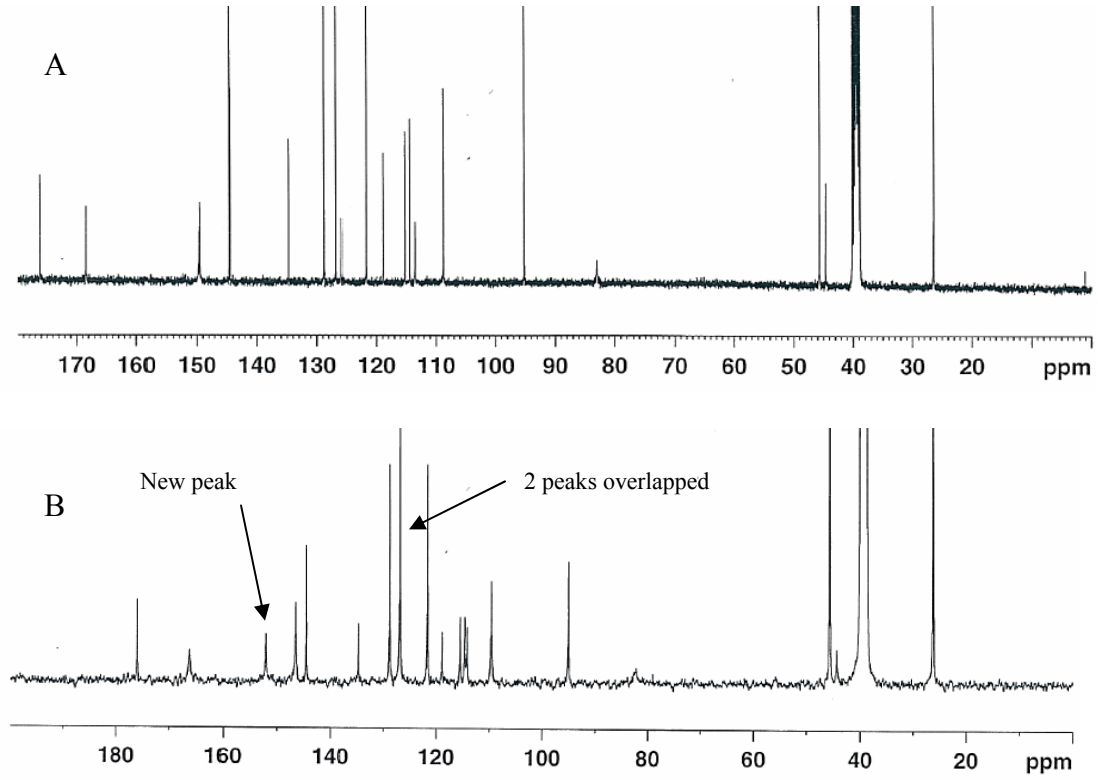

Figure 4.13. ^{13}C NMR spectra in $(CD_3)_2SO$ of A) **4.8** and B) **4.9**.

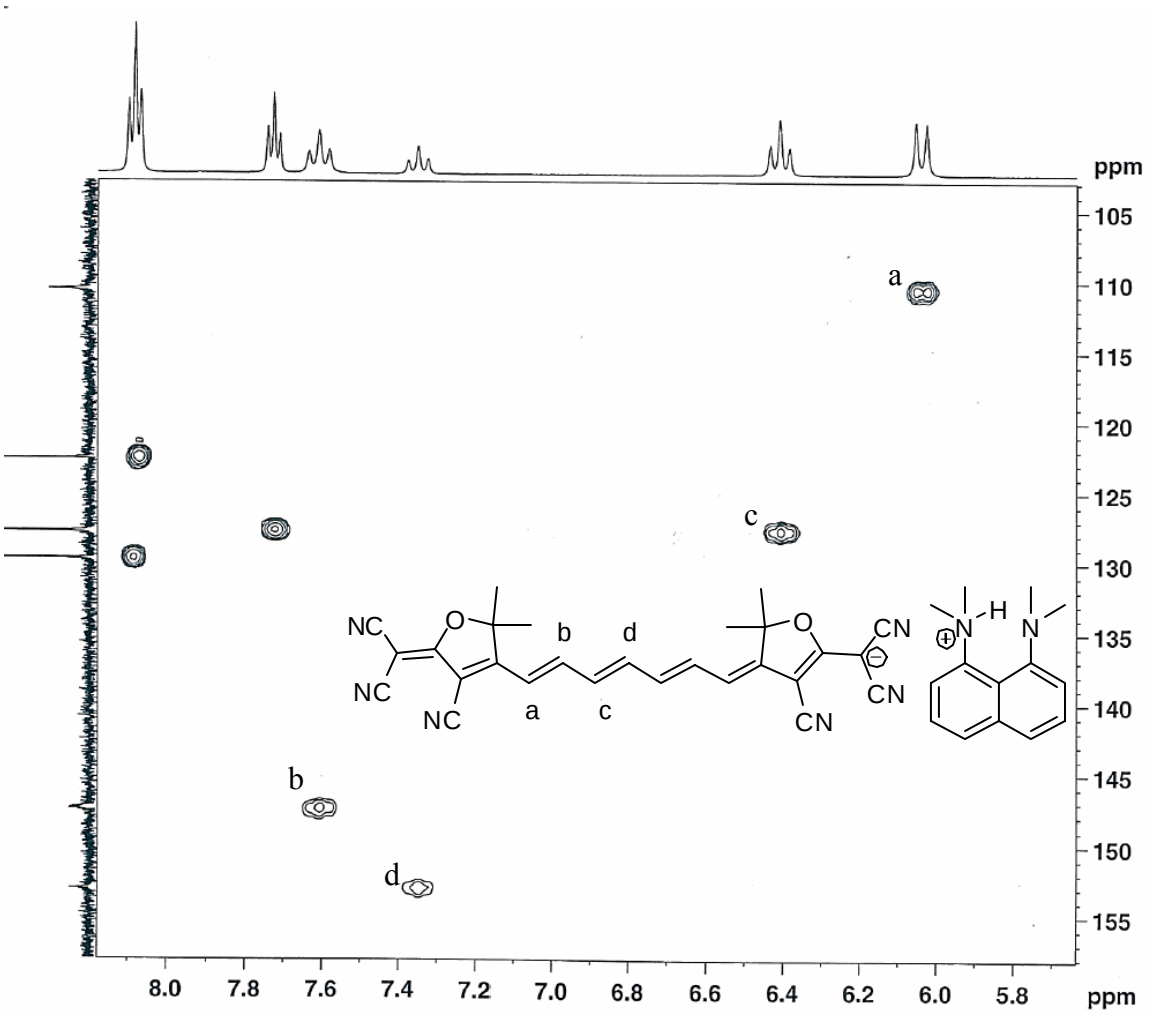

Figure 4.14. HSQC NMR spectrum (^{1}H NMR on the X-axis, ^{13}C DEPT135 on the Y-axis) in $(CD_3)_2SO$ of **4.9**.

Dye **4.10**, which differs from **4.9** in the counterion, has two carbon resonances which were not observed. There is most likely three peaks overlapped at 115 ppm, which are likely to belong to the three carbon atoms of the nitrile functionalities (Figure 4.15), since this is a typical chemical shift for the carbons of nitriles.[21] The peaks appeared separately in the spectra for similar compounds **4.8** and **4.9**, for which $(CD_3)_2SO$ was used as the solvent; however, the spectrum for **4.10** was acquired in $CDCl_3$ leading to the

overlap. Dyes **4.11** and **4.12** have ^{13}C NMR spectra that are consistent with the expected products.

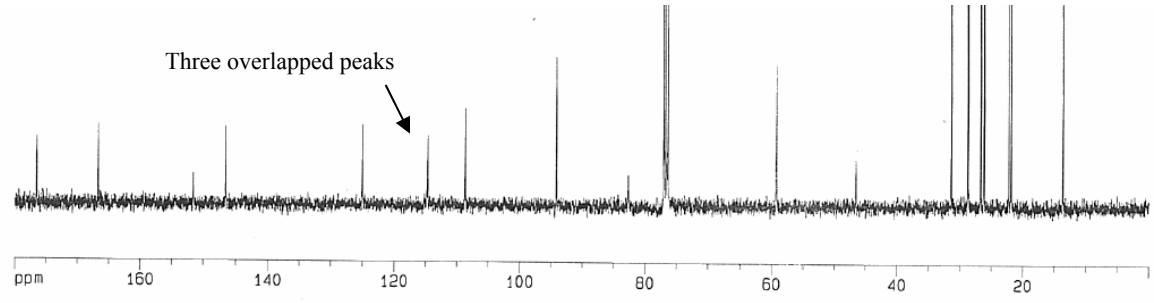

Figure 4.15. ^{13}C NMR spectrum of **4.10** in $CDCl_3$.

4.4. Linear and Nonlinear Optical Properties

4.4.1. Linear and Nonlinear Optical Properties of 4.1-4.7

Table 4.1 collects the measurements for several linear optical properties of **4.1-4.7**. **4.1-4.3** show a trend that would be expected in λ_{max}: of *ca*. 100 nm bathochromic shift per additional vinylene group. **4.6** and **4.7**, as well as **4.4** and **4.5** show a similar trend. A comparison of the trimethine dyes **4.4**, and **4.6** versus **4.1** shows a bathochromic shift in the λ_{max} of the former dyes as the effective conjugation length of the dye is increased. A 153 nm bathochromic shift is observed when the sulfone functionality of **4.1** is replaced by the dicyanomethylidene group as seen in **4.4**. Replacing the ketone functional group of **4.1** with the –ylidenemalononitrile group seen in **4.6** resulted in a 187 nm bathochromic shift in λ_{max}. Figure 4.16, 4.17 and 4.18 show the absorption spectra of **4.1-4.7** in DMSO solution.

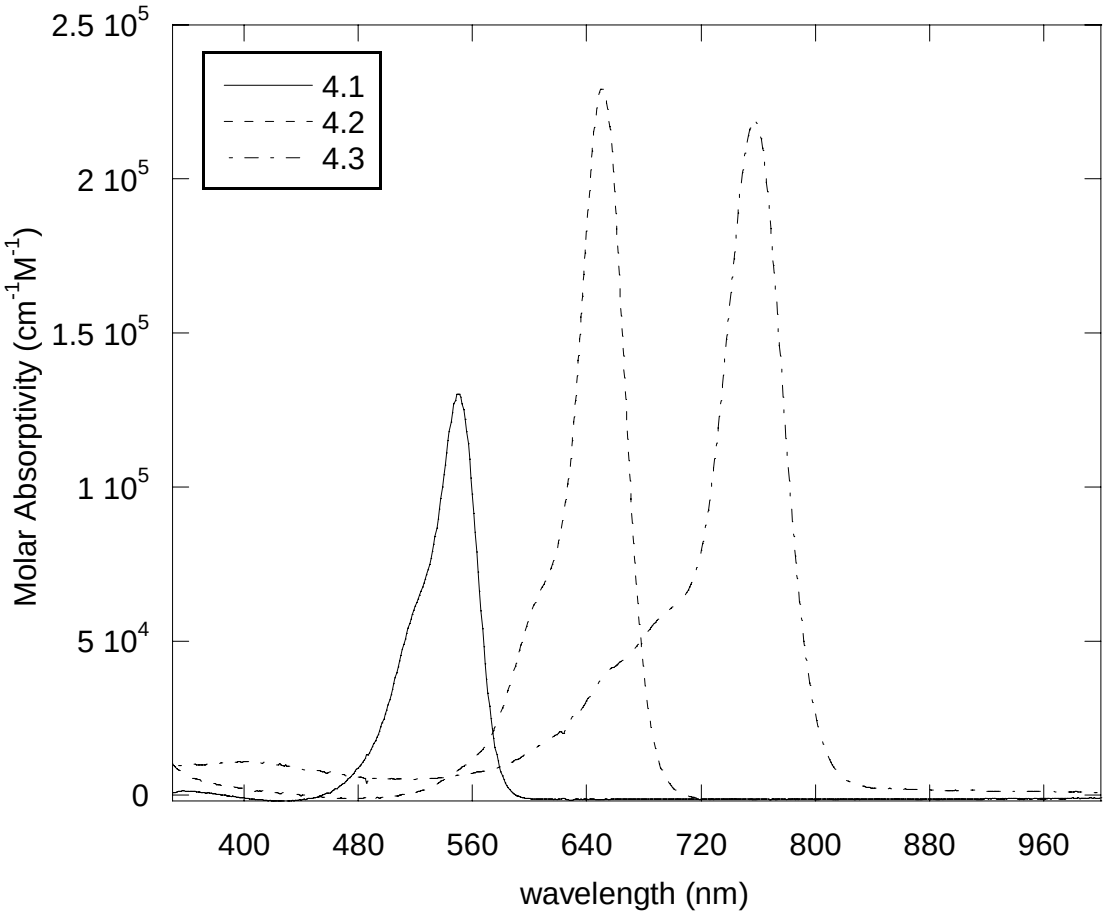

Figure 4.16. Absorption spectra in DMSO solution of **4.1-4.3**.

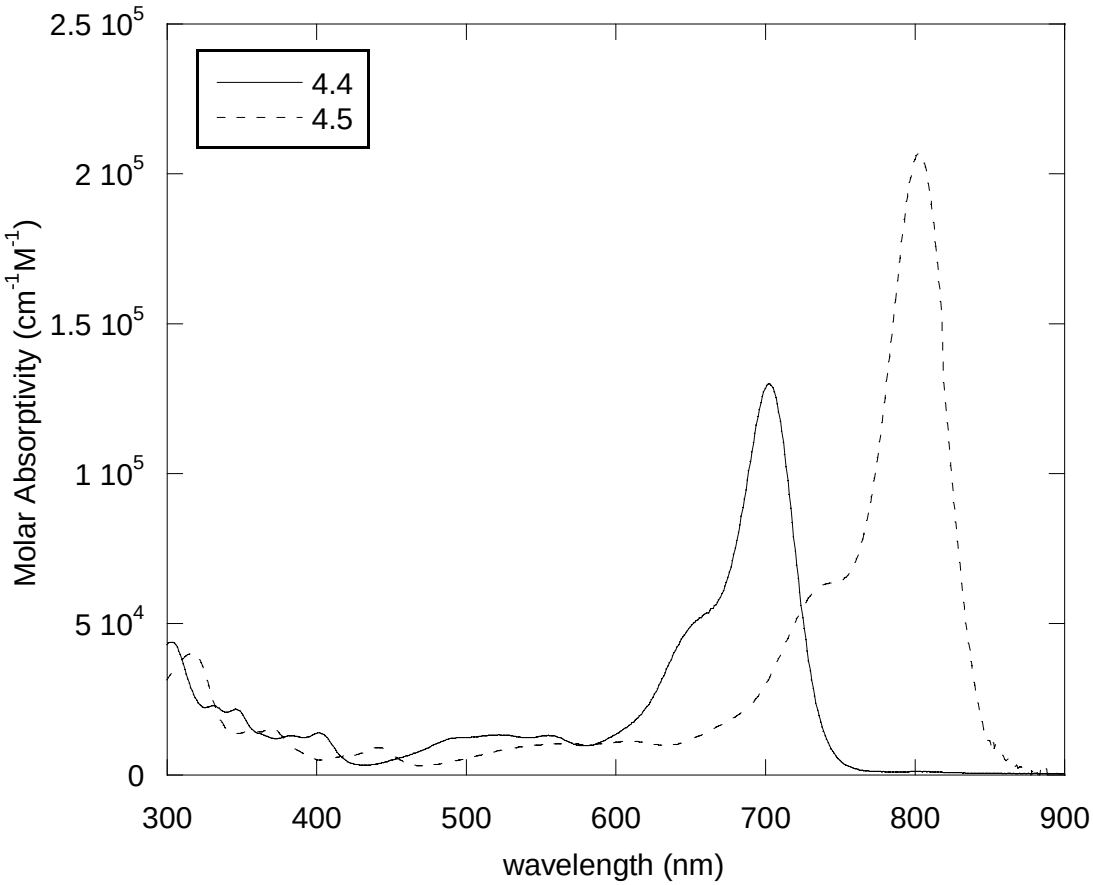

Figure 4.17. Absorption spectra in DMSO solution of **4.4** and **4.5**.

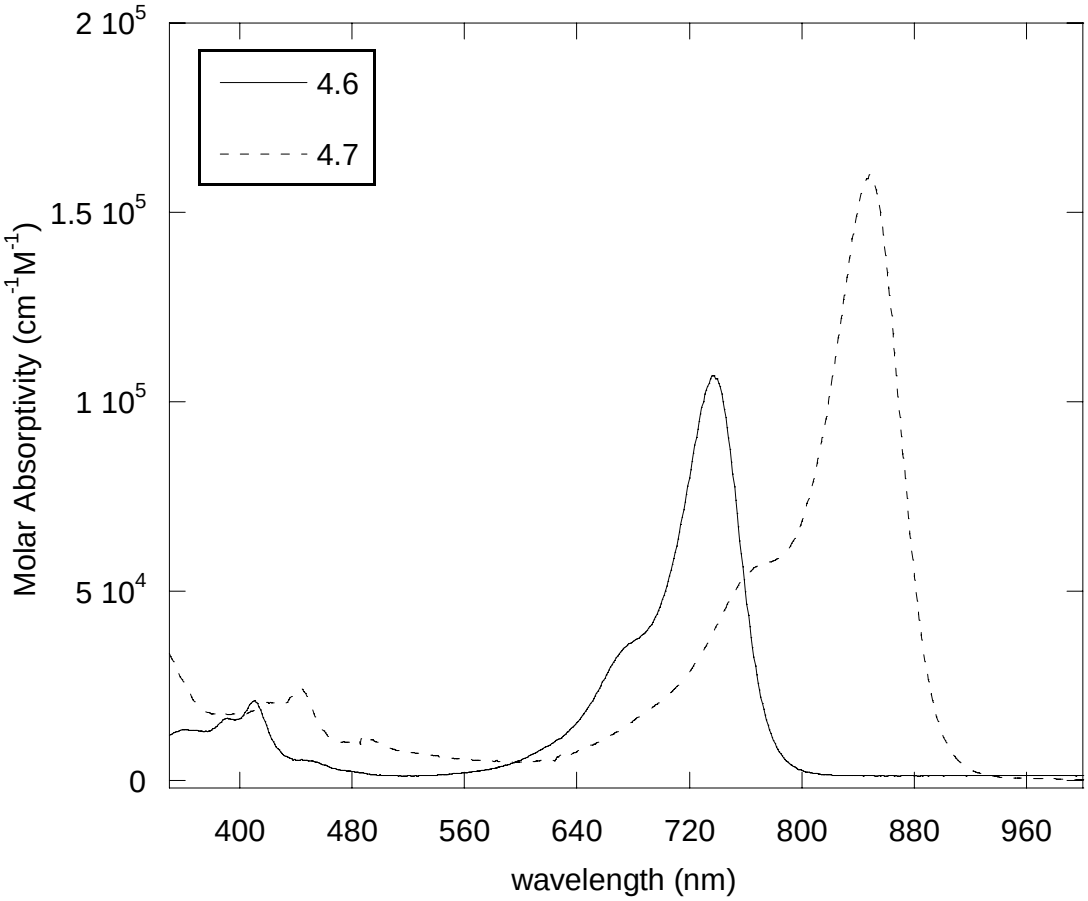

Figure 4.18. Absorption spectra in DMSO solution of **4.6** and **4.7**.

In polymethines, the sum-over-states expression[22] for Re(γ) is typically dominated by a two-state term in which the key quantities are the transition energy and transition dipole moment, both associated with the lowest energy one-photon absorption. Values of the static (zero-frequency) Re(γ) were estimated by the two-state expression introduced in Chapter 2:

$$\mathrm{Re}(\gamma)_{\mathrm{static}}) = -\left((2.998)^4 \times 10^{23}\right) \times \left(\frac{1}{5}\right) \times 4 \times \frac{M_{ge}^4}{E_{ge}^3} \tag{4.1}$$

The values from the calculations for **4.1**-**4.7** are shown in Table 4.1.

Table 4.1. λ_{max}, ε_{max}, M_{ge}, and the Re(γ)$_{static}$ of **4.1-4.7** in DMSO solution

Dye	λ_{max} (nm)	ε_{max} (10^5 M^{-1} cm^{-1})	M_{ge} (D)[a]	2-level model Re(γ)$_{static}$ (10^{-33} esu)[b]
4.1	550	1.30	10.1	-0.18
4.2	651	2.29	13.2	-0.85
4.3	757	2.19	15.2	-2.36
4.4	703	1.30	10.7	-0.47
4.5	803	2.09	14.5	-2.34
4.6	737	1.07	10.5	-0.50
4.7	848	1.60	13.8	-2.26

[a] Obtained from integration of the absorption spectra as $M_{ge} = 0.9584(\int \varepsilon d\upsilon / \upsilon_{max})^{0.5}$ where ε is in $M^{-1}cm^{-1}$ and υ is in cm^{-1}.
[b] Calculated from Eq 4.1 using experimentally determined values of M_{ge} and E_{ge} from this table.

Table 4.2 reports the nonlinear optical properties of **4.1-4.7**. The third-order nonlinear optical properties of **4.1**-**4.7** were investigated in DMSO solutions using open- and closed-aperture Z-scan techniques[23,24] to determine Im(γ) and Re(γ), respectively, with ~100 fs pulses at a wavelength of 1.3 μm. These measurements were performed by Dr. Joel Hales.

The dye with the shortest wavelength λ_{max}, **4.1**, was insensitive to the Z-scan measurements; the magnitude of real and imaginary γ being too small to measure. The Re(γ) value of **4.2** was positive and relatively weak. The positive value may be due to γ_σ-sigma effects dominating the γ_π-effects for this dye of short conjugation length.[25-28] The relatively large value of Im(γ) indicates 1300 nm is close to a TPA resonance peak. The only heptamethine dye in this study, **4.3**, displayed the largest values of Re(γ) and Im(γ). The Re(γ) and Im(γ) of trimethine **4.4** was similar to that of trimethine **4.6**. The Re(γ) was significantly larger for **4.4** and **4.6** compared to **4.1** (or even **4.2**). Pentamethines **4.5**

and **4.7** had similar magnitudes of Re(γ) to one another, which were greater than that for pentamethine **4.2**.

The trends in Re(γ) predicted from the linear absorption using the 2-level model ($Re(\gamma)_{static}$) are generally underestimated, particularly in the case of dyes **4.3-4.7**, which is most likely due to near resonance enhancement (Nonlinear optical measurements taken near 2PA resonances). **4.3** was predicted to be of similar magnitude as **4.5** and **4.7**; however, the experimental value was almost twice as large. The magnitude of Im(γ) is relatively large, indicating it is near a TPA resonance, which could give greater resonance enhancement to the magnitude of Re(γ).

Table 4.2. Re(γ), Im(γ), |γ|, Φ, and the $Re(\gamma)_{static}$ of **1-7**.[a]

Dye	2-level model $Re(\gamma)_{static}$ (10^{-33} esu)[b]	Re(γ) (10^{-33} esu)	Im(γ) (10^{-33} esu)	|γ| (10^{-33} esu)	Φ (°)
4.1	-0.18	-	-	-	-
4.2	-0.85	0.56	2.90	0.63	27
4.3	-2.36	-7.92	4.70	9.21	149
4.4	-0.47	1.28	0.91	1.57	145
4.5	-2.34	-4.00	1.46	4.26	160
4.6	-0.50	-2.20	1.21	2.51	151
4.7	-2.26	-4.26	1.09	4.40	166

[a] Measured in DMSO at 1300 nm using the Z-scan technique. The magnitude and phase of γ are defined as $|\gamma|^2 = Re(\gamma)^2 + Im(\gamma)^2$ and $\theta = \arctan[Im(\gamma)/Re(\gamma)]$, respectively.
[b] Calculated from Eq 4.1 using experimentally determined values of M_{ge} and E_{ge} from Table 4.1.

4.4.2. Linear and Non-linear Optical Properties of 4.8-4.12

4.8-4.12 all show strong absorption maxima in the visible-near-IR spectrum; the absorption spectra are shown in Figure 4.19a and Figure 4.19b. Parameters characterizing the linear absorptions are given in Table 4.3.

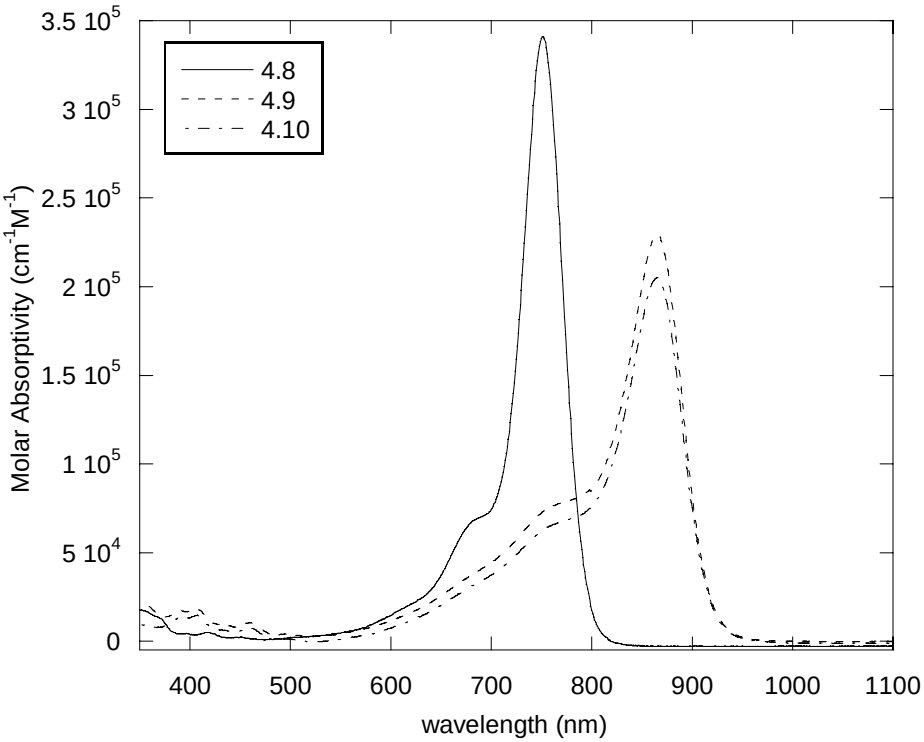

Figure 4.19a. Absorption spectra of **4.8** (—), **4.9** (----),, and **4.10** (-·-·-) in DMSO.

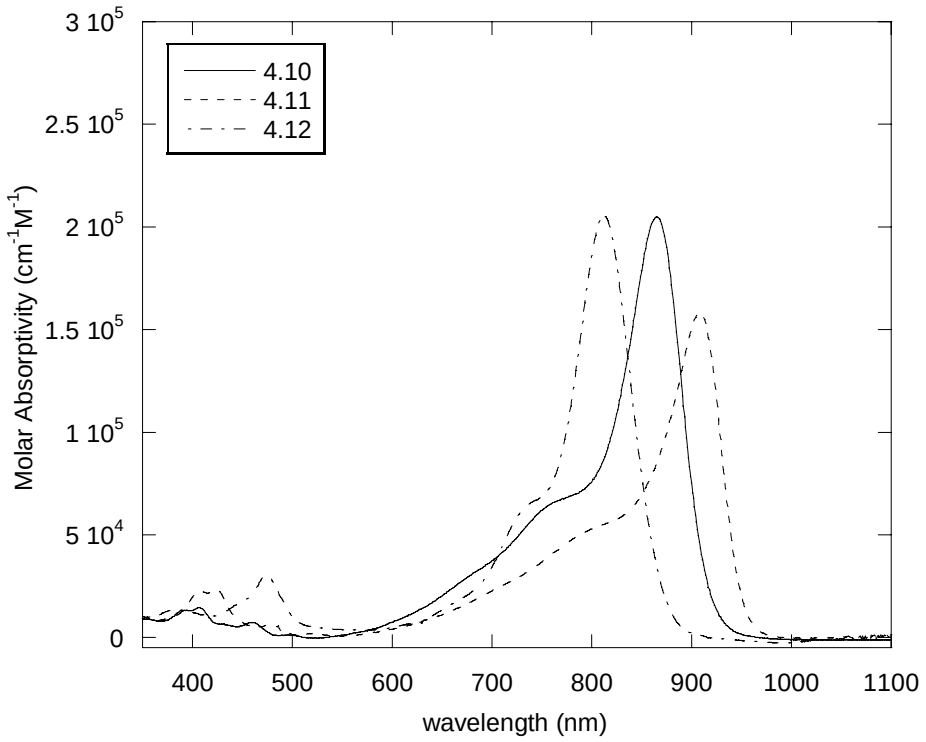

Figure 4.19b. Absorption spectra of **4.10** (—), **4.11** (----),, and **4.12** (-·-·-) in DMSO.

A *ca*. 100 nm bathochromic shift is observed in λ_{max} for **4.8** to **4.9**. This shift is expected due to the additional vinylene group of **4.9**. **4.9** and **4.10** differ by the counterion, which has little effect on the position of λ_{max}. **4.11** has a 44 nm bathochromic shift, while **4.12** has a 52 nm hypsochromic shift compared to **4.10**. The bathochromic shift of **4.11** can be explained by an increase in planarity of the conjugated bridge leading to better π-orbital overlap. Additionally, the incorporation of electron donating groups in the γ-positions (alkyl groups) and electron withdrawing groups in the δ-position (chlorine) should cause a bathochromic shift in λ_{max} by the expected effects of the Dewar-Knott rule (please see chapter three for more details).[29] The hypsochromic shift of **4.12** can be rationalized by the propensity for the indene ring on the center of the bridge to

localize the negative charge and form an aromatic five-member ring, thus disrupting the complete delocalization of the charge (Figure 4.20). Similar effects have been observed on the absorption spectra of benzothiazole terminated dyes with different bridges, which depending on the structure, could aromatize.[30] Figure 4.21 shows three benzothiazole terminated dyes, one with an unsubstituted bridge (**4.X**), one with the indene ring in a position where it can not aromatize (**4.XI**), and one where it can aromatize (**4.XII**). In ethanol the λ_{max} of **4.X** is 652 nm, **4.XI** is 755 nm and **4.XII** is 615 nm.[30] The bathochromic shift of **4.XI** relative to **4.X** may be due to increased planarity of the bridge, while the hypsochromic shift of **4.XII** relative to **4.X** is probably due to the aromatization of the central ring.

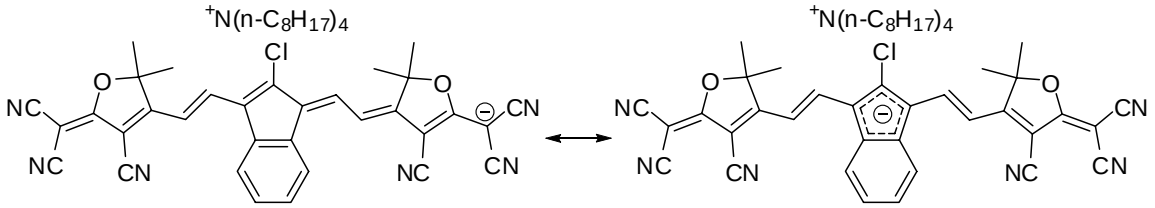

Figure 4.20. Two resonance forms contributing to the ground state of **4.12**.

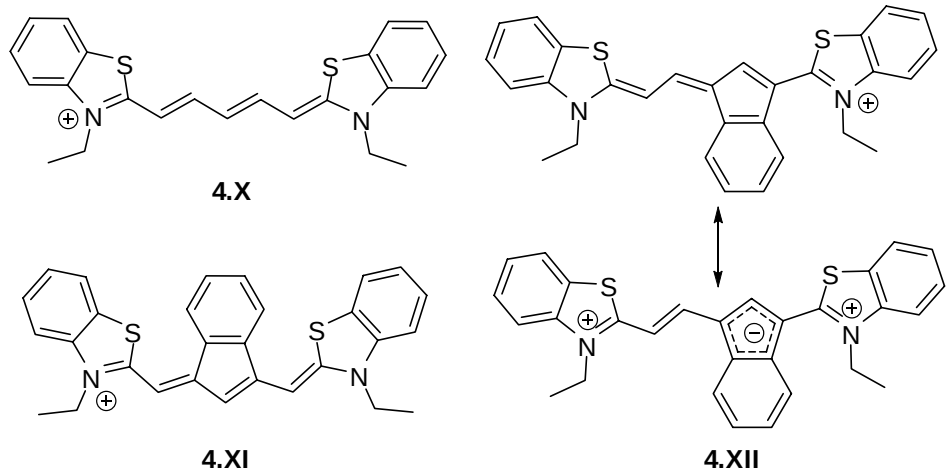

Figure 4.21. Benzothiazole terminated dyes from the literature.[30]

The relatively narrow absorption band of **4.8** was found to have a high extinction coefficient at λ_{max} with an overall transition dipole moment of 17.3 Debye for the band. **4.9** has a somewhat larger transition dipole moment (18.3 Debye); the maximum extinction coefficient is smaller at the λ_{max}, but the broader band shape compensates for this reduction. Comparing **4.9** and **4.10** reveals that the counterion has little effect on the extinction coefficient and the transition dipole moment in solution. **4.11** and **4.12** have similar transition dipole moments, which can be rationalized by comparing the broad absorption band of **4.11** with the narrower, but stronger absorption band of **4.12**.

Equation 4.1 was once again used to calculate Re(γ) using the sum-over-states expression.[22] The values from the calculations for **4.8-4.12** are shown in Table 4.3.

Table 4.3. λ_{max}, ε_{max}, M_{ge}, and the $Re(\gamma)_{static}$ of TCF-terminated polymethine dyes in DMSO solution

Dye	λ_{max} (nm)	ε_{max} (10^5 M^{-1} cm^{-1})	M_{ge} (D)[a]	2-level model $Re(\gamma)_{static}$ (10^{-33} esu)[b]
4.8	752	3.41	17.3	-3.9
4.9	865	2.29	18.3	-7.4
4.10	865	2.04	17.0	-5.5
4.11	908	1.58	15.0	-3.9
4.12	812	2.06	15.5	-3.2

[a] Obtained from integration of the absorption spectra as $M_{ge} = 0.9584(\int \varepsilon d\upsilon / \upsilon_{max})^{0.5}$ where ε is in $M^{-1}cm^{-1}$ and υ is in cm^{-1}.

[b] Calculated from Eq 4.1 using experimentally determined values of M_{ge} and E_{ge} from this table.

The third-order nonlinear optical properties of **4.8**-**4.12** were investigated in DMSO solutions using open- and closed-aperture Z-scan techniques[23,24] to determine Im(γ) and Re(γ), respectively, with ~100 fs pulses at a wavelength of 1.3 μm. The measurements were performed by Dr. Joel Hales. Data is collected and presented in Table 4.4. This trend in experimental Re(γ) at 1300 nm is reproduced by the trend obtained from the sum-over-states expression for $Re(\gamma)_{static}$. It is important to note the calculated $Re(\gamma)_{static}$ does not take into consideration resonance enhancement, while the experimental measurements are at 1300 nm where resonance enhancement can occur, thus, larger magnitudes of Re(γ) were observed experimentally. The weak response of **4.12** can be attributed to the tendency for π-electrons to aromatize in the bridge of the dye, which results in lower λ_{max} and so lower Re(γ(0)), but also less resonant pre-enhancement. Even though the |γ| for **4.11** is relatively small compared to **4.10**, the majority of γ is Re(γ). The ratio of Re(γ)/Im(γ) is 4.6 for **4.11** compared to 2.1 for **4.10**.

This is most likely due to a bathochromic shift in the peak of the 2PA peak, which would be consistent with the bathochromic shift of the 1PA peak.

Table 4.4. Re(γ), Im(γ), |γ|, Φ, and the $Re(\gamma)_{static}$ of TCF-terminated polymethine dyes.[a]

Dye	2-level model $Re(\gamma)_{static}$ (10^{-33} esu)[b]	Re(γ) (10^{-33} esu)	Im(γ) (10^{-33} esu)	|γ| (10^{-33} esu)	Φ (°)
4.8	-3.9	-6.1	3.5	7.0	150
4.9	-7.4	-9.7	3.7	10.4	159
4.10	-5.5	-8.5	4.0	9.4	155
4.11	-3.9	-7.9	1.7	8.1	168
4.12	-3.2	-5.7	2.0	6.0	160

[a] Measured in DMSO at 1300 nm using the Z-scan technique. The magnitude and phase of γ are defined as $|\gamma|^2 = Re(\gamma)^2 + Im(\gamma)^2$ and $\theta = \arctan[Im(\gamma)/Re(\gamma)]$, respectively.
[b] Calculated from Eq 4.1 using experimentally determined values of M_{ge} and E_{ge} from Table 4.3.

4.5. Conclusions

Anionic polymethine dyes were synthesized with various keto- and dicyanomethylidene-based terminal groups, conjugation lengths and in the case of TCF terminated dyes, with a variety of polymethine bridges. The linear absorption properties of the polymethine dyes follow similar trends to cationic polymethine dyes in respect to bathochromic-shifted absorption maxima and increased transition dipole moments as vinylene groups are added to the bridge.

Generally, the terminal groups with stronger withdrawing abilities led to greater bathochromic shifts and larger magnitudes of Re(γ) than those with weaker withdrawing abilities (when comparing dyes of the same core length). The anionic dyes reported do

not possess a favorable ratio of Re(γ)/Im(γ) suitable for all-optical signal processing at 1300 nm. Dyes with additional vinylene groups in the core are necessary to achieve larger magnitudes of γ, for example if TCF-terminated dyes follow trends observed in other polymethine dyes regarding a power law dependence of Re(γ) upon $N^{\pm 8}$ (where N is the number of π-electrons), then perhaps a TCF-terminated dye with nine methine units would have suitably large Re(γ) for use in a device.

It is useful to compare the nonlinear optical properties of dyes with one terminal group to another. Determination of effective conjugation lengths causes difficulty in making direct comparisons. Comparing dyes of similar λ_{max}, for example **4.8** (752 nm) and **4.6** (737 nm), may be reasonable. The larger M_{ge} of **4.8** compared to **4.6** may be the cause of a magnitude of Re(γ) being almost three times larger at 1300 nm. The similar Φ of each dye would indicate 2PA resonance enhancement is similar for each dye. Thus, dyes terminated with S4.4 may be a better choice for materials used for AOS and AOSP.

The exchange of the counter-ion has relatively small effects on the linear and nonlinear optical properties in solution when both counter-ions are non-absorbing in the region of interest as shown by comparing **4.9** and **4.10**. The bridge substituents had considerable effects upon the nonlinear optical properties at 1300 nm indicating consideration of the bridge is necessary as observed by comparing **4.10**, **4.11** and **4.12**. Careful inspection of the two-photon absorption spectrum is necessary to determine the optimal wavelength to perform measurements of γ, most likely due to the simultaneous shifting of one-photon and two-photon absorption bands.

4.6. Experimental

Starting materials were obtained from commercial sources and used without further purification. Where necessary tetrahydrofuran was dried by passage through two columns of activated alumina.[31] UV-vis.-NIR spectra were recorded in 1 cm cells using a Varian Cary 5E spectrometer. NMR spectra were recorded on a Varian 300, a Bruker 400, and a Bruker 500 MHz spectrometers. Unless otherwise noted, the NMR spectra were collected at room temperature. Elemental analyses were performed by Atlantic Microlabs. The EI mass spectra were recorded on a VG instruments 70SE and the ESI mass spectra were recorded on a Micromass Quattro LC.

4.1

S4.1 (0.214 g, 1.18 mmol), 1,8-bis(dimethylamino)naphthalene (proton sponge) (0.321 g, 1.50 mmol) and **S4.5** (0.128 g, 0.495 mmol) were dissolved in acetonitrile (10 mL) and acetic anhydride (0.25 mL). The reaction mixture was stirred and heated at reflux for 25 min. The solvent was removed under vacuum, then a residue was precipitated from chloroform by adding hexanes. The precipitate was collected by filtration to give a red solid (0.285 g). The crude product was combined with tetra-*n*-octylammonium bromide and combined in dry tetrahydrofuran (20 mL) under nitrogen. A slurry of sodium hydride (42 mg, 1.7 mmol) in dry tetrahydrofuran (10 mL) was added dropwise. After stirring for 5 min., the solution was quickly filtered. The solvent was removed from the filtrate under vacuum and the residue was dissolved in dichloromethane followed by precipitation by adding hexanes. A semicrystalline, red solid was collected by filtration and dried under vacuum (0.151 g, 0.174 mmol, 40% yield). ^{1}H NMR (400 MHz, CD_2Cl_2,

204 K): δ (ppm) 7.92 – 7.78 (m, 4H), 7.78 – 7.65 (m, 4H), 7.61 (d, J = 14 Hz, 2H), 7.31 (d, J = 13 Hz , 0.2H, lesser isomer), 6.58 (d, J = 14 Hz , 1H), 3.03 (m, 8H), 1.49 (m, 8H), 1.20 – 1.13 (m, 40H), 0.78 (t, J = 6.6 Hz, 12H). ^{13}C NMR (100 MHz, $CDCl_3$): δ (ppm) 175.7, 145.4, 143.3, 134.2, 133.0, 132.7, 123.1, 119.4, 114.6, 106.5, 58.1, 31.5, 28.9, 28.8, 26.0, 22.4, 21.7, 13.9. (Additional small peaks belonging to the minor isomer were observed in the room temperature ^{1}H NMR spectrum at 175.8, 142.0, 134.6, 122.2, 119.9, 114.7, 110.1. The peaks corresponding to the minor isomer were not observed at 333K). MS (ESI) (+) *m/z* = 466.6 [M^+ cation] (-) *m/z* = 398.9 [M^- anion]. Anal. Calcd. for $C_{51}H_{79}NO_6S_2$: C, 70.71, H, 9.19, N, 1.62. Found: C, 70.62, H, 9.16 N, 1.68.

4.2

S4.1 (0.188 g, 1.03 mmol), proton sponge (0.321 g, 1.50 mmol) and **S4.6** (0.136 g, 0.478 mmol) were dissolved in isopropanol (8 mL) and acetic anhydride (0.25 mL). The flask was stirred and heated at 90 °C for 15 min. Upon cooling, a solid was precipitated using ether, and then collected by filtration. The precipitate was then dissolved in dichloromethane and re-precipitated by adding hexanes. The crude product was collected as a sticky blue solid (0.248 g, 0.387 mmol). The crude product (0.144 g, 0.223 mmol) was combined with tetra-*n*-octylammonium bromide (0.139 g, 0.254 mmol) and dissolved in dry tetrahydrofuran (15 mL) under nitrogen. A slurry of sodium hydride (39 mg, 1.6 mmol) in dry tetrahydrofuran (5 mL) was added dropwise. After stirring for 5 min., the solution was quickly filtered. The solvent was removed from the filtrate under vacuum. The product was separated by silica gel column chromatography using dichloromethane/ethylacetate (9:1) followed by dichloromethane/ethylacetate (5:5) as dichloromethane by adding hexanes. The product was collected as an amorphous blue

solid that slowly crystallized into green needles (0.123 g, 0.138 mmol, 36% yield). ^{1}H NMR (400 MHz, CD_2Cl_2, 273 K): δ (ppm) 7.88 – 7.86 (m, 2H), 7.81 – 7.79 (m, 2H), 7.71 – 7.65 (m, 4H), 7.50 (broad d, J = 14 Hz, 2H), 7.32 (broad t, J = 13 Hz , 1H), 6.62 (broad t, 1H (should integrate to 2H; however, the peak is broad), 2.91 (m, 8H), 1.44 (m, 8H), 1.18 – 1.14 (m, 40H), 0.79 (t, J = 6.8 Hz, 12H) (a major and minor isomer can be observed in the ^{1}H NMR spectrum at 213K as shown in Figure 4.12; however, a large amount of overlap causes interpretation of the spectrum to be difficult). ^{13}C NMR (100 MHz, $CDCl_3$): δ (ppm) 175.4, 158.0, 143.2, 141.1, 134.6, 133.0, 132.9, 123.2, 119.6, 115.5, 115.0, 58.9, 31.5, 28.9 (2 peaks overlapped), 26.2, 22.5, 21.8, 14.0. MS (ESI) (+) *m/z* = 466.6 [M^+ cation] (-) *m/z* = 424.9 [M^- anion]. Anal. Calcd. for $C_{53}H_{81}NO_6S_2$: C, 71.34, H, 9.15, N, 1.57. Found: C, 71.21, H, 9.17, N, 1.63.

4.3

S4.1 (0.420 g, 2.31 mmol), and **S4.7** (0.354 g, 1.09 mmol) were dissolved in acetonitrile (6 mL) and acetic anhydride (0.4 mL). Triethylamine (0.5 mL) was added dropwise and the solution was stirred and heated at 80 °C for 5 min. Upon cooling, a solid was precipitated by the addition of ether (100 mL). The supernatant was decanted off and the residue was dissolved in ethylacetate/acetontitrile (1:1). The solution was passed through silica gel (made basic by treatment with triethylamine) using ethylacetate/methanol (3:1) as the eluent. The solvent was removed under reduced pressure and the residue was precipitated from a solution of ethylacetate/acetontitrile (1:1) by adding a mixture of ether/hexanes (2:1). The crude product was collected as a sticky blue solid (0.154 g), which was combined with tetra-*n*-octylammonium bromide (0.152 g, 0.278 mmol) and dissolved in dry tetrahydrofuran (40 mL) under nitrogen. A slurry of sodium hydride (31

mg, 1.3 mmol) in dry tetrahydrofuran (10 mL) was added dropwise. After 5 min. of stirring, the solution was quickly filtered. The solvent was removed from the filtrate under reduced pressure. The product was separated using silica gel (made basic by treatment with triethylamine) column chromatography using a gradient of eluents: dichloromethane/ethylacetate (9:1), dichloromethane/ethylacetate (3:1), dichloromethane/ethylacetate (1:3). The solvent was removed under vacuum and the product was precipitated from dichloromethane using hexanes. The product was collected as an amorphous blue solid (0.098 g, 0.107 mmol, 9.8% yield). ^{1}H NMR (400 MHz, $CDCl_3$, 333 K): δ (ppm) 7.88 (m, 2H), 7.76 (m, 2H), 7.60 (m, 4H), 7.36 (d, J = 13 Hz, 2H), 7.08 (t, J = 13 Hz, 2H), 6.89 (br t, 2H), 6.34 (t, J = 13 Hz, 1H), 3.04 (m, 8H), 1.54 (m, 8H), 1.32 – 1.20 (m, 40H), 0.87 (t, J = 7.2 Hz, 12H). ^{13}C NMR (100 MHz, $CDCl_3$, 333 K): δ (ppm) 175.1, 154.6, 143.5, 139.6, 135.2, 132.80, 132.76, 123.1, 123.0, 119.8, 117.4, 116.3, 59.3, 31.6, 29.0, 28.9, 26.4, 22.5, 22.1, 13.9. MS (ESI) (+) *m/z* = 466.6 [M^+ cation] (-) *m/z* = 451.0 [M^- anion]. Anal. Calcd. for $C_{55}H_{83}NO_6S_2$: C, 71.93, H, 9.11, N, 1.53. Found: C, 71.69, H, 9.22, N, 1.61.

4.4

S4.2 (109 mg, 0.561 mmol) and **S4.5** (69 mg, 0.267 mmol) were dissolved in absolute ethanol (5 mL), and then heated to reflux. Triethylamine (0.5 mL) and acetic anhydride (10 drops) were added. A dark solid quickly precipitated. The solution was stirred for 10 min., and then the precipitate was collected from the hot solution by filtration (97 mg, 0.185 mmol, 69%). ^{1}H NMR (400 MHz, $(CD_3)_2SO$): δ (ppm) 9.11 (t, J = 13.1 Hz, 1H), 8.83 (broad s, 1H), 8.27 (d, J = 7.2 Hz, 2H), 8.12 (d, J = 13.3 Hz, 2H), 7.68 – 7.60 (m, 6H), 3.08 (q, J = 7.3 Hz, 6H), 1.14 (t, J = 7.3 Hz, 9H). ^{13}C NMR (100 MHz, d-DMSO):

δ (ppm) 188.6, 159.3, 147.8, 139.4, 136.1, 133.5, 132.9, 123.1, 121.8, 119.4, 117.1, 116.9, 115.6, 58.3, 45.8, 8.6. MS (ESI) (+) *m/z* = 101.8 [M^+ cation] (-) *m/z* = 423.1 [M^- anion]. Anal. Calcd. for $C_{59}H_{79}N_5O_2$: C, 75.41, H, 5.18, N, 13.32. Found: C, 75.49, H, 5.00, N, 13.23.

4.5

S4.2 (0.205, 1.06 mmol) and **S4.6** (0.131 g, 0.461 mmol) were dissolved in acetonitrile (10 mL) and acetic anhydride (0.25 mL) and then heated to reflux. Triethylamine (0.5 mL) was added dropwise with stirring, then heated for 5 min. A dark precipitate was collected by filtration and rinsed with ethanol. The material was combined with tetra-*n*-octylammonium bromide (0.254 g, 0.465 mmol) under nitrogen. The solids were dissolved in dry tetrahydrofuran (15 mL), then a slurry of sodium hydride (44 mg, 1.8 mmol) in dry tetrahydrofuran (10 mL) was added dropwise. After 10 min. the solution was filtered. The solvent was removed from the filtrate under vacuum. The residue was dissolved in dichloromethane and then purified through silica gel (made basic by treatment with triethylamine) chromatography using dichloromethane/ethylacetae (9:1) as the eluent. (0.233 g, 0.254 mmol, 27%). ^{1}H NMR (400 MHz, $CDCl_3$): δ (ppm) 8.39 (dd, *J* = 6.2, 1.4 Hz, 2H), 8.17 (d, *J* = 13.1 Hz, 2H), 8.01 (t, *J* = 13.0 Hz, 2H), 7.57 (d of m, *J* = 6.2 Hz, 2H), 7.50 – 7.44 (m, 4H), 7.24 (t, *J* = 12.8 Hz, 2H), 3.16 (m, 8H), 1.64 (m, 8H), 1.40 – 1.10 (m, 40H), 0.78 (t, *J* = 6.9 Hz, 12H). ^{13}C NMR (100 MHz, $CDCl_3$): δ (ppm) 190.0, 161.0, 159.6, 144.5, 140.1, 136.8, 133.0, 132.1, 123.7, 123.5, 121.6, 117.7, 117.6, 116.3, 58.9, 58.4, 31.5, 28.99, 28.94, 26.3, 22.5, 21.9, 14.0. MS (ESI) (+) *m/z* = 466.5 [M^+ cation] (-) *m/z* = 449.0 [M^- anion]. Anal. Calcd. for $C_{51}H_{79}NO_6S_2$: C, 79.96, H, 8.91, 7.64. Found: C, 80.00, H, 9.03, N, 7.64.

4.6

S4.3 (0.266 g, 1.16 mmol), proton sponge (0.303 g, 1.42 mmol) and **S4.5** (0.131 g, 0.506 mmol) were dissolved in acetonitrile (8 mL) and acetic anhydride (0.25 mL). The solution was stirred and heated at reflux for 15 min. Upon cooling to room temperature the precipitate was collected by filtration. The coppery brown precipitate was rinsed with acetonitrile, ethanol, water and ethanol to give the crude product (0.244 mg, 0.343 mmol, 68%). The crude product (0.217 g) was combined with tetra-*n*-octylammonium bromide (0.272 g, 0.498 mmol) in dry tetrahydrofuran (20 mL). A slurry of sodium hydride (0.030 g, 1.3 mmol) in dry tetrahydrofuran (10 mL) was added dropwise and allowed to stir for 5 min., then quickly filtered. The solvent was removed from the filtrate and the residue was purified through silica gel (made basic by treatment with triethylamine) chromotagraphy using hexanes as an eluent. Removal of the solvent led to the product as a brown solid (0.155 mg, 0.161 mmol, 42%). ^{1}H NMR (400 MHz, $CDCl_3$): δ (ppm) 8.80 – 8.78 (m, 2H), 8.42 (d, J = 13 Hz, 2H), 7.76 – 7.74 (m, 2H), 7.69 – 7.63 (m, 4H) 7.43 (t, J = 13 Hz, 2H), 3.15 (m, 8H), 1.60 (s, 8H), 1.30 – 1.20 (m, 40H), 0.81 (t, J = 6.7 Hz, 12H). ^{13}C NMR (100 MHz, $CDCl_3$): δ (ppm) 147.1, 143.1, 138.5, 133.7, 132.8, 130.3, 125.4, 120.8, 118.4, 117.6, 117.5, 114.8, 58.5, 58.0, 31.6, 29.1, 29.0, 26.2, 22.5, 21.8, 14.0. MS (ESI) (+) *m/z* = 466.6 [M^+ cation] (-) *m/z* = 494.9 [M^- anion]. Anal. Calcd. for $C_{57}H_{79}N_5O_4S_2$: C, 71.14, H, 8.27, N, 7.28. Found: C, 71.29, H, 8.28, N, 7.26

4.7

S4.3 (0.275 g, 1.20 mmol), proton sponge (0.313 g, 1.46 mmol) and **S4.6** (0.137 g, 0.482 mmol) were dissolved in acetonitrile (8 mL) and acetic anhydride (0.25 mL). The flask was stirred and heated at reflux for 40 min. The solution was cooled to room temperature

and filtered. The coppery brown precipitate was rinsed with acetonitrile, and then methanol (0.202 mg, 0.274 mmol, 57%). ^{1}H NMR (400 MHz, $(CD_3)_2SO$): δ (ppm) 8.63 (d, J = 8.0 Hz, 2H) 8.25 (d, J = 14 Hz, 2H) 8.11 – 8.06 (m, 6H) 7.93 – 7.84 (m, 4H) 7.73 (t, J = 7.9 Hz, 2H) 7.47 (t, J = 13 Hz , 1H) 6.89 (t, J = 13 Hz , 2H) 3.12 (s, 6H) 3.11 (s, 6H). A ^{13}C NMR An interpretable spectrum was not obtained due to decomposition of the product in DMSO before all peaks were resolved. MS (ESI) (+) *m/z* = 215.0 [M^+ cation] (-) *m/z* = 520.9 [M^- anion]. Anal. Calcd. for $C_{41}H_{32}N_6O_4S_2$: C, 66.83, H, 4.38, N, 11.41. Found: C, 66.68, H, 4.25, N, 11.31.

4.8

S4.4 (294 mg, 1.47 mmol), **S4.5** (184 mg, 0.710 mmol) and proton sponge (400 mg, 1.87 mmol) were dissolved in acetic anhydride (0.6 mL) and acetonitrile (8 mL**)** under a nitrogen atmosphere. The solution was heated at 80 °C for 10 min. Upon cooling a green solid precipitated, which was then collected by filtration. Recrystallization in acetonitrile gave a green, crystalline solid (423 mg, 0.671 mmol, 95%). ^{1}H NMR (500MHz, $(CD_3)_2SO$): δ (ppm) 8.09 (m, 4H), 7.73 (t, J = 8 Hz, 2H), 7.71 (t, J = 13 Hz, 2H), 6.41 (t, J = 11 Hz, 1H), 6.03 (d, J = 14, 2H), 3.12 (s, 6H), 3.11 (s, 6H), 1.65 (s, 12H). ^{13}C NMR (500 MHz, $(CD_3)_2SO$): δ (ppm) 176.2, 168.5, 149.5, 144.6, 134.8, 128.8, 126.9, 126.0, 121.8, 119.0, 115.3, 114.5, 113.5, 108.9, 95.3, 83.0, 45.7, 44.6, 26.5. MS (ESI) (+) *m/z* 215.1 [M^+ cation] (-) *m/z* 433.0 [M^- anion]. Anal. Calcd. for $C_{39}H_{36}N_8O_2$: C, 72.20; H, 5.59; N, 17.27. Found: C, 72.31; H, 5.69; N, 17.14.

4.9

S4.4 (287 mg, 1.44 mmol), **S4.6** (201 mg, 0.706 mmol) and proton sponge (0.376 g, 1.76 mmol) were combined under nitrogen. A solution of acetonitrile (8 mL) and acetic

anhydride (0.4 mL) was added. The reaction mixture was stirred and heated to 80 °C for 10 min. The reaction mixture was allowed to cool to room temperature, upon which a solid precipitated. The precipitate was collected by filtration as a green solid, which was rinsed with chloroform. (308 mg, 0.456 mmol, 65%) ^{1}H NMR (400 MHz, $(CD_3)_2SO$): δ (ppm) 8.09 (m, 4H) 7.73 (t, J = 8.0 Hz, 2H) 7.61 (t, J = 13 Hz, 2H) 7.36 (t, J = 13 Hz, 1H) 6.42 (t, J = 13 Hz, 2H) 6.04 (d, J = 14 Hz, 2H) 3.12 (s, 6H) 3.11 (s, 6H) 1.58 (s, 12H). ^{13}C NMR (125 MHz, $(CD_3)_2SO$): δ (ppm) 176.1, 166.2, 152.2, 146.6, 144.6, 134.8, 128.9, 126.9 (2 peaks), 121.8, 119.0, 115.5, 114.7, 114.2, 109.7, 95.1, 82.4, 45.7, 44.0, 26.4. MS (ESI) (+) *m/z* 215.1 [M^+ cation] (-) *m/z* 459.1 [M^- anion]**.** Anal. Calcd. for $C_{41}H_{38}N_8O_2$: C, 72.98; H, 5.68; N, 16.61. Found: C, 73.12; H, 5.77; N, 16.80.

4.10

4.9 (430 mg, 0.637 mmol) and tetra-*n*-octylammonium bromide were dissolved in dry THF (20 mL). A slurry of sodium hydride (92 mg, 3.8 mmol) in tetrahydrofuran (10 mL) was added dropwise under nitrogen with stirring. The solution was quickly filtered after 5 min. The solvent was removed from the filtrate under reduced pressure. The residue was dissolved in dichloromethane, and then separated using silica gel chromatography with dichloromethane as the eluent. The solvent was removed under vacuum to give the product (450 mg, 0.486 mmol, 76%). ^{1}H NMR (400 MHz, $CDCl_3$, 333 K): δ (ppm) 7.67 (t, J = 13 Hz, 2H), 7.04 (t, J = 13 Hz, 1H), 6.22 (t, J = 13 Hz, 2H), 5.80 (d, J = 14 Hz, 2H), 3.15 (m, 8H), 1.68 (m, 8H), 1.38 – 1.26 (m, 40H), 0.88 (t, J = 7.0 Hz, 12H). ^{13}C NMR (125 MHz, $CDCl_3$, 333 K) δ (ppm) 176.8, 166.9, 151.9, 146.9, 125.3, 114.9 (3 peaks), 108.9, 94.4, 82.9, 59.5, 46.8, 31.6, 29.0 (2 peaks), 27.0, 26.4, 22.5, 22.1, 13.9.

MS (ESI) (+) *m/z* 466.5 [M^+ cation] (-) *m/z* 458.9 [M^- anion]**.** Found: C, 76.50; H, 9.47; N, 10.58. Calcd for $C_{59}H_{87}N_7O_2$: C, 76.76; H, 9.64; N, 10.51.

4.11

S4.4 (0.17 g, 0.86 mmol), sodium acetate (0.20 g, 2.4 mmol) and **S4.8** (0.150 g, 0.417 mmol) were dissolved in methanol (5 mL) under a nitrogen atmosphere. The solution was stirred overnight at reflux. Upon cooling a precipitate formed which was collected by filtration and rinsed with diethyl ether. The precipitate was run through a silica plug using ethylacetate as the eluent. The solvent was removed under vacuum and the residue (0.130 mg) was combined with tetra-*n*-octylammonium bromide (0.140 mg, 0.256 mmol) and dissolved in dichloromethane (10 mL) and sonicated for 1 min. The solution was filtered and the solvent was removed under reduced pressure. The product was obtained through silica gel chromatography with hexanes/ethylacetate (1:1) eluent (0.172 g, 0.172 mmol, 41%). ^{1}H NMR (300 MHz, CD_3CN): δ (ppm) 8.22 (d, J = 14 Hz, 2H), 6.01 (d, J = 14 Hz, 2H), 3.07 (m, 8H), 2.58 (t, J = 6 Hz, 4H), 1.81 (p, J = 6 Hz, 2H), 1.60 (m, 20H), 1.34 (m, 40H), 0.91 (t, J = 7.5 Hz, 12H). ^{13}C NMR (100 MHz, CD_3CN): δ (ppm) 177.5, 168.1, 147.4, 140.6, 128.4, 116.1, 115.4, 115.2, 107.5, 96.0, 84.5, 59.23, 46.7, 32.3, 29.6, 29.5, 27.00, 26.97, 26.75, 23.3, 22.2, 21.7, 14.3. MS (ESI) (+) *m/z* = 466.6 [M^+ cation] (-) *m/z* = 533.1 [M^- anion]. Anal. Calcd. for $C_{62}H_{91}ClN_7O_2$: C, 74.33; H, 9.16; N, 9.79. Found: C, 74.40; H, 9.09; N, 9.74.

S4.9

The hexafluorophosphate salt was synthesized through a modified procedure of that used by Arnold to prepare the perchlorate salt.[18] Phosphorous oxychloride (13.5 mL) was added dropwise to a solution of DMF (18 mL) cooled in an ice bath. The solution was

heated at 45 °C for 30 min., and then dry dichloromethane (100 mL) was added after cooling. The solution was cooled in an ice bath and 2-indanone (6.7 g, 50 mmol) was added dropwise. The solution was stirred for 10 min. in the ice bath and 3.5 h. at room temperature. The solution was poured onto ice (400 mL) and the product was precipitated as a solid upon the addition of an aqueous solution of potassium hexafluorophosphate (10.3 g, 56.0 mmol). The dark yellow solid was collected by filtration (13.32 g, 32.75 mmol, 66%). The material was of sufficient purity to use as collected for the formation of **4.12**, but the **S4.9** can be further purified by dissolving it in acetonitrile and slowly adding ether, after which the product quickly crystallizes as yellow needles. ^{1}H NMR (400 MHz, CD_3CN): δ (ppm) 8.39 (s, 2H), 7.54 (m, 2H), 7.27 (m, 2H), 3.59 (s, 6H), 3.54 (s, 6H). ^{13}C NMR (125 MHz, CD_3CN): δ (ppm) 160.1, 145.1, 132.3, 124.2, 121.9, 111.4, 49.1, 45.3. MS (ESI) (+) *m/z* = 248.0 [Condensation with MeOH to form $C_{14}H_{15}ClNO^{+}$] (-) *m/z* = 144.7 [M^{-} anion]. Anal. Calcd. for $C_{15}H_{18}ClF_6N_2P$: C, 44.29; H, 4.46; N, 6.89. Found: C, 44.11; H, 4.38; N, 6.93.

4.12

S4.4 (201 mg, 1.01 mmol), proton sponge (325 mg, 1.52 mmol) and **S4.9** (195 mg, 0.479 mmol) were dissolved in acetonitrile (4 mL) and acetic anhydride (0.25 mL). The solution was stirred for 5 min., upon which a large amount of solid formed, which was collected by filtration. The precipitate was dissolved in dimethylformamide and precipitated by the addition of ether, and then collected by filtration. Tetra-*n*-octylammonium bromide (0.231 g, 0.42 mmol) was combined with the crude material (0.315 g) and dissolved in dry tetrahydrofuran (10 mL). A slurry of sodium hydride (48 mg, 2.0 mmol) in dry tetrahydrofuran (10 mL) was added dropwise will stirring under

nitrogen. The solution was quickly filtered after 5 min. The solvent was removed from the filtrate under vacuum. The residue was then purified by silica gel chromatography using dichloromethane as the eluent. Removal of the solvent under vacuum gave the product (0.20 g, 0.19 mmol, 48%). ^{1}H NMR (300 MHz, CD_3CN): δ (ppm) 8.26 (d, J = 15 Hz, 2H), 7.81 (m, 2H), 7.29 (m, 2H), 6.85 (d, J = 15 Hz, 2H), 3.07 (m, 8H), 1.73 (s, 12H), 1.60 (m, 8H), 1.34 (m, 40H), 0.91 (t, J = 7.5 Hz, 12H). ^{13}C NMR (125 MHz, $CDCl_3$): δ (ppm) 177.0, 172.4, 143.0, 138.7, 134.7, 124.9, 124.4, 120.5, 114.5, 114.1, 113.6, 107.3, 95.6, 86.8, 59.0, 49.3, 31.6, 29.0, 27.3, 26.3, 22.5, 21.9, 14.0. MS (ESI) (+) m/z = 466.5 [M^+ cation] (-) m/z = 567.1 [M^- anion]. Anal. Calcd. for $C_{65}H_{88}ClN_7O_2$: C, 75.44; H, 8.57; N, 9.47. Found: C, 75.47; H, 8.65; N, 9.25.

4.7. References

1. Patel, R. C.; Thien, T. V.; Warner, D., Preparation and Use of Dyes. US patent, **1993**, 5208135.
2. Wariishi, K.; Ishida, T.; Morishima, S., Information Recording Medium. US patent, **2003**, 6670475 B2.
3. Batsanov, A. S.; Bryce, M. R.; Davies, S. R.; Howard, J. A. K.; Whitehead, R.; Tanner, B. K., Studies on p-Acceptor Molecules Containing the Dicyanomethylene Group. X-Ray Crystal Structure of the Charge-transfer Complex of Tetramethyltetrathiafulvalene and 2,3-Dicyano-1,4-naphtoquinone:$(TMTTF)_3$-$(DCNQ)_2$. *J.Chem. Soc. Perkin Trans. 2* **1993**, 313-319.
4. Kirsanov, A. V.; Levchenko, E. S.; Tret'yakova, G. S., Diphenylamidines of carboxylic acids. *Ukrains'kii Khemichnii Zhurnal* **1953,** 19, 622-630.
5. Ahlheim, M.; Barzoukas, M.; Bedworth, P. V.; Blanchard-Desce, M.; Fort, A.; Hu, Z.-Y.; Marder, S. R.; Perry, J. W.; Runser, C.; Staelhelin, M.; Zysset, B., Chromophores with Strong Heterocyclic Acceptors: A Poled Polymer with a Large Electro-Optic Coeffiecient. *Science* **1996,** 271, 335-337.
6. Shi, Y.; Zhang, C.; Zhang, H.; Bechtel, J. H.; Dalton, L. R.; Robinson, B. H.; Steier, W. H., Low (sub-1-Volt) halfwave Voltage Polymeric Electro-optic Modulators Achieved by Controlling Chromophore Shape. *Science* **2000,** 288, 119-122.
7. Zhang, C.; Todorova, G.; Wang, C.; Londergan, T.; Dalton, L. R., Synthesis of New Second-order nonlinear optical chromophores: implementing lessons learned from theory and experiment. *Proc. SPIE Int. Soc. Opt. Eng.* **2000,** 4114, 77-87.
8. Beverina, L.; Fu, J.; Leclercq, A.; Zojer, E.; Pacher, P.; Barlow, S.; Van Stryland, E. W.; Hagan, D. J.; Brédas, J.-L.; Marder, S. R., Two-Photon Absorption at

Telecommunications Wavelengths in a Dipolar Chromophore with a Pyrrole Auxiliary Donor and Thiazole Auxiliary Acceptor. *J. Am. Chem. Soc.* **2005,** 127, 7282-7283.
9. Zheng, S.; Leclercq, A.; Fu, J.; Beverina, L.; Padilha, L. A.; Zojer, E.; Schmidt, K.; Barlow, S.; Luo, J.; Jiang, S.-H.; Jen, A. K.-Y.; Yi, Y.; Shuai, Z.; Van Stryland, E. W.; Hagan, D. J.; Brédas, J.-L.; Marder, S. R., Two-Photon Absorption in Quadrupolar Bis(acceptor)-Terminated Chromophores with Electron-Rich Bis(heterocycle)vinylene Bridges. *Chem. Mater.* **2007,** 19, 432-442.
10. Bouit, P.-A.; Di Piazza, E.; Rigaut, S.; Le Guennic, B.; Aronica, C.; Toupet, L.; Andraud, C.; Maury, O., Stable Near-Infrared Anionic Polymethine Dyes: Structure, Photophysical, and Redox Properties. *Org. Lett.* **2008,** 10, 4159-4162.
11. Bouit, P.-A.; Rauh, D.; Neugebauer, S.; Delgado, J. L.; Di Piazza, E.; Rigaut, S.; Maury, O.; Andraud, C.; Dyakonov, V.; Martin, N., A "Cyanine-Cyanine" Salt Exhibiting Photovoltaic Properties. *Org. Lett.* **2009,** 11, 4806-4809.
12. Peng, X.; Song, F.; Lu, E.; Wang, Y.; Zhou, W.; Fan, J.; Gao, Y., *J. Am. Chem. Soc.* **2005,** 127, 4170-4171.
13. Brooker, L. G. S.; Heseltine, D. W., Merocyanine Dyes Containing a Sulfone Group. US patent, **1956**, 2748114.
14. Shang, Y.; Wen, Y.; Li, S.; Du, S.; He, X.; Cai, L.; Li, Y.; Yang, L.; Gao, H.; Song, Y., A Triphenylamine-Containing Donor-Acceptor Molecule for Stable, Reversible, Ultrahigh Density Data Storage. *J. Am. Chem. Soc.* **2007,** 129.
15. Baumann, W., Improvements in or relating to organic compounds. GB patent, **1980**, 2026528.
16. Liu, S.; Haller, M. A.; Ma, H.; Daltron, L. R.; Jang, S.-H.; Jen, A. K.-Y., Focused Microwave-Assisted Synthesis of 2,5-Dihydrofuran derivatives as electron acceptors for Highly efficient nonlinear optical chromophores. *Adv. Mater.* **2003,** 15, 603-607.
17. Nikolajewski, H. E.; Dähne, S.; Hirsch, B., Vilsmeir-Formylierung von Polenaldehyden. *Chem. Ber.* **1967,** 100, 2616-2619.
18. Arnold, Z., Synthetic Reactions of Dimethyl Formamide. XXII, Formation and Preparation of Formyl Derivatives of Indene. *Collect. Czech. Chem. Commun.* **1965,** 30, 2783-2791.
19. Rumyantseva, L. I.; Gonta, S. D.; Kardash, G. G.; Perepelkin, A. N., Thionaphthen-3-one 1,1-Dioxide derivatives as Antihalation Dyes in Photography. USSR patent, **1980**, 19801015.
20. Patel, R. C.; Ferguson, I. J.; Pennicott, H. J., Oxidative Imaging. European Patent Office, **1984**, 84301156.
21. Silverstein, R. M.; Webster, F. X.; Kiemle, D. J., *Spectrometric Identification of Organic Compounds*. Seventh ed.; John Wiley & Sons, Inc: 2005.
22. Dirk, C. W.; Cheng, L.-T.; Kuzyk, M. G., A Simplified Three-Level Model Describing the Molecular Third-Order Nonlinear Optical Susceptibility. *Int. J. of Quantum Chem.* **1992,** 43, 27-36.
23. Thorley, K. J.; Hales, J. M.; Anderson, H. L.; Perry, J. W., Porphyrin Dimer Carbocations with Strong Near Infrared Absorption and Third-Order Optical Nonlinearity. *Angew. Chem. Int. Ed.* **2008,** 47, 7095-7098.
24. Sheik-bahae, M.; Said, A. A.; Van Stryland, E. W., High-sensitivity, single-beam n_2 measurements. *Opt. Lett.* **1989,** 14, 955-957.

25. Flytzanis, C., Third Order Electric Polarizabilities of the H_2-molecule and C-C and C-H sigma-bonds. *Chem. Phys. Lett.* **1975,** 33, 555-559.
26. Levine, B. F.; Bethea, C. G., Second and Third Order Hyperpolarizabilities of Organic Molecules. *J. Chem. Phys.* **1975,** 63, 2666-2682.
27. Meredith, G. R.; Buchalter, B.; Hanzlik, C., Third-order Susceptibility Determination by Third Harmonic Generation. II. *J. Chem. Phys.* **1983,** 78, 1543-1551.
28. Kajzar, F.; Messier, J., Cubic Hyperpolarizabilities and Local Electric Field in Alkanes and Substituted Alkanes. *J. Opt. Soc. Am. B.* **1987,** 4, 1040-1046.
29. Dewar, M. J. S., Colour and Constitution. Part I. Basic Dyes. *J. Chem. Soc.* **1950**, 2329-2334.
30. Daehne, S.; Dekhyar, M. L., Molecular Engineering of NIR Dyes. In *Near-Infrared Dyes for High Technology Applications*, Daehne, S.; Resch-Genger, U.; Wolfbeis, O. S., Eds. Kluwer Academic Publishers: Dordrecht, 1998; Vol. 52, pp 327-362.
31. Pangborn, A. B.; Giardello, M. A.; Grubbs, R. H.; Rosen, R. K.; Timmers, F. J., Safe and Convenient Procedure for Solvent Purification. *Organometallics* **1996,** 15, 1518-1520.

Chapter 5

Nonlinear Optical Properties of Chalcogenopyrylium-Terminated Dyes

5.1. Introduction

A survey of the linear optical properties of several types of polymethine dyes identified chalcogenopyrylium-terminated dyes as being good candidates to achieve large third-order polarizabilites. Several chalcogenopyrylium dye derivatives were synthesized with a variable number of vinylene groups in the bridge. The dyes were made highly soluble by exchanging the counterion of the dyes for tetrakis(3,5-bis(trifluoromethyl)phenyl)borate. The third-order nonlinear optical properties of the dyes were then characterized. A significant amount of the work reported in this chapter was previously published.[1]

As discussed in Chapter 1, the third-order nonlinear optical properties have a strong dependence on the number of vinylene groups in the polymethine bridge. However, at long chain lengths a localization of the charge tends to occur, known as symmetry breaking. A route for achieving large nonlinearities while avoiding symmetry breaking in polymethine dyes is to optimize Re(γ) for a fixed conjugation length. Based on the three-term perturbative expression for γ, discussed in Chapter 1, the critical term to optimize is the "N" term. Therefore one approach to optimize gamma involves identifying polymethine dyes with absorptions that occur at low energy (small energy gap between the ground and excited state, E_{ge}), even at moderate chain lengths, and that are very strong (large transition dipole moment between the ground and excited state, M_{ge}). While, to a first approximation, many cyanines meet these requirements, modification of

the terminal groups in such systems can still profoundly impact the corresponding optical properties. An appropriate choice for a terminal group should provide good energy matching of terminal group orbitals to the highest occupied π-orbitals of the polymethine bridge and possess π-orbital wave functions that show substantial overlap with the highly delocalized electrons in the conjugated backbone. In this manner, the terminal group (1) participates efficiently in extending the overall conjugation length and (2) increases the transition densities towards the periphery, which introduces large contributions to the transition dipole moment, all while maintaining a bridge of modest length that could help prevent the onset of symmetry breaking.

5.1.1. Brief Literature Survey of Optical Properties of Polymethine Dyes[2]

To determine the extent to which the choice of terminal group can help generate large values of Re(γ) at modest chain lengths, an analysis of data from the literature was used for comparison of the progression of E_{ge} and M_{ge} as a function of conjugation length (L) for a number of polymethine systems with various terminal units was performed. A number of vinylogous polymethine systems with various terminal units (Figure 5.1) were chosen for a comparison of the progression of the lowest lying excited-state transition energies and dipole moments (E_{ge} and M_{ge}, respectively) as a function of L. The optical properties of these systems were extracted from data provided in the literature: dimethyamino (**5.I**)[3], pyridinium (**5.II**)[4], benthiazolium (**5.III**)[5], dithiole (**5.IV**)[6], dioxaborine (**5. V**)[7], and thiopyrylium (**5.VI**)[5]. Extraction of E_{ge} values was straightforward, determination of M_{ge} values first required qualitatively reproducing the linear absorption spectra. Scaling the reproduced spectrum to the appropriate peak molar

extinction coefficient (ε_{max}) then allowed for integration of the absorption spectra, according to the equation given in Table 5.2, to determine M_{ge}.

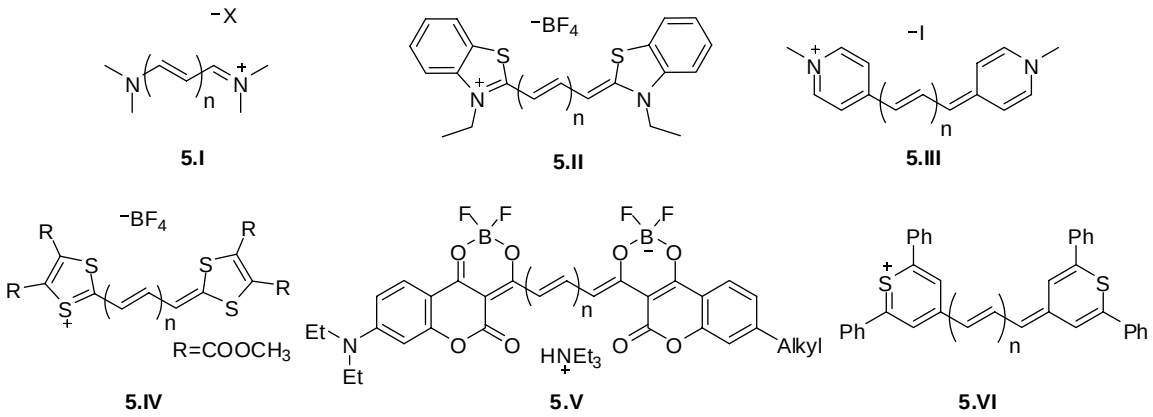

Figure 5.1. Polymethine dyes from the literature.[3-7]

Since each terminal group is different, a quantitative determination of its contribution to the overall conjugation length of the molecule was necessary. This was calculated based on the following formula[4]:

$$E_{ge} = k/(N_{\pi} + 2 \times N_{extra}) \qquad \text{(E5.1)}$$

where k is a constant, N_{π} is the number of π-electrons along the polymethine chain (two π-electrons per C=C bond were assumed) and N_{extra} is the effective number of π-electrons contributed by a terminal group (two terminal groups per dye). Figure 5.2 shows a representative plot of N_{π} versus E_{ge} (in eV). The solid lines represent fittings of the experimental data to E5.1, from which values of k and N_{extra} were determined. Values of N_{extra} were extracted for **5.I-5.VI**, which the values are shown in Table 5.1.

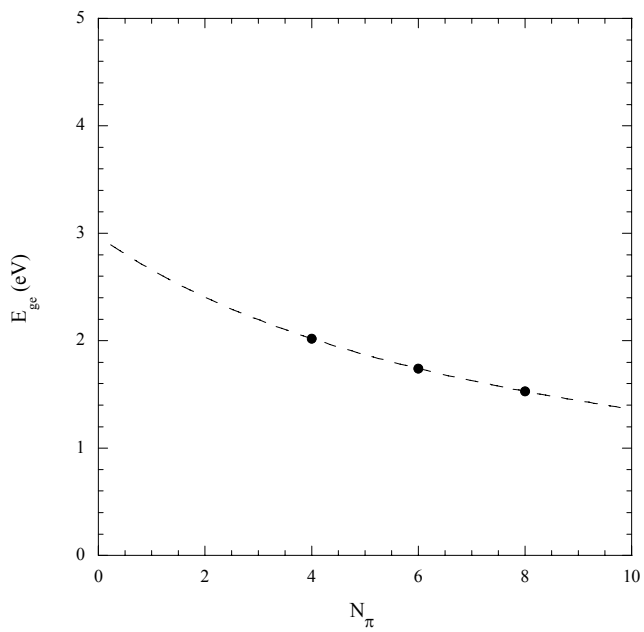

Figure 5.2. Plot of E_{ge} versus N_{π} for representative systems with the dioxaborine terminal units. The solid lines represent fittings to the experimental values from which k and N_{extra} were determined.

Table 5.1. N_{extra} of terminal groups for **5.I-5.VI**

Terminal group	N_{extra}
5.I	1.0
5.II	3.4
5.III	3.2
5.IV	2.5
5.V	4.2
5.VI	3.7

Once these values of N_{extra} are known (Table 5.1), one can then plot M_{ge} and E_{ge} versus effective conjugation length, L_{eff} (where $L_{eff} = N_{\pi} + 2 \times N_{extra}$). The trends for **5.I-5.VI** are plotted in Figure 5.3. The thiopyrylium-terminated dyes have a combination of the linear optical properties superior for use in AOSP applications (properties to achieve large Re(γ): low E_{ge} and high M_{ge}) compared to those with the other terminal groups.

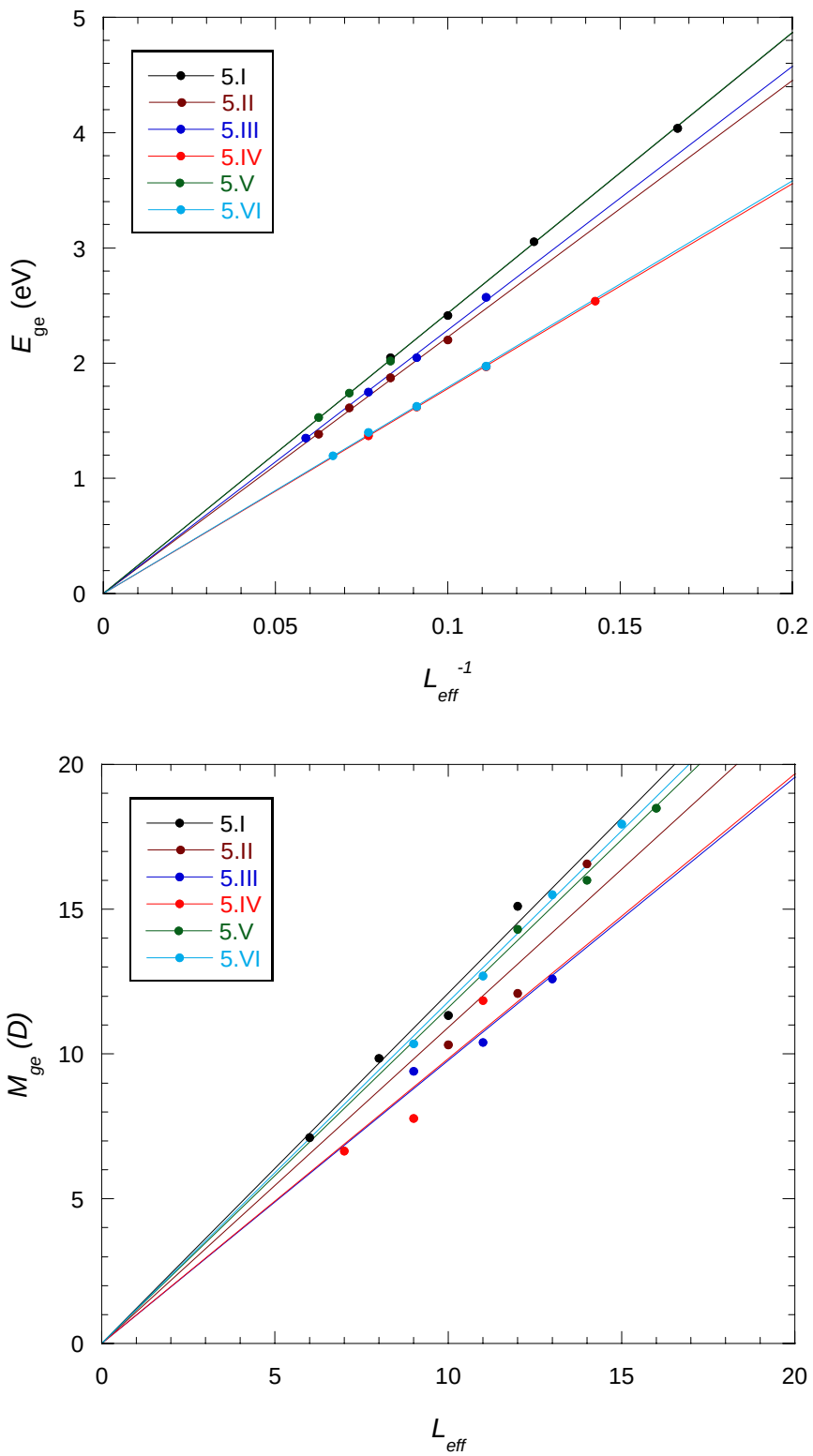

Figure 5.3. Plots of (a) E_{ge} versus L_{eff}^{-1} and (b) M_{ge} versus L_{eff} for polymethines with various terminal groups.

5.1.2. Chalcogenopyrylium-Terminated Polymethines

Chalcogenopyrylium-terminated dyes can be found in the literature with oxygen, sulfur, selenium and tellurium chalcogens. The size of the chalcogen atom increases in size as one moves down the periodic table (O<S<Se<Te). Even though the chalcogenopyrylium heteroatom rings are considered aromatic[8], the increase in atomic size tends to decrease the π-overlap of the conjugated carbon framework. An example of this is provided by Detty *et al.*[9] who solved the crystal structure of the asymmetric monomethine **5.VII** (Figure 5.4), which contains a telluropyrylium ring and a pyrylium ring joined by one methine carbon. The C-Te bond lengths were found to be 2.07 Å, compared to the much shorter C-O bond lengths of 1.38 Å. The plane formed by the tellurium and its adjacent carbons was found to be bent out of plane 8.7° from the plane formed by the five carbons of the ring. This angle was more than twice that for the angle formed by the pyrylium ring (4.2°). The reduced planarity and long bond lengths are both affects attributed to the larger atomic radius.

Moving down the periodic table also results in a decrease in electronegativity (O>>S>Se>>Te)[10], which is related to σ-withdrawing and donating effects. Detty *et al.*[9] sought to determine the σ and π contributions to the HOMO and LUMO levels of a series of chalcogenopyrylium salts shown in Figure 5.4 (**5.VIII**). Cyclic voltammetry was consistent with HOMO energy increasing as the electronegativity of the chalcogen decreased (HOMO energy increased Te>Se>S>O), while the energy level of the LUMO decreased as the electronegativity decreased (LUMO energy decreased O>S>Se>Te). This is consistent with the observed bathochromic shift in λ_{max} (Te>Se>S>O) for chalcogenopyryliums of type **5.VIII**. A similar bathochromic shift was observed in

chalcogenopyrylium polymethine dyes similar to **5.1** (Figure 5.6), in which the chalcogen has been varied and a hexafluorphosphate counterion was used.[11] In aqueous solution the trend in λ_{max} for the varied chalcogenopyrylium dyes was as follows: O (593 nm) < S (685 nm) < Se (730 nm) < Te (810 nm).

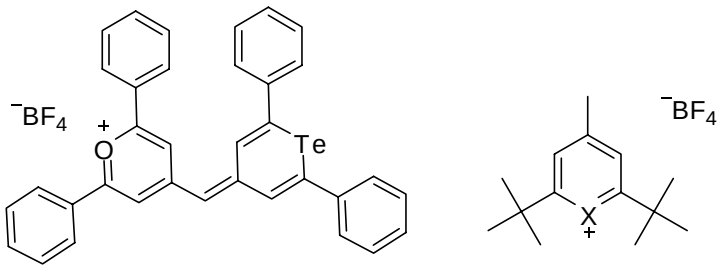

5.VII **5.VIII**

Figure 5.4. Chalcogenopyrylium general structure studied by Detty *et al.*[9]

The favorable linear optical properties of chalcogenopyrylium-terminated polymethine dyes have not gone unnoticed and have been investigated by others in the context of nonlinear optics. Pyrylium-terminated polymethine dyes were among various dyes investigated by Maloney *et al.*[12] who measured resonant γ values using degenerate four wave mixing (DFWM) with 160 ps pulses (Figure 5.5, **5.IX**). **5.IX** displayed one of the largest resonant γ values of the set of molecules examined ($\gamma = 1.35 \times 10^{-28}$ esu). The excitation wavelength used to measure γ was 1064 nm, while the λ_{max} absorption of the dye was ~1080 nm. This resonant value of γ has an impressive magnitude; however, strong 1PA would be unsuitable for AOSP applications at 1064 nm. Ganeev *et al.*[13] used the Z-scan technique to characterize a similar thiopyrylium-based dye (Figure 5.5, **5.X**). Once again the excitation wavelength was resonant (measured at 1064 nm, while the λ_{max} was ~1060 nm), at which wavelength 1PA is prohibitive for AOSP. Examination of the

sample using the open aperture Z-scan technique resulted in no nonlinear change in the refractive index. This may be due to the excitation wavelength overlapping in a region of the refractive index dispersion curve that goes through zero (note the change in sign of the Re(χ^3) at the maximum of Im(χ^3) as discussed in Chapter 1).

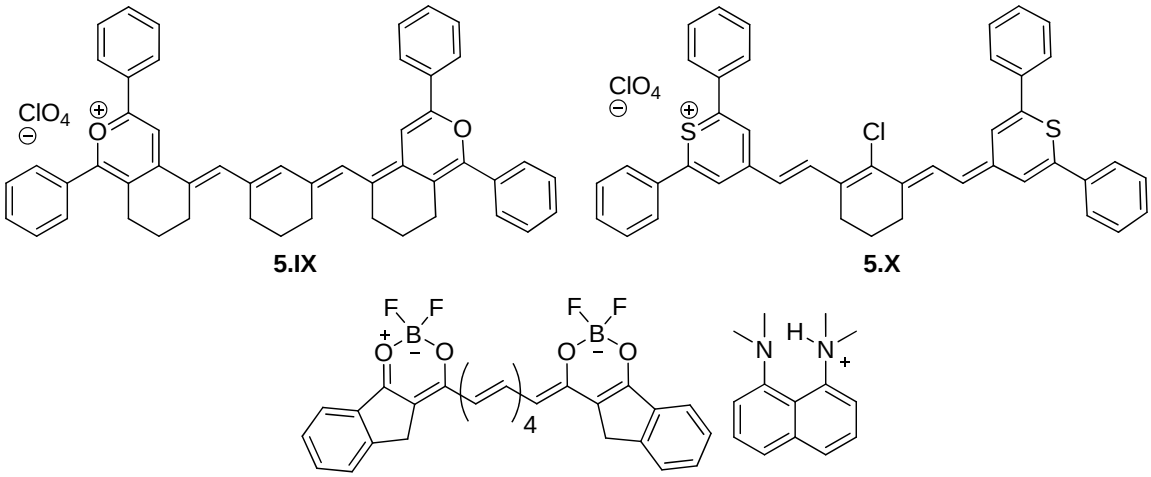

Figure 5.5. Polymethine dyes, which had γ values measured.[12-14]

Non-resonant measurements of γ have not been reported for pyrylium-terminated dyes, so the NLO properties warrant further investigation. Encouraging nonresonant measurements of γ for a polymethine dye were reported by Hales *et al.*[15] for a bis(dioxaborine)-terminated anionic nonamethine (Figure 5.5, **5.XI**), which resists symmetry breaking despite the reasonably long conjugation length and low-energy absorption. Sizable values of Re(γ) ($\approx -5 \times 10^{-32}$ esu) were reported, while the dye maintained a reasonable ratio of |Re(γ)/Im(γ)| (≤ 10) throughout the telecommunications spectral region (1300-1550 nm). Despite these promising results, additional improvements along this route are limited by the complicated molecular designs needed

to further extend the delocalization pathway and the synthetic challenges in the preparation of such systems.

5.1.3. Goals of Chapter 5

The need for enhanced properties relative to **5.XI**, led to the investigation of the chalcogenopyrylium-terminated dyes discussed in this chapter. The linear optical properties of this class of materials, as discussed earlier, would expectedly effect the necessary optical properties to achieve large Re(γ), which is consistent with previous observations that such end-groups can produce very low energy absorptions.[16] In particular, thio- and selenopyrylium-terminated polymethine dyes were investigated. The pyrylium-terminated dyes, where the chalcogen would be oxygen, would be expected to have inferior optical properties to the S and Se analogues (larger E_{ge}). The telluropyrylium-terminated dyes would be expected to have superior optical properties (smaller E_{ge}); however, telluropyrylium-terminated dyes are more synthetically challenging due to instability (oxidative and photochemical) of the tellurium atom and the highly toxic nature of this element. The investigated dyes were synthesized with varying polymethine bridges and a tetrakis(3,5-bis(trifluoromethyl)phenyl)borate ($^{-}$BAr'$_4$) counter ion to improve solubility. The dyes, **5.1-5.6**, are shown in Figure 5.6. The third-order NLO properties were then characterized.[17]

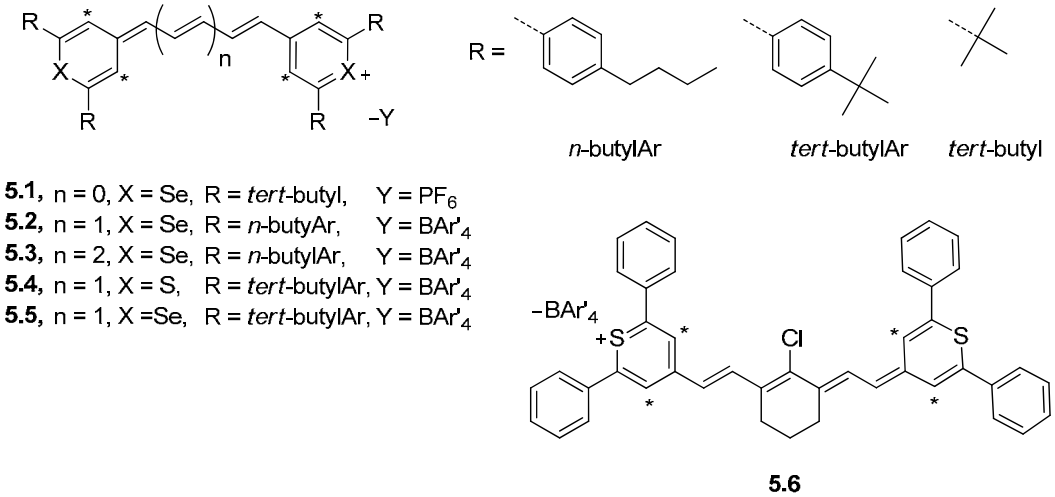

Figure 5.6. Chalcogenopyrylium-terminated dyes, **5.1-5.6**, discussed in this study. The starred positions identify the carbons (and hydrogens attached to them) that consistently did not appear in the room temperature ^{1}H and ^{13}C NMR spectra.

5.2. Synthesis and NMR Characterization

The reaction scheme to synthesize the 2,6-bis(4-butylphenyl)-4-methylchalcogenopyrylium tetrafluoroborate salts (**S5.8, S5.9,** and **S5.10**) is shown in Scheme 5.1. Synthesis of analogous compounds can be found in the literature.[18, 19] The synthesis of cyanine precursors **S5.11** and **S5.12** can be found in the literature.

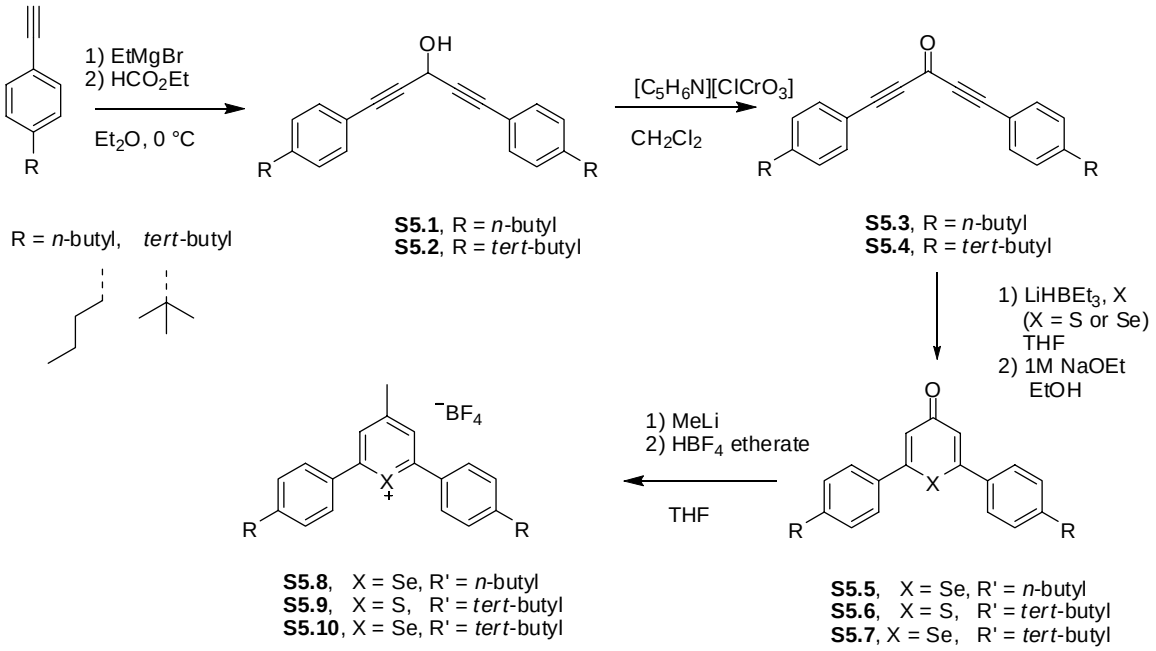

Scheme 5.1. Scheme for the synthesis of **S.8, S5.9** and **S5.10**.

5.1 was synthesized according to literature procedures by Michael Detty.[11] The synthesis of **5.2**, **5.3, 5.4,** and **5.5** was accomplished through Scheme 5.2. The sodium tetrakis(3,5-bis(trifluoromethyl)phenyl)borate ($NaBAr'_4$) used for the ion exchange reaction was prepared according to a literature procedure.[20] **5.6** was prepared via ion metathesis on commercially available dye IR-1061 (Sigma-Aldrich).

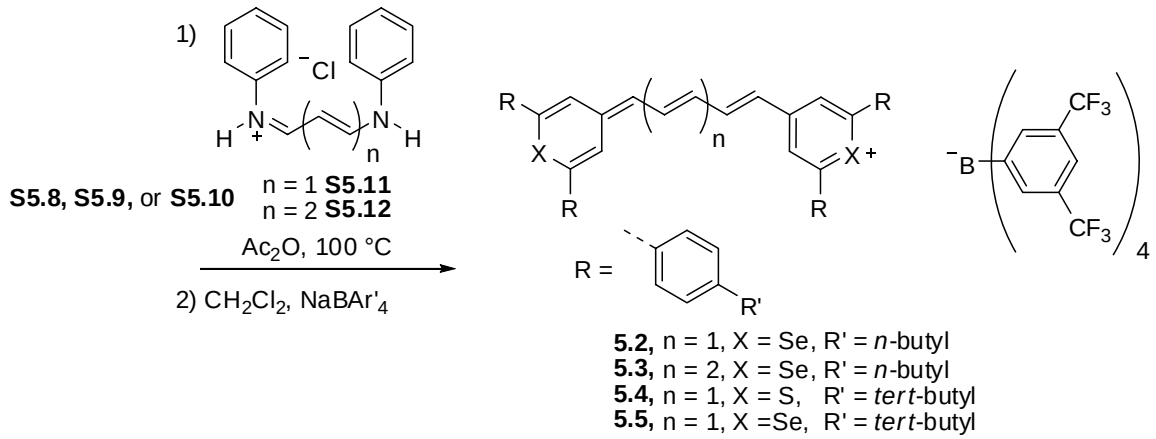

Scheme 5.2. Synthetic scheme for dyes **5.2, 5.3, 5.4,** and **5.5**.

The dyes were characterized using ^{1}H and ^{13}C NMR, mass spectrometry and elemental analysis. At room temperature the resonance for the proton and the carbon atoms in the starred (*) position (Figure 5.6) consistently did not appear in the ^{1}H and ^{13}C NMR spectra, respectively. It was assumed there was restricted rotation in the molecule causing the broadened peaks. Variable temperature NMR at 333 K was used in an attempt to identify the missing resonances for **5.2, 5.4, 5.5,** and **5.6**. Figure 5.7 shows the aromatic region (6.4-8.0 ppm) of the ^{1}H NMR spectrum of **5.2** at 295 K and 333 K. An additional peak is observed at 7.69 ppm in the 333 K spectrum. In a similar manner, the ^{1}H resonance of the * position of **5.4** and **5.5** were found to appear at ~7.60 (overlapped with other peaks) and 7.65 ppm at 333 K, respectively. The missing peak in the ^{13}C NMR spectra for **5.2, 5.4** and **5.5** were not observed, even at 333 K. The ^{1}H resonance for the * position for **5.6** occurred at a chemical shift of 7.69 ppm (overlapped with other peaks) in the NMR spectrum at 333K. The ^{13}C chemical shift for the * position of **5.6** was observed at 125.5 ppm in the NMR spectrum at 333 K (Figure 5.8).

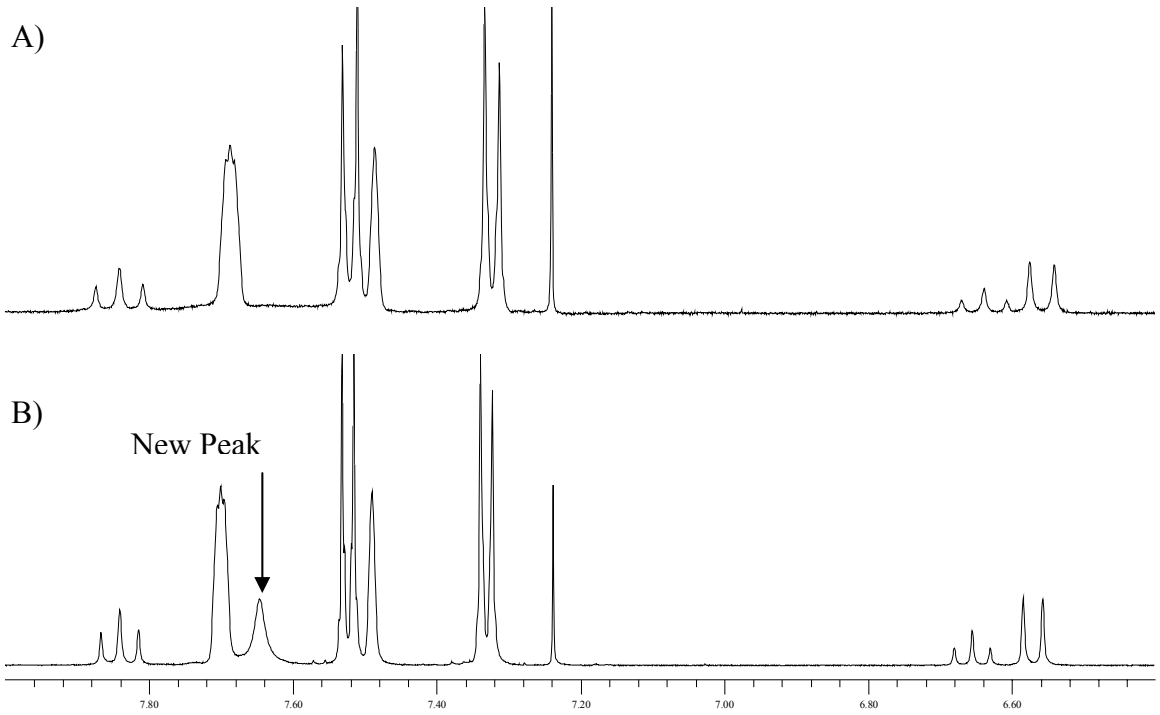

Figure 5.7. The aromatic region of the ^{1}H NMR spectra of **5.2** in $CDCl_3$ at A) 295 K and B) 333 K.[1]

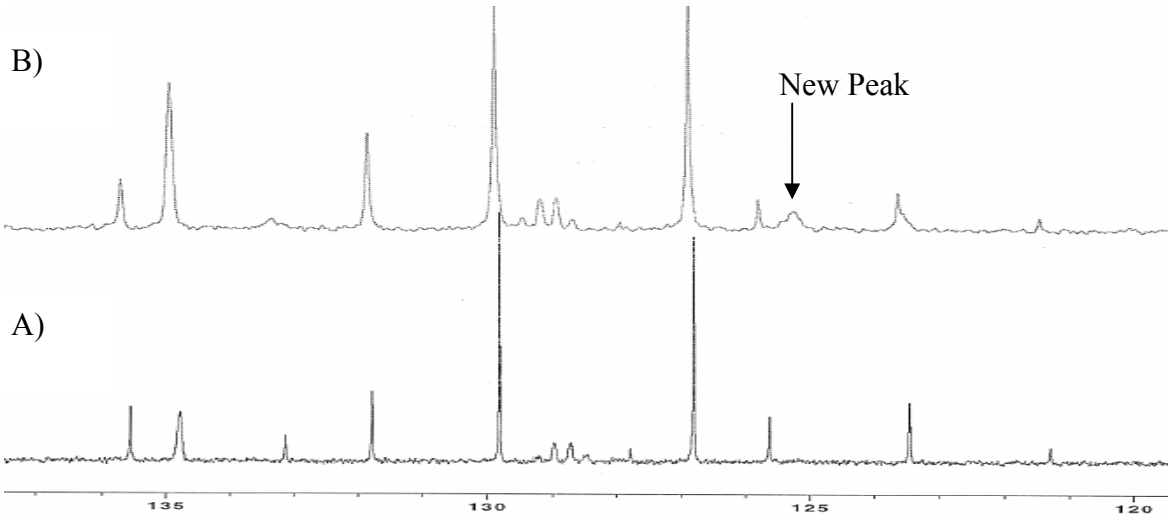

Figure 5.8. The aromatic region of the ^{13}C NMR spectra of **5.6** in $CDCl_3$ at A) 295 K and B) 333 K.[1]

5.3. Linear optical properties

A summary linear optical parameters (λ_{max}, ε_{max}, and M_{ge}) of **5.1-5.6** are collected in Table 5.2. Estimates of Re(γ) based on the two-level model at 1300 nm and at the static (∞) wavelength are also included.

Table 5.2. λ_{max}, ε_{max}, M_{ge}, and the Re(γ)$_{calc}$ of chalcogenopyrylium terminated polymethine dyes in Chloroform solution

Dye	λ_{max} (nm)	ε_{max} (10^5 M^{-1} cm^{-1})	M_{ge} (D)[a]	Re(γ)$_{static}$ (10^{-33} esu)[b]	Re(γ)$_{1300\ nm}$ (10^{-33} esu)[b]
5.1	750	3.00	12.7	-1.1	-14
5.2	946	3.60	16.4	-6.1	-230
5.3	1081	3.90	19.4	-18	-1400
5.4	902	3.21	15.8	-4.6	-130
5.5	947	2.85	15.5	-4.9	-180
5.6	1068	3.68	18.2	-13	-990

[a] Obtained from integration of the absorption spectra as $M_{ge} = 0.9584(\int \varepsilon d\upsilon / \upsilon_{max})^{0.5}$ where ε is in $M^{-1}cm^{-1}$ and υ is in cm^{-1}.
[b] Calculated from E5.2 using experimentally determined values of M_{ge} and E_{ge} from this table.

An increase in both λ_{max} and M_{ge} was observed as vinylene groups were added from **5.1** to **5.2** to **5.3**. The aryl groups on the chalcogopyrylium terminal groups are known to increase the overall conjugation of similar dyes relative to alkyl groups.[21, 22] **5.2** has increased conjugation compared to **5.1** in both the terminal aryl groups (versus *tert*-butyl) and the additional vinylene group. Vinylene shift (V) is the shift in λ_{max} as an additional vinylene group is added to the polymethine bridge ($V = \lambda_n - \lambda_{n-1}$, where n is the number of vinylene groups) was found to be greater than 100 nm for these compounds. König was the first to report the vinylene shift to be ~100 nm for polymethine dyes.[23] Kachkovski *et al*. compared the vinylene shift of several polymethine dyes from the

literature and indeed, many of the dyes followed the relationship V = 100 nm.[24] The vinylene shift for chalcogenopyrylium-terminated dyes is generally larger than 100 nm (λ_{max} of **5.3** minus the λ_{max} of **5.2** is 135 nm). One explanation for the large vinylene shift is due to increased contributions of higher vibrational transitions leading to broadened band shapes; comparing the average position of the bands gave much closer values to 100 nm.[25, 26] The absorption spectra of **5.1-5.3** are shown in Figure 5.9.

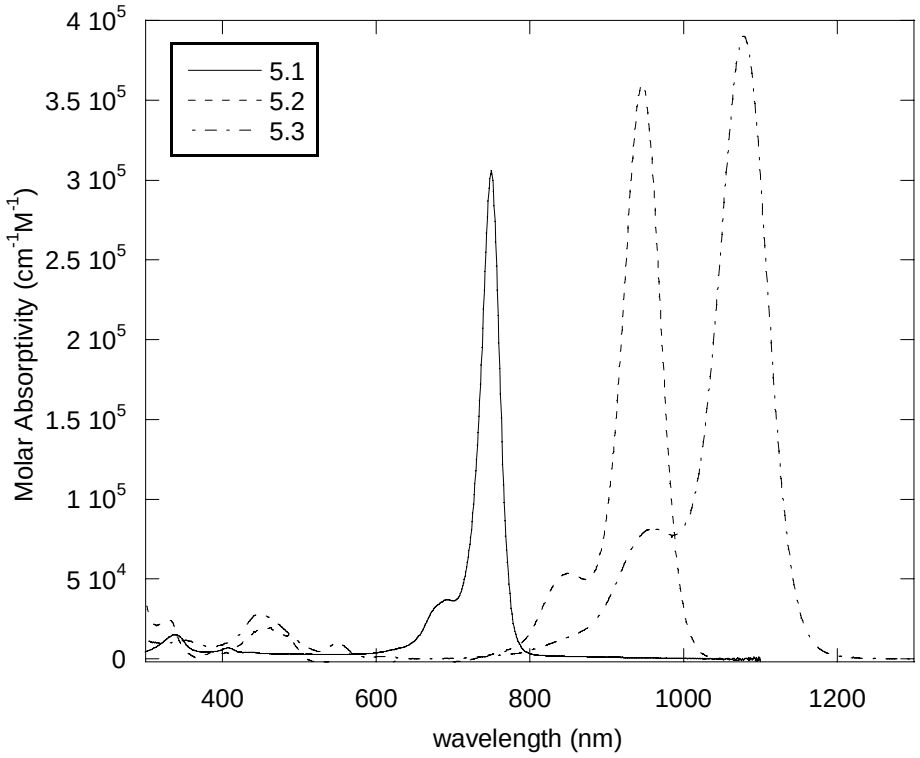

Figure 5.9. Absorption spectra of **5.1** (—), **5.2** (----), and **5.3** (-·-·-) in chloroform.

The absorption spectra of pentamethine dyes (**5.2**, **5.4**, and **5.5**) are shown in Figure 5.10. All three have similarly large extinction coefficients at λ_{max} and large transition dipole moments. The hypsochromic shift in λ_{max} of the sulfur compound, **5.4,**

relative to the selenium analogues, **5.2** and **5.5,** is caused by the heteroatom and consistent with the observations of known compounds described in the introduction.

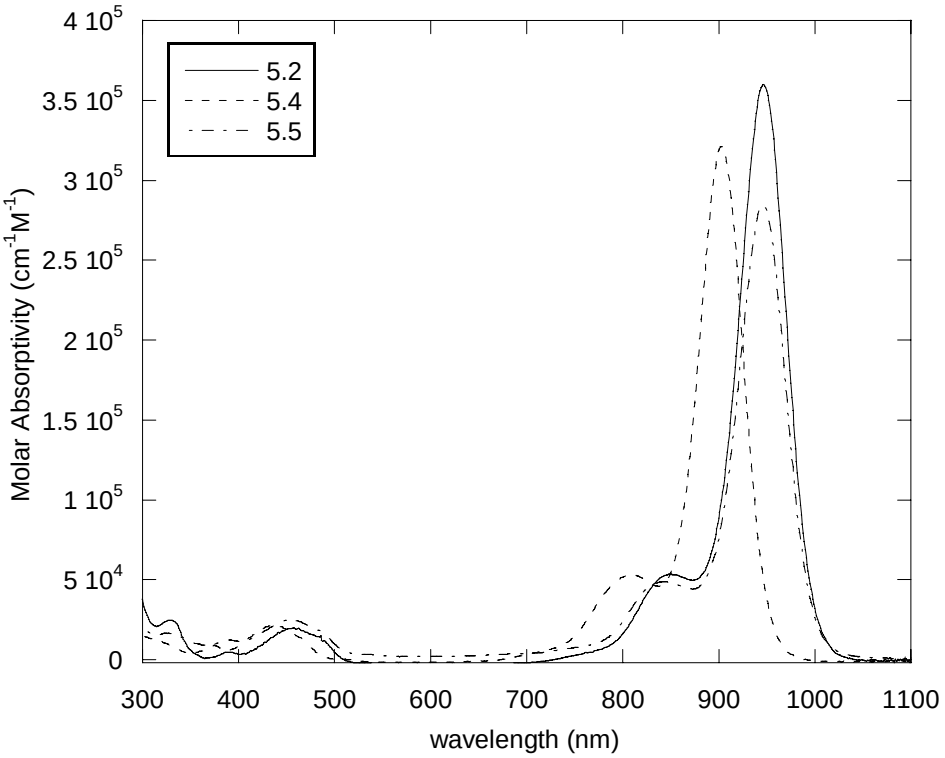

Figure 5.10. Absorption spectra of **5.2** (—), **5.4** (----), and **5.5** (-·-·-) in chloroform.

The absorption spectra of **5.3** and **5.6** are shown in Figure 5.11. The difference in λ_{max} of the heptamethine dyes with various chalcogens (S and Se) is much smaller than the difference in the pentamethine dyes **5.4** and **5.5** (13 nm versus 45 nm). The structural modifications in the bridge (the ring and chlorine substituents) of the sulfur containing compound, **5.6,** are the most likely cause of the narrowing of the gap. The substituents effects, causing a bathochromic shift in λ_{max}, are consistent with the Dewar-Knott rules, as discussed in Chapter 3.

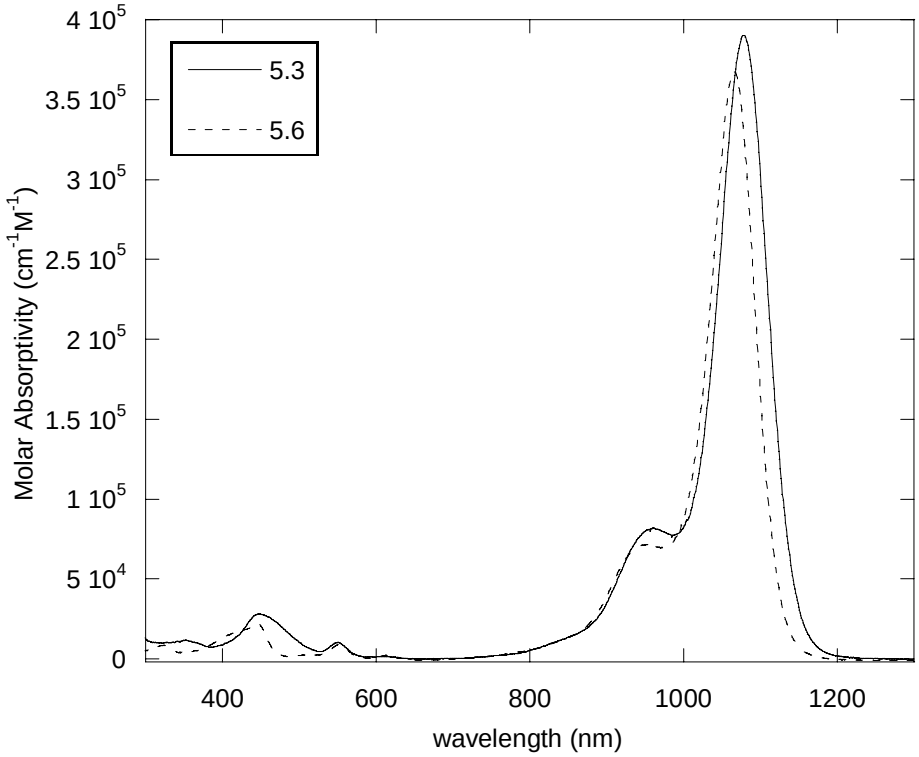

Figure 5.11. Absorption spectra of **5.3** (—) and **5.6** (----) in chloroform.

A simplified version of the perturbation theory, two-term expression of static Re(γ) was given in previous chapters (2, 3, and 4) because resonance enhancement from 1PA bands was less important. A more complete expression is given below:

$$\gamma(\omega) = -\left((2.998)^4 \times 10^{23}\right) \times \left(\frac{1}{5}\right) \times 2 \times \left(\frac{M_{ge}^4}{(\Omega_{ge} - \hbar\omega)^3} + \frac{M_{ge}^4}{(\Omega_{ge} - \hbar\omega)^2 \times (\Omega_{ge}^* - \hbar\omega)}\right) \qquad \text{(E5.2)}$$

where g denotes the ground state, e the first excited state, M the transition dipole moment between states, $\Omega_{ge} = E_{ge} - i\Gamma_{ge}$ (where Γ_{ge} is the damping of the transition (damping is introduced to account for the broadness of each band, usually approximated to be 0.1 eV), E is the energy gap, Ω_{ge}^* is the complex conjugate of Ω_{ge}, $\hbar\omega$ term is the frequency of use, which will account for the detuning energy of the measurement ($\Omega_{ge} - \hbar\omega$). The

detuning takes into account the difference between the wavelength at which γ is measured and the absorption band. The factor of 1/5 is due to orientation averaging of the molecules, and the prefactor is simply a conversion factor between the input MKS units (values for E_{ge}, M_{ge}, and Γ_{ge}) and the resulting cgs (esu) units for two-level $\mathrm{Re}(\gamma)_{\omega}$.

When the linear optical quantities given in Table 5.2 (i.e. E_{ge} and M_{ge}) are used in E5.2, the 2-level values of Re(γ) for **5.1-5.6** could be estimated. These values, for two different incident photon energies, are shown in Table 5.2. $\mathrm{Re}(\gamma)_{static}$ is the value of the nonlinearity at zero photon energy, representing the off-resonant value of γ ($\Omega_{ge} = E_{ge}$, $\hbar\omega$=0). $\mathrm{Re}(\gamma)_{1300nm}$ is the value of the nonlinearity at a photon energy corresponding to an excitation wavelength of 1300 nm. The calculated values ($\mathrm{Re}(\gamma)_{1300nm}$ and $\mathrm{Re}(\gamma)_{static}$) show the expected large negative contributions to Re(γ) and reproduce the experimentally observed trends (See nonlinear optical section). It should be noted that the $\mathrm{Re}(\gamma)_{static}$ differ from the $\mathrm{Re}(\gamma)_{1300nm}$ values by up to two orders-of-magnitude. This is a consequence of pre-resonance enhancement and demonstrates its significant role in the resulting magnitudes of Re(γ).

5.4. Nonlinear optical properties[17]

The third-order nonlinear optical properties of these dyes were investigated in chloroform solutions using the femtosecond-pulsed Z-scan technique (to determine Im(γ) and Re(γ)). The nonlinear optical properties of the compounds at 1300 nm are summarized in Table 5.3 as well as |Re(γ)/Im(γ)|. As discussed in Chapter 1 a ratio of |Re(γ)/Im(γ)| > 12 is desirable for AOSP, so all dyes except **5.1** have favorable figures of merit (FOM) at 1300 nm. It is worth noting that the magnitude of Re(γ) increases by an

order of magnitude with the addition of each vinylene group, leading to an exceptionally high value of -2.2×10^{-31} esu for dye **5.3**, with a $|\mathrm{Re}(\gamma)/\mathrm{Im}(\gamma)|$ greater that 150.

Table 5.3. $\mathrm{Re}(\gamma)^a$, $\mathrm{Im}(\gamma)^a$, $|\gamma|^a$, Φ^a, and the $\mathrm{Re}(\gamma)_{calc}{}^b$ of chalcogenopyrylium terminated polymethine dyes.

Dye	$\mathrm{Re}(\gamma)_{1300\ nm}$ (10^{-33} esu)[b]	$\mathrm{Re}(\gamma)$ (10^{-33} esu)	$\mathrm{Im}(\gamma)$ (10^{-33} esu)	$\lvert\gamma\rvert$ (10^{-32} esu)	Φ (°)	$\lvert\mathrm{Re}(\gamma)/\mathrm{Im}(\gamma)\rvert$
5.1	-14	-2.79	0.711	0.29	166	3.9
5.2	-230	-22.6	0.197	2.26	~180	114
5.3	-1400	-221	1.16	22.1	~180	190
5.4	-130	-14.6	0.280	1.46	179	52.1
5.5	-180	-21.9	0.726	2.19	178	30.2
5.6	-990	-143	0.998	14.3	~180	143

[a] Measured in CHloroform at 1300 nm using the Z-scan technique. The magnitude and phase of γ are defined as $|\gamma|^2 = \mathrm{Re}(\gamma)^2 + \mathrm{Im}(\gamma)^2$ and $\theta = \arctan[\mathrm{Im}(\gamma)/\mathrm{Re}(\gamma)]$, respectively.
[b] Calculated from E5.2 using experimentally determined values of M_{ge} and E_{ge}.

The calculated values for the magnitude of $\mathrm{Re}(\gamma)_{static}$ (Table 5.2) scale in the expected manner, given the progression of the calculated linear optical properties and the dominance of the N-term as discussed in Chapter 1. The values of $\mathrm{Re}(\gamma)_{1300nm}$ provide a slightly better reproduction of the experimentally-determined trends as one might expect given the role of pre-resonant enhancement in the experimental values. However, the calculated values are found to be significantly larger in magnitude than the experimental nonlinearities given in Table 5.3. This is likely due to the limitations inherent in the truncated perturbation theory expression used, which excludes other terms that would serve to moderate these large negative values. Incorporation of the T and D terms (which are in opposition to the N term) in the three-state equation can be added to obtain calculated $\mathrm{Re}(\gamma)$ values that more closely match the experimental values (please refer to

the supporting information by the manuscript by Hales *et al.*[1] for further details). Importantly, the full set of observations made here is consistent with the notions outlined in the introduction that chalcogenopyrylium-terminal groups have excellent γ for a fixed conjugation length.

The unprecedented two-photon FOMs indicate that detrimental 2PA can be avoided in compounds of this type. While **5.2, 5.4-5.6** exhibit a $|\mathrm{Re}(\gamma)/\mathrm{Im}(\gamma)|$ at 1300 nm greater than the acceptable 12, **5.3** possesses similarly large values but maintains this over the entire spectral region of interest. The value of $|\mathrm{Re}(\gamma)/\mathrm{Im}(\gamma)|$ at 1450 was 190, while at 1550 nm it was 72. It is also interesting to note that these ratios dwarf those of **5.XI**, a system known for showing promise in terms of good two–photon FOMs.[15]

In order to determine the positions of the two-photon resonances in these cyanine systems, non-degenerate (ND) 2PA spectra were measured for **5.1-5.3** in solution; the spectra for **5.1-5.3** are shown in Figure 5.12a-c. A salient feature is that *all* spectra exhibit a favorable region over which 2PA is relatively weak; this low-loss window appears to be tunable simply by modifying the position of E_{ge} (or equivalently molecular length). These observables are a result of a number of characteristics that are, as a whole, unique to polymethine dyes. Typical of polymethine dyes[27], the 2PA transitions lie at $E_{ge'} \approx 1.1 \times E_{ge}$ and $E_{ge''} \approx 1.7 \times E_{ge}$ leading to a large energy gap between these resonances. The bands are also reasonably narrow, likely due to similar ground- and excited-state equilibrium geometries leading to absorption spectra that are dominated by the [0-0] vibronic transition.[28] In comparison, 2PA spectra can be significantly broader for dipolar-type compounds that have different ground- and excited-state equilibrium geometries.[29] The strengths of the 2PA transitions are also modest. The lower lying

transition ($E_{ge'}$) is typically relatively weak, as it is ascribed to vibronically-assisted 2PA.[27, 30] into a state that would otherwise be 2PA-forbidden. An additional two-photon resonance at ~650 nm in the ND-2PA spectrum of **5.XI** (Figure 5.12d) explains the reduced two-photon FOMs (values of $|\mathrm{Re}(\gamma)/\mathrm{Im}(\gamma)| < 10$)

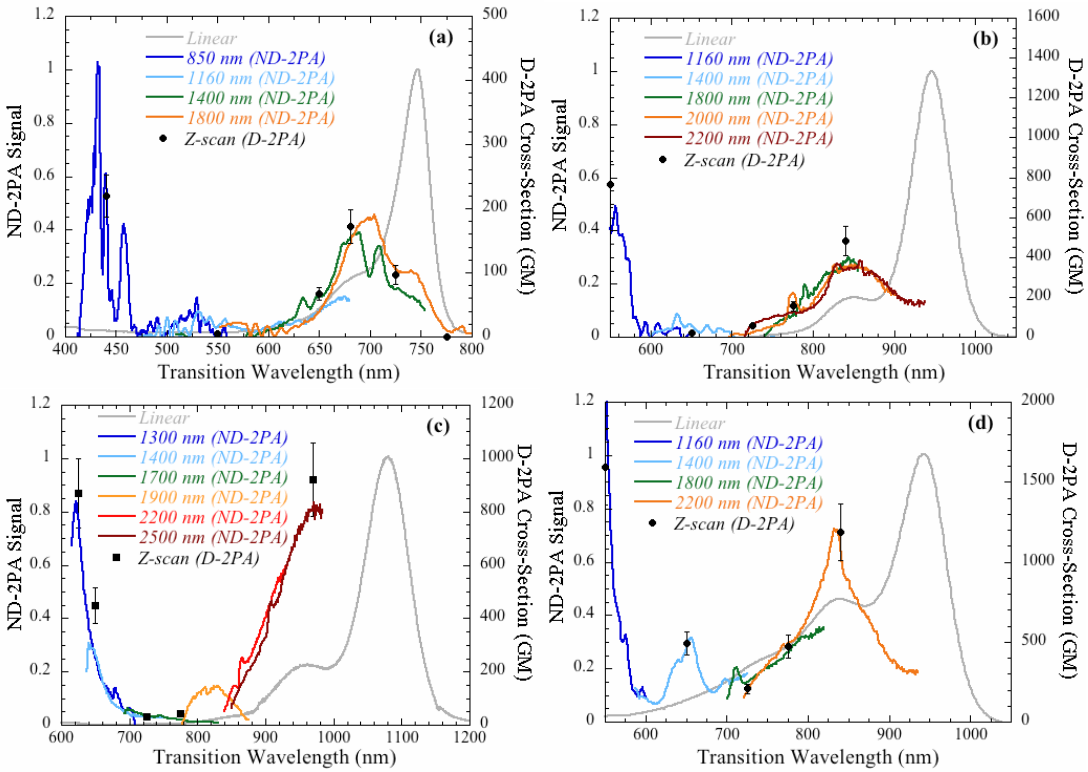

Figure 5.12. Non-degenerate 2PA (ND-2PA) spectra in chloroform: (a) **5.1**, (b) **5.2**, (c) **5.3**, and (d) **5.XI**. Different pump wavelengths (shown in legend) were employed to observe the full ND-2PA spectra. Filled circles are degenerate 2PA (D-2PA) cross-sections derived from femtosecond-pulsed Z-scan measurements. 1 GM is defined as 1×10^{-50} cm^4 s photon^{-1}. Experimental uncertainties in the values were estimated to be ±15%. Linear absorption spectra are shown as references.[1]

5.5. Conclusions

In conclusion, a strategy for improving the third-order polarizability and two-photon figures-of-merit of polymethine chromophores intended for all-optical switching

was explored. This strategy required the operational wavelength (a telecommunications wavelength) to lie between the 1PA and 2PA, which would allow Re(γ) to be very large due to the exploitation of pre-resonance enhancement of the nonlinearity. Operating between the bands would allow 1PA and 2PA to be low, which provided the excellent |Re(γ)/Im(γ)|. This strategy was demonstrated using chalcogenopyrylium-terminated polymethine dyes. A selenopyrylium-terminated dye with a heptamethine chain (**5.3**) was found to exhibit a remarkably large value of Re(γ) at 1300 nm and yet possessed an unprecedented molecular two-photon FOM compared to other chromophores previously reported. It is noteworthy that even though selenopyrylium-terminated dyes (such as **5.5)** had larger Re(γ) and a better |Re(γ)/Im(γ)| than the thiopyrylium-terminated dyes (such as **5.4)**, thiopyrylium-terminated dyes still had significant magnitudes of each, which may make it unnecessary to use toxic heavy-chalcogen atoms to further develop these materials.

The FOMs extend over a broad wavelength range, for example: ~300 nm for **5.3**. The FOMs can be tuned to specific frequency ranges by changing the molecular length of the dye and thereby modifying the energy gap of the molecule. Thus, the observations here have important implications for the design of a new generation of materials that could enable low power and high contrast all-optical switching. Incorporation of such materials at high number density into appropriate architectures for photonic applications remains a challenge. However, numerous synthetic pathways can be explored to address this issue.

5.6. Experimental

Starting materials were obtained from commercial sources and used without further purification. Where necessary tetrahydrofuran and dichloromethane was dried by passage through three columns of activated alumina.[31] UV-vis.-NIR spectra were recorded in 1 cm cells using a Varian Cary 5E spectrometer. A Varian 300, Bruker 400 and Bruker 500 megahertz NMR spectrometers were used to record NMR spectra. Elemental analyses were performed by Atlantic Microlabs. The EI mass spectra were recorded on a VG instruments 70SE and the ESI mass spectra were recorded on a Micromass Quattro LC.

1,5-Bis(4-butylphenyl)penta-1,4-diyn-3-ol **S5.1**

Under a nitrogen atmosphere, 3 M ethylmagnesiumbromide in diethylether (10 mL, 30 mmol) was added dropwise to a solution of 1-butyl-4-ethynylbenzene (5.33 g, 33.7 mmol) in dry diethylether (30 mL) cooled in an ice bath. The solution was warmed to room temperature and stirred for 17 h. The solution was cooled in an ice bath and ethyl formate (1.2 mL, 15 mmol) was added dropwise. After 5 min 10% aqueous hydrochloric acid (25 mL) was added dropwise. The organic layer was separated and additional product was extracted from the aqueous phase using diethylether (30 mL × 3). The organic layer was dried using magnesium sulfate, and then filtered. The solvent was removed under vacuum and the residue was recrystallized from hexanes to give a white solid (4.05 g, 11.8 mmol, 78%). ^{1}H NMR (400 MHz, $CDCl_3$): δ (ppm) 7.39 (d, J = 8.1 Hz, 4H), 7.12 (d, J = 8.1 Hz, 4H), 5.56 (d, J = 7.5 Hz, 1H), 2.59 (t, J = 7.8 Hz, 4H), 2.44 (d, J = 7.5 Hz, 1H), 1.59 (quint., J = 7.3 Hz, 4H), 1.34 (sextet, J = 7.5 Hz, 4H), 0.91 (t, J = 7.3 Hz, 6H). ^{13}C NMR (100 MHz, $CDCl_3$): δ (ppm) 143.8, 131.7, 128.3, 119.0, 85.3,

84.6, 53.2, 35.4, 33.2, 22.1, 13.8. (ES) (+) m/z = 344.1 [M+]. Anal. Calcd. for $C_{25}H_{28}O$: C, 87.16, H, 8.19. Found: C, 86.77, H, 8.26.

5-Bis(4-butylphenyl)penta-1,4-diyn-3-one, **S5.2**

S5.1 (4.05 g, 11.8 mmol) in dry dichloromethane (20 ml) was added to a solution of pyridinium chlorochromate (3.84 g, 17.9 mmol) in dry dichloromethane (50 mL) under a nitrogen atmosphere with stirring. After three hours diethylether (100 mL) was added to precipitate a dark material, which was then filtered through a silica plug using diethylether as the eluent. The solvent from the filtrate was removed under vacuum and the remaining residue was purified through silica gel chromatography using dichloromethane/hexanes (1:1) as the eluent to give a yellow oil (3.43 g, 10.0 mmol, 85%). ^{1}H NMR (300 MHz, $CDCl_3$): δ (ppm) 7.55 (d, J = 8.4 Hz, 4H), 7.20 (d, J = 8.4 Hz, 4H), 2.63 (t, J = 8.1 Hz, 4H), 1.59 (quint., J = 7.8 Hz, 4H), 1.34 (sextet, J = 8.0 Hz, 4H), 0.91 (t, J = 7.2 Hz, 6H). ^{13}C NMR (100 MHz, $CDCl_3$): δ (ppm) 161.0, 146.9, 133.4, 128.8, 116.6, 92.2, 89.5, 35.8, 33.2, 22.3, 13.9. (ES) (+) m/z = 342.1 [M+]. Anal. Calcd. for $C_{25}H_{26}O$: C, 87.68, H, 7.65. Found: C, 87.41, H, 7.69.

2,6-Bis(4-butylphenyl)-4*H*-selenopyran-4-one, **S5.3**

Under a nitrogen atmosphere selenium powder (0.252 g, 3.19 mmol) was reduced using 1 M lithium triethylborohydride in tetrahydrofuran (6.5 mL, 6.5 mmol)). 1 M sodium ethoxide was added (7 mL) after 1 h. **S5.2** (1.14 g, 3.32 mmol) in tetrahydrofuran (5 mL) and 1 M sodium ethoxide (5 mL) was added dropwise, while the reaction mixture was on an ice bath. The solution was stirred for 20 h, and then partitioned between dichloromethane and water. The product was extracted from the aqueous layer with additional dichloromethane (30 mL × 4), the organic solutions were combined, and the

solvent was removed under vacuum. The product was purified by silica gel chromatography using dichloromethane/ethyl acetate (3:1) as the eluent to give the product (1.07 g, 2.52 mmol, 76%). ^{1}H NMR (400 MHz, $CDCl_3$): δ (ppm) 7.49 (d, J = 8.2 Hz, 4H), 7.27 (d, J = 8.4 Hz, 4H), 7.26 (s, 2H), 2.65 (t, J = 7.8 Hz, 4H), 1.61 (quint., J = 7.7 Hz, 4H), 1.36 (sextet, J = 7.6 Hz, 4H), 0.92 (t, J = 7.4 Hz, 6H). ^{13}C NMR (100 MHz, $CDCl_3$): δ (ppm) 184.6, 155.5, 146.0, 135.1, 129.4, 127.5, 126.7, 35.4, 33.3, 22.3, 13.9. (ES) (+) m/z = 424.2 [M+]. Anal. Calcd. for $C_{25}H_{28}OSe$: C, 70.91, H, 6.66. Found: C, 71.14, H, 6.61.

2,6-Bis(4-butylphenyl)-4-methylselenopyrylium tetrafluoroborate, **S5.4**

Under a nitrogen atmosphere 1.6 M methyllithium in diethylether (2.5 mL, 4 mmol) was added dropwise to a solution of **S5.3** (0.844 g, 1.98 mmol), cooled in a dry ice/acetone bath. After 15 min hydrofluoroboric acid (50-54% w/v in diethylether, 1 mL) was added dropwise and the reaction mixture was stirred for 10 min. The solution was then warmed to room temperature and after 1 h diethylether (100 mL) was added. A dark residue precipitated which was collected, dissolved in dichloromethane and partitioned with water. The organic layer was then collected, dried using magnesium sulfate, filtered and then the solvent was removed under vacuum to give a brown solid (0.625 g, 1.23 mmol, 62%). ^{1}H NMR (400 MHz, $CDCl_3$): δ (ppm) 8.42 (s, 2H), 7.84 (d, J = 8.4 Hz, 4H), 7.40 (d, J = 8.4 Hz, 4H), 2.85 (s, 3H), 2.64 (t, J = 7.6 Hz, 4H), 1.60 (quint., J = 7.6 Hz, 4H), 1.34 (sextet, J = 7.6 Hz, 4H), 0.92 (t, J = 7.2 Hz, 6H). ^{13}C NMR (100 MHz, $CDCl_3$): δ (ppm) 179.4, 166.8, 150.5, 133.3, 132.6, 130.8, 128.4, 35.6, 33.0, 27.9, 22.3, 13.9. (ESI) (+) m/z = 423.1 [M+] (-) m/z = 86.8 [M-]. Anal. Calcd. for $C_{26}H_{31}BF_4Se$: C, 61.32, H, 6.14. Found: C, 61.68, H, 6.22.

5.2

S5.4 (333 mg, 0.653 mmol) and **S5.5** (77 mg, 0.30 mmol) were dissolved in acetic anhydride (4 mL) and heated at 100 °C for 30 min. The reaction was cooled under a nitrogen flow, which was also used to concentrate the solution. The residue was mixed with $NaBAr'_4$ (321 mg, 0.362 mmol) in dichloromethane (5 mL), then purified by silica gel chromatography by loading the material using dichloromethane onto a column packed with hexanes and eluted with dichloromethane/hexanes (1:1). The compound was then precipitated from dichloromethane by the addition of hexanes. The precipitation was repeated three times and the product was collected by filtration as a semicrystalline dark solid (123 mg, 0.0706 mmol, 24%). ^{1}H NMR (333 K, 500 MHz, $CDCl_3$): δ (ppm) 7.84 (t, J = 12.8 Hz, 2H), 7.69 (s, 8H), 7.65 (s, 4H), 7.52 (d, J = 8.0 Hz, 8H), 7.49 (s, 4H), 7.32, (d, J = 8.0 Hz, 8H), 6.64 (t, J = 12.8 Hz, 1H), 6.56 (d, J = 13.6 Hz, 2H), 2.67 (t, J = 7.6 Hz, 8H), 1.62 (quint., J = 8.0 Hz, 8H), 1.36 (sextet, J = 7.2 Hz, 8H), 0.95 (t, J = 7.3 Hz, 12H). ^{13}C NMR (100 MHz, $CDCl_3$): δ (ppm) 161.7 (1:1:1:1 q, J_{CB} = 50 Hz), 157.8, 151.4, 147.6, 147.2, 135.0, 134.8, 131.1, 129.9, 129.0, 128.8 (q, J_{CF} = 37 Hz), 126.7, 124.5 (q, J_{CF} = 271 Hz), 117.4, 35.5, 33.3, 22.3, 13.8. (1 peak missing). (ESI) (+) m/z = 881.5 [M+ cation] (-) m/z = 863.1 [M- anion]. Anal. Calcd. for $C_{87}H_{73}Se_2BF_{24}$: C, 59.94, H, 4.22. Found: C, 59.81, H, 4.23.

5.3

S5.4 (255 mg, 0.500 mmol) and **S5.6** (70 mg, 0.254 mmol) were dissolved in acetic anhydride (4 mL) and acetic acid (0.5 mL) heated at 100 °C for 15 min. Upon cooling to room temperature a precipitate formed, which was collected by filtration (68 mg crude). The crude product was mixed with a solution of $NaBAr'_4$ (240 mg, 0.270 mmol) in

dichloromethane, then purified by silica gel chromatography using dichloromethane/ hexanes (1:1) as the eluent. The fractions containing product were concentrated, then precipitated by adding hexanes. The product was collected by filtration as a brown solid (61 mg, 0.0345 mmol, 14%). ^{1}H NMR (500 MHz, CD_2Cl_2): δ (ppm) 7.77 (t, J = 12.5 Hz, 2H), 7.70 (s, 8H), 7.65 (s, 4H) 7.57 (d, J = 8.0 Hz, 8H), 7.54 (s, 4H), 7.36, (d, J = 7.5 Hz, 8H), 7.29 (t, J = 13.0 Hz, 1H), 6.72 (t, J = 13.0 Hz, 2H), 6.62 (d, J = 13.5 Hz, 2H), 2.69 (t, J = 8.1 Hz, 8H), 1.63 (quint., J = 7.8 Hz, 8H), 1.38 (sextet, J = 7.6 Hz, 8H), 0.94 (t, J = 7.4 Hz, 12H). ^{13}C NMR (125 MHz, CD_2Cl_2): δ (ppm) 162.1 (1:1:1:1 q, J_{CB} = 50 Hz), 156.4, 152.2, 150.4, 147.8, 145.8, 135.5, 135.2, 132.4, 130.2, 129.8, 129.2 (q, J_{CF} = 31.3 Hz), 127.1, 125.0 (q, J_{CF} = 270 Hz), 117.8, 35.8, 33.8, 22.7, 14.0 (1 peak missing). (ESI) (+) *m/z* 907 [M^+ cation] (-) *m/z* 863 [M^- anion]. Anal. Calcd. for $C_{89}H_{75}Se_2BF_{24}$: C, 60.42, H, 4.27. Found: C, 60.58, H, 4.14.

1,5-Bis(4-tert-butylphenyl)penta-1,4-diyn-3-ol, **S5.5**

4-*tert*-butylphenylacetlyne (22.61 g, 142.9 mmol) was combined with dry diethylether (90 mL) under a nitrogen atmosphere and cooled in an ice bath. 3 M ethylmagnesiumbromide in diethylether (43 mL) was added dropwise over ten min, then was allowed to stir for 18 h. Ethyl formate (5.2 mL, 64.5 mmol) was added dropwise, then the solution was quenched with 10% aqueous hydrochloric acid (50 mL). The organic phase was separated and diethylether was used to extract the product (3 × 50 mL). The organic layers were combined and concentrated under vacuum. The product was obtained as a white solid after recrystallization from hexanes (15.0 g, 43.5 mmol, 68%). ^{1}H NMR (400 MHz, $CDCl_3$): δ (ppm) 7.43 (d, J = 8.6 Hz, 4H) 7.35 (d, J = 8.7 Hz, 4H) 5.6 (d, J = 7.3 Hz, 1H) 2.39 (d, J = 7.6 Hz, 1H) 0.13 (s, 18H). ^{13}C NMR (100 MHz,

$CDCl_3$): δ (ppm) 152.0, 131.5, 125.2, 118.8, 85.3, 84.5, 53.2, 34.7, 31.0. MS (EI) m/z = 344.2 [M^+]. Anal. Calcd. for $C_{25}H_{28}O$: C, 87.16, H, 8.19. Found: C, 87.19, H, 8.16.

5-Bis(4-*tert*-butylphenyl)penta-1,4-diyn-3-one, **S5.6**

S5.5 (3.15 g, 9.14 mmol) was combined with pyridiniumchlorochromate (3.01 g, 14.2 mmol) in dry dichloromethane (80 mL). After 5 h of stirring diethylether (150 mL) was added. The solution was filtered through a short pad of silica using dichloromethane as the eluent. The filtrate was concentrated and purified through silica gel column chromatography using dichloromethane/hexanes (1:1) as the eluent. The product was collected as a yellow solid, then recrystallized in hexanes (2.07 g, 6.03 mmol, 70%). ^{1}H NMR (400 MHz, $CDCl_3$): δ (ppm) 7.58 (d, J = 8.5 Hz, 4H) 7.42 (d, J = 8.6 Hz, 4H) 1.31 (s, 18H). ^{13}C NMR (100 MHz, $CDCl_3$): δ (ppm) 161.0, 155.0, 133.2, 125.7, 116.4, 92.1, 89.4, 35.1, 31.0. MS (ES) m/z = 342.1 [M^+]. Anal. Calcd. for $C_{25}H_{28}O$: C, 87.68, H, 7.65. Found: C, 87.60, H, 7.77.

2,6-Bis(4-*tert*-butylphenyl)-4H-thiopyran-4-one, **S5.7**

Sulfur powder (0.349 g, 10.9 mmol) was reduced using 1 M lithium triethylborohydride in tetrahydrofuran (22 mL), which was added dropwise under a nitrogen atmosphere. After 1.5 h a solution of 1 M sodium ethoxide in ethanol (20 mL) was added. The solution was added dropwise for 5 min to a solution of **S5.6** (3.80 g, 11.1 mmol) in tetrahydrofuran (20 mL) and 1 M sodium ethoxide in ethanol (20 mL) under a nitrogen atmosphere, while being cooled in an ice bath. The solution was stirred for 18 h, then concentrated under vacuum to a viscous oil. The residue was partitioned between dichloromethane and water. The organic layer was separated and product was extracted from the aqueous layer repeatedly using dichloromethane (5 × 40 mL). The organic

layers were combined and the solvent was removed under vacuum. The residue was dissolved in hexanes and filtered to remove a small amount of insoluble material. The solid was recrystallized from hexanes to give orange crystalline solid (2.38 g, 6.32 mmol, 51%). ^{1}H NMR (400 MHz, $CDCl_3$): δ (ppm) 7.57 (d, J = 8.5 Hz, 4H), 7.50 (d, J = 8.5 Hz, 4H), 7.20 (s, 2H), 1.34 (s, 18H). ^{13}C NMR (100 MHz, $CDCl_3$): δ (ppm) 182.6, 154.3, 153.2, 133.2, 126.55, 126.50, 126.3, 34.9, 31.1. GC-MS *m/z*: 376 [M^+]. Anal. Calcd. for $C_{25}H_{28}OS$: C, 79.74, H, 7.49. Found: C, 79.47, H, 7.60.

2,6-Bis(4-*tert*-butylphenyl)-4*H*-selenopyran-4-one, **S5.8**[32]

Selenium powder (0.576 g, 7.30 mmol) was reduced using 1 M lithium triethylborohydride in tetrahydrofuran (14.6 mL), which was added dropwise under a nitrogen atmosphere. After 2 h a solution of 1 M sodium ethoxide in ethanol (30 mL) was added. The solution was added dropwise for 5 min to a solution of **S5.6** (2.5 g, 7.3 mmol) in tetrahydrofuran (20 mL) and 1 M sodium ethoxide in ethanol (30 mL) under nitrogen and cooled on an ice bath. The solution was stirred for 18 h, then concentrated to a viscous oil. The residue was partitioned between dichloromethane (100 mL) and water. The organic layer was separated and product was extracted from the aqueous layer repeatedly (2 × 50 mL). The organic layers were combined and dried over magnesium sulfate. The magnesium sulfate was filtered and the filtrate was concentrated to give an orange solid. It was further purified by recrystallization in acetonitrile (1.24 g, 2.92 mmol, 40% yield). ^{1}H NMR (400 MHz, $CDCl_3$): δ (ppm) 7.56-7.49 (m, 8H), 7.29 (s, 2H), 1.36 (s, 18H). ^{13}C NMR (100 MHz, $CDCl_3$): δ (ppm) 184.6, 155.5, 154.2, 134.9, 127.6, 126.5, 126.4, 34.9, 31.2. MS (EI) m/z = 424.2 [M^+]. Anal. Calcd. for $C_{25}H_{28}OSe$: C, 70.91, H, 6.66. Found: C, 71.21, H, 6.71.

2,6-Bis(4-*tert*-butylphenyl)-4-methylthiopyrylium tetrahydrofluoroborate, **S5.9**

S5.7 (2.12 g, 5.62 mmol) was dissolved in tetrahydrofuran (20 mL) under nitrogen and cooled in a dry ice/acetone bath. 1-2 M methyllithium in diethylether (5 mL) was added dropwise. After stirring for 10 min hydrofluoroboric acid (1.5 mL, 50-54% w/v in diethylether) was added dropwise. After 10 min the solution was warmed to room temperature. The solution was concentrated, then dissolved in dichloromethane (100 mL) and washed with water (150 mL × 2). The organic layer was then concentrated and the addition of hexanes caused a solid to precipitate. The product was then collected by filtration as a yellow solid (1.53 g, 2.80 mmol, 49.8%). ^{1}H NMR (400 MHz, $CDCl_3$): δ (ppm) 8.58 (s, 2H), 7.92 (dd, J = 2.0, 6.8 Hz, 4H), 7.64 (dd, J = 1.9, 6.9 Hz, 4H), 2.97 (s, 3H), 1.33 (s, 18H). ^{13}C NMR (100 MHz, $CDCl_3$): δ (ppm) 168.6, 167.4, 158.3, 133.0, 130.7, 128.3, 127.6, 35.3, 30.9, 26.4. (ESI) (+) m/z = 375.2 [M+], (-) m/z = 86.7 [M-]. Anal. Calcd. for $C_{26}H_{31}BF_4S$: C, 67.54, H, 6.76. Found: C, 67.38, H, 6.78.

2,6-Bis(4-*tert*-butylphenyl)-4-methylselenopyrylium tetrahydrofluoroborate, **S5.10**[32]

S5.8 (5.5 g, 13 mmol) was dissolved in tetrahydrofuran (100 mL) under nitrogen and cooled in a dry ice/acetone bath. 1-2 M methyllithium in diethylether (16 mL) was added dropwise. After stirring for 30 min hydrofluoroboronic acid (8.5 mL, 50-54% w/v in diethylether) was added dropwise. After 30 min the solution was warmed to room temperature and stirred for 1 h. Water (200 mL) and dichloromethane (200 mL) were added onto the reaction mixture and he organic layer and the aqueous layer were separated. The aqueous layer was extracted with dichloromethane (2 × 50 mL). The organic layers were combined and dried over magnesium sulfate. The magnesium sulfate was removed by filtration and the solvent was removed under vacuum. The black residue

was dissolved in dichloromethane (20 mL), then hexanes (15 mL) was added and the mixture was allowed to stand overnight. The product was then collected by filtration as a dark orange solid (3.4 g, 6.7 mmol, 52%). ^{1}H NMR (400 MHz, $CDCl_3$): δ (ppm) 8.47 (s, 2H), 7.90 (d, J = 8.7 Hz, 4H), 7.67 (d, J = 8.7 Hz, 4H), 2.93 (s, 3H), 1.37 (s, 18H). ^{13}C NMR (100 MHz, $CDCl_3$): δ (ppm) 179.3, 166.9, 158.5, 133.1, 132.7, 128.2, 127.8, 35.4, 30.9, 27.9; MS (ESI) m/z = 423.2 [ES^+], 86.7 [ES^-]. Anal. Calcd. for $C_{26}H_{31}BF_4Se$: C, 61.32, H, 6.14. Found: C, 60.86, H, 6.21 (The product did not pass elemental analysis after attempting to recrystallize the product in acetonitrile, followed by recrystallization in hexanes. Dissolving the product in dichloromethane and extracting impurities (presumably hydrofluoroboric acid) with water gave the closest elemental analysis, which is the one reported above).

5.4

S5.9 (302 mg, 0.65 mmol) and **S5.5** (80 mg, 0.31 mmol) were dissolved in acetic anhydride (4 mL) and heated at 100 °C for 25 min. The reaction was cooled in an ice bath, then filtered to obtain the crude product (80 mg). The crude product was mixed with $NaBAr'_4$ (200mg, 0.226 mmol) in dichloromethane, then purified by silica gel chromatography by loading the material using dichloromethane onto a column packed with hexanes and eluted with dichloromethane followed by a second silica gel column packed with hexanes, the product was dissolved in dichloromethane and loaded onto the column, which was eluted with dichloromethane/hexanes (1:1). The compound was then precipitated from dichloromethane using hexanes. The product was collected by filtration as a semicrystalline brown solid (118 mg, 0.0715 mmol, 23.1%). ^{1}H NMR (333 K, 500 MHz, $CDCl_3$): δ (ppm) 7.73 (t, J = 13.1 Hz, 2H), 7.69 (m, 8H), 7.60 (dm, J = 8.6

Hz, 12H), 7.55 (d, J = 8.6 Hz, 8H) 7.49 (s, 4H), 6.56, (t, J = 12.8 Hz, 1H), 6.42 (d, J = 13.7 Hz, 2H), 1.35 (s, 36H). ^{13}C NMR (100 MHz, $CDCl_3$): δ (ppm) 161.7 (1:1:1:1 q, J_{CB} = 50 Hz) 155.9, 153.4, 150.8, 147.6, 134.8, 132.7, 129.7, 128.9 (q, J_{CF} = 31 Hz) 126.8, 126.6, 125.5, 124.6 (q, J_{CF} = 271 Hz) 117.4, 35.1, 31.1 (1 peak missing). (ESI) (+) m/z = 785.4 [M+ cation] (-) m/z = 863 [M- anion]. Anal. Calcd. for $C_{87}H_{73}S_2BF_{24}$: C, 63.35, H, 4.46. Found: C, 63.48, H, 4.52.

5.5

S5.10 (333 mg, 0.653 mmol) and **S5.5** (81 mg, 0.31 mmol) were dissolved in acetic anhydride (5 mL) and heated at 100 °C for 20 min. The reaction was cooled under a nitrogen flow overnight, then filtered to obtain the crude product. The crude product was mixed with $NaBAr'_4$ (287 mg, 0.324 mmol) in dichloromethane, then purified by silica gel chromatography by loading the material using dichloromethane onto a column packed with hexanes and eluted with dichloromethane. The compound was then precipitated from dichloromethane using hexanes. The product was collected by filtration as a black solid (194 mg, 0.111 mmol, 36%). ^{1}H NMR (333 K, 500 MHz, $CDCl_3$): δ (ppm) 7.83 (t, J = 13.0 Hz, 2H), 7.70 (m, 8H), 7.65 (s, 4H), 7.55 (s, 16H), 7.49 (s, 4H), 6.65 (t, J = 12.5 Hz, 1H), 6.57 (d, J = 13.5 Hz, 2H), 1.38 (s, 36H). ^{13}C NMR (333 K, 125 MHz, $CDCl_3$): δ (ppm) 161.9 (1:1:1:1 q, J_{CB} = 50 Hz), 158.1, 156.1, 151.7, 147.3, 135.0, 134.9, 131.2, 129.2, 129.1 (q, J_{CF} = 33.8 Hz), 127.0, 126.7, 124.7 (q, J_{CF} = 270 Hz), 117.5, 35.2, 31.1 (1 peak missing). (ESI) (+) m/z = 881.3 [M+ cation] (-) m/z = 863.0 [M- anion]. Anal. Calcd. for $C_{87}H_{73}Se_2BF_{24}$: C, 59.94, H, 4.22. Found: C, 59.97, H, 4.24.

5.6

4-((*E*)-2-((*E*)-2-chloro-3-(2-(2,6-diphenyl-4*H*-thiopyran-4-ylidene)ethylidene)cyclohex-1-enyl)vinyl)-2,6-diphenylthiopyrylium tetrfluoroborate was purchased from Sigma-Aldrich as IR-1061. IR-1061 (135 mg, 0.180 mmol) was mixed with $NaBAr'_4$ (166 mg, 0.187 mmol) in dichloromethane (5 mL) for 5 min. The product was purified using silica gel chromatography with dichloromethane/hexanes (1:1) as the eluent followed by precipitation from dichloromethane by the addition of hexanes. The product was collected as a black solid (231 mg, 0.151 mmol, 84%). ^{1}H NMR (333 K, 500 MHz, $CDCl_3$): δ 8.29 (d, J = 13.9 Hz, 2H), 7.69 (m, 12H), 7.67 (d, J = 7.0 Hz, 8H), 7.57-7.51 (m, 12H), 7.49, (s, 4H), 6.58 (d, J = 13.8 Hz, 2H), 2.66 (m, 4H), 1.86 (m, 2H). ^{13}C NMR (333 K, 125 MHz, $CDCl_3$): δ (ppm) 162.0 (1:1:1:1 q, J_{CB} = 49 Hz), 153.0, 150.3, 149.5, 140.4, 135.7, 135.0, 133.4, 131.9, 129.9, 129.1 (q, J_{CF} = 34 Hz), 126.9, 125.3, 124.7 (q, J_{CF} = 271 Hz), 117.5, 27.1, 20.9. (ESI) (+) m/z = 661.1 [M+ cation] (-) m/z = 862.7 [M- anion]. Anal. Calcd. for $C_{76}H_{46}S_2BClF_{24}$: C, 59.84, H, 3.04. Found: C, 59.61, H, 2.87.

5.7. References

1. Hales, J. M.; Matichak, J.; Barlow, S.; Ohira, S.; Yesudas, K.; Brédas, J.-L.; Perry, J. W.; Marder, S. R., Design of Polymethine Dyes with Large Third-Order Optical Nonlinearities and Loss Figures of Merit. *Science* **2010,** 327, 1485-1488.
2. *A significant contribution is from Dr. Joel Hales*.
3. Johr, T.; Werncke, W.; Pfeiffer, M.; Lau, A.; Dähne, L., Third-order Nonlinear Polarizabilities of a Homologous Series of Symmetric Cyanines. *Chem. Phys. Lett.* **1995,** 246, 521-526.
4. Tolbert, L. M.; Zhao, X., Beyond the Cyanine Limit: Peierls Distortion and Symmetry Collapse in a Polymethine Dye. *J. Am. Chem. Soc.* **1997,** 119, 3253-3258.
5. Kachkovski, O. D.; Tolmachov, O. I.; Slominskii, Y. L.; Kudinova, M. O.; Derevyanko, N. O.; Zhukova, O. O., Electronic Properties of Polymethine Systems 7: Soliton Symmetry Breaking and Specral Features of Dyes with Long Polymethine Chain. *Dyes Pigm.* **2005,** 64, 207-216.
6. Simonsen, K. B.; Geisler, T.; Petersen, J. C.; Arentoft, J.; Sommer-Larsen, P.; Greve, D. R.; Jakobsen, C.; Becher, J.; Malagoli, M.; Bredas, J. L.; Bjornholm, T., Bis(1,3-dithiole) polymethine Dyes for Third-Order Nonlinear Optics - Synthesis,

Electronic Structure, Nonlinear Optical Properties, and Structure-Property Relations. *Eur. J. Org. Chem.* **1998**, 2747-2757.
7. Gerasov, A. O.; Shandura, M. P.; Kovtun, Y. P., Series of polymethine dyes derived from 2,2-difluoro-1,3,2-(2*H*)-dioxaborine of 3-acetyl-7-diethylamino-4-hydroxycoumarin. *Dyes Pigm.* **2008,** 77, 598-607.
8. Kassaee, M. Z.; Jalalimanesh, N.; Musavi, S. M., Effects of Group 14-16 Heteroatoms on theAromaticity of Benzene at DFT Level. *J. Mol. Struct. (THEOCHEM)* **2007,** 816, 153-160.
9. Detty, M. R.; McKelvey, J. M.; Luss, H. R., Tellurapyrylium Dyes. 2. The Electron-Donating Properties of the Chalcogen Atoms to the Chalcogenapyrylium Nuclei and Their Radical Dications, Neutral Radicals, and Anions. *Organometallics* **1988,** 7, 1131-1147.
10. Mullay, J., Atomic and Group Electronegativities. *J. Am. Chem. Soc.* **1984,** 106, 5842-5847.
11. Detty, M. R.; Merkel, P. B., Chalcogenapyrylium Dyes as Potential Photochemotherapeutic Agents. Solution Studies of Heavy Atom Effects on Triplet Yields, Quantum Efficiencies of Singlet Oxygen Generation, Rates of Reaction with Singlet Oxygen, and Emission Quantum Yields. *J. Am. Chem. Soc.* **1990,** 112, 3845-3855.
12. Maloney, C.; Blau, W., Resonant Third-order Hyperpolarizablities of Large Organic Molecules. *J. Opt. Soc. Am. B* **1987,** 4, 1035-1039.
13. Ganeev, R. A.; Tugushev, R. I.; Ishchenko, A. A.; Derevyanko, N. A.; Ryasnyansky, A. I.; Usmanov, T., Characterization of Nonlinear Optical Parameters of Polymethine Dyes. *Appl. Phys. B* **2003,** 76, 683-686.
14. Hales, J. M.; Zheng, S.; Barlow, S.; Marder, S. R.; Perry, J. W., Bisdioxaborine Polymethines with Large Third-Order Nonlinearities for All-Optical Signal Processing. *J. Am. Chem. Soc.* **2006,** 128, 11362-11363.
15. Hales, J. M.; Zheng, S.; Barlow, S.; Marder, S. R.; Perry, J. W., Bisdioxaborine Polymethines with Large Third-Ordr Nonlinearities for All-Optical Signal Processing. *J. Am. Chem. Soc.* **2006,** 128, 11362-11363.
16. Kachkovski, A. D.; Kudinova, M. A.; Shapiro, B. I.; Derevjanko, N. A.; Kurkina, L. G.; Tolmachev, A. I., Electronic Energy Levels and Electron Donor Ability of γ-Pyrylocyanines and Their Heteroanalogues. *Dyes Pigm.* **1984,** 5, 295-306.
17. *Performed by Dr. Joel Hales*.
18. Detty, M. R.; Murray, B. J.; Seidlar, M. D., Preparation of 2,6-diphenyl-4H-chalcogenapyran-4-ones. *J. Org. Chem.* **1982,** 47, 1968-1969.
19. Hori, H.; Yamazaki, S.; Yamamoto, K.; Murata, I., A Monocyclic Selenepine: Synthesis and Characterization of Dieethyl 2,7-Di-tert-butyl-4,5-selenepinedicarboxylate. *Angew. Chem. Int. Ed.* **1990,** 29, 424-425.
20. Brookhart, M.; Grant, B.; Volpe Jr., A. F., $[(3,5\text{-}(CF_3)_2C_6H_3)_4B]^-[H(OEt_2)_2]^+$. *Organmetallics* **1992,** 11, 3920-3922.
21. Kudinova, M. A.; Kachkovski, A. D.; Kurdyukov, V. V.; Tolmachev, A. I., Nature of the Absorption Bands of Pyrylocyanines. 2. Influence of *t*-Bu, Ph and Th Ring Substituents. *Dyes Pigm.* **2000,** 45, 1-7.

22. Panda, J.; Virkler, P. R.; Detty, M. R., A Comparison of Linear Optical Properties and Redox Properties in Chalcogenopyrylium Dyes Bearing Ortho-Substituted Aryl Substituents and tert-Butyl Substituents. *J. Org. Chem.* **2003,** 68, 1804-1809.
23. König, W., *Angew. Chem.* **1925,** 38, 743-748.
24. Kachkovski, A. D.; Kovalenko, N. M., Electronic Properties of Polymethine Systems. Part 4. Vinylene Shift. *Dyes Pigm.* **1997,** 35, 131-148.
25. Kudinova, M. A.; Derevyanko, N. O.; Dyadyusha, G. G., *Khimia Geterotzikl. Soed.* **1980**, 898.
26. Tolmachev, A. I.; Derevianko, N. A.; Ischenko, A. A., *Khimia Geterotzikl. Soed.* **1982**, 1178.
27. Fu, J.; Padilha, L. A.; Hagan, D. J.; Van Stryland, E. W., Molecular Structure—Two-Photon Absorption Property Relations in Polymethine Dyes. *J. Opt. Soc. Am. B: Opt. Phys.* **2007,** 24, 56-66.
28. Lu, D.; Chen, G.; Perry, J. W.; Goddard, W. A. I., Valence-Bond Charge-Transfer Model fro Nonlinear Optical Properties of Charge-Transfer Organic Molecules. *J. Am. Chem. Soc.* **1994,** 116, 10679-10685.
29. Beverina, L.; Fu, J.; Leclercq, A.; Zojer, E.; Pacher, P.; Barlow, S.; Van Stryland, E. W.; Hagan, D. J.; Brédas, J.-L.; Marder, S. R., Two-Photon Absorption at Telecommunications Wavelengths in a Dipolar Chromophore with a Pyrrole Auxiliary Donor and Thiazole Auxiliary Acceptor. *J. Am. Chem. Soc.* **2005,** 127, 7282-7283.
30. Scherer, D.; Dörfler, R.; Feldner, A.; Vogtmann, T.; Schwoerer, M.; Lawrentz, U.; Grahn, W.; Lambert, C., Two-Photon States in Squaraine Monomers and Oligomers. *Chem. Phys.* **2002,** 279, 179-207.
31. Pangborn, A. B.; Giardello, M. A.; Grubbs, R. H.; Rosen, R. K.; Timmers, F. J., Safe and Convenient Procedure for Solvent Purification. *Organometallics* **1996,** 15, 1518-1520.
32. *Synthesized by Dr. Tissa Sajoto*.

Chapter 6

Conclusions and Future Work

6.1. Conclusions

The aim of this thesis was to explore the third-order nonlinear optical properties of a variety of polymethine dyes. The structural modification of polymethine dyes and subsequent nonlinear characterization was employed to determine structure-property relationships that effect the third-order polarizability. The investigation of the dyes was directed at the identification of potentially useful materials to be used for an all-optical switching or all-optical signal processing application (AOSP).

The majority of the compounds reported in this thesis have not been previously reported in the literature. However, in most cases close analogues of the dyes can be found in the literature with relatively modest modifications. Primarily three classes of reactions were used to synthesize the materials: Vilsmeyer-like formylations, the Knoevenagel condensation, and ion metathesis. The Vilsmeyer-like formylation was used to synthesize cyanine precursors, which were necessary to modify bridge length and bridge substituents. The Knoevenagel condensation, a reaction used to combine a simple cyanine bridge with peripheral electron donating or accepting groups, added complexity to simple cyanine dyes by providing a means to make dyes with a variety of terminal groups. Finally the ion metathesis reactions were used to purify the materials and increase the solubility of the dyes in common organic solvents.

Figure 6.1 shows a general structure of a polymethine dye, which can be modified in several positions: at the terminal groups; at the polymethine bridge; at the counterion;

and the number of vinylene groups can be modified. This thesis explored all the possible positions of modification to some degree.

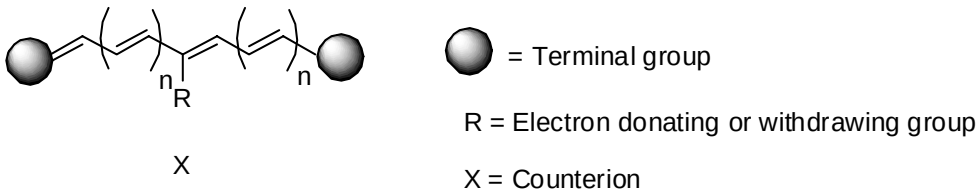

Figure 6.1. General structure of a polymethine dye with tunable positions.

In this thesis modification of the counterion was not explored as heavily as the other tunable positions of polymethine dyes outlined in Figure 6.1. The counterion was predominantly used to aide in the purification of materials and to enhance the solubility of the dyes rather than improving the nonlinear optical properties. The ion metathesis reaction involving sodium hydride and a tetra-*n*-alkylammonium bromide salts in tetrahydrofuran (used extensively in Chapters 2, 3 and 4) provided a means to purify and increase the solubility of anionic dyes. The use of the $^{-}BAr'_4$ counterion aided in the purification of cationic dyes (as seen in Chapters 3 and 5) while increasing the solubility of the dyes in common organic solvents. The effects of the counterion upon the solution phase third-order nonlinear optical properties were small as seen in Chapter 2 (comparing **2.XVI**, **2.1** and **2.2**) and Chapter 4 (comparing **4.9** and **4.10**). However, the range of types of counterions used in this study was not diverse. The counterions used in this thesis (proton sponge, triethylammonium, tetra-*n*-alkylammonium, Iodide, $^{-}BAr'_4$) would not be expected to contribute to the third-order nonlinearity. The pairing of ions which are both known to have substantial contribution to the third-order nonlinearity would

make an interesting study in the future. The counterion clearly has an effect on the solid state linear optical properties, as opposed to the solution phase. As seen in Chapter 2, the counterion will play an important role in solid state studies and eventual device applications. More extensive studies should be conducted regarding the counterion in order to understand the effects upon the linear and nonlinear optical properties of polymethine dyes in the solid state.

Modifications of the bridge were preformed in each Chapter, either through lengthening the bridge by the addition of vinylene groups or adding substituents. The simple addition of vinylene groups generally leads to larger γ values. While the effects upon the linear absorption spectra are well known through the vinylene shift, the series in Chapter 5 (**5.1-5.3**) showed the position of 2PA bands can also be controlled through the use of the bridge length. In Chapter 3, a survey of the literature was performed regarding ε of substituted heptamethine dyes. The survey revealed that the σ and π-electron effects can be fairly well explained through the modified Swain-Lupton coefficients. A series of dioxaborine-terminated pentamethine dyes and a series of indole-terminated heptamethine dyes were synthesized to show that the linear absorption properties and redox properties were fairly consistent with the Swain-Lupton coefficients. It was found that by tuning the position of the 1PA peak using bridge substitution, the effects on the position of the 2PA peak could be predicted. Subsequently, the relative magnitudes of real and imaginary γ could be tuned for a specific wavelength. Chapter 4 supported the findings in Chapter 3 using TCF-terminated dyes with ring substituents on the polymethine bridge, which had similar effects on the third-order nonlinear optical properties.

It is important to note that dyes with atypical absorption band shapes have unpredictable effects on γ. Dyes **2.8** and **3.3** were dioxaborine terminated pentamethine dyes which had nitro substituents on the periphery of the terminal groups and at the center of the bridge respectively. Both positions of substitution lead to atypical linear absorption spectra. Eventhough the λ_{max} of **2.8** exhibited a bathochromic shift relative to dyes of similar length, the broad spectrum and atypical vibronic coupling lead to relatively small γ values. **3.3** exhibited an atypically broad absorption spectrum and an additional peak, which also had relatively small γ values.

A wide variety of terminal groups was studied in this thesis. Chapter 2 provided examples of similar terminal groups (all dioxaborine-terminal groups) with moderate variation in conjugation length, can still effect the magnitude of Re(γ). As expressed in the introduction of Chapter 5, it is difficult to directly compare the effects upon the linear and nonlinear optical properties caused by terminal groups if the terminal groups are very different. This thesis could be used as a starting point for a library of polymethine dyes and the third-order nonlinear optical properties of those dyes.

Wavelengths at which molecules will have both large Re(γ) and small Im(γ) can be predicted with a fairly high degree of reliability. Additionally, structural modifications can be performed in order to tune a molecule to have optimized properties at the desired wavelengths. Pyrylium-terminated polymethine dyes identified in this study outperformed the other dyes in terms of large magnitudes of Re(γ) and ratios of Re(γ)/Im(γ). The selenopyrylium-terminated dye with a heptamethine chain (**5.3**) was found to exhibit a remarkably large value of Re(γ) at 1300 nm and yet possessed an

unprecedented ratio Re(γ)/Im(γ) of greater than 150. The pyrylium-terminated dyes have set a new benchmark in organic materials designed for AOSP applications.

6.2. Future directions

This thesis focused on the development of structure-property relationships of polymethine dyes in the solution phase, which is not a practical phase for device applications. A device to be used for AOSP will require materials at high number density in the solid state. Large magnitudes of Re($\chi^{(3)}$) are necessary to allow the optical power of laser pulses and power consumption of the pulses to be kept low. Additionally, large magnitudes of Re($\chi^{(3)}$) would permit devices to be fabricated with small interaction lengths (*i.e*. the path length of the light through the nonlinear optical material could be minimized). The large magnitudes of Re($\chi^{(3)}$) need to be coupled with low loss (linear, nonlinear, and scattering losses) to provide flexibility in the interaction length and minimize the buildup of heat caused by absorption that could potentially damage the nonlinear medium. To a first approximation based upon the solution properties, the pyrylium-terminated dyes identified in Chapter 5 fulfill many of these requirements. Therefore, pyrylium-terminated dyes would be the most likely candidates to further develop for use in the solid state.

Future work will focus upon the processing of the materials in the solid state. It will be desirable to spin-coat or melt process a thick film (1 μm) of the nonlinear material on a device as an amorphous film (in order to minimize scattering losses). This thesis did not attempt to address this issue; however, certain aspects of material processing were considered. For example, a material will require high solubility in solvents if it is to be spin-coated on a device. The ion metathesis reactions described in this thesis has

addressed this issue by identifying counterions that can be paired with cationic or anionic dyes that will allow them to be soluble in a large variety of solvents.

The preliminary work in Chapter 2 regarding the counter-ion effects upon the linear absorption spectra of dioxaborine-terminated dyes (**2.XVI**, **2.1** and **2.2**) in the solid state serves as an indication that control of aggregation (the most likely cause of the different absorption spectra) will play an important role in the solid state processing of polymethine dyes. Polymethine dyes are well known to aggregate in the solution phase[1] and particularly in the solid state where number density is generally much higher. It is not clear whether aggregation is advantageous or detrimental to third-order nonlinearites. Two important aspects to consider are the band shape and the band position. Aggregation which can cause broadening of the absorption bands would most likely be detrimental. An important feature of the shape of polymethine absorption bands that makes them amenable for third-order materials is the steep curve of the low energy side of the band. Excitation wavelengths (*e.g.* operational wavelengths of a device) near the absorption edge of the material will receive resonance enhancement, which will be reflected in large magnitudes of Re(γ). However, this advantage would be lost if the absorption band is broadened, because the excitation wavelength would be farther from the peak of the band. Along the same lines of argument, aggregation that causes the absorption band to hypsochromically shift compared to the solution phase peak may be undesirable because the peak absorption would be more greatly detuned from the measurement wavelength (*e.g.* 1300 nm). While moderate shifts in the peak of the solid state spectrum may be tolerable, a large bathochromic shift may push the absorption edge too close to the excitation wavelength, leading to detrimental linear absorption.

While it may be advantageous to control aggregation, it may be more practical to prevent aggregation altogether. Insulating the chromophores from each other is one approach to achieve solid state behavior that is similar to solution-phase behavior. The remainder of this Chapter will outline several strategies, which may be useful to achieve this goal. It is important to note that these strategies will "dilute" the active chromophore in the solid film. Using one of these strategies may improve the effectiveness of a single chromophore; however, the number density of chromophores in a film will be reduced. A balance between these two opposing effects must be met in order to make practical materials for devices.

The first strategy involves adding substantial bulk to the chromophore, which would rely on steric hindrance to keep the chromophores separate. Bouit *et al.*[2] used dendrimers to increase the solubility and to prevent aggregation for polymethine dyes in solution. Doctors Annabelle Scarpaci and Arpornrat Nantalaksakul have prepared dendronized derivatives of pyrylium-terminated polymethine dyes, which the bulky dendrimer substituents are intended to prevent aggregation. Figure 6.2 shows a general diagram of a polymethine dye with three possible combinations of dendrimer substitution: 1) in the peripheral positions (on the terminal group, labeled X), on the center of the chromophore (on the polymethine bridge, labeled Y), or a combination of the two. While effects in the aggregation behavior were demonstrated (by Dr. Scarpaci and Dr. Nantalaksakul) for substitution of dendrimers in the X or Y positions, they did not achieve complete isolation of the chromophores from one another. The more heavily dendronized version (where X and Y are both substituted with dendrimers) remains to be explored.

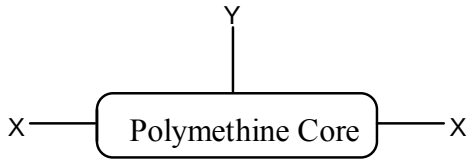

A) X = Dendrimer
B) Y = Dendrimer
C) X and Y = Dendrimer

Figure 6.2. Possible positions to decorate a polymethine dye with dendritic substituents.

An alternative approach to prevent aggregation may be the route taken by Yau *et el.*[3] which is to encapsulate the polymethine core in a supramolecular rotaxane structure. The strategy used a α-cyclodextrin to encapsulate a polymethine dye. While the core of the dye was completely surrounded by the α-cyclodextrin, a possible disadvantage to this approach is the opportunity for the terminal groups to interact (π-π stacking of the terminal groups were observed in the crystal structure). A second drawback to this approach arises from synthetic difficulties. An aqueous solution is necessary to perform the synthesis of a rotaxane: first a pseudo-rotaxane forms as the cyanine precursor threads through the hydrophobic core of the α-cyclodextrin, then the terminal groups are attached to the cyanine precursor to form the capped rotaxane (Figure 6.3). Unfortunately many polymethine dyes lack sufficient stability in an aqueous environment for this to be a viable strategy.

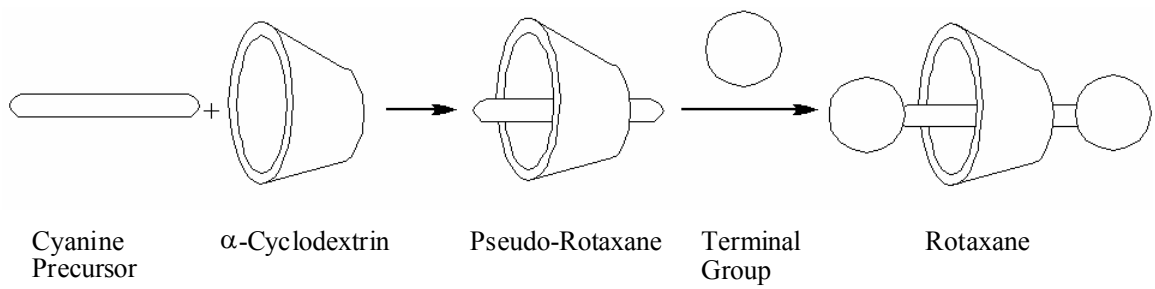

Figure 6.3. Scheme to form an encapsulated polymethine dye.

A third possible strategy to synthesize a solution processable polymethine dye without aggregation would be to attach the polymethine dye as a side group on a polymer backbone. Polymers have high viscosity in solution, which is beneficial for forming high quality films using the spin-coating technique. Copolymerizing a combination of monomers, one with the polymethine chromophore and one with a bulky substituent, could be used as a strategy to separate the polymethine chromophores from one another. Varying the ratio of monomers would allow the determination of the maximum loading of chromophore that could be used before aggregation occurred. Furthermore, covalently attaching polymethine dyes to a polymer backbone would prevent phase separation between the optically inactive and optically active species. Figure 6.4 represents a diagram of such a polymeric system.

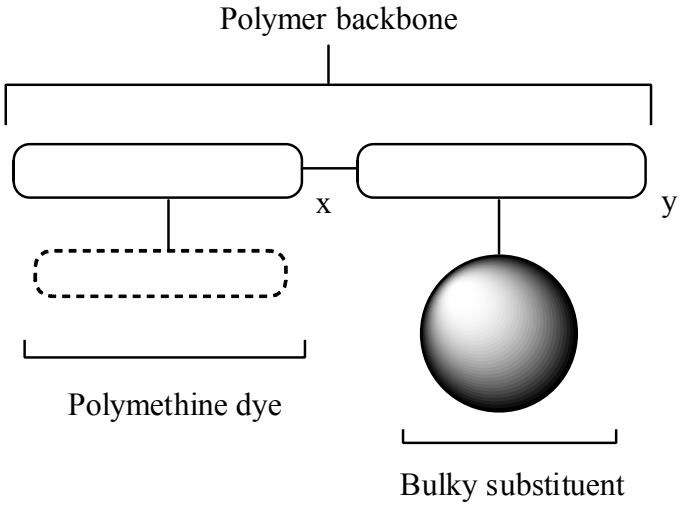

Figure 6.4. A representation of a random copolymer with a polymethine sidegroup intended to provide third-order nonlinearity and a bulky substituent intended to provide steric bulk.

6.3. References

1. Shapiro, B. I., Molecular Assemblies of Polymethine Dyes. *Russ. Chem. Rev.* **2006,** 75, (5), 433-456.
2. Bouit, P.-A.; Westlund, R.; Feneyrou, P.; Maury, O.; Malkoch, M.; Malmström, E.; Andraud, C., Dendron-Decorated Cyanine Dyes for Optical Limiting Applications in the Range of Telecommunication Wavelengths. *New J. Chem.* **2009,** 33, 964-968.
3. Yau, C. M. S.; Pascu, S. I.; Odom, S. A.; Warren, J. E.; Klotz, E. J. F.; Frampton, M. J.; Williams, C. C.; Coropceanu, V.; Kuimova, M. K.; Phillips, D.; Barlow, S.; Brédas, J.-L.; Marder, S. R.; Millar, V.; Anderson, H. L., Stabilisation of a Heptamethine Cyanine Dye by Rotaxane Encapsulation. *Chem. Commun.* **2008**, 2897-2899.